Damage Stability of Ships as a Safety Criterion for Optimisation Tools

Thesis for the degree of Doctor of Philosophy

Deniz Saydan
Faculty of Engineering, Science & Mathematics
School of Engineering Sciences

UNIVERSITY OF SOUTHAMPTON

FACULTY OF ENGINEERING, SCIENCE & MATHEMATICS

School of Engineering Sciences

Damage Stability of Ships as a Safety Criterion for Optimisation Tools

by

Deniz Saydan

Thesis for the degree of Doctor of Philosophy

July 2006

dedicated to

my beloved mother, father and sister

UNIVERSITY OF SOUTHAMPTON

ABSTRACT

FACULTY OF ENGINEERING, SCIENCE & MATHEMATICS

SCHOOL OF ENGINEERING SCIENCES

Doctor of Philosophy

DAMAGE STABILITY OF SHIPS AS A SAFETY CRITERION FOR OPTIMISATION TOOLS

by Deniz Saydan

A literature overview of past optimisation studies revealed that whilst satisfaction of intact stability requirements has been built into existing alternative hull form optimisation packages, seeking improved hydrodynamic hull forms in terms of seakeeping, calm water resistance and added resistance, damage stability is not an automated feature. Within the context of the hydrodynamic hull form optimisation techniques their application to novel hull forms would only permit use of deterministic damage stability analysis and as this is not straight-forward damage is applied after the hull is optimised. The damage must be relevant to ship type and applied in appropriate locations with sensible extents of damage. To fulfil this need both the Marine Accident Investigation Branch (MAIB) damage data base and a damage data base generated by Lutzen (2002) are interrogated and findings are reported.

The hydrodynamic analysis of the optimised hull and basis hull for the intact and damage cases is thereafter carried out using a three-dimensional singularity distribution method. The relative vertical motion responses of both intact and damaged hull forms are determined with greater structural cross-coupling than is usually applied in the solution of the equations of ship motions. This has necessitated the development of a novel approach to implement the calculation of the pure and product moment of inertias for the intact and damaged hull forms to facilitate meaningful comparison of intact and damaged ship motions. The processes are equally applicable to any kind of ship.

CONTENTS

LIST OF TABLES

LIST OF FIGURES

ACKNOWLEDGEMENTS

I would like to thank to all of the following people without whom this research could not have been undertaken.

In particular, I would like to thank to Dr. Ö. Belik, Professor P. Temarel and Professor P.A. Wilson, without their presence such a research could not have started. It was a great pleasure to work under the supervision of Professor G.E. Hearn. I am really grateful for his support and encouragement. In addition his and Jenny Hearn's excellent hospitability is greatly appreciated. My thanks are also directed to the members of the Department of Ship Science, staff and students.

The opportunity to meet Dr. Lützen arose at just the right time. I greatly appreciate the discussions with her during this research.

I would like to acknowledge Özgür for his invaluable help, support and encouragement.

Last, but certainly not least, I am grateful to my late Grandfather and Grandmother, Mum and Dad, my sister, Özgür's family and my friends at the University for always being there for me spiritually and physically.

NOMENCLATURE

At the end of variable definitions a list of acronyms used within the text are defined.

a	Distribution density of damage location along ship's length
a_{wpc}	Waterplane area of compartment, that is, area between selected bulkheads
A	Attained survival probability index
$[A]$	Linear motions coefficient matrix including hydrodynamic, hydrostatic and mass distribution influences
$\left[A_{kj}\right]$	Added mass matrix for intact ship. Elements A_{kj} denote added mass coefficient for hydrodynamic reaction in k^{th} direction arising from motion in the j^{th} direction. The pure added mass coefficient for j, k = 1,2,3 is given in kg, whereas the pure added mass coefficient for j, k = 4,5,6 is presented in kg m^2. Finally, the cross-coupled added mass coefficients are given in kg m
$\left[A'_{kj}\right]$	Added mass matrix of damaged ship. A'_{kj} is value of A_{kj} for damaged ship
$A_{\max}$	Required subdivision index associated with probabilistic approach to damaged stability of a ship
A_{wps}	Waterplane area of intact ship
A'_{wps}	Waterplane area of damaged ship
AP , FP	Aft and forward perpendiculars of ship
AP , AS	Subscripts indicating quantity associated with aft portion of ship either to port or starboard
b	Either penetration of damage (m) or base points for the objective function in Hooke-Jeeves optimisation method

B	Breadth (or moulded beam) of ship
$\left[B_{kj}\right]$	Fluid damping matrix of intact ship. B_{kj} denotes fluid damping coefficient for hydrodynamic reaction in k^{th} direction arising from motion in the j^{th} direction. The pure fluid damping coefficient for j, k = 1,2,3 is given in kg rad/s, whereas the pure fluid damping coefficient for j, k = 4,5,6 is presented in kg m^2 rad/s. Finally, the cross-coupled fluid damping coefficients are given in kg m rad/s
$\left[B'_{kj}\right]$	Fluid damping matrix of damaged ship. B'_{kj} is value of B_{kj} for damaged ship
B_{WL}	Breadth of ship at still waterline
C_B	Block coefficient
$\left[C_{kj}\right]$	Hydrostatic restoring matrix of intact ship. C_{kj} is hydrostatic coefficient for restoration in k^{th} direction arising from motion in the j^{th} direction. The pure hydrostatic coefficient for j, k = 3 is given in kg/s^2, whereas the pure hydrostatic coefficient for j, k = 4,5 is presented in kg m^2/s^2. Finally, the cross-coupled hydrostatic coefficients are given in kg m/s^2
$\left[C'_{kj}\right]$	Hydrostatic restoring matrix of damaged ship. C'_{kj} is value of C_{kj} for damaged ship
C_N	Conditioning number of hydrodynamic fluid structure interaction influence matrix of ship being analysed
C_P	Prismatic coefficient
C_{WP}	Waterplane area coefficient
dm	Elemental constituent mass for ship
dm'	Elemental constituent mass of ingressed water
D	Depth of intact ship

F	Factor of subdivision, assumed distribution function of damage location along ship's length and wave exciting forces and moments matrix.
F_k	Time dependent wave exciting force/moment in k^{th} direction for intact ship. F_k used to form k^{th} row of F. The wave exciting force for j, k = 1,2,3 is given in kg m/s^2, whereas the wave exciting moment for j, k = 4,5,6 is presented in kg m^2/s^2
F_k'	Corresponding value of F_k for damaged ship
FP , FS	Subscripts indicating quantity associated with forward portion of ship either to port or starboard
g	Acceleration due to gravity
$g(x)$	Objective function in Hooke-Jeeves optimisation method
GM	Metacentric height
GZ	Righting lever
$GZ_{\max}$	Maximum righting lever
h	Either elevation of water on deck, measured with respect to undisturbed free surface or height of damage (m) presented as a proportion of the ship depth D
$H(\omega)$	Motion transfer function
H_S	Catamaran demi-hull separation parameter
HJ	Step length in Hooke-Jeeves optimisation method

i, j, k subscripts used singly or in pairs to denote a member of a group of values.

I_{XX} , I_{YY} , I_{ZZ}	
or	Pure moments of inertia of intact ship
I_{55} , I_{66} , I_{44}	
I'_{XX} , I'_{YY} , I'_{ZZ}	
or	Pure moments of inertia of damaged ship
I'_{55} , I'_{66} , I'_{44}	

I_{XY}, I_{ZX}, I_{YZ}	
or	Products of inertia for intact ship
I_{56}, I_{54}, I_{46}	
$I'_{XY}, I'_{ZX}, I'_{YZ}$	
or	Products of inertia for damaged ship
$I'_{56}, I'_{54}, I'_{46}$	
$J_{\max}$	Maximum non-dimensional damage length
k_{XX}, k_{YY}, k_{ZZ}	Radius of gyration with respect to X, Y and Z axis respectively
l	Extent of damage (m)
l_p, l_r	Levers for pitch and roll motions
L	Length of ship between perpendiculars
L_{OA}	Overall length of ship
L_S	Moulded length of ship
L_{WL}	Length of vessel at still water waterline
LCB	Longitudinal centre of buoyancy
LCF	Longitudinal centre of flotation
LCG	Longitudinal centre of gravity
m_w	Total mass of ingressed water
M	Ship mass
$M_{AP}, M_{AS}, M_{FP}, M_{FS}$	Representative point masses for intact ship
$M'_{AP}, M'_{AS}, M'_{FP}, M'_{FS}$	Representative point masses for damaged ship made up from intact ship point masses and ingressed water
$\left[M_{kj}\right]$	Generalised mass matrix of intact vessel
$\left[M'_{kj}\right]$	Generalised mass matrix of damaged vessel
M_l	Mass of liquid contained within a compartment of the intact ship

M_{XYZ}	Earth-fixed right-handed Cartesian frame of axes (X, Y, Z) with its origin, M, located at the intersection of the undistributed free-surface, the mid-ship section and the longitudinal central plane of symmetry of the ship in its intact position of static equilibrium.
n	Iteration number
p_i	Probability of damage of either the ith ship compartment or ith group of ship compartments
R	Required subdivision index, often used in stability regulations as being an equivalent alternative designation for $A_{\max}$
$R(\omega)$	Response spectrum
$RVM(z,x)$	Amplitude of vertical relative displacement
s_i	Probability of survival of either the ith ship compartment or ith group of ship compartments
$S(\omega)$	Wave spectrum
$S_V(z,x)$	Amplitude of vertical displacement
S_W	Wetted surface of ship
t	Time
T	Draught of ship
V	Service speed of ship
w_{lost}	Structural mass loss due to ship damage
x	Variables for the objective function in Hooke-Jeeves optimisation method
x_1, x_2	Distance from the aft terminal of L_S to the foremost/ aftermost portion of the aft/forward end of the compartment being considered

X_P, X_S	Transverse distance of port and starboard specified point masses with respect to M_{XYZ}
$Y_{AP}, Y_{AS}, Y_{FP}, Y_{FS}$	Vertical distance of aft and forward located port and starboard point masses
Y_B	Vertical centre of buoyancy for intact ship
Y'_B	Vertical centre of buoyancy for damaged ship
Y_{SINK}	Measure of extent of parallel sinkage
z	Vertical position of damage (m)
Z, X, Y	Distance of elemental ship mass coordinates with respect to the M_{XYZ} reference system
Z, X, Y_1	New location of X, Y, Z after ship experiences parallel sinkage
Z_A, Z_F	Longitudinal distance of aft and forward located point masses
Z'_A, X'_P, Y'_{AP}	Location of M_{AP} for the damaged ship
Z''_A, X'_S, Y'_{AS}	Location of M_{AS} for the damaged ship
Z_C, X_C, Y_C	Centre of flotation for intact ship
Z'_C, X'_C, Y'_C	Centre of flotation for damaged ship
Z'_F, X''_P, Y'_{FP}	Location of M_{FP} for the damaged ship
Z''_F, X''_S, Y'_{FS}	Location of M_{FS} for the damaged ship
Z_G, X_G, Y_G	Centre of gravity for intact ship
Z'_G, X'_G, Y'_G	Centre of gravity for damaged ship
Z_m, X_m, Y_m	Location of elemental constituent mass for intact ship
Z'_m, X'_m, Y'_m	Location of elemental constituent mass for damaged ship
Z_w, X_w, Y_w	Location of elemental mass of water
Z_1, X, Y_2	New location of X, Y, Z after ship heels
Z_1, X_1, Y_3	New location of X, Y, Z after ship trims

α	Angle to determine the position of bulkheads
Δ	Displaced weight for intact ship
Δ'	Displaced weight for damaged ship
$\zeta(z,x,t)$	Complex wave amplitude
η	Six degree of freedom motion displacement column matrix
η_j	Time dependent motion response of intact ship in j^{th} degree of freedom. The motion response amplitude for j=1,2,3 is given in metres, whereas the motion response amplitude for j=4,5,6 is presented in radians.
η'_j	Time dependent motion response of damaged ship in j^{th} degree of freedom
$\dot{\eta}_j$	Velocity in j^{th} degree of freedom for intact ship
$\dot{\eta}'_j$	Velocity in j^{th} degree of freedom for damaged ship
$\ddot{\eta}_j$	Acceleration in j^{th} degree of freedom for intact ship
$\ddot{\eta}'_j$	Acceleration in j^{th} degree of freedom for damaged ship
η_{ja}	Complex amplitude of j^{th} degree of freedom motion response of intact ship
η'_{ja}	Complex amplitude of j^{th} degree of freedom motion response of damaged ship
η_{ji}, η_{jr}	Imaginary and real parts of η_{ja}
η'_{ji}, η'_{jr}	Imaginary and real parts of η'_{ja}
η_k	Generalised direction cosine in the k^{th} direction
θ	Heel angle
μ_c	Volumetric permeability of the damaged compartment
μ_2	Surface permeability of the damaged compartment
v_c	Compartment volume

v_i	Intact volume of i^{th} compartment or i^{th} grouping of compartments
v_{jn}	Normal velocity component of point on wetted surface of ship due to oscillation in the j^{th} degree of freedom
v_{lost}	Lost buoyancy volume
ρ	Associated material density
ρ_l	Fluid density
ρ_s	Sea water density
ϕ	Either trim angle or time independent velocity potential
ϕ_D	Diffraction velocity potential
ϕ_j	Radiation velocity potential associated with motion in j^{th} degree of freedom
ϕ_{ji} , ϕ_{jr}	Imaginary and real parts of j^{th} radiation velocity potential
ϕ_W	Velocity potential of incident wave
Φ	Time dependent velocity potential defined
ω	Wave frequency
∇	Displaced volume for intact ship
∇'	Displaced volume for damaged ship
CEM	Concept exploration model
CFD	Computational fluid dynamics
HARDER	Harmonization of rules and design rationale
IMCO	Inter-governmental maritime consultative organisation
IMO	International maritime organisation
ITTC	International towing tank conference
MAIB	Marine accident investigation branch
MARPOL	The international convention for the prevention of pollution from ships
O.B.O	Oil-bulk-ore

RAO	Response amplitude operator
RBM	Relative bow motion
RO - RO	Roll on roll off
SEM	Static equivalent method
SOLAS	Safety of life at sea
UK	United Kingdom

1. INTRODUCTION

This dissertation addresses the impact of damage upon the hydrodynamic and hydrostatic characteristics and the motion responses of a ship hull form optimised for seakeeping with no increase in calm water resistance. To appreciate how optimisation may assist the ship design process, a short overview of ship design approaches is provided in the next section. This is followed by a brief overview of what optimisation can achieve and this provides the identification of a possible shortcoming in existing optimisation tools for improved hydrodynamic performance. It is this possible defect and its consequences that drive the research.

1.1 The Ship Design Concept

Ship design is an interesting and demanding task. It provides the best opportunity of combining theoretical analysis, scientific knowledge of hydrostatics, hydrodynamics, dynamics, materials and structures, with the historical experience that include ‘perceived’ beneficial ratios of geometric dimensions and form factors.

Depending on the ship type a ‘volumetric’ or ‘deadweight’ design will be undertaken to identify the principal hull form characteristics for the required cargo capacity, ship speed and range. Volumetric design is used when the ship must provide a specific amount of cargo space. This approach is applied to passenger ships, containerships and most naval ships. Deadweight design is based on equating the sum of the lightship component masses and the cargo masses to the ship displacement. It is used mainly in the design of tankers and bulk carriers.

An important step in the earlier stages of design is the selection of principal ship dimension related parameters such as displacement, length, beam, draught, depth and block coefficient. At this stage of design few naval architecture tools can be applied.

The preliminary design stage is generally carried out in three ways. The first method is known as the basis ship approach. This technique, which uses a particular existing hull form to lead the families of designs. This approach was very useful when the number of new ships being constructed was high, so that design can be optimised by small improvements from ship to ship and class to class. However, when the number of new ships constructed decreases, such as at the present time and single vessel classes become more common this method looses its effectiveness.

Another design method is to use the ‘trend curves’. This method is based on the plots of the data gathered from existing ships (see, for example, Watson (1962) and Watson & Gilfillan (1977)). This technique provides an interval of values for specific ship sizing parameters to be used. Consequently, the quality of new designs based on this approach depends on both the relevance and inappropriateness of previous designs included in the associated database. This aspect of design is also discussed by Sarioz (1993). Furthermore, this method limits the capability of the designer to create novel designs, as the new designs based on this method will have similar features.

The third option is the ‘parametric survey’ (see, for example, Murphy et al. (1965) and Gilfillan (1969)). This approach looks for the most advantageous combination of overall ship dimensions and form parameters within defined limits of the design study. This method tries to find the optimum hull form for the prescribed criteria but it does not look at different alternatives.

All these methods provide an initial estimate of the indicated principal hull form parameters. After the basic ship parameters are defined the resulting design must be examined to check its technical and economic feasibility in terms of intact stability, cargo carrying capacity and freeboard & power requirements and if it achieves the goals necessary for the intended service. Consequently, the design is developed iteratively.

The indicated technical analyses are usually carried out when the design geometric characteristics are well established. Therefore, some required changes may not be accommodated due to the level of commitment to the design and the perceived costs in design re-development. The failure to reflect the results of the most accurate analysis in the design process limits the usefulness of empiricism and experience based design methods. An alternative approach is to apply rational computer-based searches or optimisation tools in the earlier design stages to improve the measures of merit for seakeeping, resistance, structural and economic qualities.

The complexity of the design relies on different features of the technical design, the construction of the ship and its operation. As the ship dimensions have a direct effect on material and construction cost the ship-builder requires a design with minimum dimensions to achieve the prerequisites of the ship owner. At the same time the operator of the ship restricts the design for the minimum operational and capital costs.

Because of these different objectives and its multidisciplinary nature the ship design process is developed iteratively. This iterative process can be expressed schematically as a design spiral (see, for example, Andrews (1981)). At the design spiral early estimates of the ship sizing parameters are made. As the design proceeds along the spiral these estimates are altered and developed as different levels of analysis of differing complexity are applied. This continuous evolution of the design is the result of the feedback provided at subsequent steps and increased information about the sensitivities of the design. The process continues until convergence and a final economic and technical feasible design is produced.

The outcome of this process represents a compromise of choices as influenced by; the route of the ship, the physicals limitations associated with water depth and canal dimensions, the complicated environment the ship must survive, the type of cargo carried, port operating restrictions and the minimum requirements of Classification Authorities on intact and damage stability.

The internal subdivision of the ship by means of transverse and/or longitudinal watertight bulkheads or by horizontal subdivisions like double bottoms in commercial ships might add to the cost of the ship. This unavoidably involves a compromise between safety and cost. The more severe the standard adopted for subdivision and stability, the greater the probability that capital and operating costs will increase and the economic viability of the ship may be compromised. Therefore, the stability requirements are usually satisfied at the minimum level required by the Classification Authorities.

1.2 Optimisation Tools

A design based optimisation tool generally determines a technically more advantageous set of design parameters. The parameters may be related through specific mathematical functions or defined by some empirical formulae. These parameters will be subject to physical, technical, legal and economic restrictions. If more than one combination of the design variables satisfies all these conditions, the algorithm within the optimisation tools determines that combination of design variables that optimises the hull form for some measure of merit specified by the designer (see, for example, Schneekluth & Bertram (1998)). This ability to iterate several hull form parameter changes at the design stage encourages the designer to carry out alternative modifications of the design parameters in a way that was not previously possible.

1.3 A Possible Shortcoming of Existing Optimisation Tools

Seakeeping and resistance qualities of a ship have significant impact on the operability of the ship and hence upon the economic viability of the design. Consequently most ship design optimisation tools addressing ship hydrodynamic aspects consider seakeeping or resistance or both as primary tasks whereas intact stability is usually treated as a design constraint to be fulfilled (see, for example, Sarioz (1993) and Keane

et al. (1991)). However, it is not evident that damage stability is addressed at all in such optimisation tools. Therefore, it could be the case that the computer based optimisation programs, which are used for improving the behaviour of the 'non-damaged' hull form in terms of seakeeping, resistance, structural strength and economy may lead to ship designs that are less survivable when damaged. Essentially this is the question addressed in this research programme (see Saydan and Hearn (2004)).

1.4 Aims and Outline of the Research

The absence of damage stability considerations in an optimisation routine that addresses hydrodynamic performance subject to intact stability may be viewed as incomplete. To determine whether this is the case one must either include damage stability in the optimisation process and examine its impact on the computer programme outcomes, or, undertake hydrodynamic and motion analyses of an assumed non-optimised hull form and its optimised hull form to try and demonstrate a shortcoming in the optimisation process. At this stage there is no need to comment on the pros and cons of either possible approach since it is necessary to investigate all aspects of the posed problem and to identify a possible feasible way forward. Certainly it would be extremely perverse if one were to find that a damaged optimised hull form was less survivable than the associated damaged conceptual form.

Improving hydrodynamic performance requires appropriate modification of the geometric form of the basis hull. Modifying the hull form is not an easy task without an appropriate wealth of design/operational experience related to the ship type addressed. Hence a systematic process to try and identify the beneficial changes is required. This could be undertaken by using design charts, that is, plots of ship behaviour characteristics as a function of different design pairings. These pairings are designated primary or secondary parameter changes ('L and B/T' form the first set and C_{WP}, LCB and LCF' the second set) when creating new/novel designs.

Having perceived which changes are beneficial in terms of the vessel designed, the continuous iteration of the selected parameters should be undertaken by using a suitable algorithm in order to produce new hull forms. This could be achieved using so called ‘inverse analysis’ whereby hull form shapes have preferable seakeeping and resistance responses (compared to the initial designed ship) are sought by seeking out beneficial geometric changes. In Chapter 2 this inverse analysis is explained and the approach of different researchers is reviewed. Various researchers have used different objective functions (or drivers). The Hooke-Jeeves optimisation process (see, for example, Hooke & Jeeves (1961), Kowalik & Osborne (1968), Aoki (1971) and Walsh (1975)) is used to provide an optimised hull form.

Prior to attributing damage to any ship (optimised or otherwise) it is necessary to understand what damage is most likely together with most likely location and the expected extent of the damage. These aspects are discussed and appropriate statistical results presented in Chapter 3.

Chapter 4 reviews the development of ship regulations and stability analysis and identifies why certain developments have taken place over the past 76 years. Two possible methods of examining the stability of a ship when it is damaged are discussed. The first one is deterministic and is mandatory, whereas the second one is probabilistic approach and is used when the deterministic method is found unsatisfactory. An intense analysis of the two different stability methods provides their advantages and disadvantages for the intended damage research. Selection of the deterministic approach is justified in the care of general optimisation used with novel hull forms.

The seakeeping analysis of intact and damaged ships is, in principle, the same but the data required to carry out motion analysis of damaged ships is not always available. In Chapter 5 frequency versus time domain analysis together with the presentation of the required generalised motion equations is provided. A novel method of providing products of inertia is also presented.

The hydrodynamic analysis of the optimised hull and basis hull for the intact and damage cases is carried out using the Matthew Diffraction Suite (Hearn (1978)). In Chapter 6 the Hooke-Jeeves optimisation process as built into the Optistanbul Suite (Sarioz (1993)) is applied to the selected Derbyshire hull form. The reasons for its selection and the objective function and constraints used are explained. Validation of the intact stability of both basis and optimised hull forms are provided together with approval of the bulkhead division in each case. The damage statistics of Chapter 3 are used to determine the orientation of the parent and optimised Derbyshire hull form for four distinct damage scenarios.

Chapter 7 then undertakes a three-dimensional hydrodynamic analysis of all selected ten hull forms and justifies the quality of the results prior to undertaken relative vertical motion response calculations in Chapter 8.

Chapter 9 provides a closure to the thesis with general comments and observations, conclusions and an indication of the future research that could prove beneficial.

2. THE OPTIMISATION PROCESS

The improvement of ship design using optimisation techniques requires selection of an appropriate optimisation tool, the selection of an objective function that reflects the improvements sought and appropriate supporting analysis to undertake evaluation of the parameters (variables) included in the selected objective function. The process is essentially iterative with the initial independent parameters (variables) being gradually modified so as to generate improvements in the selected metric or metrics of interest. Optimisation can be misleading if one aspect of the design is improved with little or no consideration of other equally important aspects. The quality of the outcomes can also depend upon the ability of the analysis tools to properly reflect the impact of changes in the governing design parameters selected. The governing parameters selected, if inappropriate may limit the capability of the optimisation process to identify a true global optimal solution.

Thus optimisation tools may provide a large number of alternative designs within a relatively short time with better characteristics than the parent design. In many cases important constraints will have influenced the outcome. In this chapter previously applied optimisation tools, applied in the context of improved hydrodynamic and motion characteristics, will be reviewed and assessed in terms of their strengths and weaknesses and their potential to include damage stability assessments.

Since this PhD study will use tools generated initially at the University of Newcastle the first part of the review will summarise the research carried out at the University of Newcastle. Thereafter many other examples of analysis used in other aspects of ship design optimisation are presented and discussed.

2.1 Background

2.1.1 A Specific Motion and Resistance Driven Optimisation Research Programme

In the late 1980s, Hearn et al. (1988) developed a Frank close-fit (see Frank (1967)) velocity potential based strip theory for in-house seakeeping analysis within the design offices of British Shipbuilders. Since there was little familiarity (within the design offices) with the mathematical formulation and solution of either the ship motions & the dynamic shear force/bending moment characteristics or the associated fluid structure interaction analysis the computer system developed 'Lynette Suite (Hearn et al. (1988))' required many self correcting and automatic recovery processes. Because the designers in British Shipbuilders would not agree to geometric data being provided in a preferred form, automatic spline fitting through arbitrary defined waterplanes and transverse sections was necessary to generate required geometric data at the usual 21 stations. This in turn also required automatic discretisation of the stations to allow the necessary hydrodynamic analysis. Availability of robust friendly software with error detection and recovery was thought by the authors to be a necessary tool to allow improved initial designs within British Shipbuilders. It was soon evident that the designers could not control the development of the hull forms using fully automated analysis. A search methodology was required to indicate what level of changes was needed to achieve the desired performance improvements. Thus the need for seeking an optimisation process was industry based not research driven within the academic environment.

An approach developed by Hearn et al. (1990, 1991 and 1992), Sarioz et al. (1992) and Hearn et al. (1994 and 1995a) addressed the search methodology for improved seakeeping with consideration of frictional resistance, wave making resistance, added resistance and satisfaction of IMO intact stability requirements. Their initial approach was designated the 'Forward technique' because it simply looked at straightforward use of the analysis tools, whilst investigating which geometric hull design parameters were

influential in affecting the design and the sensitivity of the different hydrodynamic characteristics to different level of changes in different hull form parameters. Having gained some insight through the 'Forward technique', a fully automated optimisation approach the 'Inverse technique' was developed since it used the analysis to identify the hull form design parameter values. Both techniques seek cause and effect information regarding the hydrodynamic characteristics dependence upon hull form parameters.

The forward technique simply analyses the required engineering responses for defined variations of the selected hull form parameters. The literature search undertaken by Hearn et al. (1990) indicated the dependence of ship motions upon the secondary parameters of C_{WP}, LCB and LCF. Consequently, these secondary parameters were investigated on the basis they influenced seakeeping and related quantities, but were not present in standard empirical resistance calculation formulae. Hence it was argued that seakeeping could be influenced without significantly influencing resistance characteristic. This information is used to generate so called 'design charts' that provide a three-dimensional graphical representation of the 'cause and effect' relationship for different engineering responses as a function of different pairs of hull form parameters. In theory one could use the resulting surface plots to try and identify beneficial changes of the 'initial' hull. Secondary parameters are investigated using the Lackenby transformation (see Lackenby (1950)) to change the sectional area curve (to change LCB) and the waterline curve (to change LCF and C_{WP}). Each parameter can be modified without influencing the other two parameters. A year later, Hearn et al. (1991) included the effect of altering the primary parameters of L and B/T. The primary parameters are modified by using linear distortion methods in which the displacement of the ship and its block coefficient remain fixed. Thus any proportional change in ship length is balanced by appropriate adjustments of the value of the product of beam and draught subject to B/T remaining invariant.

The inverse method systematically modifies all permitted hull form parameters to identify a more beneficial hull form. That is, those combinations of hull form parameter

changes that provide improved engineering responses per se. In each step a hull form is generated and analysed. Initially, the Landweber-Macagno three parameter conformal mapping procedure (see Landweber & Macagno (1959)) was used to develop each modified transverse section. The hydrodynamic characteristics of these sections are then determined using a Frank close-fit method. A year later, the generation of alternative hull forms is produced using the Lackenby transformation by Hearn et al. (1991).

In the inverse approach the optimisation technique of Hooke-Jeeves (see Appendix A) was employed. The responses investigated were seakeeping responses selected from a menu of possibilities, the wave making resistance and the frictional resistance subject to the intact stability characteristics complying with the IMO requirements (outlined in Section 6.4 of this dissertation). The objective function was a linear combination of the selected hydrodynamic responses, each scaled with respect to the response of the parent (initial) design. Initially the objective function has a value of unity. The parameter changes allowed were specified as part of the input data on the basis it should be the designer who stipulates no-change or specifies permissible levels of change for each parameter. Similarly the selection of those responses that are considered more critical for the efficient operation of the ship operating on a specific route should be specified by the designer prior to applying either the 'forward' or 'inverse' analyses.

Ship responses in random waves are modelled by Hearn et al. (1990 and 1991) using the linear spectral analysis (see, for example, Lloyd (1998) and Saydan (1999)), that is, irregular waves are assumed to correspond to the superposition of regular waves having different wave lengths, wave amplitudes and directions. Having selected a wave spectrum, $S(\omega)$, representation of the operational area of the sea and calculated the motion transfer functions, $H(\omega)$, of the ship (and its variants resulting from the optimisation search) the response spectrum or spectra can be calculated using $R(\omega) = |H(\omega)|^2 S(\omega)$.

The term $\left|H\left(\omega\right)\right|^2$ is often referred to as the response amplitude operator (RAO). Various statistical parameters of the response may be determined such as probability of slamming, acceleration thresholds being exceeded, deck wetnesses et cetera.

The area under the response spectrum defines the variance of the ship responses to the selected sea-state. Firstly this area is minimised for all sea states. In practice, Hearn et al. (1992) and Sarioz et al. (1992) found it more suitable to reduce the peak value of the response amplitude operator of selected response(s). This approach required less computational effort and produced the same optimised hull form parameter values given by the initial computationally intensive approach. The reduction of peak values leads to a general reduction in the response amplitude operator amplitudes and the response motion spectrum values are automatically decreased for all sea-states.

Sarioz et al. (1992) found that application of other researchers' optimisation techniques such as that of Lloyd (1991) based on optimising in a specific sea-state often meant the optimised form was better in the selected sea-state but not all sea-states. Hearn et al. (1990, 1991 and 1992) and Sarioz et al. (1992)'s approach does not exhibit this characteristic. Their optimisation method produced new hull forms which showed better hydrodynamic characteristics for all sea-states. In these mono-hull studies strip theory (see, for example, Salvesen et al. (1970)) is implemented for the seakeeping analysis; whereas a selection of resistance prediction techniques were included such as the method of Holtrop & Mennen (see Holtrop & Mennen (1982) and Holtrop (1984)) together with thin-ship wave-making resistance of Michell (1898) and International Towing Tank Conference (ITTC) 1957 frictional resistance correlation curve, see, for example, Hearn & Wright (1999). Intact stability is usually checked against the International Maritime Organisation's criteria contained within IMO A-749 (see Section 6.4). Manoeuvring analysis was added to the forward technique by Furukawa & Hearn (2000). It is based on IMO manoeuvring requirements see, IMO (1993). Hearn et al. (2000) added manoeuvring analysis to the inverse part of the optimisation process.

The mono-hull studies by Hearn et al. (1990, 1991 and 1992) and Sarioz et al. (1992) were restricted to vertical motions in head waves such as heave, pitch, relative bow motion (RBM) and slamming. This was because the authors, like Lloyd (1991), believed that if a ship is optimised for vertical motions in head seas, it will generally show better characteristics in other motions. In the study of multi-hull vessels by Hearn et al. (1994, 1995a and 1995b) the same motion characteristics are analysed in head seas with the inclusion of roll in bow and quartering seas; whereas again only the vertical motions are analysed in head waves in Hearn et al. (1995c) and Hearn & Wright (1997, 1998a and 1998b).

For the twin-hull vessels the demi-hull separation parameter 'H_S' is added to the primary parameters because the graphs of hydrodynamic coefficients of the twin hulls plotted by Hearn et al. (1994) were significantly different for variations of this demi-hull separation parameter. The wave-making resistance is calculated in these twin-hull studies using a modified Michell thin-ship theory (see Lunde (1951)) so that interaction between demi-hulls is included as necessary, this is dependent upon demi-hull separation and forward speed of advance (see, for example, Hearn & Wright (1997) and Tuck (1987)). The Michell thin-ship theory is chosen because it has the advantage of consistency of treatment regarding seakeeping and wave resistance in the sense that both analysis methods use actual hull form shape rather than global hull form parameters. In order to facilitate a wider range of hull parameter combinations, the secondary parameters were extended to include 'C_P' in Hearn & Wright (1998a and 1999). C_P does not directly influence the optimisation results, but facilitates seakeeping and resistance conflict resolution through greater variation of the other parameters with practical ship forms maintained.

Significantly different behaviour of twin-hull hydrodynamic coefficients compared to mono-hull hydrodynamic coefficients is outlined by Hearn et al. (1994). This necessitated preparing a significantly larger database of catamaran hydrodynamic coefficients, compared to the mono-hull database (see Hearn et al. (1994 and 1995a)),

for efficient and accurate motion analysis without real-time calculation of required hydrodynamic coefficients using Frank close-fit in-line. However, once the database is provided the hydrodynamic coefficients for several alternative hull forms are generated within a small amount of time. Then as in mono-hull studies, linear distortion methods and the Landweber-Macagno three parameter conformal mapping procedure or Lackenby transformation techniques are used in order to generate new hull forms.

For mono-hulls, in order to minimise a selected response of the ship, standard optimisation techniques such as Hooke-Jeeves can be used. This is possible because the objective function associated with the selected response of the ship has only one minimum. However, the hydrodynamic coefficients of twin hulls plotted for heave motion by Hearn et al. (1994) for two different non-dimensional hull separation coefficients show the highly nonlinear variation of the catamaran responses with hull geometry variations. Thus, whilst linear analyses were used in the calculation it was found that the responses were very nonlinear with respect to the hull form design parameter changes and so the Hooke-Jeeves approach was not appropriate. So a new 'evolutionary programming' based search strategy was proposed by Hearn et al. (1995a and 1995b) to cope with the nonlinear nature of the catamaran objective function. This 'Genetic Algorithm' (see Hearn et al. (1995a and 1995b) and Bertram (2003)) made it possible to converge to the global minimum despite the design charts being full of local minima.

2.1.2 Ship Design Optimisation with Different Design Drivers

Other than the particular ship design optimisation research programme just reviewed, one finds many other good examples of analysis being coupled with optimisation techniques. One of the earliest procedures to identify the principal ship dimensions in concept or preliminary design was that of Watson (1962) and Watson & Gilfillan (1977). In this technique experience in previous designs is stored in a series of graphs and presented as a ratio of ship hull form parameters such as L/B, B/D and D/T. Here

design process starts by the assumption of three ship lengths, then by using the plots and relations provided in Watson (1962) and Watson & Gilfillan (1977) it is possible to determine beam, draught and block coefficient and hence obtain a displacement. Once the lightship weight for each ship is calculated through the plots and relations of Watson (1962) and Watson & Gilfillan (1977), it is subtracted from the displacement to obtain deadweight values for three different ships. The three deadweight values plotted versus length gives the possibility to identify the required ship length for the deadweight specified at the beginning of the design. This procedure used historical data. Thus it is possible that new designs generated, using this data, may be influenced by both relevant and inappropriate previous designs. Another disadvantage of the method lies in the fact that the use of historical data limits the capability of the designer to create novel designs, as the new designs will have features similar to those of the database.

Over the period 1965-1985 several attempts were undertaken to solve the problem of identifying ship sizing parameters by computer algorithms. They were developed by Murphy et al. (1965), Mandel & Leopold (1966), Gilfillan (1969), Nowacki et al. (1970), Fisher (1972) and Lyon & Mistree (1985). There were two basic optimisation methods used in these cited papers.

The first approach is of Murphy et al. (1965) and Gilfillan (1969). In the work of Murphy et al. (1965) the ship dimensions affecting the size and cost of the ship are varied over a finite range of step sizes. The size of this multi-dimensional method is determined by the number of variables together with the step size and the permissible range of each variable chosen. Whilst the design charts readily allow identification of suitable hull form parameters the minimum cost of building and operating such a ship for a year is less readily identified. To seek minimum cost a great deal of graphical data has to be systematically searched. This approach is thus relatively cumbersome, since data has to be graphically manipulated before the desired result is obtained. Gilfillan (1969) used a procedure in which the vessel length is increased in steps until the deadweight satisfies the owner's requirements, while all other design variables (B, C_B

and T) were expressed as functions of ship length. Then all calculations regarding the power, weight, stability and cost were carried out by the computer code for each trial length. Again the desired design was not available directly, but it was selected by examination of the output of the computer code.

However, in the second method mathematical programming is employed to achieve optimum solutions. The final result arrived at the computer algorithm is the desired result sought by the designer, whereas in the first approach the output from graphical manipulation or the computer code does not lead directly to an optimum. There is always some further refinement of the process. In the computer oriented optimisation techniques either direct or random search techniques (see, for example, Fisher (1972) and Mandel & Leopold (1966)) or nonlinear programming (see, for example, Nowacki et al. (1970) and Lyon & Mistree (1985)) are applied.

The preliminary ship design stage has frequently been viewed as an economic optimisation problem with the physical, technical and legal aspects treated as restrictions or constraints. Consequently, the design process becomes a multi-criteria optimisation problem as demonstrated by Sen (1992) and Ravn (2002). In the earlier cited papers, Murphy et al. (1965) used only the ship construction cost in their economic criteria; whereas Fisher et al. (1972) considers it better to render some approximation to all factors rather than disregard some of them entirely. Therefore Fisher et al. (1972) include impact of taxes, bank interest and borrowed capital to owner's capital ratio. The optimisation problem is that of seeking minimum cost of each ton of cargo each year as a function of fleet size.

Liu et al. (1981) stresses the advantage of applying optimisation tools in the preliminary design stage by two facts. Firstly, use of these tools in the early stages of design offers the designer large potential savings in initial ship structural cost. Secondly, early analysis of the design parameters improves the quality of the detailed design depending on the inputs of the preliminary design.

An investigation of the seakeeping performance of the British Ship Research Association merchant series is carried out by Wilson (1986). By his method it is possible to consider large number of different designs at early design stage at a small cost penalty which is only a function of the speed of the processor in the computer used. The need of a philosophy, which uses recent advances in computer graphics to understand the nature of the design process and to create radically new ship design synthesis, is extensively discussed in Andrews (1981, 1986 and 2003).

Different optimisation techniques (random and direct) are compared by Keane et al. (1991) for the minimum resistance of a frigate of 3300 tonnes displacement. Such an optimisation process requires generation of the mathematical hull forms see Keane (1988).

Doctors & Day (1995) introduced the genetic algorithm into their research to improve catamaran ferries in terms of wave resistance so as to reduce the erosions of river banks by wash. Later, their analysis was extended to include also vertical acceleration in head seas (Day & Doctors (1997)). The wave resistance is calculated by either Holtrop & Mennen in Keane et al. (1991) or Michell thin-ship theory in Doctors & Day (1995) and Day & Doctors (1997). The first method has the advantage of covering a wide range of ship types of varying sizes; whereas the thin-ship theory of Michell is more sensitive to the change of hull form parameters, since it uses the actual hull form shape rather than global hull form parameters to determine the wave resistance. The Michell thin-ship theory has also been used extensively by Tuck & Lazauskas (1998) for predicting the wave resistance for multi-hulls.

Work on resistance of high speed displacement catamarans has also been accomplished by Insel & Molland (1992), Molland et al. (1996) and Molland & Lee (1997). Insel & Molland (1992) presented the resistance experiments on NPL series of models with changes in length displacement ratio. This work is extended by Molland et al. (1996) by including beam draught ratio. A further extension is carried out by Molland & Lee

(1997) by investigating the influence of prismatic coefficient on catamaran resistance. Whilst all these works have been performed in calm water, Molland et al. (2001) examined the performance characteristics of catamarans in head and oblique waves. Finally, Ghani (2003) investigated the influence of bulbous bows on the high speed displacement catamaran performance in shallow water condition.

Keane & Robinson (1999) suggested that research in the conceptual design of ships should not focus only on dealing with different hull form 'innovation', but also should seek to find better search techniques in optimisation. Different optimisation techniques in the sense of Keane & Robinson (1999) are provided by Schneekluth & Bertram (1998) and Holden et al. (2002).

In automatic optimisation designer interaction is not needed (see, for example, Janson & Larsson (1996)). However, such an approach risks the optimum design not being practical. Therefore an interactive optimisation that does not leave the designer out of the design process, but supports him with his decision making is more preferred. However, the designer should be clear with respect to what his/her objectives are as the computer program cannot automatically perform the optimisation without a clear framework.

Concept exploration models (CEM) are an alternative to the automatic optimisation. In this method a pool of candidate solutions is generated by varying design variables. Each of these solutions is evaluated and the optimum is selected between them. An application of the CEM for small warship design is provided by Eames & Drummond (1977); whereas the development of a model for the conceptual exploration of alternative high-speed ferry types is presented by Molland & Karayannis (1997). In the optimisation process known as 'optimisation shells' (see, for example, Schneekluth & Bertram (1998)) the designer provides all necessary knowledge in the form of relationships and then the shell checks if all the given relationships are (a) necessary and (b) sufficient to solve the problem.

In the use of expert systems (see, for example, Dai et al. (1994) and Bertram (2003)) a knowledge database is built up from the knowledge of experts within a particular specialisation. In this technique the designer may specify the appropriate inputs but the outputs are purely a function of the inbuilt expertise, there is usually little scope for the designer to strongly influence the process outputs. This method has the disadvantage of producing similar ships to those of an experienced designer. The need for a full automatic or an interactive optimisation procedure is considered by Schneekluth & Bertram (1998), Liu et al. (1981) and Keane & Robinson (1999). It is suggested that an efficient optimisation technique coupled with the interaction of the ship designer is more suitable for the optimisation process. In the papers of Hearn et al. (1990, 1991 and 1992) it is also assumed that constraints on parameter variation and objective function context are the responsibility of the designer. That is, the final range of ship dimensions should be selected by a naval architect who understands the relationships between different design parameters and the information presented by optimisation tools. Therefore, an optimisation procedure should not absolve the designer of his responsibility, but assist him with his decisions.

Usually, the safety of a ship is regarded as a design constraint. Whilst it should be fulfilled it does not directly drive the design optimisation process. Attempts to include the safety of a ship in the optimisation process are achieved by Sen et al. (1997) and Cramer & Tellkamp (2002 and 2003). Sen et al. (1997) investigated safety issues in the context of lifeboat design. Different safety analysis methods are discussed prior to their choice of ‘Cause-Consequence’ analysis. This method considers every dangerous event and then traces all possible earlier events that could lead to its occurrence. After that, it examines all the consequences of the given event. Cramer & Tellkamp (2002 and 2003) followed an equivalent safety approach and showed a qualitative comparison of different ship designs with respect to their probability of survival in severe seas. While their method is a step forward towards the introduction of safety into the optimisation process, the approach does not include a mathematical optimisation technique to permit

variation of the design parameters systematically and this omits the evaluation of the effect of changes of design parameters on the hydrodynamic responses.

Pawlowski et al. (2004) proposed a way to use the floodable length curve as a function of *s*, conditional survival probability of a ship following the flooding of each compartment in turn. This method presents a novel approach for effective subdivision at the early stages of the design. However, their technique suffers from some numerical instability that presents different solutions for the same initial conditions and case.

2.2 Discussion on Past Optimisation Studies

The discussed optimisation tools could be considered incomplete, from a safety point of view, as they are only concerned about the intact stability of ships and they do not address damage stability. To assess the significance, or otherwise, of this omission it was decided to carry out the hydrodynamic analysis and hence dynamic motion responses of hull forms in the intact and damage case for the ship as 'designed' and 'when optimised', to try and understand the influence of damage upon optimised hull forms. In particular, the work carried out at the University of Newcastle has demonstrated that for different ship types (trawlers, containerships, warships and catamarans) it is possible to improve seakeeping, wave-making resistance and added resistance whilst satisfying the IMO intact stability conditions imposed. Since no apparent obvious disadvantage (in terms of the metrics used) exist with the intact ship it might be the case (however perverse) that the disadvantages show themselves when studying the damaged ship.

To produce alternative hull forms from a basis hull form to facilitate investigation of the influence of damage on the hydrodynamic and motion characteristics of the optimised and non-optimised hull forms the Hooke-Jeeves method is used. This method is selected as it is fast at finding an optimum value of the selected objective function see, for

example, Keane et al. (1991). In the next section the optimisation method applied in this research programme will be described in greater detail.

2.3 Statement of the Optimisation Process

A two-dimensional hydrodynamic analysis (strip theory) within the optimisation process provides the opportunity to analyse the effect of several hull form parameter changes on seakeeping within a very short amount of time. However, the physics of the damage cannot be captured well within such a two-dimensional approach. Hence, the possibility of developing a modified two-dimensional optimisation process, in which damage stability is simultaneously investigated with seakeeping and resistance, was rejected. Inclusion of full three-dimensional hydrodynamic analysis within the optimisation procedure is not considered a practical option because of the computational designs of three dimensional fluid-structure interaction analyses. The discretisation of the original structure and its variants would require a very robust automated process. This process would require a large amount of cross checking that the representation of the current ship and the variant ship were consistently well modelled in terms of geometry and discretisation, as this influences the quality of fluid-structure interaction results (equality of cross-terms, well conditioned influence matrices and satisfaction of Haskind equality conditions). Whilst this might not involve a large amount of processing unit time the development of the associated logic could prove to be an unwanted digression. Any evaluations included in the optimisation process must be reliably undertaken for the thousands of alternative hull forms involved in the search for an optimal hull form. Clearly, a compromise is required. It was therefore decided to optimise a selected hull form using the two-dimensional hydrodynamic analysis based optimisation process and then to create the extent of damage in the original and in the optimised hull forms and reanalyse as three dimensional structures.

The Optistanbul Suite (see Sarioz (1993)) is used in this study in order to optimise the selected basis hull form (see Section 6.2). This software represents an extension of the method originally developed at the University of Newcastle upon Tyne. As before, a database of hydrodynamic coefficients (added mass and fluid damping) for a suitable representative set of transverse sections is used for the hydrodynamic analysis. The optimisation of a hull form is provided using the Hooke-Jeeves algorithm. The primary parameters within the optimisation process are modified by using linear distortion methods and the secondary parameters are varied by using Lackenby transformation to change the sectional area curve or the waterline curve. The generation of alternative hull forms is produced by linear distortion or, in the case of Sarioz (1993) by the Lackenby transformation. Having edited the software to provide some of the omitted main and print algorithms, optimisation of the basis hull form was undertaken for an objective function based on minimisation of the peak relative bow motion (RBM) in head seas subject to the constraint that calm water resistance is not increased. RBM is selected as an objective function since it includes the amplitude and phase information of both the heave and pitch motions, which in turn are coupled to surge for the intact ship and coupled to all other motions in the case of a damaged ship.

2.4 Summary

Having reviewed optimisation process in a specific hydrodynamic/motion context and also reviewed more general aspects of optimisation, it is noted that safety aspects rarely provide the driver of the process, but may occur in the context of a constraint. Therefore, a way ahead has been suggested that permits a suitable combination of two-dimensional hydrodynamic optimisation and three-dimensional post damage hydrodynamic analysis.

Prior to present such a procedure one must examine damage statistics and identify a representative set of damaged conditions. This aspect is addressed in the next chapter.

3. ANALYSIS OF DAMAGE DATA

In this chapter the damage statistics are investigated in order to provide a general appreciation of those accidents that have led to capsize or to the loss of a ship. These damage statistics are prepared by the Marine Accident Investigation Branch (MAIB). When analysing the damage statistics, this organisation treats fishing boats and merchant vessels as two distinct industries. Hence, these two vessel types will be examined separately. In addition to the damage statistics prepared by MAIB, the 'Lutzen 2002' damage database is analysed to provide a general understanding of the damage location and the extent of the damage. These studies will influence the selection of the ship to be analysed and the location and extent of damage to be investigated on such a ship.

3.1 Damage Statistics

The MAIB investigates marine accidents involving UK registered ships in world-wide waters and non-UK registered ships in UK territorial waters. The gathered information is published as a collection of short reports and accidents statistics only for the UK registered ships. The statistics extracted are presented here as pie-charts for merchant vessels in Figures 3.1(a), 3.1(b) & 3.1(c) and for fishing boats in Figures 3.2(a), 3.2(b) & 3.2(c) respectively.

The types of accidents identified in the merchant ship pie-charts (Figures 3.1(a), 3.1(b) and 3.1(c)) are: foundering/flooding, grounding, collision/contact, fire/explosion, capsizing/listing, heavy weather damage, machinery damage, etc.

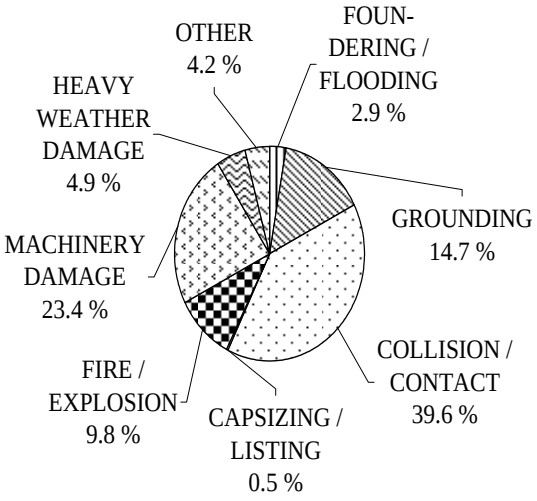

(a) 1992-2000 (MAIB (2000))

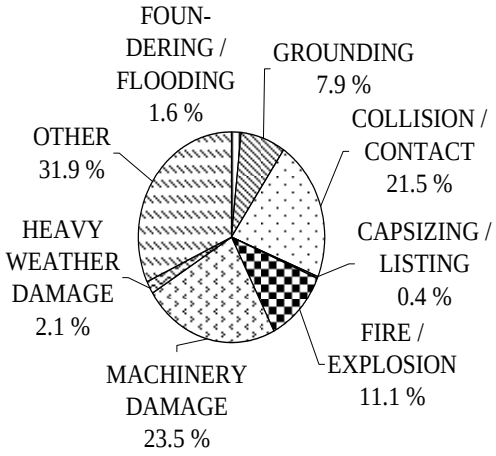

(b) 1994-2001 (MAIB (2001))

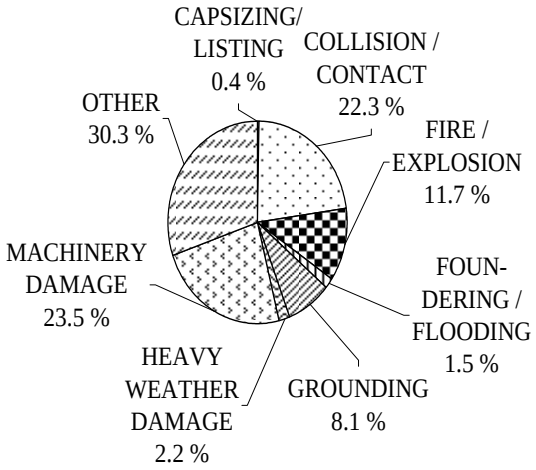

(c) 1994-2002 (MAIB (2002))

Figure 3.1: Relative occurrence of different classifications of accidents for UK registered merchant vessels.

Figure 3.1(a) indicates that the most common types of merchant vessel accidents are collision/contact, machinery damage and grounding (in that order). On the other hand, according to Figures 3.1(b) and 3.1(c) merchant vessels experience a higher percentage of machinery damage than collision/contact damage. Machinery damage and capsizing/listing provide the same overall percentage (23.9%) in the accident statistics belonging to the three different periods; even though contributions from other types of accident are quite distinct in Figures 3.1(a) and 3.1(b) or 3.1(c). There is generally a decrease in the occurrence of the accidents in the 1994-2001 with 1623 accidents and 1994-2002 with 1745 accidents compared to those of 1992-2000 with 1042 accidents. The increase in the occurrence of accident statistics belonging to different years takes place in the ‘fire/explosion’ and ‘other’ categories of the damage statistic pie-charts. The increase in the ‘other’ category (4.2% to 31.9% to 30.3%) of the pie-charts and the decreases in the remaining classification of accidents, excluding the ‘fire/explosion’ category, occurs due to the 1999 changes in accident reporting and investigation regulations (see MAIB (1999)). In particular, these new regulations changed what were

previously known as ‘dangerous occurrences’ to ‘accidents’. These new types of accidents, which are included in the ‘other’ category of the pie-chart, have decreased percentages associated with other categories.

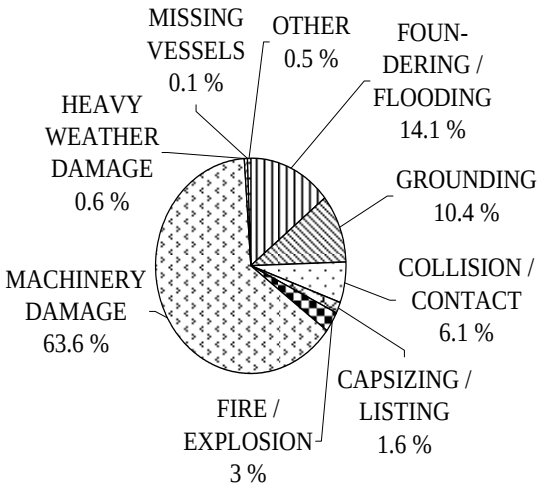

(a) 1995-2000 (MAIB (2000))

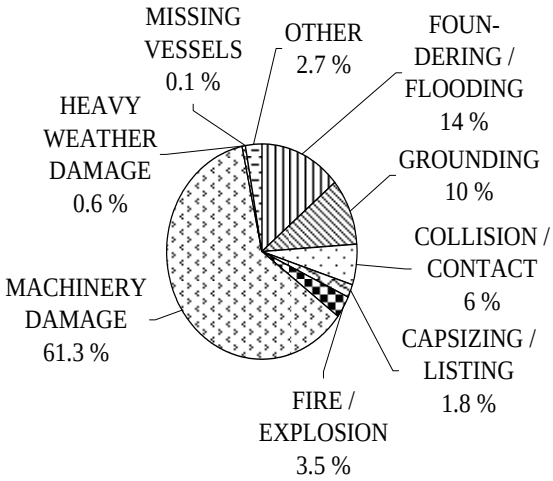

(b) 1994-2001 (MAIB (2001))

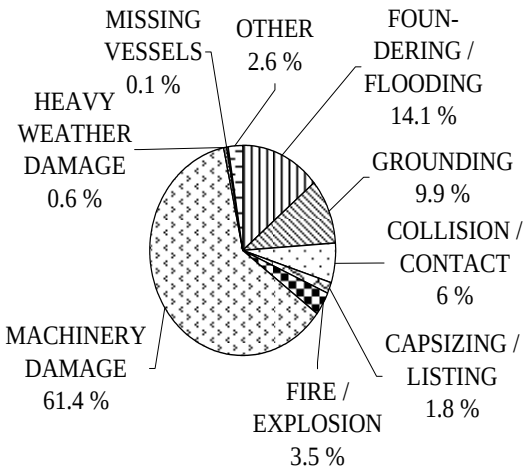

(c) 1994-2002 (MAIB (2002))

Figure 3.2: Relative occurrence of different classifications of accidents for UK registered fishing boats.

The damage statistics for fishing boat accidents (see Figures 3.2(a), 3.2.(b) and 3.2(c)) are classified according to: foundering/flooding, grounding, collision/contact, fire/explosion, capsizing/listing, heavy weather damage, machinery damage, missing vessels, etc. The accident statistics presented in Figure 3.2(a) are for the period 1995-2000 and not the period 1992-2000 used in Figure 3.1(a), simply because MAIB (2000) fishing boat data was only available for this period.

The percentages of occurrences of the different categories of accident in Figures 3.2(a), 3.2(b) and 3.2(c) are almost invariant and certainly consistent over the different time periods for each category. The only real difference arises in the ‘other’ category of the damage statistics. According to Figures 3.2(a), 3.2(b) and 3.2(c) 85.3% to 88.1% of reported fishing boats incidents are associated with machinery damage, foundering/flooding and grounding. Here foundering/flooding indicates water accumulation in the holds because of heavy waves.

The significance of machinery damage versus collision/contact changes from a ratio of approximately 23.5: 21.5 (or 23.4: 39.6 in Figure 3.1(a)) in representing 45% (or 63% in Figure 3.1(a)) of the statistics in Figures 3.1(a) to 3.1(b) or 3.1(c) to representing a total of 67.3% (or 69.7 in Figure 3.2(a)) of the statistics in a ratio of approximate in 61.3 to 6 (or 63.6 to 6.1 in Figure 3.2(a)) in Figures 3.2(a), 3.2(b) and 3.2(c). Within this research programme, damage means the hull form damage. Hence, the machinery damage and foundering/flooding are not considered in this study, as well as those denoted as 'other' in the pie-charts due to lack of information.

The MAIB statistics reviewed suggest that from a structural damage perspective fishing boats are not the primary concern regarding ship type selection. For fishing boats machinery damage is particularly significant and therefore fishing boats will not be researched further in this thesis. Merchant vessels are more likely to benefit from an analysis of their responses and the influence of damage on their responses.

Ideally the MAIB accident statistics would also indicate the extent of damage, areas most vulnerable to damage along the length of the ship, the height of damage and the position of damage. Since the MAIB statistics analysed do not give such guidance, another damage database designated 'Lutzen 2002' is investigated.

The damage database 'Lutzen 2002' is a large collection of accident data. It includes 2946 reports addressing seven different categories of accident for different ship types over the period 1935 and 1999. The sought damage related data has been extracted and processed to allow creation of appropriate pie-charts and the formation of appropriate conclusions.

Figures 3.3(a) and 3.3(b) indicate the relative percentages of each of nine ship types that have been involved in accidents and the relative percentage occurrence of each of seven accident categories.

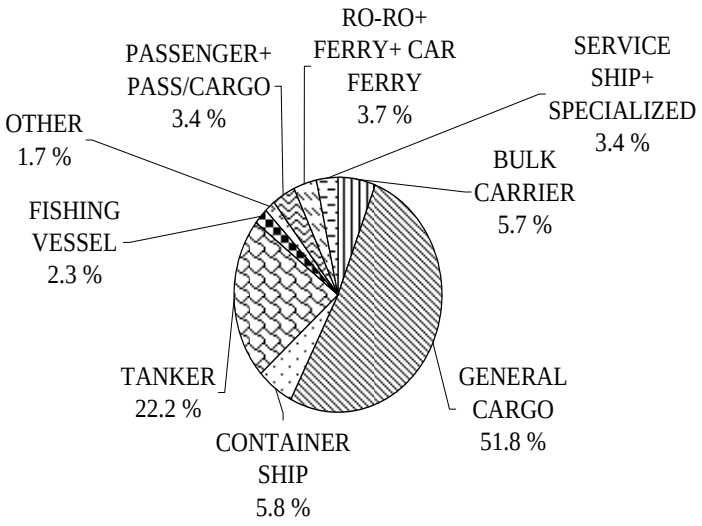

(a) Ship types

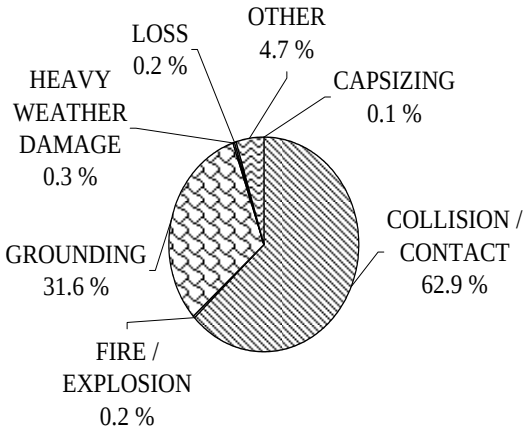

(b) Different casualties

Figure 3.3: Damage database (Lutzen (2002)).

Figure 3.3(a) indicates that general cargo ships, tankers, containerships and bulk carriers account for approximately 85.5% of all accidents reported.

Figure 3.3(b) indicates that collision/contact and grounding in the approximate ratio of 2:1 account for 94.5% of all accidents. The same conclusions are also withdrawn by Fach (2004) as a result of the analysis of structural damages on high speed crafts. Here grounding also includes collision to a rock at the bottom of the sea.

There are differences in the percentages of accident types in Figures 3.1(a), 3.1(b), 3.1(c) and Figure 3.3(b). This is due to the fact that MAIB accidents statistics present accidents that involved UK registered ships in world-wide waters and non-UK registered ships in UK territorial waters during the periods 1992-2000, 1994-2001 and 1994-2002, whereas the damage statistics included in Figure 3.3(b) are investigated by Det Norske Veritas, Lloyd's Register of Ship Repair Statistics, Hellenic Register of Shipping, DSRK (former East German authorities), IMO and Germanisher Lloyd over the significantly longer period of 1935-1999. To identify which class of merchant ship is more often the subject of collision/contact and grounding the statistics associated with Figures 3.3(a) and 3.3(b) were further analysed to produce the pie-charts of Figures 3.4(a) and 3.4(b).

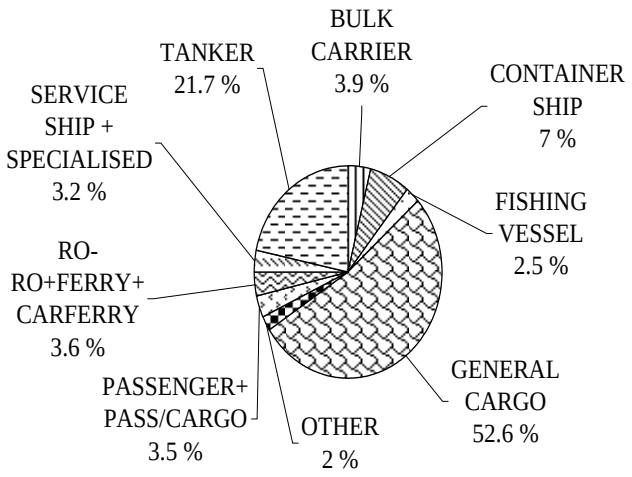

(a) Collision/contact

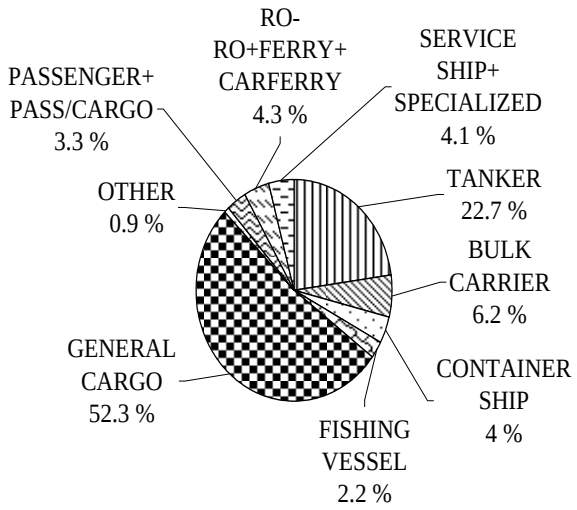

(b) Grounding

Figure 3.4: Two main accidents from damage database (Lutzen (2002)).

According to Figure 3.4(a) and Figure 3.4(b) general cargo ships and tankers account for 74.3% to 75% of the collision/contact and grounding accidents with other ship types such as containership, bulk carrier and ferries accounting for single figure amount.

The high percentage of accidents associated with general cargo ships is discussed by Spouge (2003). Spouge (2003) tried to identify the cause of this problem. He analysed several factors such as ship age, ship size, flag of registration, ship quality, ship design, domestic operations, coastal operations and classification society approval. Finally, he concluded that high loss rate on general cargo ships might be attributed to either poor quality of ship operation or this ship type might be more vulnerable to flooding.

Having identified the types of merchant ships that collide or experience grounding most often, data related to damage location is determined next by further analysis of the 'Lutzen 2002' source.

For collision incidents the damage location is examined for general cargo ships (52.6%), tankers (21.7%) and containerships (7%); whereas for grounding the damage location is considered for general cargo ships (52.3%), tankers (22.7%) and bulk carriers (6.2%). In order to specify the location of the damage, the ship hull is divided longitudinally into six regions. These regions are shown in Figure 3.5. The longitudinal location of damage for general cargo ships, tankers, containerships and bulk carriers for collision and grounding problems are presented in pie-chart form in Figures 3.6(a), 3.6(b), 3.6(c) and Figures 3.7(a), 3.7(b) and 3.7(c) respectively.

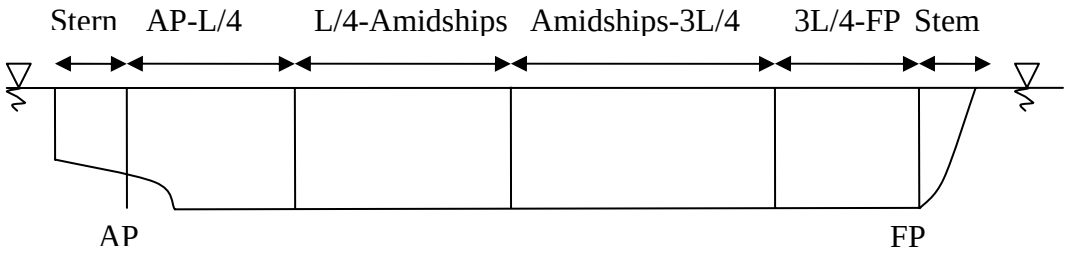

Figure 3.5: The representation of the location of the damage.

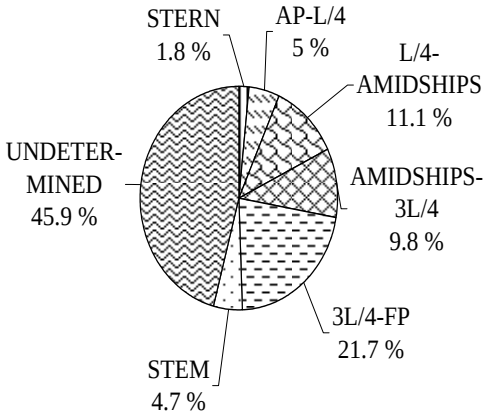

(a) General cargo ships

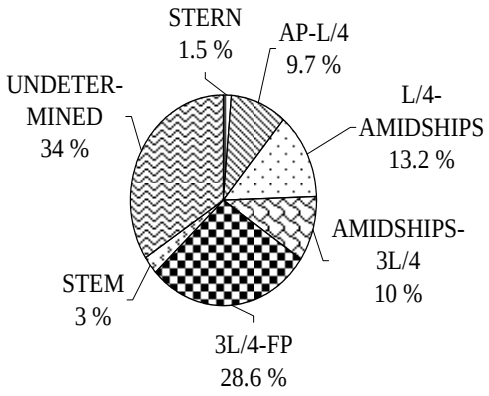

(b) Tankers

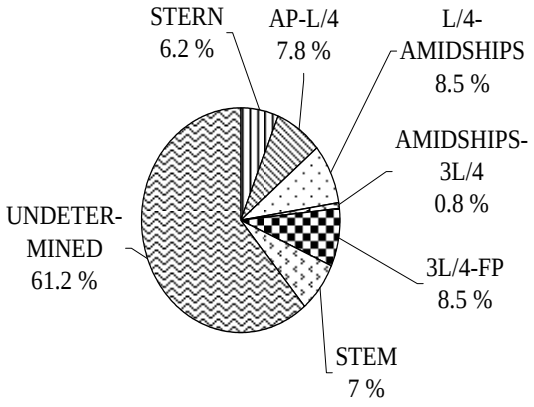

(c) Containerships

Figure 3.6: Location of damage in collision incidents for different ship types.

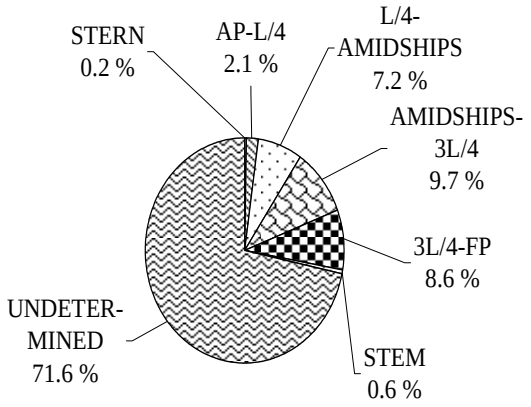

(a) General cargo ships

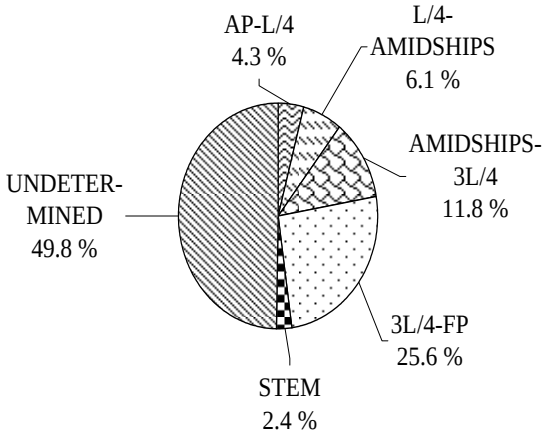

(b) Tankers

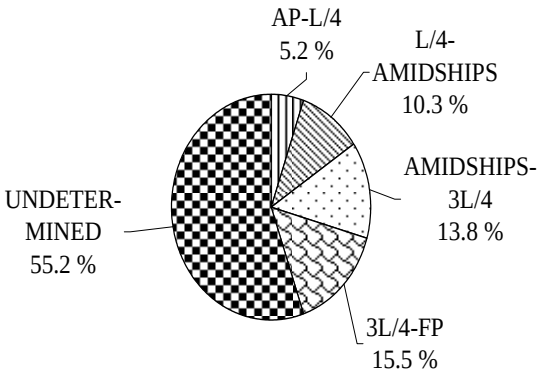

(c) Bulk carriers

Figure 3.7: Location of damage in grounding incidents for different ship types.

Figures 3.6(a), 3.6(b) & 3.6(c) and Figures 3.7(a), 3.7(b) & 3.7(c) indicate that the most vulnerable part of the ship in a collision scenario is the 3L/4-FP region for general cargo ships and tankers and L/4-amidships and 3L/4-FP regions for containerships. In a grounding scenario, when information is reported, mostly likely location of damage is in the amidships-3L/4 region for general cargo ships and then 3L/4-FP region for tankers and bulk carriers.

Figures 3.6(a), 3.6(b) and 3.6(c) show that data is available for 54.1% of general cargo ships, 66% of tankers and 38.8% of containerships for collision incidents. For grounding incidents data is reported for 28.4% of general cargo ships, 50.2% of tankers and 44.8% of bulk carriers. These different percentages of known data result in different degrees of confidence in each ship type for each accident classification.

Having indicated the most likely location of collision and grounding damage the next task is to present the extent of the data. The damage data available within the ‘Lutzen 2002’ database will be extracted and presented in non-dimensional form. In particular,

the longitudinal extent of the damage ‘l’ will be sealed using ship length between perpendiculars ‘L’, the penetration of the damage ‘b’ is sealed by ship beam ‘B’, the vertical position of the lowest point of damage ‘Y’ (measured from the baseline of the ship) and the height of the damage ‘h’ are both sealed by ship depth ‘D’.

The analysed data is now presented in Figures 3.8 to 3.14. In each figure there are five pie-charts designated (a) to (e) to denote non-dimensional extent of damage l/L, height of damage h/D, damage penetration b/B, vertical position of the lowest point of the damage Y/D and damage location in terms of port and starboard. Figures 3.8 & 3.9 provides collision damage details for the longitudinal position designated 3L/4-FP in Figure 3.5 for general cargo ships and tankers respectively. This is the most likely location for these ships as 3.6(a) & (b) indicated. Figures 3.10 & 3.11 provides the corresponding collision data for containerships at two equally likely longitudinal position designated L/4-amidships and 3L/4-FP in Figure 3.5 and confirmed in Figure 3.6(c).

Figures 3.12, 3.13 & 3.14 provide the corresponding data for grounding damage in the most likely regions amidships-3L/4 for general cargo ships and 3L/4-FP for tankers and bulk carriers respectively as indicated in Figure 3.7.

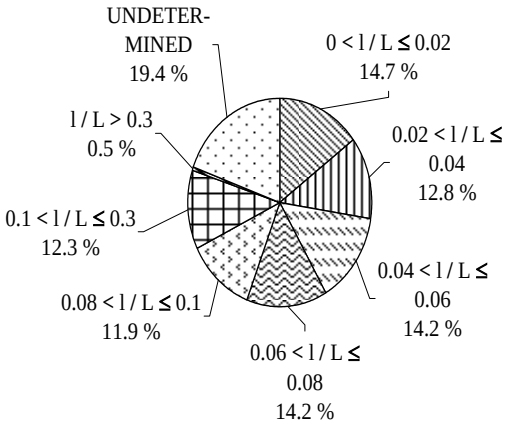

(a) The extent of the damage l/L

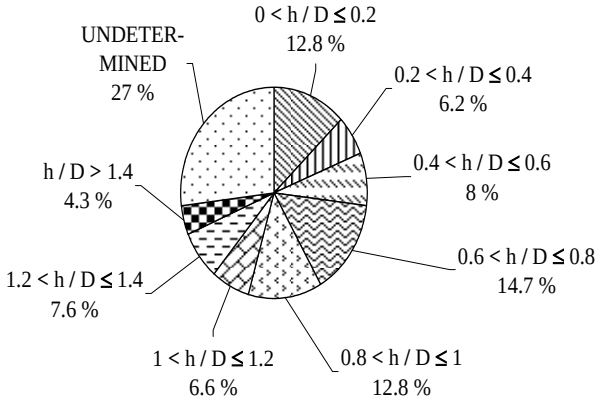

(b) The height of the damage h/D

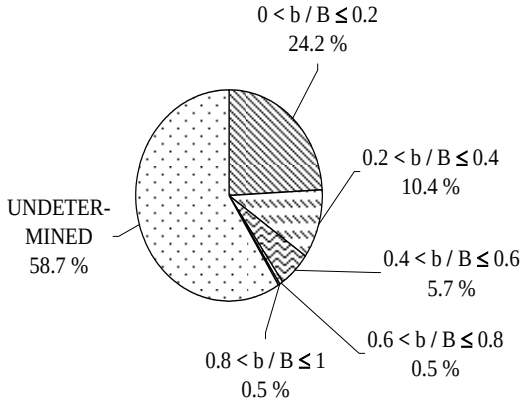

(c) The penetration of the damage b/B

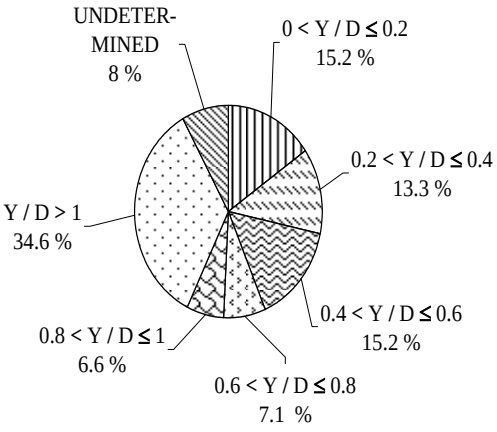

(d) The vertical position of the damage Y/D

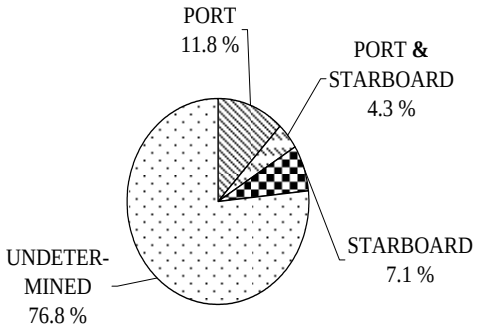

(e) The location of the damage

Figure 3.8: Damage properties in collision incidents for general cargo ships for the 3L/4-FP region.

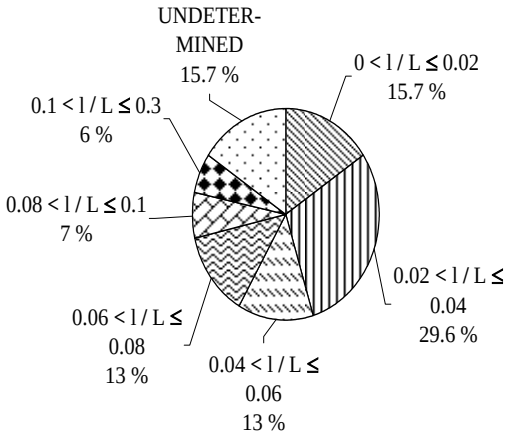

(a) The extent of the damage l/L

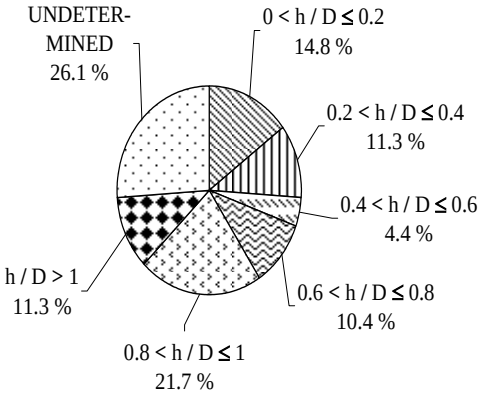

(b) The height of the damage h/D

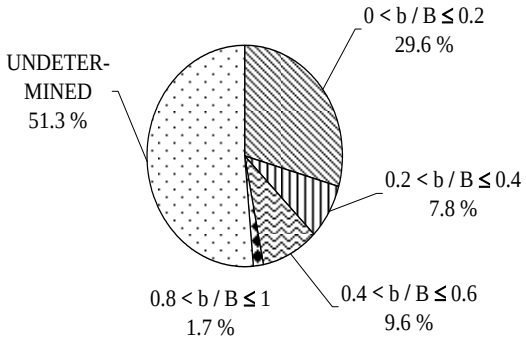

(c) The penetration of the damage b/B

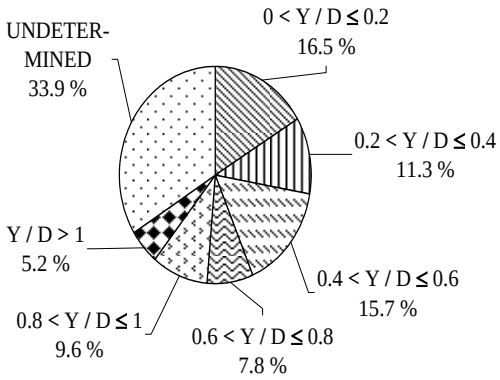

(d) The vertical position of the damage Y/D

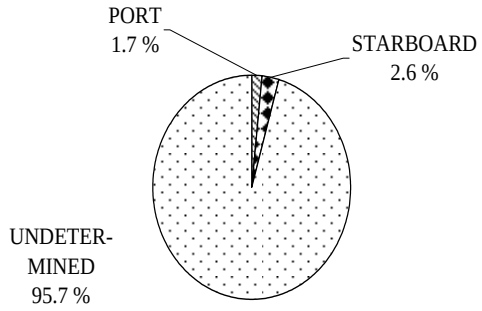

(e) The location of the damage

Figure 3.9: Damage properties in collision incidents for tankers for the 3L/4-FP region.

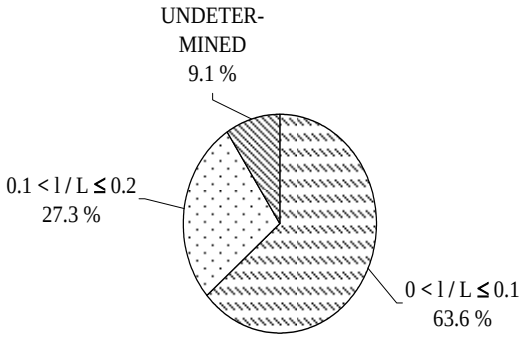

(a) The extent of the damage l/L

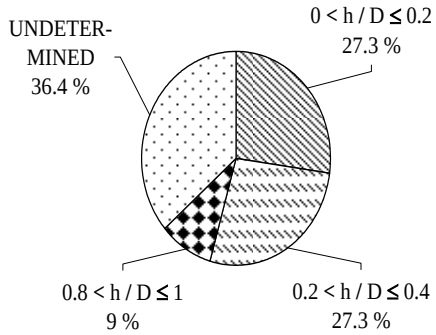

(b) The height of the damage h/D

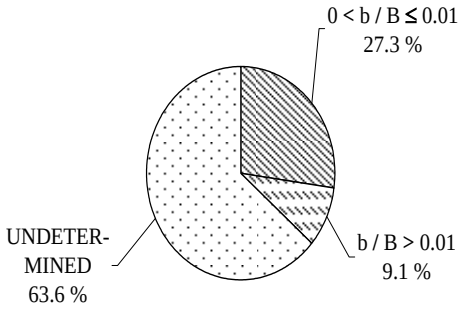

(c) The penetration of the damage b/B

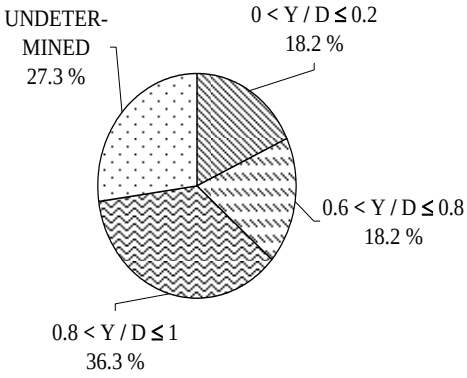

(d) The vertical position of the damage Y/D

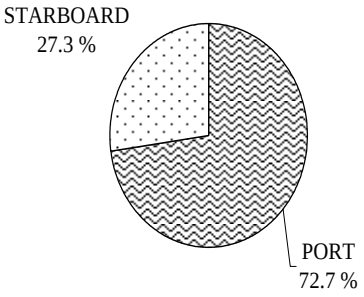

(e) The location of the damage

Figure 3.10: Damage properties in collision incidents for containerships for the L/4-amidships region.

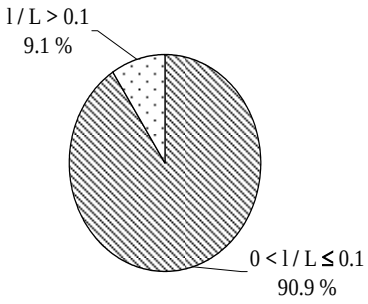

(a) The extent of the damage l/L

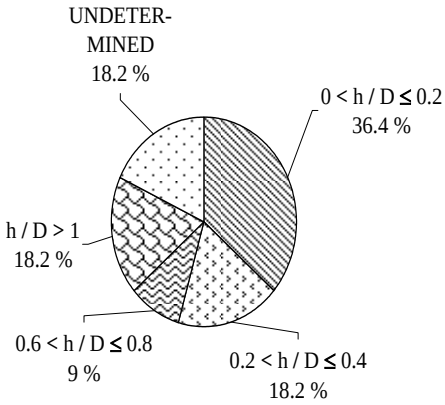

(b) The height of the damage h/D

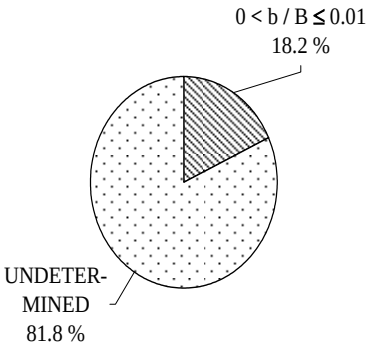

(c) The penetration of the damage b/B

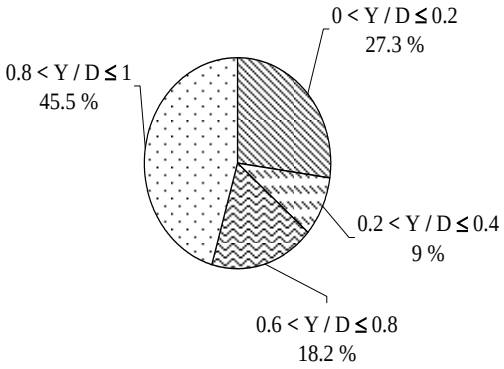

(d) The vertical position of the damage Y/D

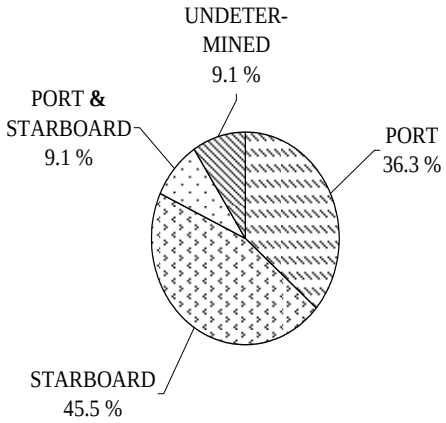

(e) The location of the damage

Figure 3.11: Damage properties in collision incidents for containerships for the 3L/4-FP region.

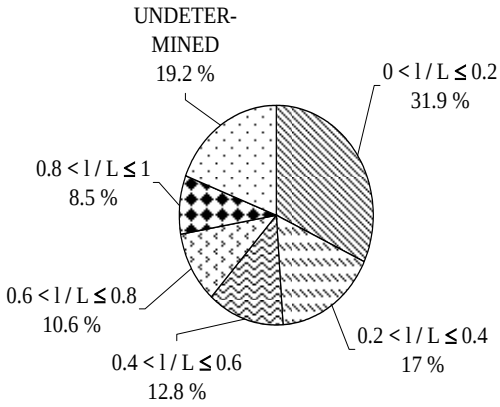

(a) The extent of the damage l/L

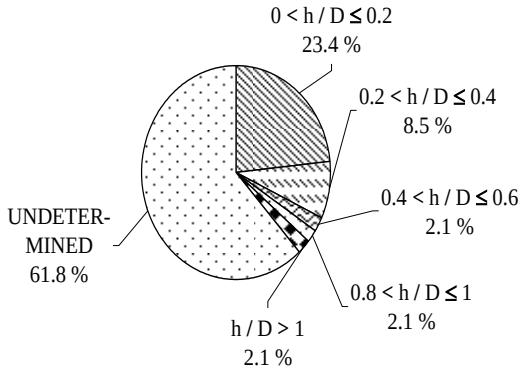

(b) The height of the damage h/D

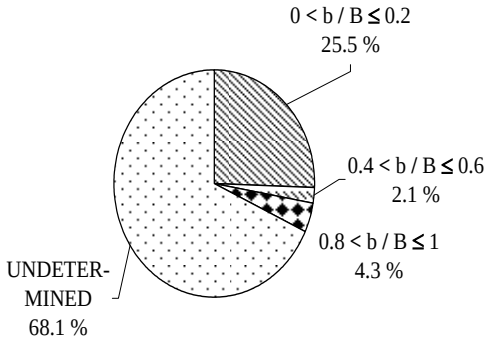

(c) The penetration of the damage b/B

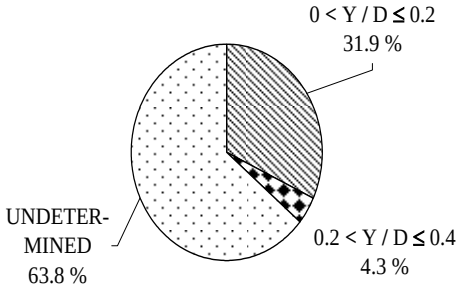

(d) The vertical position of the damage Y/D

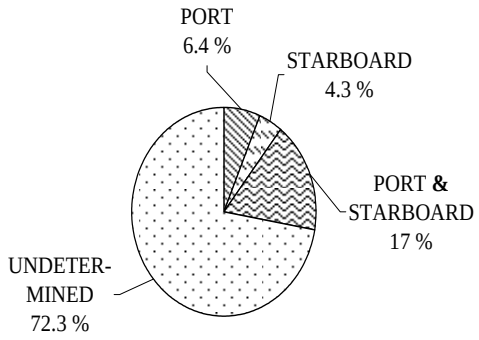

(e) The location of the damage

Figure 3.12: Damage properties in grounding incidents for general cargo ships for the amidships-3L/4 region.

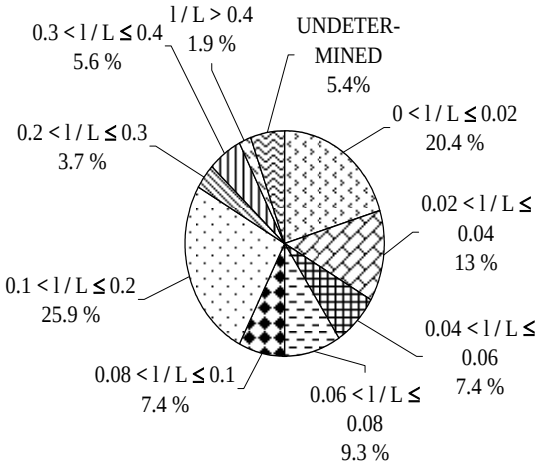

(a) The extent of the damage l/L

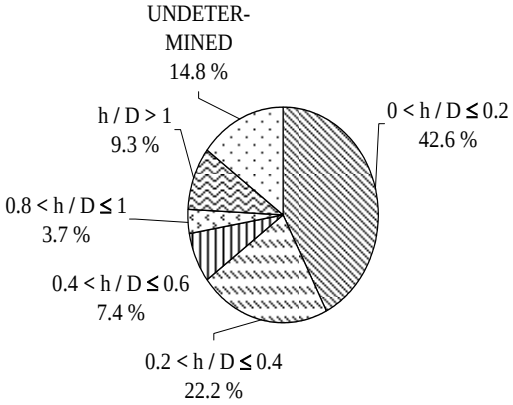

(b) The height of the damage h/D

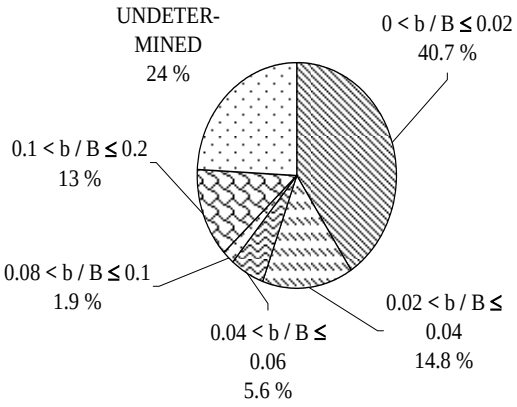

(c) The penetration of the damage b/B

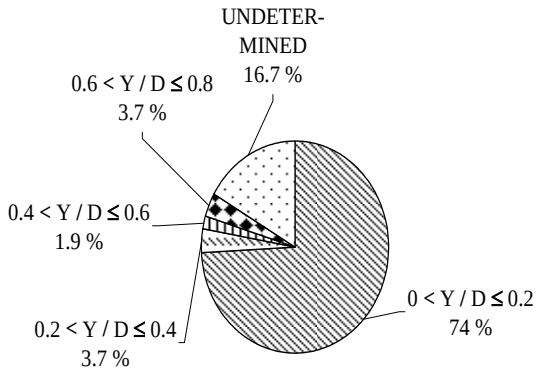

(d) The vertical position of the damage Y/D

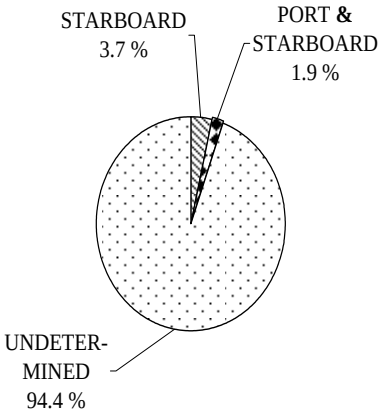

(e) The location of the damage

Figure 3.13: Damage properties in grounding incidents for tankers for the 3L/4-FP region.

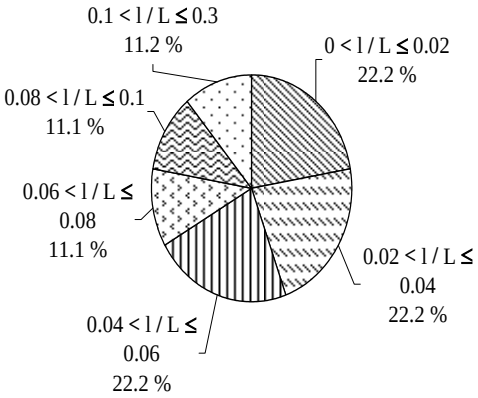

(a) The extent of the damage l/L

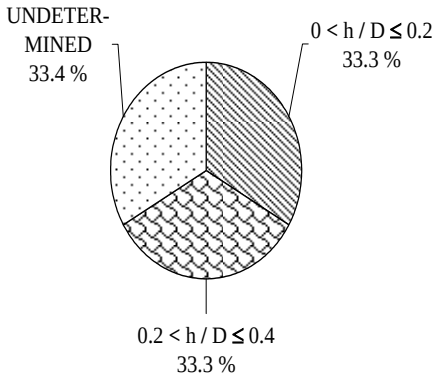

(b) The height of the damage h/D

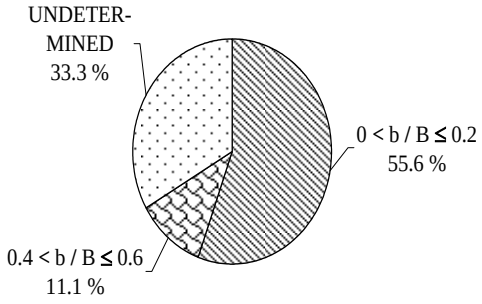

(c) The penetration of the damage b/B

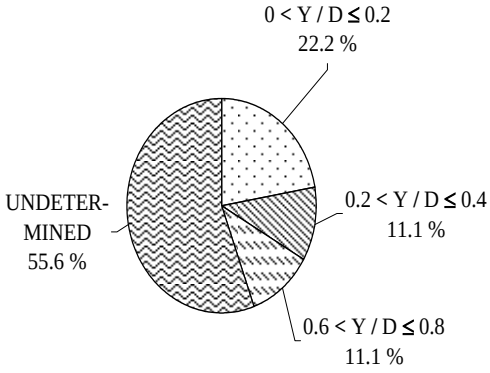

(d) The vertical position of the damage Y/D

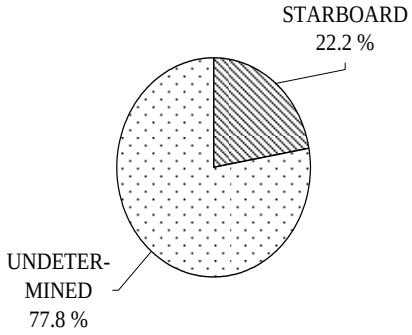

(e) The location of the damage

Figure 3.14: Damage properties in grounding incidents for bulk carriers for the 3L/4-FP region.

Having provided the detailed results of the analysis of the ‘Lutzen 2002’ database the next task is summarise the essential characteristics of the data captured in Figure 3.8 through 3.14 and to indicate (albeit simplistically) a measure of confidence in the identified data characteristics.

Table 3.1: Damage dimensions.

Damage Dimensions	Collision		Grounding	
Extension	(i) l/L≤0.1	80.6%	(i) l/L≤0.2	80.8%
	(ii) l/L≤0.1	84.3%	(ii) l/L≤0.1	94.6%
	(iii) l/L≤0.1	90.9% or 100%	(iii) l/L≤0.1	100%
Height	(i) 0.6<h/D≤0.8	73%	(i) h/D≤0.2	38.2%
	(ii) 0.8<h/D≤1	73.9%	(ii) h/D≤0.2	85.2%
	(iii) h/D≤0.4 or h/D≤0.2	63.6% or 81.8%	(iii) h/D≤0.4	66.6%
Penetration	(i) b/B≤0.2	41.3%	(i) b/B≤0.2	31.9%
	(ii) b/B≤0.2	48.7%	(ii) b/B≤0.02	76%
	(iii) b/B≤0.01	36.4% or 18.2%	(iii) b/B≤0.2	66.7%
Vertical Position	(i) Y/D>1	92%	(i) Y/D≤0.2	36.2%
	(ii) Y/D≤0.2	66.1%	(ii) Y/D≤0.2	83.3%
	(iii) 0.8<Y/D≤1	72.7% or 100%	(iii) Y/D≤0.2	44.4%
Port and Starboard	(i) Port	23.2%	(i) Port/starboard	27.7%
	(ii) Starboard	4.3%	(ii) Starboard	5.6%
	(iii) Port/starboard	100% or 90.9%	(iii) Starboard	22.2%
Notations Associated with Statistics Reported	(i) General cargo ship		(i) General cargo ship	
	(ii) Tanker		(ii) Tanker	
	(iii) Containership		(iii) Bulk carrier	

In Table 3.1 limits are placed on each of the damage dimensions of extension, height, penetration and vertical position for both collision data and grounding data. The percentage of accidents providing data for each ship type are specified as a simply measure of how confident or otherwise one may be in the data extracted. Since for container collision data there were two equally likely longitudinal locations (as defined in Figure 3.5) the first and second entries (when there is a difference) correspond to L/4-amidships and 3L/4-FP respectively.

3.1.1 Summary of Damage Statistics

Relevant accident statistics for different ship types have been extracted and processed from the records of the MAIB and the Classification Society contributions to the 'Lutzen 2002' database. The extracted statistics indicate which ship type is most vulnerable to different forms of accident and provided some indication of the likely

characteristics of the incurred damage. Some measure of confidence in the extracted statistics is provided by noting the percentage of each accident type for which reported details exist.

In the next chapter how accidents at sea have influenced the historical development of various design operation related regulations and stability analysis itself will be reviewed.

4. THE DEVELOPMENT OF SHIP REGULATIONS AND STABILITY ANALYSIS

This chapter represents an overview of the most relevant rules, regulations and stability methods applicable to practical ship design.

4.1 Development of Safety

Lessons learned from past accidents have helped designers to design safer ships. In the past the new knowledge (or understanding) gained was manifested in the form of recommendations governing appropriate proportions and ship hull dimensions that would provide improved stability and seakeeping. However, whilst this unwritten insight was passed from generation to generation it was insufficient to significantly improve the safety of ships.

There was thus a necessity to develop regulations. In the second half of the eighteenth century, the first attempt was made by Lloyd's Register of Shipping. It required that the magnitude of freeboard should be two to three inches per foot of the height of the hold (see, for example, Kobylinski & Kastner (2003)). The British Merchant Shipping Act of 1854 (see, for example, Kobylinski & Kastner (2003)) demanded that passenger ships have to be fitted with a collision bulkhead and two bulkheads around the machinery space. Towards the end of nineteenth century, Samuel Plimsoll, a British lawyer, succeeded in introducing legislation on freeboard requirements. According to this all British ships had to have a load line mark 'indicating the deepest permissible draught'. A couple of years later, the Committee of the British Board of Trade proposed a two-compartment standard for passenger ships (see Section 4.2.1). These proposals were never implemented, since they were considered unnecessarily severe by the maritime world.

After the Titanic disaster of April 1912 with 1513 lives lost, international organisations tried to improve maritime safety. The first international convention for the Safety of Life at Sea (SOLAS) was held in 1914, but the recommendations agreed did not enter into force because of the outbreak of the First World War.

In 1929, another international Safety of Life at Sea conference was convened and the recommendations designated the 'Criterion of Service' and the 'Subdivision Standard' (see, for example, Turan (1993) and Kristensen (2002)). These parameters express respectively the extent to which a ship is passenger carrying and the permissible separation of bulkheads. The parameters are discussed further and are defined in Section 4.2.1. The major thrust of the 1929 Convention was directed towards passenger ships. Consequently ships engaged in the carriage of passengers were subjected to much stricter regulations.

In the 1948 SOLAS conference additional important decisions were agreed (see, for example, Turan (1993) and Kristensen (2002)). In particular, there was the introduction of stability standards and guidance regarding permissible extent of damage. The damage length was formally defined as $(3\%L + 3.05)$m and the unlimited vertical extent of damage from the tank top was introduced. The 'Margin Line', which is 76mm below the upper side of the bulkhead deck, was introduced and defines the maximum level of ship immersion in its final damaged condition. At the United Nations hosted 1948 Geneva conference the organisation currently known as the International Maritime Organisation (IMO) was established. The original name, the Inter-Governmental Maritime Consultative Organisation (IMCO), was changed to IMO in 1982.

After the capsizing of Andrea Doria in 1956 with 52 lives lost, a passenger liner built under the 1948 convention, it became clear that the 1948 stability standard exhibited some shortcomings in its practical application. Another convention was required to identify additional necessary changes. In 1960, the SOLAS sub-committee on stability, subdivision and load lines was charged with the task of investigating the stability and

subdivision of ships (see, for example, Kobylinski & Kastner (2003)). The sub-committee analysed ship accidents and the behaviour of ships when damage occurred and proposed new ideas to deal with the subdivision of ships.

The 1960 convention decided that the damage could be unlimited vertically from the baseline of the ship and recommended that IMO should develop intact stability standards for passenger ships, cargo ships and fishing vessels (see, for example, Francescutto (2004)).

These deterministic analyses on subdivision and stability of ships were updated in 1974 (see, for example, Turan (1993) and Kristensen (2002)) and designated the probabilistic approach (IMO (1971)). The probabilistic approach (explained in detail in Section 4.2.2) was accepted as an alternative rather than a replacement of the existing deterministic stability criteria because of their perceived complexity.

In connection with the development of the first probabilistic rules two sets of model experiments were carried out to examine and systematically analyse for the first time the actual capsize mechanisms for damaged ships. One was in the United Kingdom (see Bird & Browne (1974)) and the other one was in the United States (see Middleton & Numata (1970)). This was a very important step in developing international stability standards. Furthermore, these investigations were consistent with the recommendation for a scientific approach for the development of safety standards.

In 1966, the IMO conveyed the International Convention on Load Lines. This convention recommended some limitations on the draught to which a ship may be loaded in the form of freeboard requirements (see, for example, Friis et al. (2002)). In 1969, the International Convention on Tonnage Measurements of Ships (see, for example, Friis et al. (2002)) was adopted. Whilst this does not influence stability directly it represents an example of other ship design improvements being sought.

In 1967, the Torrey Canyon tanker disaster resulted in 120,000 tonnes of oil being split into the sea between England and France killing most of the marine life. Consequently, the important problem of pollution was added to the responsibilities of IMO. In 1973, IMO introduced the International Convention for the Prevention of Pollution from Ships. Later this document was modified by the Protocol of 1978 (MARPOL 73/78), see, for example, IMO (1997).

Between 1978 and 1979 the Safeship project (see Bird & Morrall (1986)) was formulated by the United Kingdom Intact Stability Working Group. The aim of this project was to develop simple stability criteria applicable to passenger and cargo ships less than 100m in length in the short term. The long term aim was to extend the existing knowledge of large amplitude rolling motions and capsize mechanisms to establish better design criteria and regulations.

Brook (1988) discussed the incompetence of the current stability criteria, since an analysis of casualty statistics showed several vessels satisfying the existing criteria were lost as a consequence of capsize. Brook (1988) emphasized the need to take into account environmental effects when analysing the intact stability of a vessel.

In 1987, the Ro-Ro passenger car ferry Herald of Free Enterprise capsized and foundered just outside Zeebrugge Harbour, Belgium, with the loss of 193 lives. This ship had been designed according to the 1960 SOLAS convention. This accident demonstrated that the existing stability criteria were still unsatisfactory and also emphasized the necessity for more realistic rules to improve the safety of ships. After the accident, new amendments expanded the existing approach by introducing three changes namely; a value of 15° for a minimum range of positive residual righting arm, a value of 0.015 m-rad. for the area under the righting curve of the ship in the final damaged condition and a maximum GZ value of 0.1 m. These amendments, made in 1988 and known as SOLAS ‘90, increased the damage stability standards of all new

passenger ships. In 1992 similar requirements were applied to all existing passenger ships.

In 1990, residual stability standards concerning righting levers, the area under the GZ curve and limiting angles of inclination were introduced for both cargo and passenger ships. These requirements came into force at the beginning of 1992 (see, for example, Turan (1993), Turan & Vassalos (1994) and Kristensen (2002)).

The Ro-Ro passenger ferry Estonia sank in 1994 with 852 lives lost as a result of large amounts of accumulated water on the cargo decks. This water collection reduced the stability. Following the Estonia disaster, a panel of experts met in December 1994 to identify ways of improving the maritime safety of Ro-Ro passenger ships. The conference agreed that all existing Ro-Ro passenger ships must deal with the damage stability requirements of SOLAS '90 (see, for example, Kristensen (2002)).

The tragic accidents of the Herald of Free Enterprise and Estonia emphasized the magnitude of the problem presented when water enters the deck of ships with large undivided spaces (such as Ro-Ro vessels). Therefore, the Joint Northwest European project (see Vassalos et al. (1996)) was established to address the development and validation of numerical tools for assessing the damage survivability of passenger/Ro-Ro vessels. This research resulted in the development of the static equivalent method (SEM) for Ro-Ro ships (see, for example, Pawlowski (1999) and Tagg & Tuzcu (2003)). This method statically calculates the volume of water that will reduce the damage GZ curve to exactly zero (see Tagg & Tuzcu (2003)). From this neutral stability position, it follows that any lesser amounts of water will imply survivability of the ship and further additions of water will cause ship capsizing.

The 'Regional Agreements Concerning Specific Stability Requirements for Ro-Ro Passenger Ships' (otherwise known as the Stockholm Agreement (see, for example, Schroter & Juhl (2002)) is considered to provide an alternative to the deterministic

approach of stability analysis. This model test method requires that at least five experiments for each peak period should be carried out and be documented by means of a written report and a video recording of the experiments. The ship model should exhibit the same outer and internal configuration as the original ship and it should be placed in beam seas with the damage hole facing the oncoming waves. More details can be found in IMO (1997).

The development of new regulations and the revision of SOLAS still continue. In recent years much work is being undertaken within the umbrella of the Harder Project (see, IMO (2002a, 2002b) and Rusas (2002)). The aim of the 'HArmonization of Rules and DEsign Rationale (HARDER)' project is to harmonise the stability demands on passenger and cargo ships greater than 80m in length. The final outcome of the HARDER project can be found in Tagg & Tuzcu (2003). The NEREUS project commenced in 2000 has the aim of developing design tools and methodologies to improve Ro-Ro damage resistance against capsize. Some of the validation work carried out within NEREUS can be found in Woodburn et al. (2002).

Stability analysis has evolved over a considerable time with different accidents acting as catalysts for further development. Whilst a probabilistic approach exists as an alternative to the deterministic approach the designer may select the approach adopted. In the next section both approaches are examined together with their advantages and disadvantages.

4.2 The Deterministic and Probabilistic Approaches to Ship Stability Analysis

The deterministic approach to ship stability is mandatory, whereas the probabilistic method is accepted as an alternative approach when the deterministic method is found to be unsatisfactory. Each approach reviewed in turn in the next sections.

4.2.1 The Deterministic Approach to Ship Stability Analysis

The deterministic approach offers the possibility to account for the floodable length and for the disposition of transverse watertight bulkheads. The floodable length varies with longitudinal position on the ship. It is the maximum length of a compartment, which if it is flooded, will permit the vessel to float at a waterline that is below or touches the 'Margin Line'. The 'Margin Line' is a fair curve drawn 76mm below the bulkhead deck, which is the uppermost deck to which watertight bulkheads extend.

Ships are subdivided according to their 'Criterion of Service' and their 'Factor of Subdivision (or Subdivision Standard)'. The 'Criterion of Service' is a numeral that expresses the degree to which a ship is a passenger carrying ship. For example, a numeral of 23 corresponds to a ship primarily engaged in carrying cargo with a small number of passengers, whereas a numeral of 123 applies to a ship engaged, mainly, in the carriage of passengers (see, for example, Lewis (1988)). This assignment of the numeral depends on the ship length, the number of passengers, the total volume of the ship below the margin line, the volume of the machinery space and the volume of the accommodation spaces below the margin line. The lower the value of the numeral assigned the further apart the watertight bulkheads may be spaced.

The 'Factor of Subdivision', designated F, depends on ship length and the designated criterion of service. The 'Factor of Subdivision' establishes the permissible length between watertight bulkheads. It is expressed as a percentage varying from 30 to 100 percent. A factor of 'F=0.3' means the bulkheads may be spaced a separation distance only equal to 30 percent of the floodable length. If the factor of subdivision is greater than 0.5, the ship must satisfy the 'one compartment standard (any one compartment can be flooded without the ship sinking)', if F is between 0.33 and 0.5 then the vessel should satisfy the 'two compartment standard' and finally if F is smaller than 0.33 the floating structure should meet the 'three compartment standard'.

So when the floodable length at each location along the ship length is calculated (see, for example, Lewis (1988)); the permissible compartment length at each point is obtained from the multiplication of the floodable length and the factor of subdivision. In this way, a permissible length curve along the ship is derived.

However, when a ship is damaged and some compartments become open to sea, the seawater cannot fill such volumes totally as some space will already be occupied by internal ship arrangements e.g. bulkheads, main engines, auxiliaries, pumps, cargo et cetera. So before the floodable length can be calculated, definite values of the permeabilities of the spaces involved must be determined. That is, the fraction of floodable volume in a compartment. Thus the floodable length curve has to be determined for different levels of permeabilities. Figure 4.1 indicates the influence of permeability levels on the floodable length curve.

Once the floodable length curves have been determined the level of stability at the appropriate level of impermeability can be examined. For each compartment a triangle is constructed on the floodable length curve with the base line defined by the end points of the compartment and the apex constructed from the intersection of the other two sides each of which makes an angle $\alpha = \tan^{-1}(2)$ with the baseline, as illustrated in Figure 4.1. For an acceptable level of stability at the selected level of permeability the triangle apex must lie below the corresponding floodable length curve. Conversely the locations of transverse watertight bulkheads are determined by ensuing each constructed triangle meets the requirement indicated.

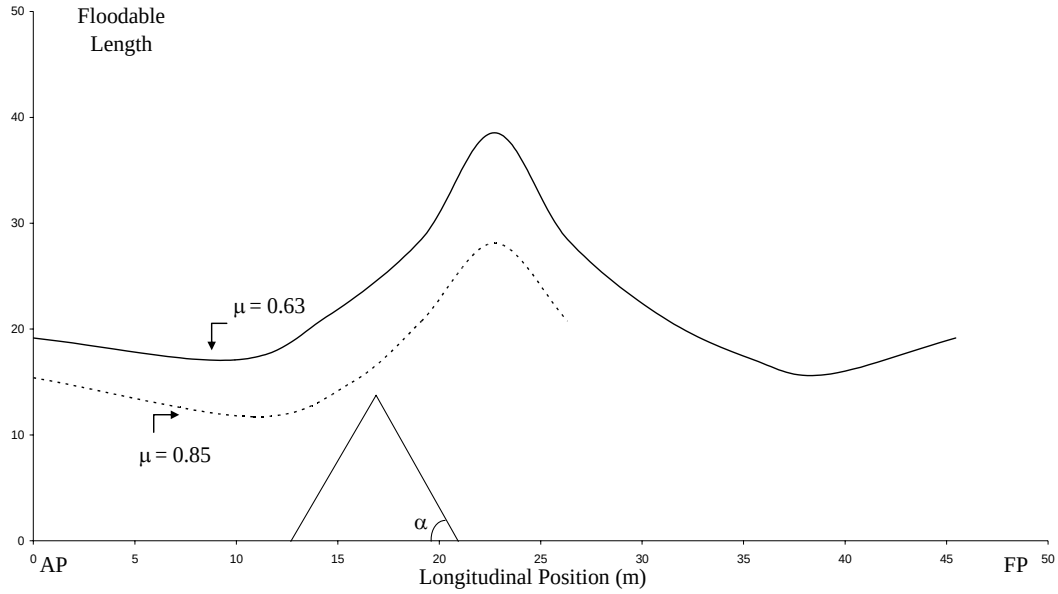

Figure 4.1: The influence of permeability on the floodable length curve for a cargo/passenger vessel of 134m in length.

More detailed information on the 'Floodable Length' and 'Factor of Subdivision' is available in the SOLAS '60 related documentation (IMCO (1960)).

In classical naval architecture, there are two principal deterministic methods to examine the stability of damaged ships: the 'Lost Buoyancy' and the 'Added Weight' techniques. Therefore as the positions of bulkheads and compartments are assigned in the design process one may use either the 'Lost Buoyancy' or the 'Added Weight' method to understand the behaviour of the damaged ship. Each method is summarised next with further discussions of the two procedures provided in Section 4.2.3.

Lost Buoyancy Method

The lost buoyancy method considers that the damaged compartments are open to the sea and the ship has lost buoyancy in these compartments. In order to compensate for the lost volume and its moments the vessel will undertake parallel sinkage, trim and heel.

The amount of parallel sinkage can be calculated from the division of the volume of the flooded compartment (or in other words lost buoyancy) by the new waterplane area of the damaged ship. The heel angle and trim are determined by equating the moments of the lost buoyancy with respect to new LCF to the moments of the buoyancy gain accompanying parallel sinkage, trim and heel attributed to the remaining non-damaged compartments of the ship.

Added Weight Method

In the added weight method the mass of water that has entered the damaged compartment(s) is treated as an additional weight on board. The additional weight changes the displacement weight and the longitudinal, vertical and horizontal positions of the centre of gravity. Hence this additional weight causes parallel sinkage, trim and heel of the ship. The parallel sinkage is calculated from the division of the volume of the water entrapped in the damaged compartment(s) by the waterplane area of the intact ship. The heel angle and trim are obtained by equating the moments of the added weight respect to LCF to the moments of the new displacement weight of the damaged ship.

Some further discussion about these two methods is presented in Section 4.2.3.

4.2.2 The Probabilistic Approach to Ship Stability Analysis

The probabilistic approach to stability analysis was initially developed in 1973. To estimate the probabilities of different damage stability related events available accident records are used. It is the known occurrence of such damage stability related events that governs the concept of stability in this procedure.

In the probabilistic approach the survival probability of a damaged ship is defined through the ‘attained survival probability index’, A. To determine this probability, one

must first estimate the conditional survival probabilities, p_i, assigned to either the i[th] damaged compartment or the i[th] specific grouping of adjacent damaged compartments. This, in turn, requires estimation of the probability of survival, s_i, after flooding the i[th] identified area or grouping of areas. Thus A is defined as

$$A = \sum_{i=1}^{N} p_i s_i . \tag{4.1}$$

Clearly i represents each compartment or group of compartments under consideration and N is the total number of individual and groups of compartments considered.

p_i for each single compartment considered is determined according to MCA (1999) as follows,

- if the compartment considered extends over L_S which is the moulded length of the ship

$$p_i = 1 \tag{4.2}$$

- if the aft limit of the compartment considered coincides with the aft terminal of L_S

$$p_i = F + 0.5ap + q \tag{4.3}$$

- if the forward limit of the compartment considered coincides with the forward terminal of L_S

$$p_i = 1 - F + 0.5ap \tag{4.4}$$

- if both ends of the compartment considered are within the aft and forward terminals of L_S

$$p_i = ap\,. \tag{4.5}$$

The assumed distribution function of damage location along the ship's length is defined as

$$F = 0.4 + 0.25E\left(1.2 + a\right). \tag{4.6}$$

The assumed distribution density of damage location along the ship's length is

$$a = 1.2 + 0.8E\text{ , which should be not more than 1.2} \tag{4.7}$$

$$E = E_1 + E_2 - 1 \tag{4.8}$$

$$E_1 = \frac{x_1}{L_s} \tag{4.9}$$

$$E_2 = \frac{x_2}{L_s} \tag{4.10}$$

Here x_1 and x_2 stand for the distance from the aft terminal of L_S to the foremost/aftermost portion of the aft/forward end of the compartment considered.

$$p = F_1 J_{\max} \tag{4.11}$$

$$F_1 = y^2 - \frac{y^3}{3}\text{ if }y<1\text{, otherwise }F_1 = y - \frac{1}{3} \tag{4.12}$$

$$y = \frac{J}{J_{\max}} \tag{4.13}$$

$$J = E_2 - E_1 \tag{4.14}$$

The maximum non-dimensional damage length ' $J_{\max}$ ' is given by

$$J_{\max} = \frac{48}{L_S}, \text{ which should be not more than 0.24} \tag{4.15}$$

$$q = 0.4F_2\left(J_{\max}\right)^2 \tag{4.16}$$

$$F_2 = \frac{y^3}{3} - \frac{y^4}{12} \text{ if } y < 1, \text{ otherwise } F_2 = \frac{y^3}{2} - \frac{y}{3} + \frac{1}{12} \tag{4.17}$$

More details and discussions about p_i can be found in IMO (2002b).

s_i can be determined for each single compartment considered according to MCA (1999) as follows,

$$s_i = C\sqrt{0.5GZ_{\max} range} \tag{4.18}$$

$$C = 1 \text{ if } \theta \le 25°,\ C = 0 \text{ if } \theta > 30°, \text{ otherwise } C = \sqrt{\frac{30-\theta}{5}}. \tag{4.19}$$

Here $GZ_{\max}$ stands for the maximum positive righting lever which should not be more than 0.1m, *range* is range of positive righting levers beyond the angle of equilibrium which should not be more than 20° and θ is the final equilibrium angle of heel.

The factor s_i can be calculated by using either a GZ based formulation (see Equation (4.18)) or the static equivalent method (summarised in Section 4.1). According to the static equivalent method, the factor s_i depends on the water head 'h' on the vehicle deck above the sea level, as shown in Figure 4.2, at the critical heel of equilibrium. The critical volume of water is the volume of water necessary to reduce the GZ curve of the ship in the damaged condition to neutral stability (see IMO (2002a)). Different formulations for the determination of the factor s_i for Ro-Ro and other types of ships are discussed by Vassalos et al. (1996), Pawlowski (1999) and IMO (2002a).

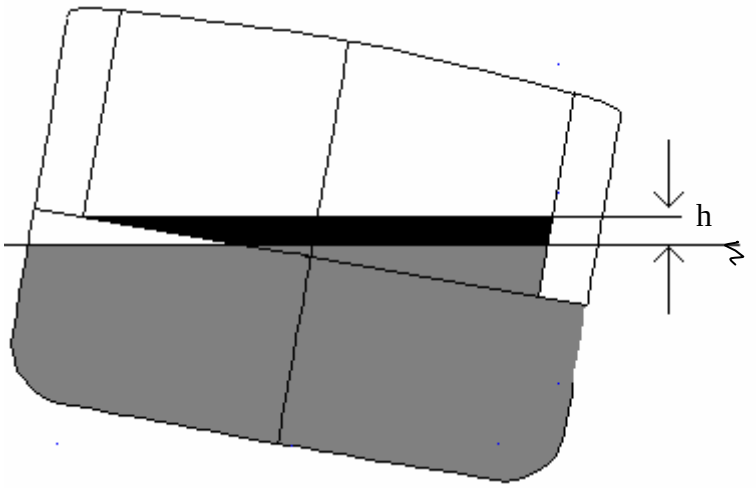

Figure 4.2: Definition of the water head, 'h' (IMO (2002a)).

A second index of subdivision, is the 'required subdivision index' designated either by R or $A_{\max}$. The calculation of the index, R, for a cargo ship (which by definition includes tankers, general cargo ships, containerships and bulk carriers) of length greater than 100m is given in Equation 4.20.

$$R = \left(0.002 + 0.0009 L_S\right)^{1/3}. \tag{4.20}$$

Equation (4.20) is different for cargo and passenger ships.

The degree of subdivision of a ship is considered sufficient if the stability of the ship in a damaged condition meets the requirements of the SOLAS '90 criteria (see, for example, Turan (1993)) and the 'attained survival probability index (A)' is not less than the 'required subdivision index (R or A_{max})'.

4.2.3 Discussion on Current Stability Methods

Having outlined two possible distinct methods of determining of the stability of a damaged ship, it is appropriate to discuss the 'marriage' of the hull form optimisation tools discussed in Chapter 2 and the stability analysis choices.

The probabilistic concept of survival, based on actual accident reports, the studying of damage stability related random events and associated probabilities, seems more realistic than the deterministic approach which is based on numerical evaluation of fixed predefined parameters.

However, the aim of this research is to examine the capability of optimised and non-optimised ships to withstand damage. Given the optimisation tools are to be applied in the earlier stages of the design to produce new improved hull forms from an initial design, the probabilistic approach is likely to be inappropriate when the initial design is particularly innovative; since the probabilistic approach requires accident statistics of existing operational ships. For less novel hull forms the designer always has the choice of allowing the probabilistic approach to influence the initial design to be optimised. Within this research programme the deterministic approach is therefore considered sufficient to ensure that modifications of the basis hull during the optimisation are constrained to satisfy the deterministic constraints with limited changes of hull form design parameters.

The lost buoyancy approach appears quite realistic as the hydrostatic calculations are carried out using the 'residual' waterplane area, that is, the original intact waterplane area minus the waterplane areas no longer contributing because of the ship damage. However, the added weight method considers the weight of water entrapped in the damaged compartments and so permits calculation of parallel sinkage either with heel or trim changes. Consequently, both approaches are adopted in combination when damage occurs below and at the still waterline.

4.3 Damage Stability Suite

Section 4.2.3 concluded that the probabilistic method could be beneficial in influencing the initial design to be optimised when well established operational statistics existed, it was not appropriate for novel designs. It has also been noted that the hull form optimisation procedures were initially developed to allow better first level iterations of design by companies without specific ship type design capability techniques.

The reported applications of such optimisation processes indicate that whereas intact stability is used as a constraint and the hull forms generated exhibit improved overall (frictional & wave-making) resistances, seakeeping and added resistance qualities stability of damaged hull forms has not been addressed. Including damage stability within the optimisation process was rejected on the basis that the structure is perceived as a series of two-dimensional transverse sections and this approach does not readily capture the three-dimensional aspects of damage stability (as discussed in Section 2.3). Hence it has been decided that the deterministic damage stability method will be applied when both the initial design and optimised design have been damaged in equivalent ways. Thereafter, the three-dimensional nature of the seakeeping motions can also be captured for both the initial and optimised hulls in their intact and damaged states.

4.3.1 Independent Damage Stability Analysis

Damage stability is an integral part of computerised stability analysis packages. However, it was found to be more convenient and faster to use the alternative equilibrium search code developed by Saydan (2004). The developed algorithm initially determines the intact hydrostatic properties of the vessel and then undertakes a damage stability analysis of the ship according to the specified extent of damage, see Section 6.6.

When a ship is damaged it may lose some of its structural mass. Assuming l, b and h denote the length, penetration and height of the damage and ρ is the associated material density the structural mass loss is estimated using

$$w_{lost} = l \times b \times h \times \rho \,. \tag{4.21}$$

With structural damage there can be the accompanying water ingress and resulting changes in trim ϕ and heel θ together with parallel sinkage. These aspects are considered next.

The volume loss, v_{lost}, within the damaged compartment is determined from knowledge of:

- the original compartment volume 'v_c'
- the volume of compartment not affected by ingressed water (e.g. closed tanks) 'v_i'
- the total mass of liquid inside the compartment prior to damage occurring 'M_l'

- the density of the fluid ' ρ_l ' and the permeability of the compartment ' μ_c '

That is

$$v_{lost} = \left[\left(v_c - v_i \right) \times \mu_c - \frac{M_l}{\rho_l} \right]. \tag{4.22}$$

The parallel sinkage is estimated taking into account the vertical position and the height of damage. If the damaged area straddles the intact still waterline (case A of Figure 4.3) then the parallel sinkage is given by Equation (4.23a), whereas if the intact ship waterplane area and its properties are conserved (case B of Figure 4.3), the parallel sinkage is determined from Equation (4.23b);

$$Y_{SINK} = \frac{v_{lost}}{A_{wps} - \mu_2 \times a_{wpc}} \tag{4.23a}$$

$$Y_{SINK} = \frac{v_{lost}}{A_{wps}} \tag{4.23b}$$

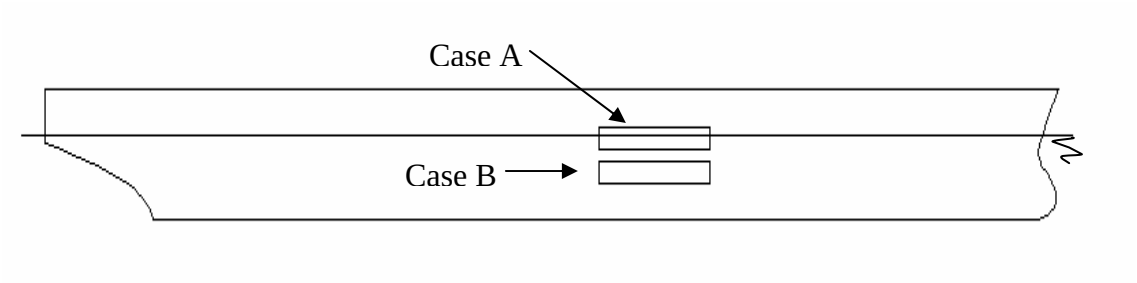

Figure 4.3: Vertical position of damage.

In Equations (4.23a) & (4.23b) A_{wps} denotes the waterplane area of the intact ship. In Equation (4.23a) μ_2 represents the surface permeability of the damaged compartment and a_{wpc} is the waterplane area of the damaged compartment.

From Euler angle descriptions of rotations one is aware that changing the order of rotations from say θ followed by ϕ (about two different axes) to ϕ by θ leads to different final positions of the structure. To determine the trim and heel angles of the damaged ship the trim and heel angles are estimated in three related ways. In the first option the hull form is trimmed first and then it is heeled, in the second option the hull form is heeled first and then it is trimmed and in the third option the equilibrium angles are determined by averaging the angles obtained from the first and second methods. The acceptability of these averaged trim and heel angle is then interrogated to establish that the implied damaged ship orientation is a position of equilibrium. If this is not the case using the current predicted ship orientation the whole process is repeated until static equilibrium is established to determine the heel and trim angles sought. As indicated earlier (Section 4.2.3) the damaged ship equilibrium position is investigated using a combination of the lost buoyancy and added weight methods (see, for example, Lewis (1988)).

4.3.2 Presentation of the Damaged Hull Forms

Downward movement, trim and heel will change the location of the hull wetted surface data points along the structure. These new positions must be determined to define the wetted surface of the damaged hull form. The necessary transformation will be achieved using vertical translation and rotation in accordance with appropriate Euler angles. The transformation of the points defining the hull form with Euler angles are presented below for a structure which trims first and then heels.

As a first step, the downward movement is applied to yield;

$$\begin{bmatrix} Z \\ X \\ Y_1 \end{bmatrix} = \begin{bmatrix} Z \\ X \\ Y \end{bmatrix} - \begin{bmatrix} 0 \\ 0 \\ Y_{SINK} \end{bmatrix} \tag{4.24}$$

whereas the trim ϕ and heel θ will lead to;

$$\begin{bmatrix} Z_1 \\ X \\ Y_2 \end{bmatrix} = \begin{bmatrix} \cos\phi & 0 & -\sin\phi \\ 0 & 1 & 0 \\ \sin\phi & 0 & \cos\phi \end{bmatrix} \times \begin{bmatrix} Z \\ X \\ Y_1 \end{bmatrix} \tag{4.25}$$

and

$$\begin{bmatrix} Z_1 \\ X_1 \\ Y_3 \end{bmatrix} = \begin{bmatrix} 1 & 0 & 0 \\ 0 & \cos\theta & \sin\theta \\ 0 & -\sin\theta & \cos\theta \end{bmatrix} \times \begin{bmatrix} Z_1 \\ X \\ Y_2 \end{bmatrix} \tag{4.26}$$

Here ϕ and θ denote the trim and heel angles and the parallel sinkage is denoted by Y_{SINK}. The reference axis system is shown in Figure 5.1.

These new data values are used in the Matthew Diffraction Suite (see Hearn (1978)) to evaluate the hydrodynamic coefficients and wave excitation forces of the damaged hull forms. This data is presented in Chapter 7 and Appendix H.

4.4 Summary

Having indicated how ship regulations and stability analysis has changed to overcome difficulties highlighted by various public attention noted accidents, a method of investigating the impact of damage upon the initial and optimal identified hull forms has

been proffered. Since investigating the impact of damage includes reassessing the motions, seakeeping aspects are discussed next.

5. SEAKEEPING

Researchers, designers and operators are interested in the dynamic behaviour of ships in waves because the seakeeping capability of a ship may determine the operational and hence the financial success of the design.

This chapter starts with a general review of seakeeping of both intact and damaged ships. Having formulated the general six degrees of freedom steady state equations of motion of an intact ship a novel technique is presented for determining the cross-products of inertia of a damaged ship.

5.1 General Review

Sea waves are irregular. Within a linear hydrodynamic theory a representation of irregular waves can be achieved by assuming that sea waves are a consequence of the linear superposition of progressing regular and harmonic waves of different wave amplitude, circular frequency and relative phasing. Furthermore, if the characteristic linear responses of a ship to progressing regular and harmonic wave components are known, then the response of that ship in an irregular seaway can be determined. Spectral analysis applied to linear dynamic systems provides the link between responses in regular waves and responses in a seaway or irregular waves (see, for example, Lloyd (1998) and Saydan (1999)).

The fluid-structure interaction associated with ship motions in regular waves can be formulated using potential flow theory. In this case viscous effects are neglected, the fluid is assumed incompressible and the fluid motion is assumed irrotational. With the additional assumption of small unsteady motions of the ship and of the surrounding fluid, linear superposition can be applied. Another consequence of linearisation is that

the wave structure interaction problem can be decomposed into diffraction and radiation problems (see, for example, Newman (1978) and Lewis (1989)).

In the diffraction problem regular harmonic incident waves act upon the otherwise 'fixed' ship. Linearisation of the fluid-structure interaction problem means that the resulting velocity potential consists of two components, the velocity potential of the undisturbed incident wave system and the velocity potential representing the diffraction or scattering of the incident waves by the 'fixed' ship. The hydrodynamic forces (moments) resulting from the incident and diffracted waves are called the excitation forces (moments) (see, for example, Newman (1978) and Lewis (1989)).

The radiation forces and moments acting on the body are a consequence of the structure being forced to oscillate in otherwise still calm water at a frequency corresponding to each incident wave frequency (for zero forward speed), or, incident encounter frequency (for forward speed case) in each of the six possible degrees of freedom in turn. This approach is adopted because linearisation implies that the forces (moments) required to induce motion in any degree of freedom are the same as those resulting from forced oscillation at the same amplitude and frequency. Since the forces (moments) are dependent upon the (as yet) unknown amplitudes of motion the radiation hydrodynamic forces are recast into an equivalent two coefficient based expression. The two coefficients, referred to as added mass and fluid damping, are essentially the force (moment) in-phase with the acceleration and velocity of the structure respectively. Hence both amplitude and phase information is encoded in these coefficients (see, for example, Newman (1978) and Odabasi & Hearn (1978)).

The excitation forces (moments) and the radiation forces (moments) are determined from integration of the associated dynamic pressures over the wetted surface of the structure (see Section 7.1 for required integral relationships). Bernoulli's equation links pressure and the corresponding velocity potentials (see, for example Bertram (2000)). In order to obtain the unknown diffraction and radiation velocity potentials, boundary

integral methods may be used (see, for example Odabasi & Hearn (1978)). Whether 3D methods or 2D based strip theory are applied appropriate boundary conditions must be satisfied. These boundary conditions (see Appendix B) are satisfied at the fluid and body boundaries. The fluid boundaries are the free surface, the sea-bed and the so-called radiation surface linking the free surface and the sea-bed in the form of a vertical cylinder to form a closed solution domain. The body boundary is the wetted surface of the ship or floating structure. Once the velocity potentials are evaluated, the hydrodynamic pressure can be derived from the linearised form of the Bernoulli pressure equation; the hydrodynamic forces can be determined from integration of the incident and diffraction or the radiation pressure over the wetted surface of the floating structure (as indicated earlier).

For a structure damaged at or below the waterline the boundary element methods may be extended to include internal wetted surfaces. In this case the appropriate boundary condition is one of a non-permeable structure, that is, normal velocity of the fluid matches the normal component of the structural velocity consistent with the radiation or diffraction problem being addressed. In the case of ingressed fluid there will be internal free-surfaces and if necessary these may be modelled as structurally massless plates with appropriate degrees of freedom (for equations of motions see Appendix K). Such an approach is not implemented here.

If the attitude of the structure is such that the deck is exposed to waves then this surface may also be included in a manner analogous to other rigid surfaces. That is, the water in contact with the deck is not considered to be entrapped on deck but to satisfy the usual continuity of normal velocity of fluid at deck.

For completeness, the problem of entrapped fluid is reviewed next.

Huang & Hsiung (1997) analysed the dynamic behaviour of the ships using a time-domain approach when a large amount of water is trapped on the deck due to spillage of

water or roll motion. Later Grochowalski et al. (1998) and Huang et al. (1998) considered the same time-domain problem with the addition of water shipping on and off the deck. The water on deck usually causes the progressive flooding of the spaces inside the hull and this may ultimately result in the loss of the ship. This problem is highlighted by Borlase (2003).

When the ship hull is damaged, water may flow into the damaged compartment(s). The water trapped within damaged compartment(s) may change the behaviour of the ship. Subramanian & Kastner (2000) examined the behaviour of a Ro-Ro ship in beam seas when water enters on deck. The model vessel was analysed in different conditions: open deck condition, a solid weight on deck (equivalent to the weight of 0.5 m depth of water) and 0.58 m depth of water on deck. It was found that if water is entrapped on the cargo deck it causes two superposed frequencies of oscillation: one is due to the frequency of oscillation of the liquid mass inside the ship and the other is due to the natural rolling frequency of the ship.

Turan (1993) and Turan & Vassalos (1994) carried out a number of different damage scenarios to investigate the dynamic behaviour of a damaged car/passenger vessel using a time simulation approach. Their mathematical model included coupled sway-heave-roll motions in beam seas. Their motion equations take into account the amount of water entering and leaving a damaged compartment and also variations in the ship mass. However, in their research there is no comparison between the computed and experimentally measured results for these damage scenarios.

Chan et al. (2002) analysed motions of a Ro-Ro ship in stern quartering waves in intact and damaged conditions using a time domain method. Their theoretical predictions and experimental measurements showed good agreement except in the roll-resonant region. The authors attributed this discrepancy to the strong coupling between all modes of motion for large amplitude responses in the roll-resonant region.

Umeda et al. (2004) suggested that the centre of harmonic motion of a damaged ship changes gradually with the increased accumulation of water inside the hull. Turan & Vassalos (1994) calculated the radiation and diffraction forces of the damaged ship without taking into account the change of the centre of harmonic motion. Four years later, Vassalos et al. (1998) calculated radiation and diffraction forces taking into account the change of centre of harmonic motion with the sinkage, heel and trim.

Traditionally, in the damaged ship dynamic calculations the free surface of the floodwater within the flooded compartment(s) is assumed to be horizontal (see, for example, IMO (1997), Vassalos et al. (1996) and Palazzi & Kat (2004)). In the probabilistic A-265 criteria the effect of floodwater is based on empirical data derived from model tests (see IMO (1971)). Woodburn et al. (2002) questioned these methods as they do not necessarily represent a realistic scenario when the ship undergoes large amplitudes of motion. Woodburn et al. (2002) used in their research a coupled model that consists of a dynamic model for the ship motions and a computational fluid dynamics (CFD) model for floodwater dynamics. Their computed results show satisfactory correlation with experimentally measured data for the mass of floodwater inside the vessel.

For the examination of the behaviour of a wall-sided, damaged Ro-Ro passenger ship in beam waves Hasegawa et al. (2000) assumed that water ingress and water egress were functions of water level inside and outside of the damaged compartment. Veer & Kat (2000) examined theoretically and experimentally the progressive flooding and sloshing in compartments. Large flow obstructions such as main engine were presented in the geometry of the model and small flow obstructions were modelled by changing only the permeability of the compartment.

Ikeda & Ma (2000) carried out an experimental study on the large dynamic roll motion of a passenger ferry at intermediate stages of flooding due to sudden ingress of water through a damage opening. It was realised that the intact stability of the vessel, the

arrangement of obstacles, the damaged area and the location of the damage opening affected the roll motion characteristics at intermediate stages.

If as a result of the frequency-domain analysis of the behaviour of the damaged and intact ship, the impact of the damage on the responses of the ship is found to be significant then these effects may have to be taken into account in a refined analysis. With this possibility in mind the problem of sloshing is reviewed next.

Faltinsen (1978) considered two-dimensional analysis of a rectangular tank forced to oscillate harmonically with small amplitudes of sway. Later, Rognebakke & Faltinsen (2001) undertook two-dimensional experiments investigating the effects of sloshing on ship motions for a box shaped ship section excited in a regular beam sea. The ship section analysed contained two tanks and it was forced to sway. The change in sway motion of the model with wave frequency, for different filling levels of the two tanks was presented. Kim (2001) worked on the coupled analysis of ship motions and sloshing flows in beam seas.

The problem of ship motions in waves is relatively complicated; therefore some simplifications may be appropriate. The transverse dimensions of the structure may be assumed to be small compared to its length. This geometric simplification of the structure leads to strip theory. Detailed reviews of the strip theory, covering its historical and mathematical development may be found in Salvesen et al. (1970), Odabasi & Hearn (1978) and Newman (1978).

For the analysis of ship motions, a representation of the wetted surface is necessary. This may be numerical using boundary elements or analytical using conformal mapping techniques. The latter technique is used to transform the sections of the ship into a circle, for which the form of the potential is known and hence the added mass and damping properties of a ship section can be determined. Mathematical details related to the conformal mapping techniques may be found in Kerczek & Tuck (1969) and

Hoffman & Zielinski (1977). A multi-parameter conformal mapping technique is presented by Westlake & Wilson (2000) and Westlake et al. (2000). This technique provides the mapping of asymmetric sections and sections with large bulbous into a circle. The conformal mapping technique could prove useful when dealing with the transverse sections of damaged ships regarding hydrodynamic aspects. However, since strip theory description of hull form is not useful for damage stability this approach has not been considered for implementation in this research programme.

5.2 Frequency and Time Domain Approach

The frequency-domain method is a standard approach in seakeeping analysis. The frequency-domain approach provides steady state amplitudes under small perturbation assumptions. The steady state approach implies that the dynamic motions are linear and the loads acting on the structure oscillate harmonically with the same frequency as the waves exciting the structure. It is a useful preliminary design tool as it uses significantly less computational time than the time-domain approach.

An alternative way of dealing with the damaged and intact structure is to use a time-domain approach. Damage and the ingress of water into the compartments are continuous phenomena and they may be analysed in detail in time steps (see, for example, Chan et al. (2002) and Turan (1993)). In the frequency-domain method this time-dependence is not modelled.

In this study the question of whether optimised hulls are more vulnerable to damage than non-optimised hulls is to be addressed. Since the damage stability analysis outlined in Chapter 4 seeks a new static equilibrium state when ship is damaged, the frequency-domain approach is useful in providing steady state motions about this heeled and trimmed ship state. The time-domain approach would be considered useful when trying to understand how different the behaviour is in detail.

5.3 Justification of Selected Approach

Different theoretical and experimental investigations of intact and damaged ships have been reviewed. Frequency-domain approaches are simpler to apply in practice but yield steady state characteristics, whereas time-domain and experimental studies may yield details of how a steady state may or may not be achieved. Since the literature has not (so far) yielded any studies related to the impact of damage on initial conceived hull forms and subsequent optimised hull forms it is considered more prudent to follow the frequency-domain approach since, as Section 5.4 will reveal, some fundamental difficulties have to be overcome if the motions of the damaged ship are to be modelled so as to make comparison with the intact ship meaningful.

The aim of this research is to analyse the capability of optimised and non-optimised ships to withstand damage. As this will be analysed in the earlier stages of the design process when different alternative hull forms are considered the selected analysis method for predicting the hydrodynamic characteristics and hence motion responses of the intact and damaged structure should be relatively fast. Thus a wealth of experience may be gained regarding the damage stability of a new hull form design. Hence a frequency-domain approach will be considered in this study. The steady state situation for both intact and damaged structure will be analysed.

The water on deck problem is not analysed in this research, since the magnitude of the orientation of the vessel for the most probable damage to be expected does not expose the deck of the vessel to the free-surface of the water. When the selected methods are applied to the selected ship it will be found that sloshing within the ship is not an issue and the changes in behaviour are relatively subtle.

5.4 Motion Analysis

The motion responses of the damaged hull forms must be determined with greater structural (mechanical) cross-coupling than is usually adhered to the solution of the equations of motions of intact ships. This has necessitated the development of a novel approach to implement the calculation of the pure and product moments of inertia for the intact and damaged hull forms to facilitate meaningful comparisons of intact and damaged ship motions. This novel method is presented in Section 5.4.3.

The responses of a damaged structure cannot be evaluated with the two-dimensional strip theory approach, since the physics of the damage will not be captured well. Hence, the hydrodynamic and the motion analysis are carried out in three-dimensions.

5.4.1 Forces and Moments Acting on a Floating Ship in Waves

Forces and Moments Acting on an Intact Ship

The presence of the intact structure in wind-generated progressive regular & harmonic waves leads to the generation of diffracted waves by the hull. The incident and diffracted waves are responsible for the loading of the structure through the resulting wave excitation forces and moments.

As a consequence of the excitation the ship will respond and this will lead to the generation of ship radiation or reaction forces and moments due to the radiation waves generated. Furthermore, there will be restoring forces and moments of an Archimedean hydrostatic nature as well as the inertial forces and moments. All depend upon the shape and orientation of the ship.

Forces and Moments Acting on a Damaged Ship

When a ship is damaged, the water that flows into the damaged compartments causes static and dynamic effects. Static effects are due to the mass of water that is entrapped in the damaged compartment and so lead to changes in the mass distribution, centre of gravity and product of inertia of the vessel. The hydrodynamic effects of water entrapped within damaged compartment(s) are ignored because this would necessitate the modelling of the internal wetted surfaces in a manner consistent with conservation of total displaced ship volume.

When a ship is damaged; the wave excitation and the radiation forces and moments change due to the changes in the extent and orientation of the wetted surface area. The Archimedean restoring forces are altered due to the change in waterplane area, centre of gravity, centre of flotation, centre of buoyancy and displacement of the ship. Furthermore, the inertial characteristics of the hull form will change because the mass distribution for the damaged ship is different to the intact ship by virtue of mass orientation changes.

All these changes must be present in the equations of motion of the damaged ship.

5.4.2 The Equations of Motion

The equations of motion of an intact ship are generally simplified due to the port-starboard geometric symmetry of the ship. Since these simplifications will not generally exist when a ship is damaged the equations of motion presented next assume their most general form.

Equations of Motion for Intact Hull Forms

Having linearised the fluid-structure interaction analysis it is consistent to linearise the governing equations of motion. With the motion responses being harmonic, the six coupled second-order ordinary differential equations can be reduced to six coupled simultaneous algebraic equations. More details of the theory can be found in Salvesen et al. (1970), Newman (1978), Lewis (1989) and Faltinsen (1990).

When determining the heel and trim of the damaged ship the longitudinal centre of the intact waterplane is used as the origin of the right-handed Cartesian reference system. Here the origin of the motion reference system must be coincident with the earth fixed hydrodynamic reference system 'M' so that the motions and the forces and moments are described with respect to the same system. Since the motion/fluid-structure interaction system is generally chosen as a convenient point in the undisturbed free-surface it will not be coincident with the centre of gravity. Consequently, mechanical cross-coupling terms originating from the inertial forces through the centre of gravity will couple the translational and rotational degrees of freedom. Any lack of mass distribution symmetry will lead to non-zero products of inertia and this will lead to mechanical coupling between the rotational degrees of freedom.

Without being too specific at this point let M denote the origin with positive X to port, positive Y directed upwards and positive Z is directed toward the bow of the ship. M and its relationship with the longitudinal centre of the intact waterplane will be specified more definitively when applying the formulated equations of relative motion in Chapter 8.

The translatory displacements of surge (η_1), sway (η_2) and heave (η_3) of the ship are thus in the positive Z, X and Y directions. The angular displacements of roll (η_4), pitch (η_5) and yaw (η_6) are right handed rotations about the Z, X and Y axes respectively as illustrated in Figure 5.1.

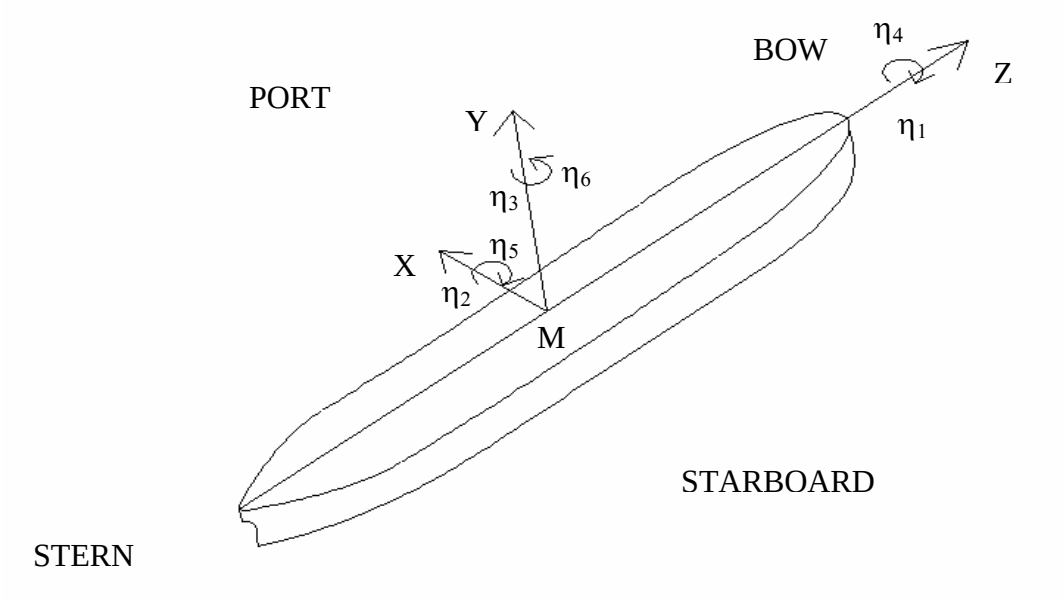

Figure 5.1: The motion-hydrodynamic Cartesian coordinate reference system.

The six linear coupled differential equations of motion for an intact hull can be written as:

$$\sum_{j=1}^{6}\left[\left(M_{kj}+A_{kj}\right)\ddot{\eta}_j+B_{kj}\dot{\eta}_j+C_{kj}\eta_j\right]=F_k \;:\; k\;=\;1,....,6 \tag{5.1}$$

The generalised mass matrix $\left[M_{kj}\right]$ elements are defined in Equation (5.2). The elements of $\left[A_{kj}\right]$ and $\left[B_{kj}\right]$ are the added mass and fluid damping coefficients for reactions in the kth direction arising from the ship motion in the jth direction. The restoration matrix $\left[C_{kj}\right]$ elements are the hydrostatic restoring force/moment coefficients for reactions in the kth direction arising from the ship motion in the jth direction. This is defined in Equation (5.3). The time-dependent wave excitation complex amplitudes are denoted by F_1, F_2 and F_3 denoting surge, sway and heave

wave exciting forces and F_4, F_5 and F_6 corresponding to roll, pitch and yaw wave exciting moments. ω is the wave circular frequency and η_j is the j[th] time-dependent displacement of the ship. Finally, $\ddot{\eta}_j$ is the acceleration and $\dot{\eta}_j$ is the velocity of the ship in the j[th] degree of freedom. Clearly subscripts j and k assume the values 1 to 6.

$$\left[M_{kj}\right]=\begin{bmatrix} M & 0 & 0 & 0 & -MY_G & MX_G \\ 0 & M & 0 & MY_G & 0 & -MZ_G \\ 0 & 0 & M & -MX_G & MZ_G & 0 \\ 0 & MY_G & -MX_G & \int\left(X_m{}^2+Y_m{}^2\right)dm & -\int X_mZ_m dm & -\int Y_mZ_m dm \\ -MY_G & 0 & MZ_G & -\int X_mZ_m dm & \int\left(Z_m{}^2+Y_m{}^2\right)dm & -\int X_mY_m dm \\ MX_G & -MZ_G & 0 & -\int Y_mZ_m dm & -\int X_mY_m dm & \int\left(X_m{}^2+Z_m{}^2\right)dm \end{bmatrix} \tag{5.2}$$

Clearly, irrespective of the geometric properties of the ship the generalised mass matrix $\left[M_{kj}\right]$ is symmetric.

$$\left[C_{kj}\right]=\begin{bmatrix} 0 & 0 & 0 & 0 & 0 & 0 \\ 0 & 0 & 0 & 0 & 0 & 0 \\ 0 & 0 & \rho_s gA_{wps} & \rho_s gA_{wps}X_C & \rho_s gA_{wps}Z_C & 0 \\ 0 & 0 & \rho_s gA_{wps}X_C & -g\Delta Y_G+\rho_s g\nabla Y_B+\rho_s gI_{XX} & -\rho_s gI_{XZ} & 0 \\ 0 & 0 & \rho_s gA_{wps}Z_C & -\rho_s gI_{XZ} & -g\Delta Y_G+\rho_s g\nabla Y_B+\rho_s gI_{ZZ} & 0 \\ 0 & 0 & 0 & 0 & 0 & 0 \end{bmatrix} \tag{5.3}$$

The restoring coefficient matrix $\left[C_{kj}\right]$ is also symmetric irrespective of shape of structure.

In the generalised mass matrix formulation $\left[M_{kj}\right]$; M is the mass of the ship, $\left(X_G, Y_G, Z_G\right)$ are the centre of gravity coordinates of the ship. The notation used assumes the centre of gravity coordinates of the intact ship are positive, but there is no loss of generality as the actual values (negative or positive) are provided once an application is to be undertaken. $\left(X_m, Y_m, Z_m\right)$ denotes the coordinates of the elemental ship mass dm.

Within the stiffness matrix $\left[C_{kj}\right]$; $\left(X_C, Y_C, Z_C\right)$ is the centre of flotation coordinates, g is the acceleration due to gravity and ρ_s is the density of sea water. Δ is the displaced mass of the ship, ∇ is the displaced volume of the ship and Y_B is the vertical coordinate of the centre of buoyancy. The moments of inertia I_{XX}, I_{ZZ} and I_{XZ} included in the stiffness matrix $\left[C_{kj}\right]$ are related to the moments of inertia in the generalised mass matrix $\left[M_{kj}\right]$ as follows:

$$I_{44} \equiv I_{ZZ} = \int \left({X_m}^2 + {Y_m}^2 \right) dm \tag{5.4}$$

$$I_{55} \equiv I_{XX} = \int \left({Z_m}^2 + {Y_m}^2 \right) dm \tag{5.5}$$

$$I_{66} \equiv I_{YY} = \int \left({X_m}^2 + {Z_m}^2 \right) dm \tag{5.6}$$

$$I_{45} \equiv I_{ZX} = -\int X_m Z_m dm = I_{XZ} \equiv I_{54} \tag{5.7}$$

$$I_{46} \equiv I_{ZY} = -\int Y_m Z_m dm = I_{YZ} \equiv I_{64} \tag{5.8}$$

$$I_{56} \equiv I_{XY} = -\int X_m Y_m dm = I_{YX} \equiv I_{65} \tag{5.9}$$

The displacement of the ship and the wave excitation loads can respectively be written in the form

$$\eta_j = \eta_{ja}\, \mathrm{e}^{-i\omega t} \equiv \left(\eta_{\mathrm{jr}} + i\eta_{ji}\right) e^{-i\omega t} \tag{5.10}$$

$$F_k = F_{ka}\, \mathrm{e}^{-i\omega t} \equiv \left(F_{\mathrm{kr}} + iF_{ki}\right) e^{-i\omega t} \tag{5.11}$$

because there is a phase shift between the incident waves and the ship reactions and excitation loads.

The equations of motion for translations can be written as follows:

$$M\ddot{\eta}_1 = F_1 - \sum_{j=1}^{6}\left(A_{1j}\ddot{\eta}_j + B_{1j}\dot{\eta}_j\right) - \left(-MY_G\ddot{\eta}_5 + MX_G\ddot{\eta}_6\right) \tag{5.12}$$

$$M\ddot{\eta}_2 = F_2 - \sum_{j=1}^{6}\left(A_{2j}\ddot{\eta}_j + B_{2j}\dot{\eta}_j\right) - \left(MY_G\ddot{\eta}_4 - MZ_G\ddot{\eta}_6\right) \tag{5.13}$$

$$M\ddot{\eta}_3 = F_3 - \sum_{j=1}^{6}\left(A_{3j}\ddot{\eta}_j + B_{3j}\dot{\eta}_j\right) - \sum_{\mathrm{j=3,4,5}} \mathrm{C}_{3\mathrm{j}}\eta_j - \left(-MX_G\ddot{\eta}_4 + MZ_G\ddot{\eta}_5\right) \tag{5.14}$$

In the case of no symmetry of mass distribution the rotational equations of motion are written:

$$\begin{aligned} I_{44}\ddot{\eta}_4 + I_{45}\ddot{\eta}_5 + I_{46}\ddot{\eta}_6 = F_4 &- \sum_{j=1}^{6}\left(A_{4j}\ddot{\eta}_j + B_{4j}\dot{\eta}_j\right) - \sum_{j=3,4,5} C_{4j}\eta_j \\ &- \left(MY_G\ddot{\eta}_2 - MX_G\ddot{\eta}_3\right) \end{aligned} \tag{5.15}$$

$$I_{54}\ddot{\eta}_4 + I_{55}\ddot{\eta}_5 + I_{56}\ddot{\eta}_6 = F_5 - \sum_{j=1}^{6}\left(A_{5j}\ddot{\eta}_j + B_{5j}\dot{\eta}_j\right) - \sum_{j=3,4,5} C_{5j}\eta_j - \left(-MY_G\ddot{\eta}_1 + MZ_G\ddot{\eta}_3\right) \quad (5.16)$$

$$I_{64}\ddot{\eta}_4 + I_{65}\ddot{\eta}_5 + I_{66}\ddot{\eta}_6 = F_6 - \sum_{j=1}^{6}\left(A_{6j}\ddot{\eta}_j + B_{6j}\dot{\eta}_j\right) - \left(MX_G\ddot{\eta}_1 - MZ_G\ddot{\eta}_2\right) \quad (5.17)$$

Equations of Motion for Damaged Hull Forms

The responses of a ship in waves are expected to change when damage occurs for a number of reasons. There will be coupling between the rotational and translational degrees of freedom whenever the damage leads to a modified orientation of the ship as a result of heel and trim. That is, any geometric symmetry present in the intact ship will no longer exist in the damaged ship. Furthermore, when a hull form is damaged, its centre of gravity and its mass distribution may change due to the water entering via the damaged area or due to structural weight loss. Damage may destroy the original waterplane area and this will cause buoyancy loss.

In order to recover the buoyancy loss and/or the additional weight (due to the water flooded into the damaged compartment) and/or structural weight loss, the vessel will in general undergo parallel sinkage, trim and/or heel.

The six linear coupled differential equations of motion for a damaged hull can be written as;

$$\sum_{j=1}^{6}\left[\left(M'_{kj} + A'_{kj}\right)\ddot{\eta}'_j + B'_{kj}\dot{\eta}'_j + C'_{kj}\eta'_j\right] = F'_k \;:\; k = 1,....,6 \quad (5.18)$$

where F_k' are the time-dependent wave exciting forces and moments for the damaged ship, η_j' is the time-dependent displacement of the damaged ship and hence $\ddot{\eta}_j'$ and $\dot{\eta}_j'$ are the acceleration and the velocity of the damaged ship in the j[th] degree of freedom.

Clearly new values of the hydrodynamic characteristics for the damaged ship $\left[A_{kj}'\right]$, $\left[B_{kj}'\right]$ and F_k' must be calculated. The contents of the generalised mass matrix $\left[M_{kj}'\right]$ will change due to extra and differently evaluated terms for the damaged case. Water ingress into the damaged ship will have the following effects:

- Change of the original total mass of the ship due to both ingressed mass of water and structural mass loss.

- The centre of gravity of the damaged ship is likely to be in a different position to that of the intact ship.

- The structural mass distribution within the ship will lead to different moment of inertia properties due to orientation of intact ship and its original mass and mass gains/losses cited.

The hydrostatic restoring coefficients $\left[C_{kj}'\right]$ will change due to new centre of flotation for damaged ship, modified still water waterplane area and the change in centre of buoyancy because of different transverse sectional area distribution as orientation of the ship changes.

The generalised mass matrix $\left[M_{kj}'\right]$ and the stiffness matrix $\left[C_{kj}'\right]$ are given by:

$$\left[M'_{kj}\right]=\begin{bmatrix} M+m_w & 0 & 0 \\ 0 & M+m_w & 0 \\ 0 & 0 & M+m_w \\ 0 & \left(M+m_w\right)Y'_G & -\left(M+m_w\right)X'_G \\ -\left(M+m_w\right)Y'_G & 0 & \left(M+m_w\right)Z'_G \\ \left(M+m_w\right)X'_G & -\left(M+m_w\right)Z'_G & 0 \end{bmatrix}$$

$$\begin{bmatrix} 0 & -\left(M+m_w\right)Y'_G & \left(M+m_w\right)X'_G \\ \left(M+m_w\right)Y'_G & 0 & -\left(M+m_w\right)Z'_G \\ -\left(M+m_w\right)X'_G & \left(M+m_w\right)Z'_G & 0 \\ \int\left(X'^{\,2}_m+Y'^{\,2}_m\right)dm+\int\left(X^2_w+Y^2_w\right)dm' & -\int X'_mZ'_m dm-\int X_wZ_w dm' & -\int Y'_mZ'_m dm-\int Y_wZ_w dm' \\ -\int X'_mZ'_m dm-\int X_wZ_w dm' & \int\left(Z'^{\,2}_m+Y'^{\,2}_m\right)dm+\int\left(Z^2_w+Y^2_w\right)dm' & -\int X'_mY'_m dm-\int X_wY_w dm' \\ -\int Y'_mZ'_m dm-\int Y_wZ_w dm' & -\int X'_mY'_m dm-\int X_wY_w dm' & \int\left(X'^{\,2}_m+Z'^{\,2}_m\right)dm+\int\left(X^2_w+Z^2_w\right)dm' \end{bmatrix}$$

(5.19)

$$\left[C'_{kj}\right]=\begin{bmatrix} 0 & 0 & 0 & 0 & 0 & 0 \\ 0 & 0 & 0 & 0 & 0 & 0 \\ 0 & 0 & \rho_s gA'_{wps} & \rho_s gA'_{wps}X'_C & \rho_s gA'_{wps}Z'_C & 0 \\ 0 & 0 & \rho_s gA'_{wps}X'_C & -g\Delta'Y'_G+\rho_s g\nabla'Y'_B+\rho_s gI'_{XX} & -\rho_s gI'_{XZ} & 0 \\ 0 & 0 & \rho_s gA'_{wps}Z'_C & -\rho_s gI'_{XZ} & -g\Delta'Y'_G+\rho_s g\nabla'Y'_B+\rho_s gI'_{ZZ} & 0 \\ 0 & 0 & 0 & 0 & 0 & 0 \end{bmatrix}$$

(5.20)

The hydrodynamic and hydrostatic quantities used for the intact and damaged ships must be calculated to reflect the geometry of the ship. In the damaged case there is a total lack of geometric symmetry. Within Equations (5.18), (5.19) & (5.20) the superscript prime indicates that values to be used relate to the damaged ship. The additional notation, associated with these equations, that needs to be defined are as follows:

- m_w is either mass of ingressed water in the damaged compartment(s), or structural mass loss or a combination of both

- dm' is the elemental mass of ingressed water, or structural loss or a combination of both at location $\left(X_w, Y_w, Z_w\right)$.

The basic displacement and wave excitation relationships and the equations of motion of the damaged ship can be written in an analogue from the intact ship equations:

$$\eta'_j = \eta'_{ja}\, \mathrm{e}^{-i\omega t} \equiv \left(\eta'_{\mathrm{jr}} + i\eta'_{ji}\right) e^{-i\omega t} \tag{5.21}$$

$$F'_k = F'_{ka}\, \mathrm{e}^{-i\omega t} \equiv \left(F'_{kr} + iF'_{ki}\right) e^{-i\omega t} \tag{5.22}$$

$$\left(M + m_w\right)\ddot{\eta}'_1 = F'_1 - \sum_{j=1}^{6}\left(A'_{1j}\ddot{\eta}'_j + B'_{1j}\dot{\eta}'_j\right) - \left(-\left(M + m_w\right)Y'_G\ddot{\eta}'_5 + \left(M + m_w\right)X'_G\ddot{\eta}'_6\right) \tag{5.23}$$

$$\left(M + m_w\right)\ddot{\eta}'_2 = F'_2 - \sum_{j=1}^{6}\left(A'_{2j}\ddot{\eta}'_j + B'_{2j}\dot{\eta}'_j\right) - \left(\left(M + m_w\right)Y'_G\ddot{\eta}'_4 - \left(M + m_w\right)Z'_G\ddot{\eta}'_6\right) \tag{5.24}$$

$$\begin{aligned}\left(M + m_w\right)\ddot{\eta}'_3 = F'_3 - \sum_{j=1}^{6}\left(A'_{3j}\ddot{\eta}'_j + B'_{3j}\dot{\eta}'_j\right) - \sum_{\mathrm{j}=3,4,5} \mathrm{C}'_{3\mathrm{j}}\eta'_j \\ -\left(-\left(M + m_w\right)X'_G\ddot{\eta}'_4 + \left(M + m_w\right)Z'_G\ddot{\eta}'_5\right)\end{aligned} \tag{5.25}$$

$$\begin{aligned}I'_{44}\ddot{\eta}'_4 + I'_{45}\ddot{\eta}'_5 + I'_{46}\ddot{\eta}'_6 = F'_4 - \sum_{j=1}^{6}\left(A'_{4j}\ddot{\eta}'_j + B'_{4j}\dot{\eta}'_j\right) - \sum_{j=3,4,5} C'_{4j}\eta'_j \\ -\left((M + m_w)Y'_G\ddot{\eta}'_2 - (M + m_w)X'_G\ddot{\eta}'_3\right)\end{aligned} \tag{5.26}$$

$$I'_{54}\ddot{\eta}'_4 + I'_{55}\ddot{\eta}'_5 + I'_{56}\ddot{\eta}'_6 = F'_5 - \sum_{j=1}^{6}\left(A'_{5j}\ddot{\eta}'_j + B'_{5j}\dot{\eta}'_j\right) - \sum_{j=3,4,5} C'_{5j}\eta'_j \\ -\left(-(M+m_w)Y'_G\ddot{\eta}'_1 + (M+m_w)Z'_G\ddot{\eta}'_3\right) \tag{5.27}$$

$$I'_{64}\ddot{\eta}'_4 + I'_{65}\ddot{\eta}'_5 + I'_{66}\ddot{\eta}'_6 = F'_6 - \sum_{j=1}^{6}\left(A'_{6j}\ddot{\eta}'_j + B'_{6j}\dot{\eta}'_j\right) \\ -\left((M+m_w)X'_G\ddot{\eta}'_1 - (M+m_w)Z'_G\ddot{\eta}'_2\right) \tag{5.28}$$

Having highlighted in this section that ship motions will change with damage, it is now necessary to consider in greater detail the evaluation of the pure moments and products of inertia for the damaged case.

It is quite common in the motion studies of intact ships to exploit the port-starboard geometric symmetry that exists and the further simply the analysis by assuming (often without any real justification, other than difficulty of specification) that the products of inertia are zero. However, even if this is the case the products of inertia are unlikely to be zero in the case of the damaged ship; hence their values must be estimated in some consistent fashion with the physics that persist in the intact ship case. The challenge is tackled next in the following section.

5.4.3 A Novel Method for Determining the Products of Inertia for Intact and Damaged Ship

The Intact Ship

The mass moment of inertia calculations for the intact ship are usually undertaken subject to the implicit assumption of port-starboard and/or fore-aft symmetry of the ship mass. This results in zero valued products of inertia of the ship. However, this is not the case for the damaged hull form, even if the ship in its intact form displayed such mass

symmetry. The water flooding into the damaged compartment(s), the structural loss occurred in the damaged part of the ship and the change of the distances of the unit masses forming the actual mass of the ship will affect the mass products of inertia. Consequently, the assumed symmetry of the mass with respect to the M_Z and M_X axes defined in Figure 5.2(a) will no longer exist.

To assist with the task of determining how the products of inertia have changed from their zero intact ship values to their non-zero damaged ship values, the actual total mass of the ship is regarded as being composed of the four representative point masses M_{AP}, M_{FP}, M_{AS} and M_{FS} defined in Figure 5.2(a) with respect to the earth-fixed right-handed coordinate system M_{XYZ}.

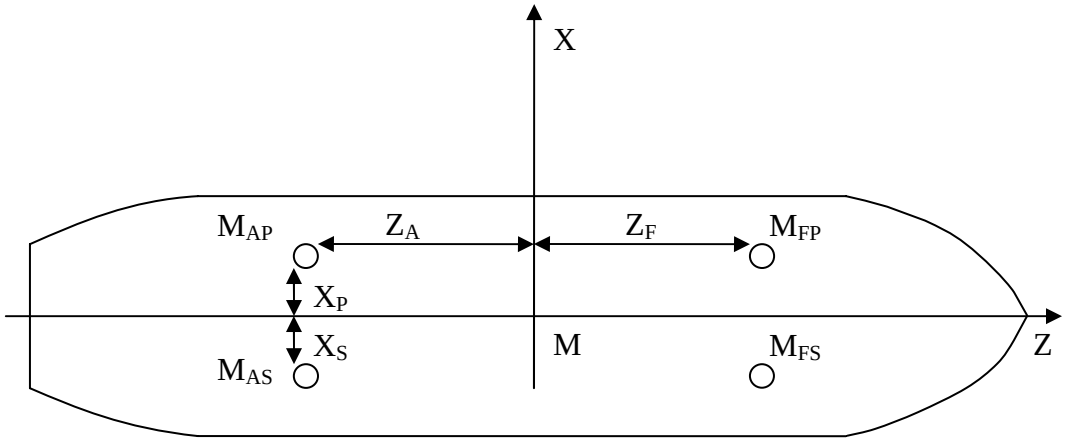

(a) Plan view

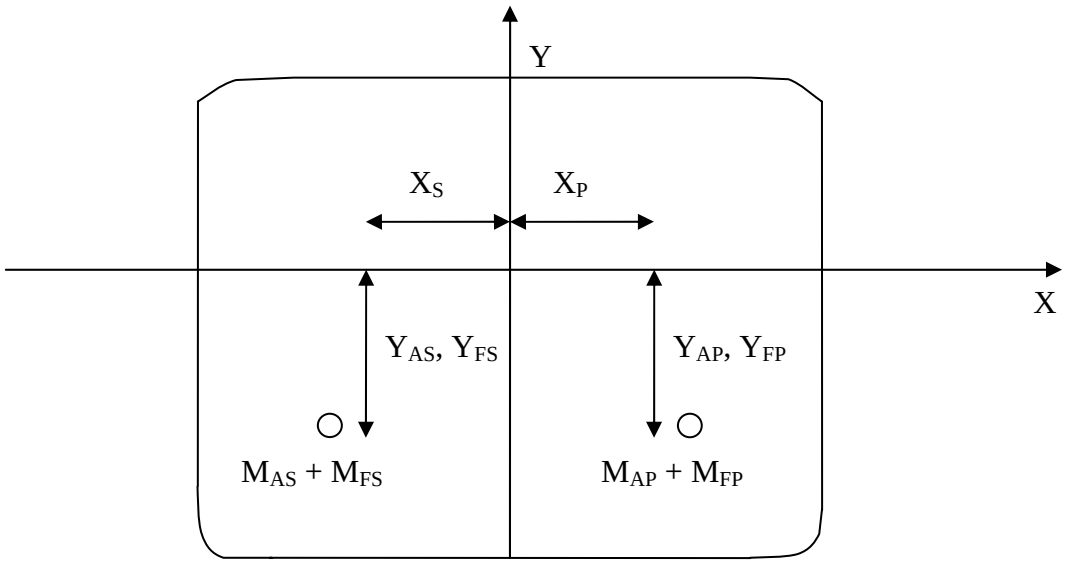

(b) Transverse view

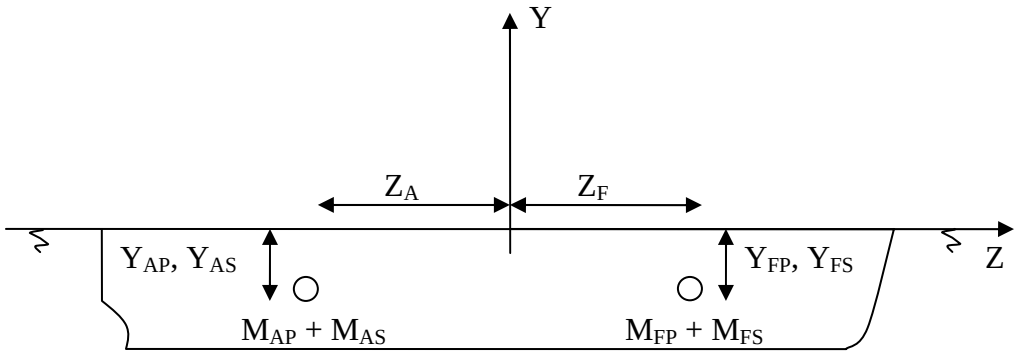

(c) Side view

Figure 5.2: Total mass of the ship represented as four equivalent point masses.

Irrespective of the geometry and thus the condition of the ship (intact or damaged), the product of inertias are symmetric; that is, $I_{45} = I_{54}$, $I_{56} = I_{65}$ and $I_{46} = I_{64}$ (see, for

example, Housner and Hudson (1966)). Using the point mass equivalence illustrated in Figure 5.2(a) it follows that;

$$I_{45} = M_{AP} Z_A X_P + M_{FP} Z_F X_P + M_{AS} Z_A X_S + M_{FS} Z_F X_S \,. \tag{5.29}$$

The right hand side of the Equation (5.29) can be equated to zero only if:

$$M_{FP} = M_{FS}$$

and

$$M_{AP} = M_{AS} \tag{5.30}$$

subject to $X_S = -X_P$.

That is, irrespective of the relationship between Z_A and Z_F, port-starboard symmetry of mass forward and aft of the midship section implies that $I_{45} = I_{54} = 0$.

Similarly, on appealing to Figure 5.2(b), it may be argued that:

$$I_{56} = M_{AS} Y_{AS} X_S + M_{FS} Y_{FS} X_S + M_{AP} Y_{AP} X_P + M_{FP} Y_{FP} X_P \,. \tag{5.31}$$

The port-starboard symmetry assumptions of Equation (5.30) for the intact ship mass distribution imply that:

$$I_{56} = M_{AS} X_S \left(Y_{AS} - Y_{AP} \right) + M_{FS} X_S \left(Y_{FS} - Y_{FP} \right). \tag{5.32}$$

Clearly, M_{AS} and M_{FS} are positive quantities, X_S is non-zero and port-starboard symmetry of the mass also means that $Y_{AS} = Y_{AP}$ and $Y_{FS} = Y_{FP}$. That is, port-starboard symmetry of the mass implies that $I_{45} = I_{54} = 0$ and $I_{56} = I_{65} = 0$.

Thus assuming that port-starboard geometric symmetry implies port-starboard mass symmetry, one can readily appreciate that four of the cross-products are zero valued. This is a common assumption when solving the equations of motion of an intact floating structure.

Next, the implications of assuming $I_{46} = I_{64} = 0$ are considered with the aid of Figure 5.2(c). The products of inertia I_{46} may be written in the form:

$$I_{46} = M_{AP} Z_A Y_{AP} + M_{AS} Z_A Y_{AS} + M_{FP} Z_F Y_{FP} + M_{FS} Z_F Y_{FS} . \tag{5.33}$$

By writing M_A for $\left(M_{AP} + M_{AS}\right)$ and M_F for $\left(M_{FP} + M_{FS}\right)$ it follows that:

$$I_{46} = M_A Z_A Y_{AS} + M_F Z_F Y_{FS} . \tag{5.34}$$

If I_{46} is to be assumed zero for the intact case, Equation (5.34) suggests two possibilities. Either the ship may have a fore-aft mass symmetry, which is not the case for most of the ships, or there should be a relationship between Y_{AS} and Y_{FS} to make the equation equal to zero. However, since the aft mass (M_A located at Z_A) and the forward mass (M_F located at Z_F) must be in equilibrium about the centre of gravity, it follows that $M_A Z_A + M_F Z_F = 0$ since Z_A and Z_F are of opposite sign. Hence from Equation (5.34) it follows that $Y_{AS} = Y_{FS}$.

With M equal to the total mass and k_{YY} denoting the radius of gyration (see, for example, Peach & Brook (1987)), I_{66} is usually expressed as:

$$I_{66} = M\ k_{YY}^2 \text{ subject to } k_{YY} \text{ lying in the range } 0.2 \text{ to } 0.25L\,, \tag{5.35}$$

where L is the length between perpendiculars of the ship.

I_{66} may also be written, upon appealing to Figure 5.2(a), in the form:

$$\begin{aligned} I_{66} = {} & M_{AP}\left(Z_A^2 + X_P^2\right) + M_{FP}\left(Z_F^2 + X_P^2\right) + M_{AS}\left(Z_A^2 + X_S^2\right) \\ & + M_{FS}\left(Z_F^2 + X_S^2\right) \end{aligned} \tag{5.36}$$

Upon adopting notation of Equation (5.30) for summing constituent masses Equation (5.36) may be written as:

$$I_{66} = M_A\left(Z_A^2 + X_P^2\right) + M_F\left(Z_F^2 + X_P^2\right). \tag{5.37}$$

Equating Equations (5.35) and (5.37) and assuming the veracity of Equation (5.35) then

$$M_A\left(Z_A^2 + X_P^2\right) + M_F\left(Z_F^2 + X_P^2\right) = \left(M_A + M_F\right) \times k_{YY}^2\,. \tag{5.38}$$

Since the details of the longitudinal mass distribution is usually more readily available than the transverse distribution of the mass, it is reasonable to assume that Z_A, Z_F, M_A and M_F are known. Hence, Equation (5.38) can be used to determine X_P.

Similarly, I_{44} can be approximated by the formula (see, for example, Peach & Brook (1987));

$$I_{44} = M\ k_{ZZ}^2 \text{ with } k_{ZZ} \text{ assuming values in the range } 0.35 \text{ to } 0.41\,B\,, \qquad (5.39)$$

where B is the beam of the ship.

I_{44} can also be written, upon appealing to Figure 5.2(b), as:

$$\begin{aligned} I_{44} = {} & M_{AS}\left(X_S^2 + Y_{AS}^2\right) + M_{FS}\left(X_S^2 + Y_{FS}^2\right) + M_{AP}\left(X_P^2 + Y_{AP}^2\right) \\ & + M_{FP}\left(X_P^2 + Y_{FP}^2\right). \end{aligned} \qquad (5.40)$$

Again using Equation (5.30), with $Y_{AS} = Y_{AP}$ and $Y_{FS} = Y_{FP}$ and equating Equations (5.39) and (5.40) leads to:

$$M_A\left(X_S^2 + Y_{AS}^2\right) + M_F\left(X_S^2 + Y_{FS}^2\right) = M \times k_{ZZ}^2\,. \qquad (5.41)$$

With X_S assumed known then

$$M_A Y_{AS}^2 + M_F Y_{FS}^2 = M \times k_{ZZ}^2 - M X_S^2\,. \qquad (5.42)$$

Thus both equations (5.34) and (5.42) provide a relationship between Y_{AS} and Y_{FS}.

I_{55} can also approximated by the formula (see, for example, Peach & Brook (1987)):

$$I_{55} = M\ k_{XX}^2 \text{ with } k_{XX} \text{ in the range } 0.2 \text{ to } 0.25\,L\,. \qquad (5.43)$$

Finally, I_{55} can also be written in the form:

$$I_{55} = M_{AP}\left(Z_A^2 + Y_{AP}^2\right) + M_{AS}\left(Z_A^2 + Y_{AS}^2\right) + M_{FP}\left(Z_F^2 + Y_{FP}^2\right) + M_{FS}\left(Z_F^2 + Y_{FS}^2\right). \tag{5.44}$$

Again using Equation (5.30) with the equivalence of Equations (5.43) and (5.44) yields the expression:

$$M_A\left(Z_A^2 + Y_{AS}^2\right) + M_F\left(Z_F^2 + Y_{FS}^2\right) = M \times k_{XX}^2 . \tag{5.45}$$

Since Z_A, Z_F, M_A and M_F are known from a knowledge of the longitudinal mass distribution (whether it is from actual data or an assumed Coffin diagram), Equation (5.45) provides a third relationship between Y_{AS} and Y_{FS}. Hence, from equations (5.34) and (5.42) or (5.45), Y_{AS} and Y_{FS} can be evaluated as there are two unknowns and three independent equations.

In particular, from Equation (5.45) it follows that:

$$M_A Y_{AS}^2 + M_F Y_{\mathrm{FS}}^2 = M \times k_{YY}^2 - \left(M_A Z_A^2 + M_F Z_F^2\right). \tag{5.46}$$

Having already deduced from Equation (5.34) the condition for $I_{46} = 0$:

$$Y_{AS} = -\left(\frac{M_F Z_F}{M_A Z_A}\right) \times Y_{FS} = Y_{FS} . \tag{5.47}$$

Y_{AS} and Y_{FS} can be readily determined from Equation (5.46). Hence the total intact ship mass may be readily equated to four point masses with determinable locations consistent with the practice of assuming zero intact ship cross-products. Applications of these equations are provided in Appendix C for the parent Derbyshire and a tanker hull form.

The Damaged Ship

Having indicated how the four equivalent point masses are to be positioned such that moments of inertias are assigned in a conventional manner and the cross-products are zero the next step is to determine the position of these equivalent point masses when the ship is in its damaged position and to identify any mass difference that might exist between the intact ship and the damaged ship. This information will allow the non-zero cross-products to be determined for the damaged ship.

In Section 4.3 a method was described to determine the orientation of the damaged ship once the consequences of the damage were known in terms of water ingress and structural mass loss. The assignment of the location of the damage and its extent will clearly influence the subsequent hydrodynamic and motion analysis of the damaged ship and thus any conclusions drawn. Assignment of damage position and extent will be based upon statistical damage data presented and discussed in Chapter 3. By using the outcome of Chapter 3, the likely changes in mass between the intact and damaged ship can be considered in this section. The damage for the selected ship is most likely to occur in the forward area of the ship (see Section 3.1) and given the mass distribution assumptions inherent in the intact ship analysis one may choose either the port or starboard side.

With this assumption it follows that the damaged ship masses satisfy

$$M'_{FS} = M_{FS} + m_w,\ M'_{AP} = M_{AP},\ M'_{FP} = M_{FP},\ M'_{AS} = M_{AS}. \qquad (5.48)$$

The location of the four damaged distinct point masses change as the ship experiences parallel sinkage (Y_{SINK}), trim (ϕ) and heel (θ) as illustrated in Figures 5.3 & 5.4. The original coordinates for M_{AP} were Z_A, X_P and Y_{AP} and after the ship orientation change they become:

$$Z'_A = Z_A \cos\phi - \sin\phi\left(Y_{AP} - Y_{SINK}\right) \tag{5.49}$$

$$X'_P = Z_A \sin\theta\sin\phi + X_P \cos\theta + \sin\theta\cos\phi\left(Y_{AP} - Y_{SINK}\right) \tag{5.50}$$

and

$$Y'_{AP} = Z_A \cos\theta\sin\phi - X_P \sin\theta + \cos\theta\cos\phi\left(Y_{AP} - Y_{SINK}\right). \tag{5.51}$$

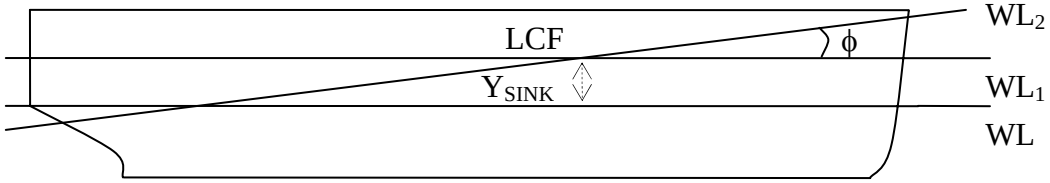

Figure 5.3: Description of the trim angle and parallel sinkage.

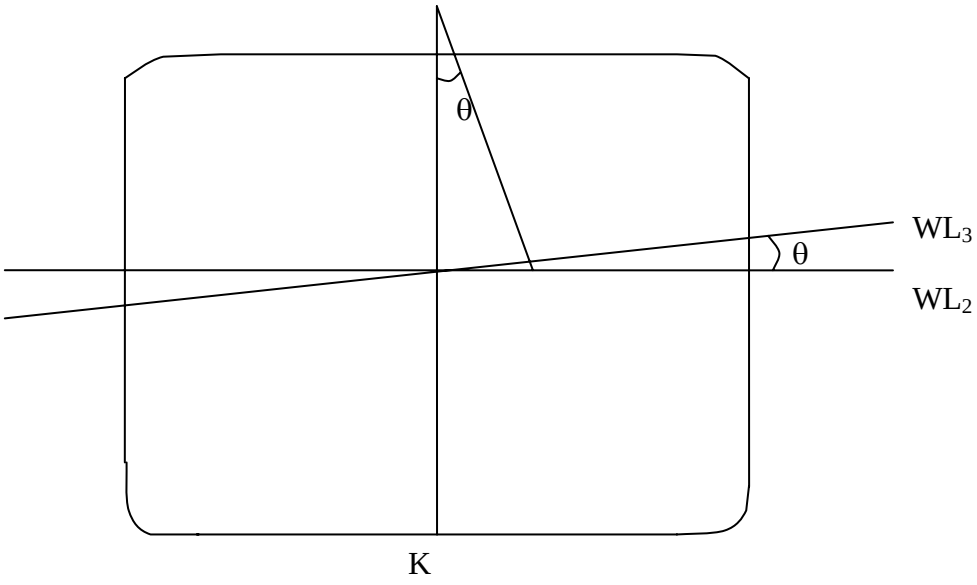

Figure 5.4: Description of the heel angle.

In the Figures 5.3 & 5.4 WL, WL_1, WL_2 and WL_3 stand for the waterlines for the initial intact ship position, after parallel sinkage, after parallel sinkage & ship trimming and after parallel sinkage & ship trimming & ship heeling respectively.

Similarly the coordinates for M_{AS} in the intact condition were Z_A, X_S and Y_{AS} and they become:

$$Z_A'' = Z_A \cos\phi - \sin\phi\left(Y_{AS} - Y_{SINK}\right) \tag{5.52}$$

$$X_S' = Z_A \sin\theta\sin\phi + X_S \cos\theta + \sin\theta\cos\phi\left(Y_{AS} - Y_{SINK}\right) \tag{5.53}$$

$$Y_{AS}' = Z_A \cos\theta\sin\phi - X_S \sin\theta + \cos\theta\cos\phi\left(Y_{AS} - Y_{SINK}\right). \tag{5.54}$$

That is, Equations (5.49) to (5.51) with X_P and Y_{AP} replaced by X_S and Y_{AS} respectively.

The coordinates $\left(Z_F, X_P, Y_{FP}\right)$ for M_{FP} in the intact condition become:

$$Z_F' = Z_F \cos\phi - \sin\phi\left(Y_{FP} - Y_{SINK}\right) \tag{5.55}$$

$$X_P'' = Z_F \sin\theta\sin\phi + X_P \cos\theta + \sin\theta\cos\phi\left(Y_{FP} - Y_{SINK}\right) \tag{5.56}$$

$$Y_{FP}' = Z_F \cos\theta\sin\phi - X_P \sin\theta + \cos\theta\cos\phi\left(Y_{FP} - Y_{SINK}\right) \tag{5.57}$$

As expected X_P'' of Equation (5.56) is identical in form with X_P' of Equation (5.50) with Z_A replaced with Z_F and Y_{AP} replaced with Y_{FP}. Finally for M_{FS} the original coordinates $\left(Z_F, X_S, Y_{FS}\right)$ are transformed to:

$$Z_F'' = Z_F \cos\phi - \sin\phi\left(Y_{FS} - Y_{SINK}\right) \equiv Z_F' \tag{5.58}$$

$$X_S'' = Z_F \sin\theta\sin\phi + X_S \cos\theta + \sin\theta\cos\phi\left(Y_{FS} - Y_{SINK}\right) \tag{5.59}$$

which is similar to X_S' with Z_A replaced with Z_F and Y_{AS} replaced with Y_{FS}.

$$Y_{FS}' = Z_F \cos\theta\sin\phi - X_S \sin\theta + \cos\theta\cos\phi\left(Y_{FS} - Y_{SINK}\right). \tag{5.60}$$

With the equivalent point masses and their new positions known the damaged ship's pure and product moment of inertias can be readily determined.

5.4.4 Determination of Motion Characteristics

The hydrodynamic coefficients, the hydrostatic restoring coefficients and the wave excitation forces and moments for the intact ship and damaged ship are evaluated using the Matthew Diffraction Suite. The motion characteristics for the intact and damaged ship for its basis hull form and optimised hull forms are determined using the Motion code of the author (see Saydan (2003)).

The Motion code solves the linear equations of motions in their most general form. That is, a set of six linear coupled equations symbolised by:

$$\left[A\right]\vec{\eta} = \vec{F}, \tag{5.61}$$

where $\left[A\right]$ includes the generalised masses, the added masses, the fluid damping and hydrostatic restoring coefficients indicated in Equation (5.1) and specified in Equation

(5.2) & (5.3). $\vec{\eta}$ is the displacement vector for the six degrees of freedom (surge, sway, heave, roll, pitch and yaw) and $\vec{F}$ contains the wave exciting forces and moments.

The linear algebraic simultaneous equation formulated may be solved analytically by using Cramer's rule (see Greenberg (1998)) to derive mathematical expressions for each degree of freedom. Alternatively one may use classical numerical methods such as the Gaussian Elimination method (see Greenberg (1998)) whereby $[A]$ is reduced to upper triangle form and the complex amplitudes for each degree of freedom determined from back substitution (see Greenberg (1998)). Equivalently $[A]$ can be reduced to the unit matrix to provide the motion amplitudes directly.

To cross check the solutions determined in the intact and damaged case the numerically solved solutions $\vec{\eta}$ and the original coefficient matrix $[A]$ are multiplied to cross check equality of $\vec{F}$ so calculated and $\vec{F}$ provided originally. Furthermore, since for the intact ship (surge, heave and pitch) and (sway, roll and yaw) are independent Cramer's rule can be used for each three degrees of freedom system to compare with numerically derived solutions.

5.4.5 Discussion

The forces acting on an intact ship and a damaged ship have been discussed in Section 5.4.1 together with the changes in the governing equations of motion for an intact and a damaged structure (see Section 5.4.2). The equations of motion are written in their most general form for both cases.

The variations in the equations of motion due to the damage (discussed in Section 5.4.2) are valid for damage cases below and at the waterline. For damage cases analysed in this study, the damage is modelled as a change in mass distribution in the damaged

region. This causes some changes in the added mass coefficients, the damping coefficients and the wave excitation forces since the damage changes the orientation of the wetted surface area of the ship. The hydrostatic restoring coefficients vary as the damage changes the displacement weight and the centre of gravity of the ship.

The hydrodynamic coefficients addressing the intact and damaged original ship hull form and its optimised intact and damaged hull forms are presented in Chapter 7 and Appendix H. The relative vertical motion responses for the original intact and damaged ship and for its optimised intact and damaged hull form are plotted in Chapter 8 and Appendix J.

Selection of an appropriate candidate merchant ship for investigating the impact of damage on its responses in its ‘as designated’ and ‘optimised’ form must take into account the extent of knowledge required to undertake the optimisation and subsequently the detailed stability (intact and damaged), hydrodynamic and motion response analyses addressed in the following chapters.

The following chapter provides the ship selection rationale and the application of the optimisation process and other indicated analyses.

6. SELECTION AND FUNDAMENTAL ANALYSIS OF BASIS SHIP

The optimisation of a basis hull form may be undertaken using the 'secondary' parameters of C_{WP}, LCB and LCF, the 'primary' parameters of L and B/T or both. Ship trims with respect to LCF. Once damaged the ship LCB will change in accordance with the extent and location of the damage and the amount of water ingressed. To permit sensible comparisons of the motions of alternative intact and damaged ships the secondary parameters will not be modified in the optimisation undertaken. Consequently, motions can be defined with respect to a common origin located at the intact LCF and motions differences of the damaged ships will not be complicated by any combination of LCF and LCB changes that might take place in secondary parameter optimisation. With C_B and intact displacement remaining unchanged L and B/T will be modified to improve intact ship motions subject to the constraint of no increase in calm water resistance. Hence there are no changes in the engine requirements, structural mass distribution of the alternative designs or in engine room bulkheads. The difference will be a consequence of damage and optimisation for seakeeping only.

In the following sections details of the selected hull form, its optimisation and the IMO stability requirements addressed will be considered together with details related to mass distribution and damage scenarios to be investigated.

6.1 Choice of Hull Form

The collisions and groundings statistics of Figure 3.4(a) & (b) clearly indicate that general cargo ships and tankers should be the principal ship types investigated (having average percentages of 52.45% and 22.2%). Thereafter containerships and bulk carriers exhibit comparable average statistics (5.5% against 5.05%). However, such a clear and

obvious selection was not possible due to the detailed mass distribution data required to determine cross-products of inertia. Furthermore, when the bulk carrier 'Liverpool Bridge' (re-named Derbyshire in 1978) was selected based on the in-depth investigations available in the literature (Department of Transport (1989), Bishop et al. (1991), Vassalos et al. (2001) and Paik & Faulkner (2003)), it was discovered that whilst some very detailed structural aspects were available they were insufficient to produce accurate cross-products of inertia for the intact ship. Consequently, it was necessary to develop the novel cross-products of inertia estimation scheme of Chapter 5 for the damaged ship, whilst assuming the zero valued inertia product for the intact ship. This choice is not ideal in the face of the statistics presented in Chapter 3, but it simply reflects the fact that ship data sufficient to undertake really detailed analysis is not readily released in the public domain or under the umbrella of confidentiality within a university based research project.

6.2 Public Domain Particulars for Derbyshire

The principal Derbyshire hull form parameters are presented in Table 6.1. A general arrangement drawing of the Derbyshire is given in Appendix D (drawing is taken from the Department of Transport (1989)).

Table 6.1: Main particulars of the Derbyshire taken from the Department of Transport (1989).

Length Overall (m)	L_{OA}	293.25
Length Between Perpendiculars (m)	L	281.94
Longitudinal Centre of Gravity (from AP) (m	LCG	144.4906
Breadth (m)	B	44.196
Draught (m)	T	17.035
Depth (m)	D	24.994
Service Speed (knots)	V	15.5

The body plan for the Derbyshire is provided in Figure 6.1.

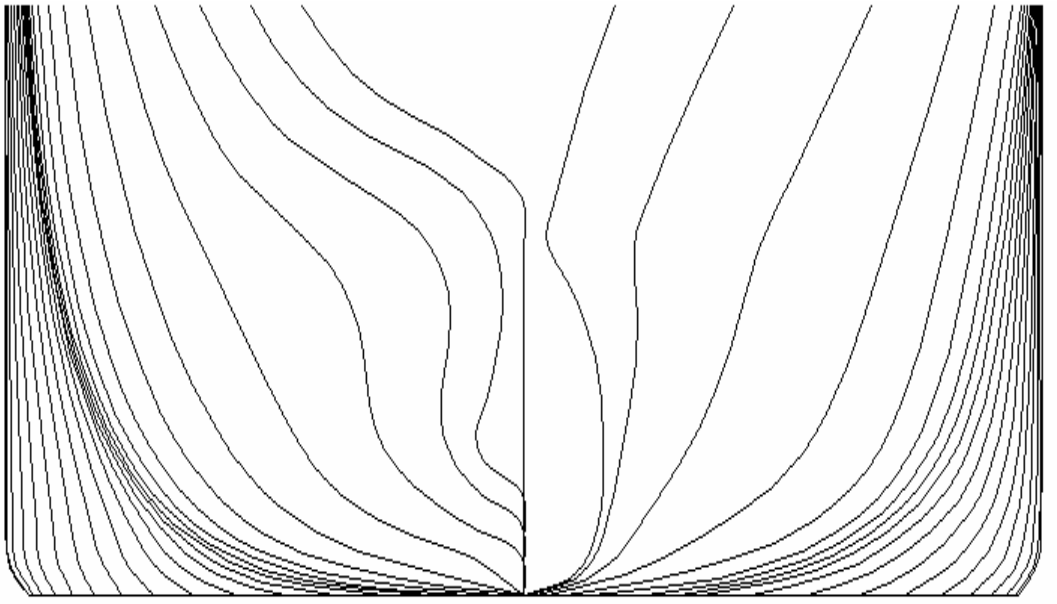

Figure 6.1: The parent hull form.

The longitudinal mass distribution given in Bishop et al. (1991) leads to a longitudinal centre of gravity (LCG) of 147.6 metres measured from the aft perpendicular. Since this does not coincide with the longitudinal centre of buoyancy (LCB), but in fact implies a bow down trim ballast water and fuel are added to the wing tanks in holds 6, 7, 8, 9 and in the after peak tank to establish a level trim state. To keep total mass constant water and fuel were removed from forward tanks and added to cited aft tanks to achieve required level trim. The resulting longitudinal distribution of mass for the Derbyshire now assumes the form provided in Figure 6.2.

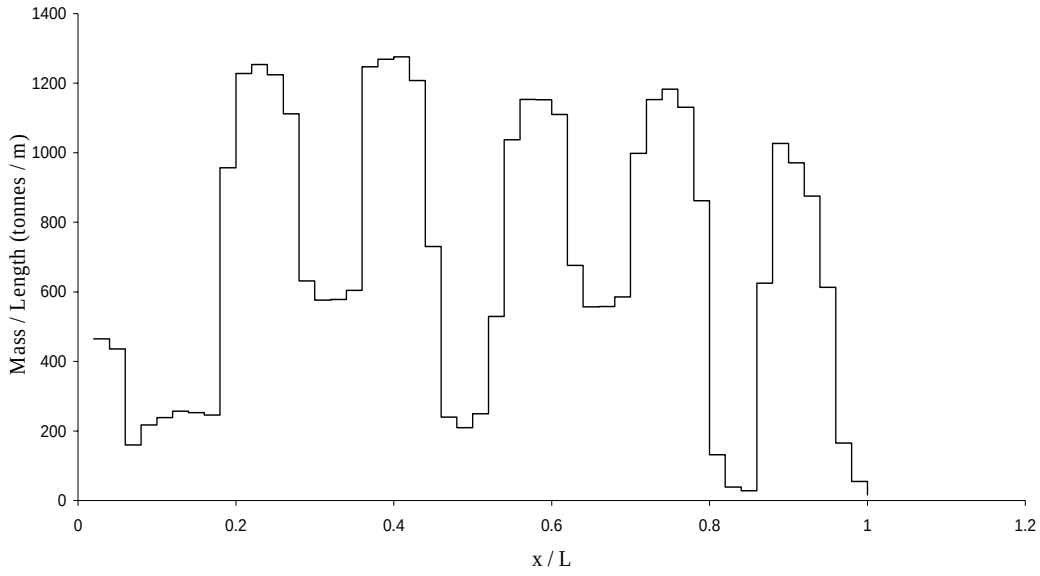

Figure 6.2: The modified longitudinal mass distribution of the Derbyshire.

The mass distribution is very peaky and quite unlike the often assumed coffin diagrams. For accurate calculation of the products of inertia, corresponding sectional distributions are required at a representative number of stations. Since such details cannot be provided at arbitrary selected ship stations the equivalent four-point masses and their location are determined assuming intact products of inertia are zero with respect to centre of gravity. However, from the longitudinal distribution of the mass one may readily estimate the pitch associated radius of gyration.

Summing the forward and aft masses separately, and their first moments with respect to the longitudinal centre of gravity, the four equivalent point masses M_{AP}, M_{FP}, M_{AS} and M_{FS} and their longitudinal positions can be readily determined to yield the details presented in Table 6.2.

Table 6.2: The four masses and their longitudinal positions for parent Derbyshire.

M_A	94686.6 (t)
M_F	104793.6 (t)
Z_A from LCG	64.1 (m)
Z_F from LCG	57.9 (m)
$M_{AP} = M_{AS}$	47343.3 (t)
$M_{FP} = M_{FS}$	52396.8 (t)

From Equation (5.38) the coordinate X_P can be determined assuming $k_{YY} = 0.225L$. Hence from Equation (5.30) it is clear that $X_S = -X_P$. With X_S known Equation (5.42) can be used to determine $Y_{AS} = Y_{FS}$, subject to the assumption that $k_{ZZ} = 0.41B$ together with the deduction made earlier from Equation (5.34). Finally, to check consistency of assumed radii of gyration $Y_{AS} = Y_{FS}$ is re-determined using Equation (5.45) with $k_{XX} = 0.2163L$.

The results of applying the indicated procedure just outlined are presented in Table 6.3. Clearly Y_{AS} and Y_{FS} are consistent.

Table 6.3: The horizontal and vertical positions of the four masses for parent Derbyshire.

Equation	Quantity Determined	Radii of Gyration
5.38	X_P =17.795 (m)	k_{YY} = 0.225
5.30	X_S =-17.795 (m)	k_{YY} = 0.225
5.42	$Y_{AS} = Y_{FS}$ = 3.41579 (m)	k_{ZZ} =0.410
5.45	$Y_{AS} = Y_{FS}$ = 3.41579 (m)	k_{XX} = 0.2163

Details of the intermediate calculations are presented for completeness in Appendix C. The process is in someway artificial as the need to present the total mass as four

equivalent points is only carried out to allow motions of damaged ship to be facilitated in a manner consistent with the intact motion analysis. To achieve moments of inertia and the consistent coordinate points (X_P, X_S) and (Y_{AS}, Y_{FS}) some iteration is necessary. One is not guarantying a unique set of answers and, furthermore, the radius of gyration values used to solve equations indicated in Table 6.3 will seem a little lower than expected for pitch and yaw values used in general motion calculations. The process presented is a compromise to overcome a difficulty that could be readily resolved if a full description of the mass distribution were readily available.

6.3 Optimisation Objective Function and Design Parameters

Having provided the basis known details and body plan for the intact Derbyshire the next task is to identify an 'optimised' hull form of Derbyshire.

Prior to presenting the results of the optimisation process it is worth noting, if only for completeness and to demonstrate how this approach sits with other investigated optimisations, to briefly indicate some of the public literature investigations essentially based on modifications of the primary hull form characteristics.

Lewis (1959) achieved reduction in the pitching amplitude and vertical bow acceleration by selecting a longer hull. Vossers et al. (1960) showed that heave, roll, pitch and RBM amplitudes are sensitive to changes of L/T. Abkowitz et al. (1966) concluded that the reduction of the draught of the ship results in better vertical motion responses. Robson (1988) emphasized that vertical seakeeping performances could be improved by increasing L_{WL}/B_{WL} and B_{WL}/T ratios.

The effects of primary and secondary parameters on vertical motions and added resistance characteristics are presented in a tabular form in Sarioz (1993) for monohulls and in Wright (2004) for catamarans.

Generation of alternative hull forms in this case is undertaken using linear distortion methods.

Prior to initiating the optimisation procedure, preliminary studies are undertaken to estimate the maximum practical percentage changes permissible in the primary parameters. The changes that led to impractical transverse sections were identified together with the upper and lower bounds on the changes in L and B/T permitted in the optimisation process, corresponding to $\pm$ 10% of the intact Derbyshire values. These limits are consistent with those used and discussed by Sarioz (1993). Other constraints imposed were fixed C_B, fixed displacement and fixed depth.

6.3.1 Choice of the Objective Function

The objective function selected is the peak relative bow motion in head seas in the Optistanbul Suite (see Hearn et al. (1992) and Sarioz et al. (1992)) subject to the constraint that calm water resistance is not increased. The relative bow motion is chosen since it includes the amplitude and phase information of the heave and pitch motions. As the Hooke-Jeeves algorithm proceeds, the hull form is modified and the resulting hydrostatic properties, resistance (wave and frictional) and relative bow motion values are determined. In this case the process converged after 52 iterations. According to Figure 10.4 of Sarioz (1993) this iteration number is satisfactory for the convergence of the optimisation variables. The calm water resistance values together with the selected objective function magnitudes are plotted against iteration number in Figure 6.3.

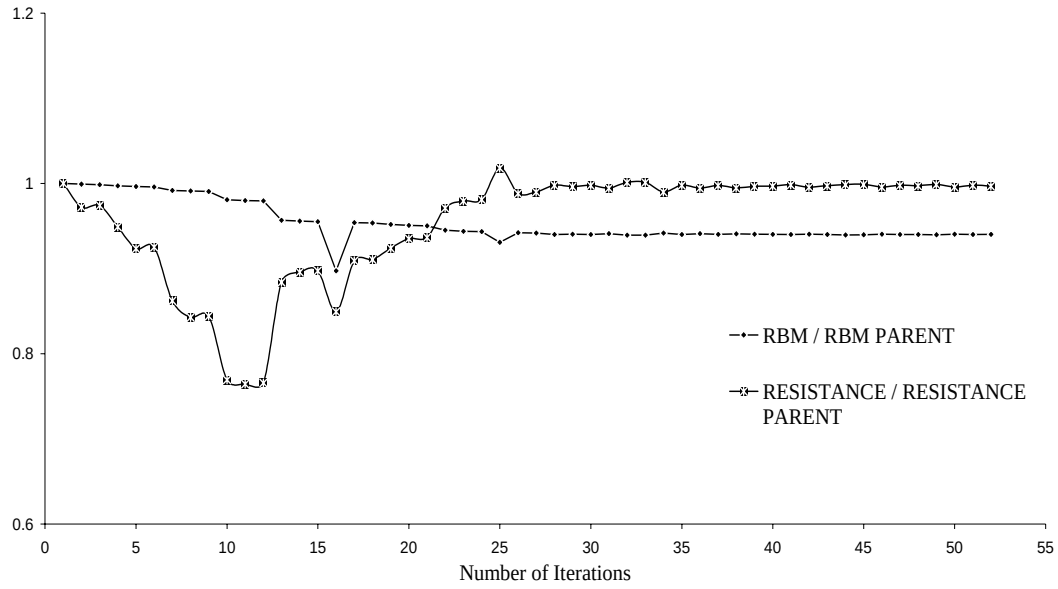

Figure 6.3: The variation of the objective function and the calm water resistance with iteration number.

Figure 6.3 indicates that the objective function (RBM of alternative designs non-dimensionalised with respect to RBM of intact parent Derbyshire) fluctuates as the optimisation process proceeds. However, not all these small values of the objective function are acceptable since they do not satisfy either the constraint of intact stability requirements or the constraint that calm water resistance is not increased. The apparent solutions determined just after 15 iterations were unacceptable due to the failure to satisfy the intact stability requirements.

The body hull forms for the parent hull and for the optimised hull form are presented in Figure 6.4.

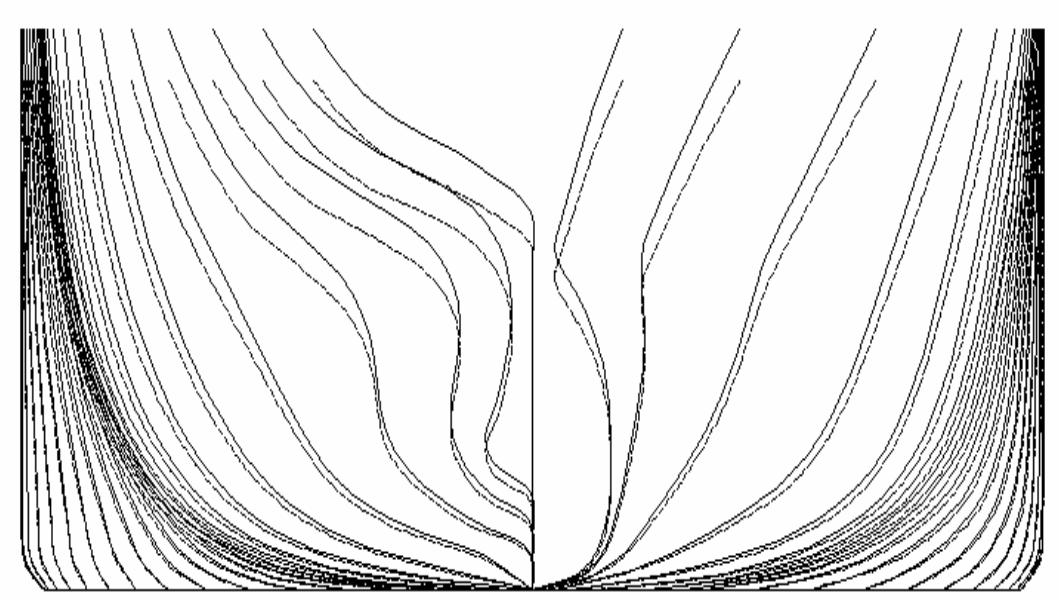

Figure 6.4: The parent (continuous) and optimised (dashed) hull forms.

It is clear from Figure 6.4 that as the ship is optimised the section curves generally expand. Fore body is now more round-formed than the original one. The lines of the aft body are more V-shaped than the original ones. Maximum draught is now decreased over the fore and aft body. Since the volume was constant during the optimisation this means that the volume lost due to the decrease of draught is balanced by the expansion of the sections' half beam distributions along the hull. The depth was one of the fixed parameters in the optimisation process. Therefore, in the case of the optimised ship, a decrease in the ship's draught resulted in an increase in the freeboard height.

The hull form parameters for the parent (intact Derbyshire) hull form and for the optimum design are presented in Table 6.4. Comparisons of the relative bow motion values for these alternative hulls are provided in Figure 6.5.

Table 6.4: Parameters for the parent and optimised hull forms.

Geometric Parameters	Parent Form	Optimised Form
Length (m)	281.94	310.134
Beam (m)	44.196	44.196
Draught (m)	17.97	16.34
Depth (m)	24.994	24.994
Displacement (t)	199480	199480
RBM (m)	2.534	2.382
Resistance (KN)	14617	14580
Service Speed (knots)	15.5	15.5

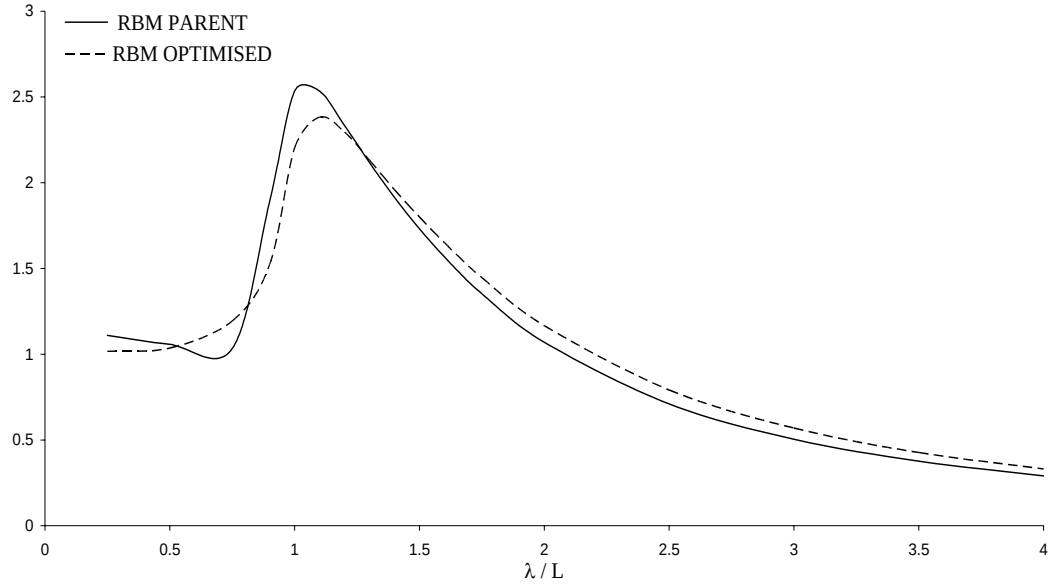

Figure 6.5: Relative bow motion responses for the parent and optimised Derbyshire from Optistanbul Suite.

Whereas the peak RBM has been reduced by 6% and the resistance has decreased by 0.25% the improved RBM and calm water resistance in the optimised hull form corresponds to a +10% change in L and +9.46% change in B/T. The draught for the parent hull form in Table 6.4 is slightly different to the original value quoted in Table

6.1. This change reflects the mass distribution consistent with change of location of ballast water and fuel to establish zero trim angle in Section 6.2.

6.4 IMO Intact Stability Requirements and Related Analysis

The Derbyshire was a B-60 designed ship, namely a ship of type B with a 60% reduction in the allowable freeboard. In the damage case the requirement was one-compartment damage that resulted in no unprotected or protected openings being compromised rather than any requirement concerning the margin line (or line of protected openings, which is applicable to passenger and special purpose ships).

As already indicated in Chapter 2 the optimised hull form has been checked for some satisfaction of the IMO intact stability rules. The actual full IMO (A-749 criteria) requirements are as follows:

- The area under the righting lever curve (GZ curve) up to 30° angle of heel should be equal to/or greater than 0.055 m.rad.

- The area under the GZ curve between 30° and 40° should be equal to/or greater than 0.03 m.rad.

- The area under the GZ curve up to 40° should be equal to/or greater than 0.09 m.rad.

- Initial GM should be equal to/or greater than 0.15m.

- The maximum righting arm should occur at an angle of heel preferably exceeding 30° but not less than 30°.

- The righting lever GZ should be at least 0.2m at an angle of heel equal to/or greater than 30°.

The first three requirements of A-749 criteria are included in the optimisation process as an intact stability check for the optimised hull form. To cross check the intact stability curves of the parent and optimised hull forms two different computer algorithms are applied, the 'Wolfson unit hydrostatics and stability program' (Wolfson (2001a)) and the 'Optistanbul suite'. The resulting intact stability curves are illustrated in Figure 6.6.

The 'Optistanbul suite' only provides GZ curve up to 40° since this is the largest angle considered in the first three requirements of the IMO criteria and within an optimisation process one undertakes sufficient calculation not more than necessary. Furthermore the ships within the 'Optistanbul suite' are defined using just 21 two-dimensional transverse sections, whereas the 'Wolfson unit hydrostatics and stability program' has a three-dimensional description of the entire hull. Within the 'Optistanbul suite' constrained cubic spline interpolation (see Kruger (2004)) is applied and within the 'Wolfson unit hydrostatics and stability program' traditional cubic spline technique is used (see ShipShape (1992)). Thus in viewing Figure 6.6 one is not comparing like with like in terms of the geometric description or the calculation performed. Here the alternative 'Wolfson unit hydrostatics and stability program' is utilised to simply demonstrate that the intact Derbyshire (parent) hull form complies with all the requirements of the IMO criteria cited.

Details related to areas under the intact stability curve for both two hulls are presented in Tables 6.5 and 6.6 together with the minimum IMO requirements. Clearly, both hulls far exceed the limits stipulated by IMO irrespective of means of calculation of quantities required.

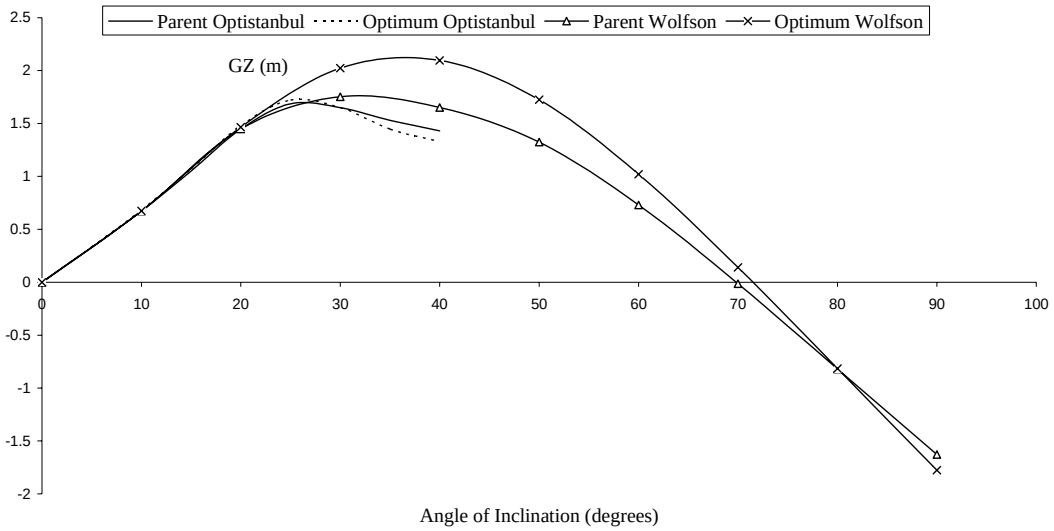

Figure 6.6: The intact stability curves for the parent and for its optimised configuration.

Table 6.5: Intact stability curve areas calculated using Optistanbul suite.

Area under GZ Curve (m.rad)	Parent Form	Optimised Form	Required Condition
Up to 30 Degrees	0.528	0.537	≥0.055
Up to 40 Degrees	0.796	0.792	≥0.03
Between 30 and 40 Degrees	0.268	0.255	≥0.090

Table 6.6: Intact stability curve areas calculated using Wolfson unit hydrostatics and stability code.

Area under GZ Curve (m.rad)	Parent Form	Optimised Form	Required Condition
Up to 30 Degrees	0.532	0.554	≥0.055
Up to 40 Degrees	0.833	0.921	≥0.03
Between 30 and 40 Degrees	0.301	0.367	≥0.090

Prior to cross checking fulfilment of the last three IMO intact stability requirements it is worth noting that the initial GM value is calculated automatically in the ‘Optistanbul suite’ and determined manually from the ‘Wolfson unit hydrostatics and stability code’ GZ curve. The heel angle at which the maximum GZ value occurs and the maximum

GZ value must be provided manually from the generated GZ curves. The calculated values of the initial GM value, the locations and values of the maximum GZ are provided in Tables 6.7 and 6.8.

Table 6.7: Calculated IMO intact stability curve properties from Optistanbul suite.

Hull Forms	Initial GM (m)	Angle of the Maximum GZ (degrees)	Maximum GZ (m)
Parent Hull Form	3.95	25	1.687
RBM Optimised Hull Form	3.98	25	1.721
Required Condition	≥0.15	≥30°	≥0.2

Table 6.8: Calculated IMO intact stability curve properties from Wolfson unit hydrostatics and stability code.

Hull Forms	Initial GM (m)	Angle of the Maximum GZ (degrees)	Maximum GZ (m)
Parent Hull Form	4	30	1.753
RBM Optimised Hull Form	4.2	40	2.095
Required Condition	≥0.15	≥30°	≥0.2

Although the two different codes yield different values for the magnitude and location of maximum GZs and for initial GMs, according to the cited IMO criteria, both hull forms significantly exceed the minimum limits for initial GM and for the maximum value of GZ. Table 6.8 is sufficient to demonstrate that the intact Derbyshire hull form and its optimised hull form fully comply with the IMO criteria. Further development of the ‘Optistanbul suite’ might address the complete rather than a subset of the IMO requirements.

The equilibrium search code developed could be improved to determine the critical KG, namely the maximum value at which all the IMO stability requirements are satisfied for a particular condition. This would provide an additional single measure to compare the performance of the optimised hull against the basis design.

6.5 Floodable Length Curve and Bulkhead Locations

Whereas longitudinal bulkheads are generally omitted in the design of O.B.O (Oil-Bulk-Ore) ships a large number of transverse bulkheads are used in their design. The number of necessary transverse watertight bulkheads depends upon the ship dimensions and is determined according to classification regulations (see, for example, Friis et al. (2002), Lloyd's Register (2003), American Bureau of Shipping (1992) and Bureau Veritas (1986)). However, there is no limitation in the total number of bulkheads for the Derbyshire or other ships longer than 198m.

According to the cited regulations ships other than passenger ships should have a collision bulkhead, an after peak bulkhead and a watertight bulkhead at each end of the machinery space. There are limits only on the location of the collision bulkhead from the fore perpendicular. This distance has to be more than 10m or 0.05 of the 96% of the waterline length of vessel and this waterline length should be measured at 85% of least moulded depth. This distance should also be less than 0.08 of the 96% of the waterline length of vessel. Due to lack of technical information this distance is taken as 96% of the length between perpendiculars of the vessel. Therefore, the position of the collision bulkhead for the Derbyshire should be between 10m and 21.65m. For both the parent and optimised Derbyshire this condition is satisfied as the position of the collision bulkhead stands in the region of 10 to 11 metres from the fore perpendicular in these two ships.

The transverse bulkheads of the intact Derbyshire are maintained and within the optimised form of the Derbyshire the positions of the bulkheads are proportionally changed in accordance to the increased length of the optimised ship. Since LCF, LCB and C_{WP} have not be modified and hence LCG cannot be modified, if level trim is to be maintained in the optimised hull form, then some adjustment of the equivalent point masses and the relationship between parent and optimised hull form geometry requires some clarification. In the Figure 6.7 the relative position of the alternative geometric

hull form relative to the fixed Z-X datum plane together with hull form parameter changes noted in the preceding subsections are captured systematically.

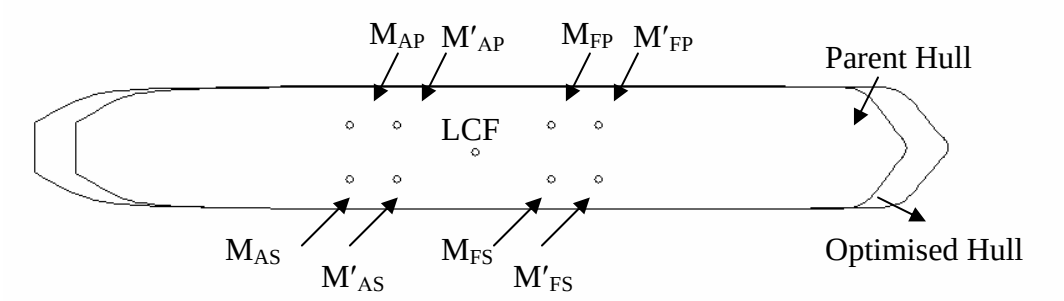

Figure 6.7: The presentation of the four point masses for the parent and optimised hull forms.

M'_{AP}, M'_{FP}, M'_{AS}, M'_{FS}, Z'_A and Z'_F are found in exactly the same way as M_{AP}, M_{FP}, M_{AS}, M_{FS}, Z_A and Z_F with mass distribution of the intact Derbyshire stretched to new length.

For the optimised ship the point mass and inertia radii data corresponding to Tables 6.2 and 6.3 are provided in Tables 6.9 and 6.10 respectively.

Table 6.9: The four masses and their longitudinal positions for optimised Derbyshire.

M_A	106709.6 (t)
M_F	92770.8 (t)
Z_A from LCG	61.9 (m)
Z_F from LCG	71.2 (m)
$M_{AP} = M_{AS}$	53354.8 (t)
$M_{FP} = M_{FS}$	46385.4 (t)

Table 6.10: The horizontal and vertical positions of the four masses for optimised Derbyshire.

Equation	Quantity Determined	Radii of Gyration
5.38	X_P =17.945 (m)	k_{YY} = 0.2217
5.30	X_S =-17.945 (m)	k_{YY} = 0.2217
5.42	$Y_{AS} = Y_{FS}$ = 1.7868 (m)	k_{ZZ} =0.41
5.45	$Y_{AS} = Y_{FS}$ = 1.7868 (m)	k_{XX} = 0.2142

The movement of the bulkheads in the optimised hull form, as a result of the ship lengthening, now needs to be justified in terms of their acceptability through consideration of the floodable length curves estimated using the 'Wolfson unit floodable length software' (Wolfson (2001b). Using a typical permeability coefficient of 0.63 in the cargo regions and a permeability of 0.85 in the engine rooms floodable length curves for parent and optimised hulls are presented in Figure 6.8. In Figure 6.8 the dash-dot broken line indicates optimised hull form and the continuous line represents the parent hull form.

As initially discussed in Section 4.2.1 and illustrated in Figure 4.1, bulkhead divisions of the original and optimised Derbyshire hull forms are acceptable at the different permeabilities investigated as the clearance between the floodable length curves and the constructed 'compartment triangles' is more than acceptable.

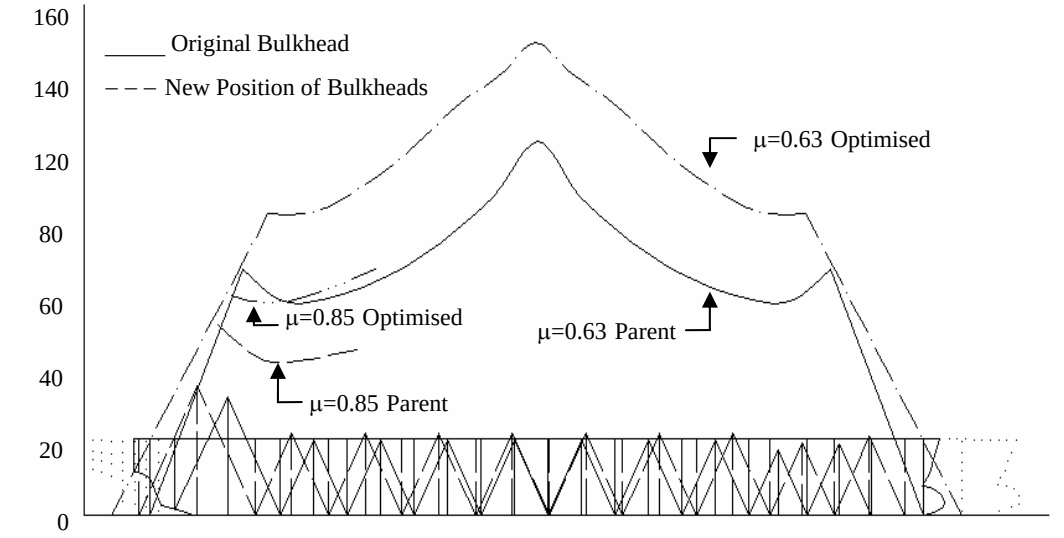

Figure 6.8: The floodable length curves for the parent and optimised hull forms for different levels of permeability.

6.6 Damage Properties of the Derbyshire

As indicated in Section 3.1 bulk carriers are more vulnerable to grounding damage. In this case the damage position is generally in the region designated 3L/4-FP (see Figure 3.5). The extent of the damage is readily identified from Figure 3.14(a), that is, with equal possibilities there are three possible length scales:

- $0 < l / L \leq 0.02$
- $0.02 < l / L \leq 0.04$
- $0.04 < l / L \leq 0.06$

For the damage height there are two possibilities (see Figure 3.14(b)) with the same probability of occurrence, namely

- $0 < h / D \leq 0.2$
- $0.2 < h / D \leq 0.4$.

The most likely damage penetration is between $0 < b / B \leq 0.2$ (see Figure 3.14(c)) and the vertical position of the damage is most likely to satisfy $0 < Y / D \leq 0.2$ (see Figure 3.14(d)). The damage is to be created on the starboard side of the ship (see Figure 3.14(e)).

Using the most likely damage characteristics four distinct scenarios will be considered as defined in Table 6.11.

Table 6.11: Damage scenarios.

Scenario	l/L	h/D	b/B	Y/D	Hold
A	0.02	0.2	0.2	0.2	2
B	0.06	0.2	0.2	0.2	2
C	0.06	0.4	0.2	0.2	1 & 2
D	0.06	0.4	0.2	0.2	2 & 3

The possibility of three holds being simultaneously damaged is unlikely using the statistics available to this study. Whilst more than two holds damaged is unlikely to appreciate the impact of more damaged holds on the attitude of the ship results are provided in Appendix E. However, only one or two hold damaged will be considered here and in subsequent chapters.

The fact that the scenarios suggested in Table 6.11 are based on grounding data it is perhaps surprising that Y/D the vertical position of the lowest point of the damage has a

value of 0.2. However, these are the findings of all reported accidents over the period 1935 and 1999.

From Figure 3.7(c) one notes that the next probable regions of damage after the selected 3L/4-FP region are the regions L/4-amidships and amidships-3L/4. To confirm that the selected 3L/4-FP region is the more important region, holds in these other cited regions were damaged and found to yield insignificant trimming moments and hence will not be considered further. Also an analysis of bulk carriers in collision incidents indicated that the most likely location of damage stands in the region L/4-amidships. As discussed earlier this results in an insignificant trimming moment.

Having indicated why the selected scenarios are worth of further in-depth analysis the next task is to provide details of attitude changes in both the original and optimised Derbyshire hull forms as each scenario is implemented.

6.7 The Damage Analysis

Each of the damaged ship scenarios presented in Table 6.11 results in a change in heel and trim attitude of the ship. The different changes in trim and heel angles lead to different equilibrium positions of the damaged hull. The parallel sinkage of the ship is calculated first. Then the trim angle is determined before the heel angle is predicted. Justification of the equilibrium angles found is presented in Appendix F.

6.8 Orientation of Damaged Hull Forms

The damages created in the hull form of the Derbyshire and in its optimised hull form are relatively minor and are therefore modelled as a change in mass distribution in the damaged region(s). Since there are no longitudinal bulkheads in the Derbyshire (apart from the engine room) water entering the damage area creates only trim. Therefore only

structural loss to the damage area causes heel. Parallel sinkage, heel and trim following the damage in the hull form of the Derbyshire and of its optimised design are presented in Tables 6.12, 6.13, 6.14 and 6.15 for the damaged scenarios A, B, C and D as defined in Table 6.11.

Table 6.12: Parallel sinkage, trim and heel angles for damage Scenario A.

Attitude of the Damaged Structure	Parent Form	Optimised Form
Parallel Sinkage (m)	1.037	0.939
Trim Angle (degrees)	0.964	0.796
Heel Angle (degrees)	1.224	1.223

Table 6.13: Parallel sinkage, trim and heel angles for damage Scenario B.

Attitude of the Damaged Structure	Parent Form	Optimised Form
Parallel Sinkage (m)	1.243	1.130
Trim Angle (degrees)	1.192	1.000
Heel Angle (degrees)	1.287	1.265

Table 6.14: Parallel sinkage, trim and heel angles for damage Scenario C.

Attitude of the Damaged Structure	Parent Form	Optimised Form
Parallel Sinkage (m)	1.992	1.811
Trim Angle (degrees)	1.875	1.551
Heel Angle (degrees)	2.000	1.500

Table 6.15: Parallel sinkage, trim and heel angles for damage Scenario D.

Attitude of the Damaged Structure	Parent Form	Optimised Form
Parallel Sinkage (m)	2.035	1.851
Trim Angle (degrees)	1.470	1.216
Heel Angle (degrees)	2.000	1.500

The reason for increased parallel sinkage and increasing trim and heel angles as scenario A passes to scenario B and then to scenario C is the increase in the dimensions of the damaged region. In scenarios C and D the heel angles are the same as the damage properties are identical. However, there is a decrease in the trim angle in D as the distance of the damaged holds from the LCF is reduced. The increased parallel sinkage for damage scenario D is due to the larger breadth of hold 3 relative to hold 1.

The optimised ship has a longer length and a higher beam to draught ratio than the parent hull form. Consequently the parallel sinkage, trim and heel angles are quite sensibly smaller due to the changes in the hull form dimensions.

As indicated in Section 6.5 (Figure 6.7) the equivalent point masses for the Derbyshire and its optimised hull form are quite distinct (see Appendix C for parent Derbyshire derivation and Table 6.9 for corresponding values of the optimised hull form). To determine the motions of the two hull forms for the cases of interest the location of the centre of gravity and the new location of the point masses are required to provide structural cross-terms and products of inertia of generalised mass matrix. The centre of gravity details are provided in Tables 6.16 and 6.17 for the parent and optimised hull forms. The corresponding pure moments and cross-products of inertia data is provided in Appendix G. The new location of the point masses are provided in Tables 6.18-6.25.

Table 6.16: Position of the centre of gravity for different damage scenarios for the parent Derbyshire.

Cases	X	Y	Z
Intact	0.0000	-3.4158	2.6527
Scenario A	0.0961	-4.4958	2.5775
Scenario B	0.1059	-4.7118	2.5553
Scenario C	0.1917	-5.4883	2.4744
Scenario D	0.1925	-5.5137	2.5120

Table 6.17: Position of the centre of gravity for different damage scenarios for the optimised Derbyshire.

Cases	X	Y	Z
Intact	0.0000	-1.7868	2.6527
Scenario A	0.0590	-2.7618	2.6146
Scenario B	0.0654	-2.9619	2.6014
Scenario C	0.0960	-3.6670	2.5544
Scenario D	0.0967	-3.6920	2.5749

Table 6.18: Position of the point masses for damage scenario A for the parent Derbyshire.

X_P,Y_{AP},Z_A	17.8640	-3.0375	-61.5135
X_P,Y_{FP},Z_F	17.9078	-5.0895	60.4692
X_S,Y_{AS},Z_A	-17.7179	-3.7977	-61.5135
X_S,Y_{FS},Z_F	-17.6741	-5.8498	60.4692

Table 6.19: Position of the point masses for damage scenario B for the parent Derbyshire.

X_P, Y_{AP}, Z_A	17.8664	-2.9790	-61.5309
X_P, Y_{FP}, Z_F	17.9234	-5.5163	60.4427
X_S, Y_{AS}, Z_A	-17.7146	-3.7783	-61.5309
X_S, Y_{FS}, Z_F	-17.6576	-6.3156	60.4427

Table 6.20: Position of the point masses for damage scenario C for the parent Derbyshire.

X_P, Y_{AP}, Z_A	17.9026	-2.7713	-61.5913
X_P, Y_{FP}, Z_F	18.0419	-6.7606	60.3433
X_S, Y_{AS}, Z_A	-17.6657	-4.0134	-61.5913
X_S, Y_{FS}, Z_F	-17.5264	-8.0027	60.3433

Table 6.21: Position of the point masses for damage scenario D for the parent Derbyshire.

X_P, Y_{AP}, Z_A	17.9193	-3.2493	-61.5669
X_P, Y_{FP}, Z_F	18.0285	-6.3771	60.3929
X_S, Y_{AS}, Z_A	-17.6490	-4.4913	-61.5669
X_S, Y_{FS}, Z_F	-17.5398	-7.6192	60.3929

Table 6.22: Position of the point masses for damage scenario A for the optimised Derbyshire.

X_P, Y_{AP}, Z_A	17.9815	-1.5190	-59.2795
X_P, Y_{FP}, Z_F	18.0210	-3.3677	73.8077
X_S, Y_{AS}, Z_A	-17.9003	-2.2850	-59.2795
X_S, Y_{FS}, Z_F	-17.8608	-4.1337	73.8077

Table 6.23: Position of the point masses for damage scenario B for the optimised Derbyshire.

X_P, Y_{AP}, Z_A	17.9822	-1.4857	-59.2892
X_P, Y_{FP}, Z_F	18.0335	-3.8081	73.7905
X_S, Y_{AS}, Z_A	-17.8991	-2.2781	-59.2892
X_S, Y_{FS}, Z_F	-17.8478	-4.6004	73.7905

Table 6.24: Position of the point masses for damage scenario C for the optimised Derbyshire.

X_P, Y_{AP}, Z_A	17.9910	-1.5224	-59.3230
X_P, Y_{FP}, Z_F	18.0853	-5.1238	73.7283
X_S, Y_{AS}, Z_A	-17.8867	-2.4619	-59.3230
X_S, Y_{FS}, Z_F	-17.7924	-6.0633	73.7283

Table 6.25: Position of the point masses for damage scenario D for the optimised Derbyshire.

X_P, Y_{AP}, Z_A	18.0011	-1.9091	-59.3112
X_P, Y_{FP}, Z_F	18.0751	-4.7327	73.7589
X_S, Y_{AS}, Z_A	-17.8766	-2.8486	-59.3112
X_S, Y_{FS}, Z_F	-17.8026	-5.6722	73.7589

The coordinates in Tables 6.16-6.25 are given respect to LCF, intact waterline and centreline for the parent and optimised Derbyshire.

6.9 Summary

In this chapter, the intact stability of the Derbyshire and of its optimised configuration is investigated. This forms the static part of the analysis. The dynamic part of the research is presented in the next chapters. Therefore, the hydrodynamic characteristics and the relative vertical motion response analysis of the parent and optimised hull forms when intact and damaged are presented in Chapters 7 & 8.

7. HYDRODYNAMIC CHARACTERISTICS OF INTACT AND DAMAGED SHIPS

The previous chapters established:

- How the bulk carrier Derbyshire might be damaged using analysed damage statistics.

- The most likely damage scenarios would not lead to ship loss.

- Required intact stability criteria were satisfied for parent and optimised hull forms.

- Determined the orientation and mass-inertia characteristics of original and optimised intact and damaged hull forms.

The next key step is to undertake the hydrodynamic analysis of each hull form for each damage scenario in order that the subsequent motion analyses may be undertaken.

Whilst forward speed was included in the optimisation process, it does not necessarily have to be included in the damaged ship motion analysis. The forward speed of the ship is not addressed simply because it is assumed that once the ship is damaged it will either stop to permit passengers and the crew to abandon the ship (if necessary), or, to assess extent of damage possible low speed advance to harbour. In the latter case forward speed effect has to be examined. Here the fluid-structure interaction analysis is undertaken for zero forward speed using the Matthew Diffraction Suite.

The wetted surface boundary elements over the damage area are not removed since the automatic quantity data checking of the Matthew Diffraction Suite is so through that it

would refuse to proceed to the interaction analysis on the basis that the hole in one side leads to inconsistent estimate of volume. To model the hole it would be necessary to model the internal wetted volumes and this was considered too complex as a first step in analysing the damaged ship.

In the following sections the method of calculation will be briefly described together with an assessment of the quality of the calculations completed prior to discussing the predictions completed for both intact and damaged parent and optimised hull forms.

7.1 Calculation of Hydrodynamic Coefficients and Excitation Forces

The general fluid-structure interaction problem can be formulated as an elliptic partial differential equation subject to linear free surface boundary conditions expressing continuity of pressure and velocity across the free surface. On the structure itself and on the stationary seabed continuity of normal velocity across these boundaries is required. In the far-field the radiation and diffraction waves generated are required to be outgoing cylindrical waves. Since the partial differential equation formulation requires modelling the fluid domain explicitly alternative Fredholm integral equation formulations have been developed that only requires solution of the unknown velocity potential on the wetted surface of the structure (see, for example, Hearn (1991)). This greatly reduces the computational demands of solving free surface based fluid-structure interaction problems. The boundary elements (small subdivisions of the wetted surface of a structure) may be triangular, quadrilateral or polygonal with any mix required to represent the geometrical form being permitted. The selection of the boundary elements is generally subjective and hence the quality of the solutions produced for the radiation potential, ϕ_j, and the diffraction potentials for different wave frequencies and wave headings must be checked.

In this study the numerical stability of the equations solved is monitored through the conditioning number provided by the Matthew Diffraction Suite. The quality of modelling the fluid structure interaction is judged through the quality of the cross-terms of the reactive coefficients ($A_{kj} = A_{jk}$ and $B_{kj} = B_{jk}$ for zero forward speed) and the equality of the wave excitation forces and moments calculated directly and calculated indirectly using the relationship of Haskind (1954).

Without proof or detailed explanations the basic relationships required to indicate how each hydrodynamic quantity is determined is presented next.

Assuming

$$\Phi(Z, X, Y, t) = \phi(Z, X, Y) e^{-i\omega t} \tag{7.1}$$

and the incident wave potential is described by

$$\phi_W(Z, X, Y) = \alpha \frac{ag}{\omega} \frac{\cosh k(y+d)}{\cosh(kd)} e^{ik(Z\cos\beta + X\sin\beta)}, \tag{7.2}$$

where β is the wave heading, ω is the wave frequency, a is the wave amplitude and d is the water depth. Specification of α is discussed in Chapter 8.

The wave excitation force/moment in the kth direction is given by

$$F_k(\omega, \beta) = -i\,\rho\,\omega \iint_{S_W} (\phi_W + \phi_D)\, n_k \, dS . \tag{7.3}$$

Alternatively the Haskind relationship uses

$$F_k(\omega, \beta) = \frac{\rho\, e^{-i\omega t}}{a_j} \iint_{S_W} \left(\phi_W \frac{\partial \phi_j}{\partial n} - \phi_j \frac{\partial \phi_W}{\partial n} \right) dS \tag{7.4}$$

where n_k is the generalised direction cosine associated with the wave excitation force (k=1, 2, 3) or moment (k=4, 5, 6), S_W is the wetted surface area of the vessel, ϕ_D is the diffraction velocity potential and t denotes time.

The hydrodynamic reactive coefficients of added mass and fluid damping are determined from the radiation velocity potentials ϕ_j associated with the structure executed the jth mode of motion. Since the reactive loads will not be in phase with the incident wave the velocity potential ϕ_j is complex to model the phase difference. In particular:

$$\phi_j = \left(\phi_{jr} + i\,\phi_{ji}\right) e^{-i\omega t} \tag{7.5}$$

with ϕ_{jr} and ϕ_{ji} denoting the real and imaginary parts of the jth velocity potential.

The added mass and fluid damping coefficients are essentially resolved components of the reactive force (moment) in-phase with the structure's acceleration and velocity respectively. These are calculated using the standard relationships:

$$A_{kj} = \frac{\rho}{\omega\,\eta_{ja}} \iint_{S_W} \phi_{jI}\, n_k\, dS \tag{7.6}$$

and

$$B_{kj} = -\frac{\rho}{\eta_{ja}} \iint_{S_W} \phi_{jR}\, n_k\, dS\,. \tag{7.7}$$

Irrespective of the geometric characteristics of the ship, independently of whether it is intact or damaged the zero forward speed hydrodynamic coefficients A_{kj} and B_{kj} may

be mathematically shown to be symmetric. Part of the analysis quality check is to establish if the calculated reactive coefficients satisfy

$$A_{kj} = A_{jk} \tag{7.8}$$

and

$$B_{kj} = B_{jk} \text{ for all } j \text{ and } k. \tag{7.9}$$

A mathematical proof of equations (7.8) and (7.9) is provided by Odabasi and Hearn (1978). The details are not reported here. When the vessel has a forward speed, the cross-coupling terms must then satisfy the Timman-Newman relationship (see Timman and Newman (1962)).

7.2 Validation of Hydrodynamic Analysis of Intact and Damaged Forms of Derbyshire

The wetted surface discretisation must satisfy two distinct aspects. Initially the definition of the wetted surface should represent the actual geometric form so that wetted surface and volumetric properties are consistent with hull form characteristics of original hull. Next the distribution of boundary elements should provide sufficient definition of the normal velocity components at their centroid to allow good modelling of the fluid structure interaction problem being investigated.

In this particular case several different forms of the basis hull form and optimised hull forms are to be analysed. Whereas the intact hull forms exhibit port-starboard symmetry the damaged hulls do not exhibit such geometric symmetry. The maximum number of boundary elements available is 1500 for the case of no planes of symmetry, so that intact and damaged hull forms are modelled consistently.

For the intact Derbyshire and the intact optimised hull form of Derbyshire a total of 1314 boundary elements were used; 1294 quadrilateral and 20 triangular elements. The discretisation for each case is pictorially presented in Figures 7.1 and 7.2.

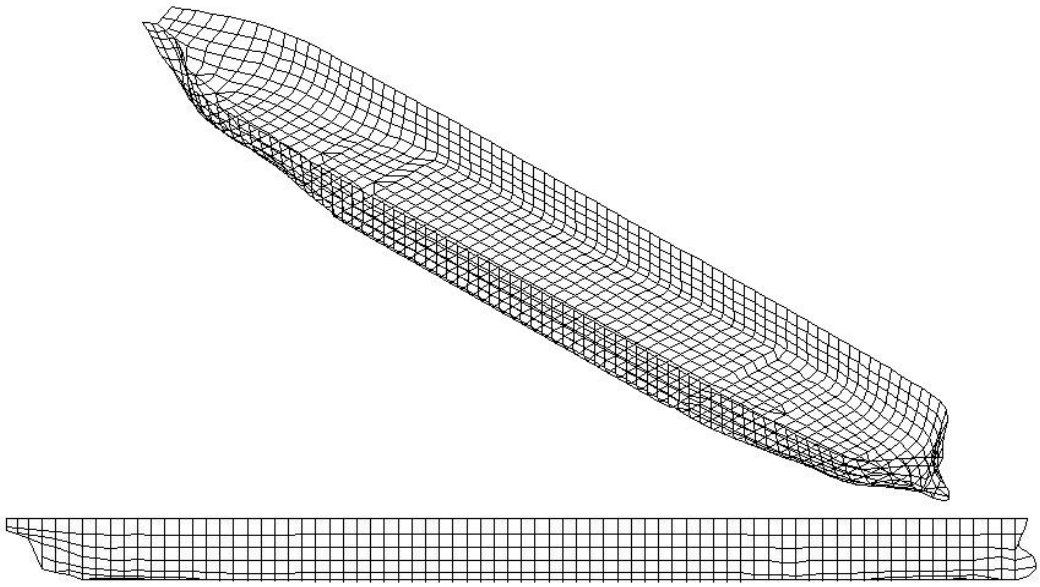

Figure 7.1: Discretisation of the intact Derbyshire.

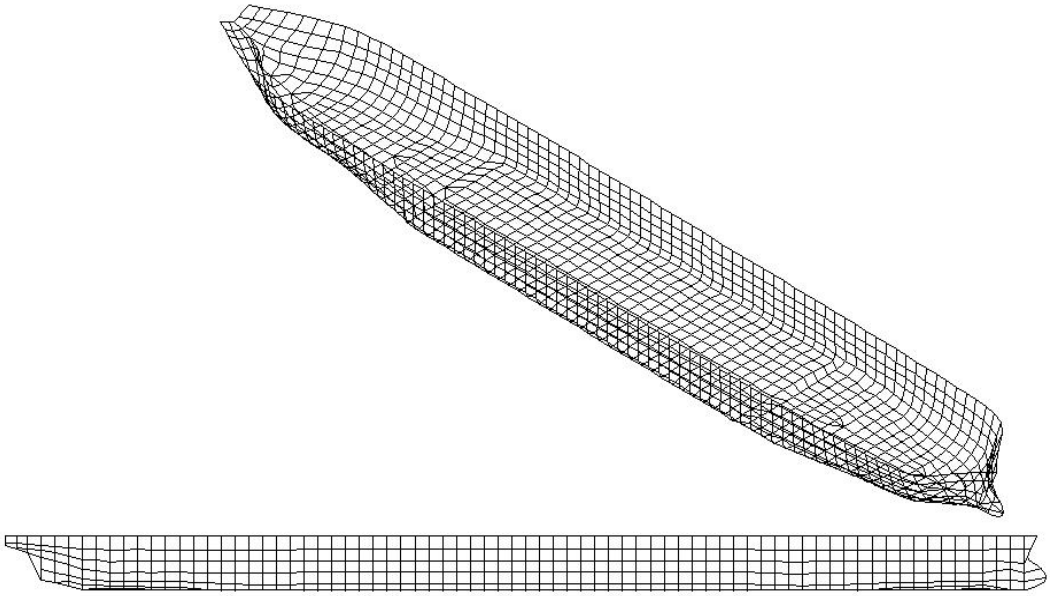

Figure 7.2: Discretisation of the intact optimised Derbyshire.

As discussed earlier a measure of the numerical stability of the calculations performed to complete the hydrodynamic calculations is the so-called ‘conditioning’ number of the equations solved. This number ideally should have the value of unity. This is a ‘necessary’ rather than a ‘sufficient’ condition. It cannot be sufficient because if one used considerably fewer boundary elements to model the fluid-structure interaction the equations solved could be very stable, but the quality of hydrodynamic predictions could be totally unacceptable because the distribution of the boundary conditions is insufficient to capture the true nature of the interaction.

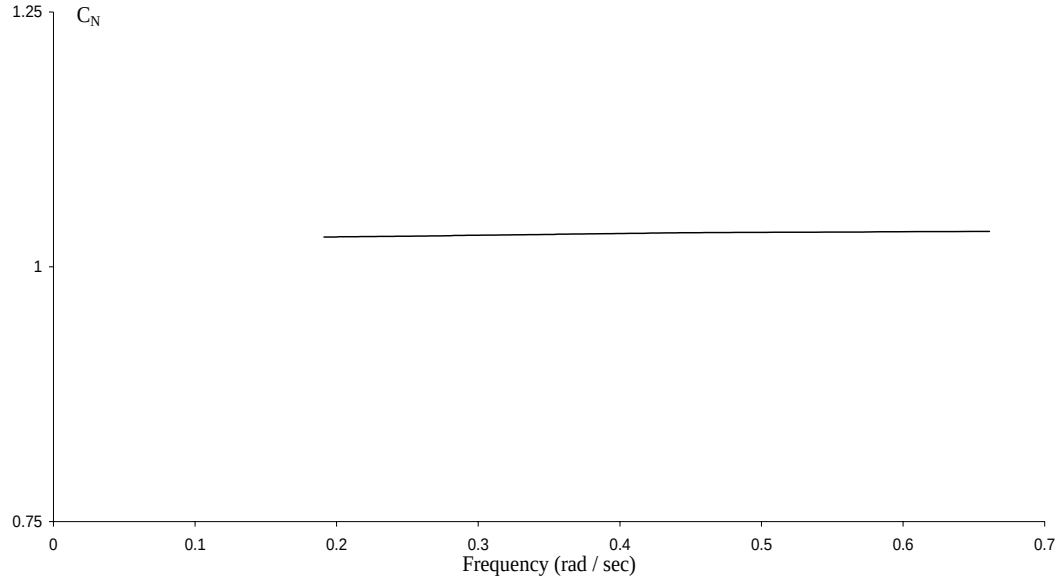

Figure 7.3: Conditioning number for the intact Derbyshire.

In Figure 7.3 the calculated conditioning number values of the hydrodynamic analysis for the intact Derbyshire is presented. Clearly the values are very close to the ideal value of unity and so it is worthwhile moving on to the next step of accessing the equality of the hydrodynamic cross-coupling reactive coefficients.

The port-starboard geometric symmetry of the intact case means that only the sway-roll-yaw and surge-heave-pitch added mass and fluid damping reactive coefficients are coupled. For the same reason only the heave-pitch hydrostatic restoring coefficients are coupled. The non-zero horizontal and vertical motions associated cross-coupling hydrodynamic terms for the intact Derbyshire are presented in Appendix H through Figures H.1-H.6 respectively. Only sway-roll and roll-sway added mass and fluid damping coefficients plot is presented in Figure 7.4 (also in Figure H.4).

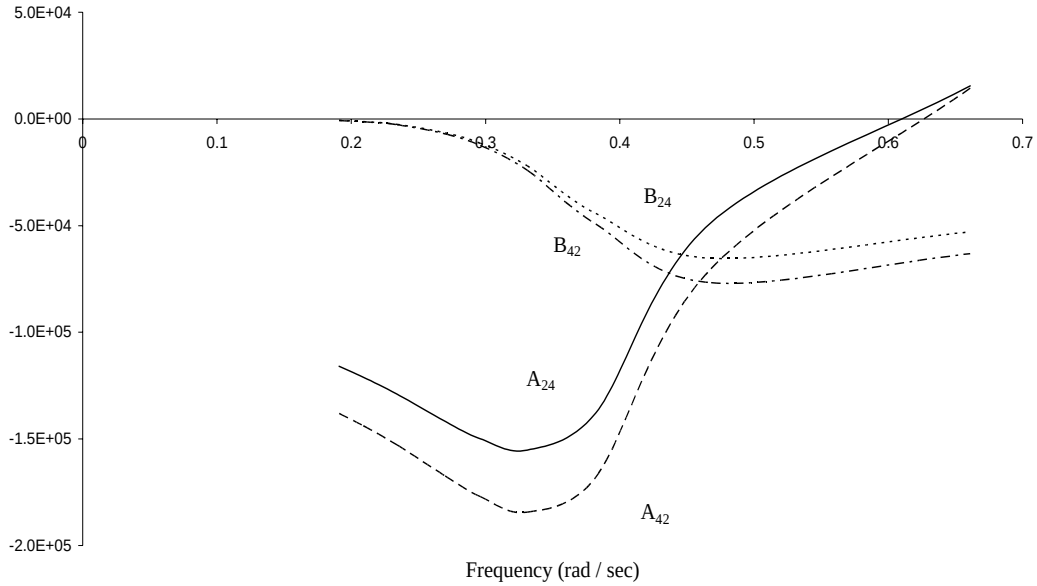

Figure 7.4: Sway-roll and roll-sway added mass and fluid damping coefficients for the intact Derbyshire.

The largest difference for the cross-coupling reactive hydrodynamic coefficients is found in Figure 7.4 for the sway-roll and roll-sway coefficients. The very close agreement of all the other cross-terms implies that all hydrodynamic calculations are stable and further improvement would require more circumferential boundary elements so as to model more precisely the roll and sway fluid-structure interactions. The number of circumferential strips of boundary elements is of the order of 75. Hence for symmetry of the boundary elements (port-starboard) 150 facets would be required to improve the sway-roll modelling. Since this would conflict with the initial plan to model the internal free-surfaces for the damaged ships (subject to 1500 upper limit) further refinement was not undertaken.

The next quality check is the prediction of wave excitation loads using direct calculation based on Equation (7.3) and the Haskind relationship of Equation (7.4). The surge, heave and pitch wave excitation loads for the intact Derbyshire calculated using Matthew Diffraction Suite for head seas are compared in Figures 7.5 to 7.7.

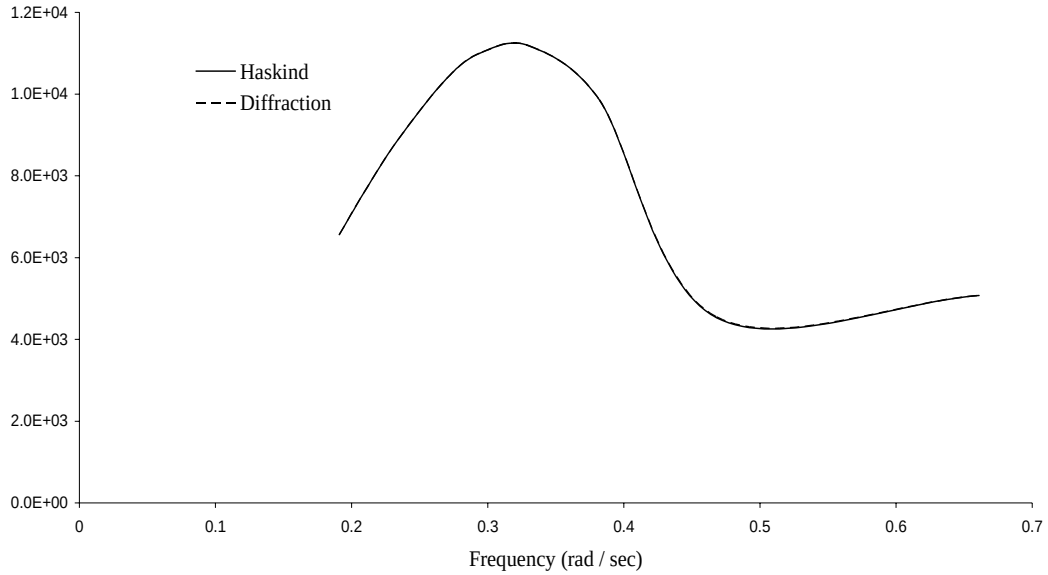

Figure 7.5: Surge wave excitation forces for the intact Derbyshire (in head seas).

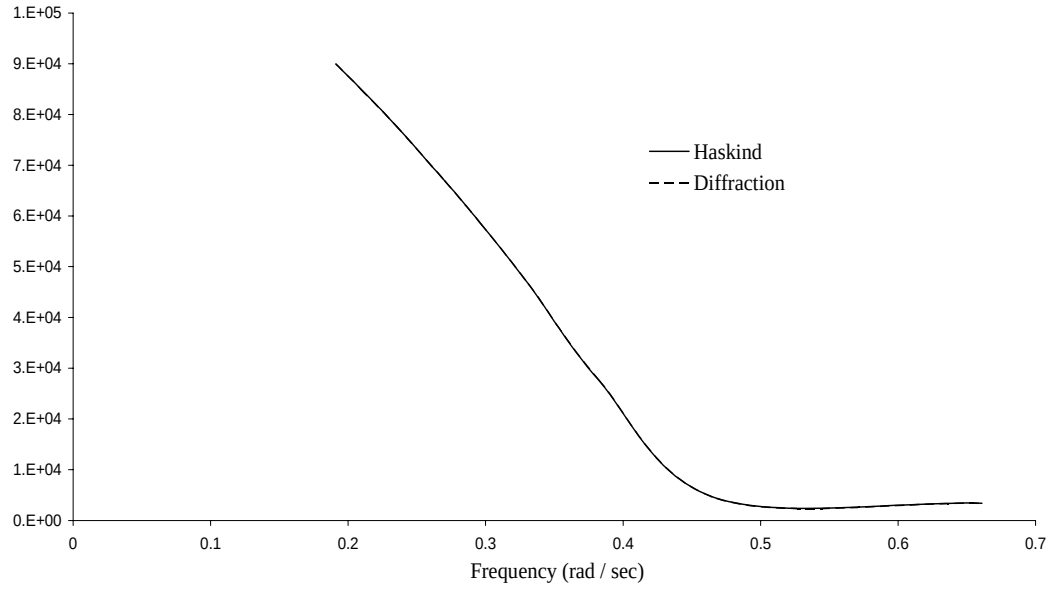

Figure 7.6: Heave wave excitation forces for the intact Derbyshire (in head seas).

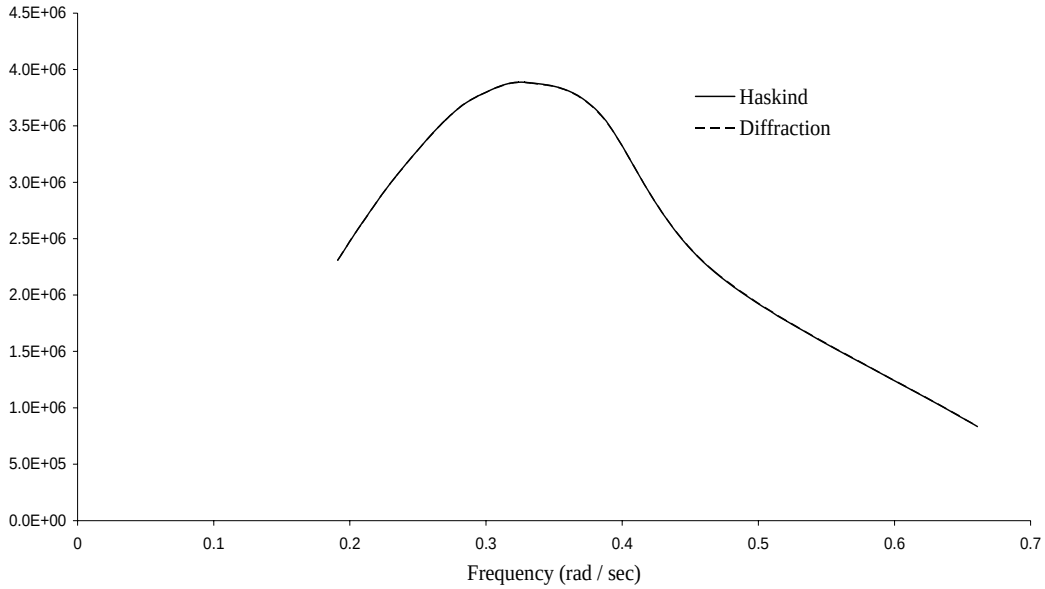

Figure 7.7: Pitch wave excitation moments for the Intact Derbyshire (in head seas).

The plots of the head sea wave excitation forces and moments for the intact Derbyshire associated with surge, heave and pitch that are calculated by using these alternative methods match very well. This set of results thus suggests that the modelling of surge, heave and pitch radiation problems is consistent with the modelling of the diffraction problems.

To demonstrate that the quality of the coupled hydrodynamic coefficients and the numerical stability of the equations processed is also maintained in the damaged scenarios the damage scenario A is addressed. The discretisation for the damage scenario A is pictorially presented in Figures 7.8. In this case the parent Derbyshire hull form is damaged in the region 3L/4-FP as specified in Figure 3.7 (c) previously. An indication of the quality of the calculated conditioning number is provided in Figure 7.9. The vertical plane and horizontal plane based cross-coupling terms are provided in Figures H.7 to H.9 and Figures H.10 to H.12 respectively. As noted with the intact parent Derbyshire form it is only the sway-roll cross-terms that exhibit any real difference as shown in Figure 7.10 or in Figure H.10.

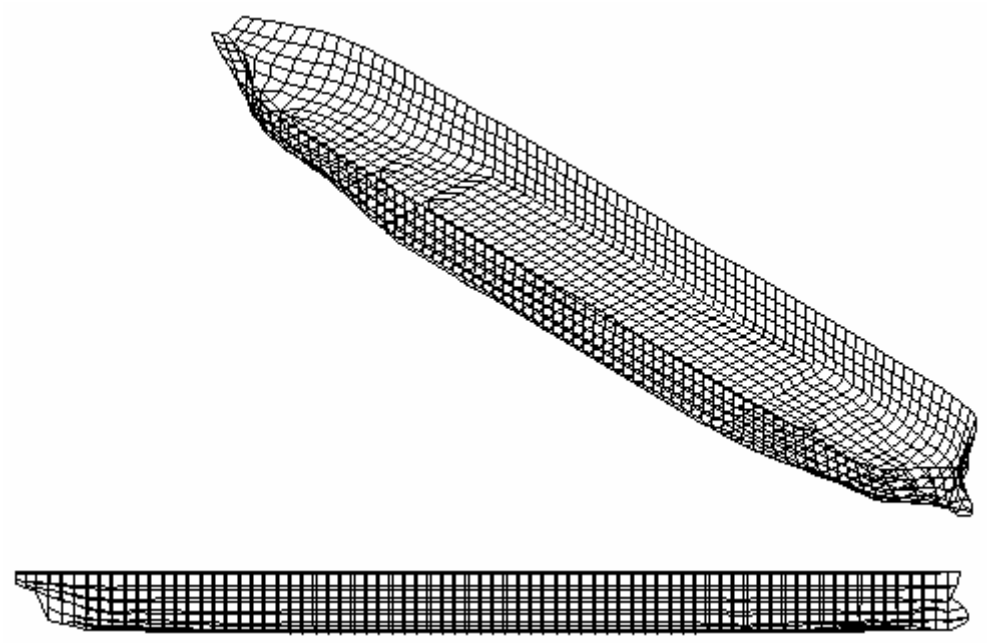

Figure 7.8: Discretisation of the damaged Derbyshire scenario A.

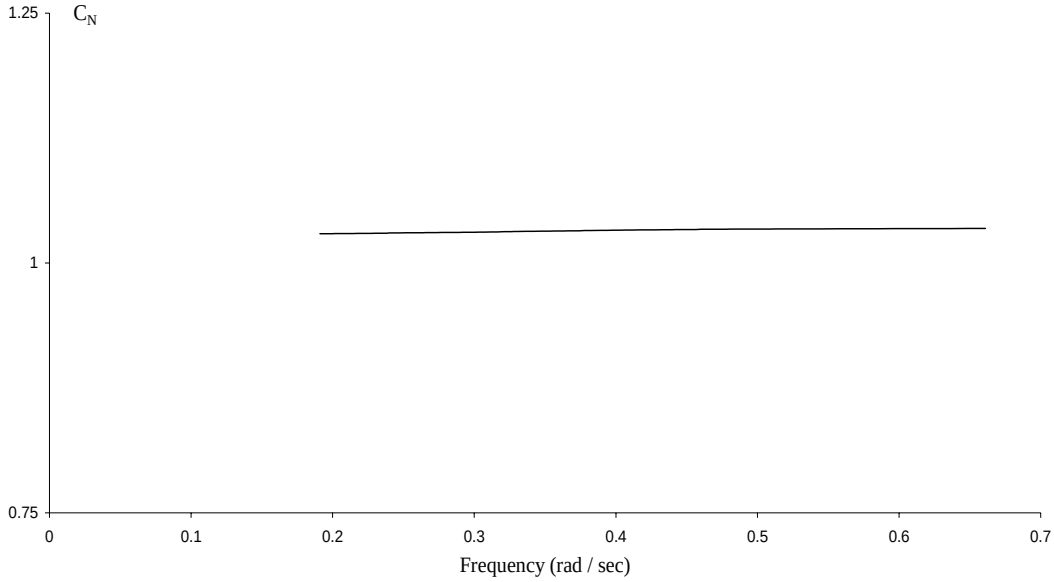

Figure 7.9: Conditioning number for the damaged Derbyshire (scenario A).

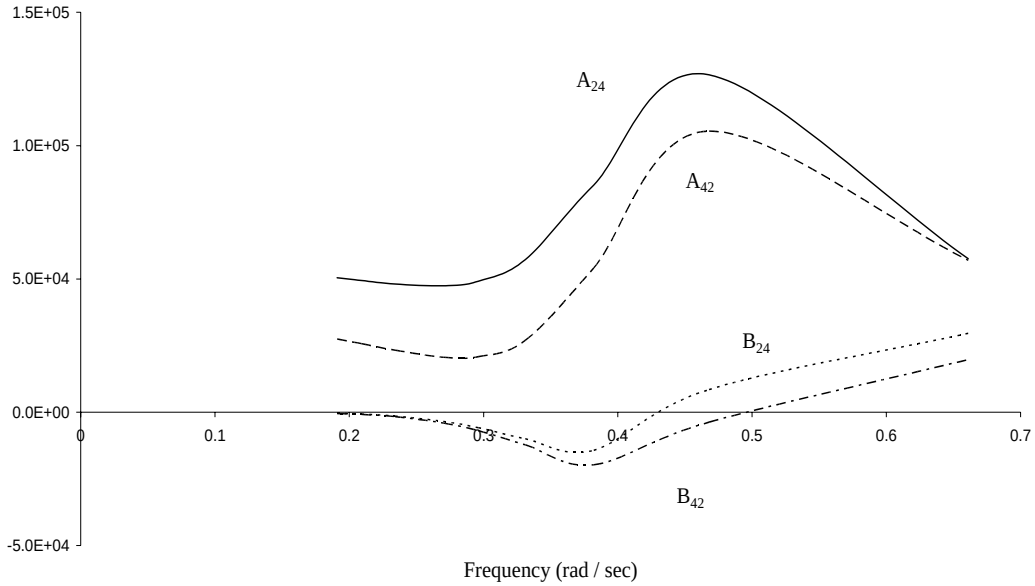

Figure 7.10: Sway-roll and roll-sway added mass and fluid damping coefficient for the damaged Derbyshire (scenario A).

For completeness the surge, heave and pitch wave excitation loads for the damaged Derbyshire (scenario A) calculated using Matthew Diffraction Suite for head seas are compared in Figures 7.11 to 7.13.

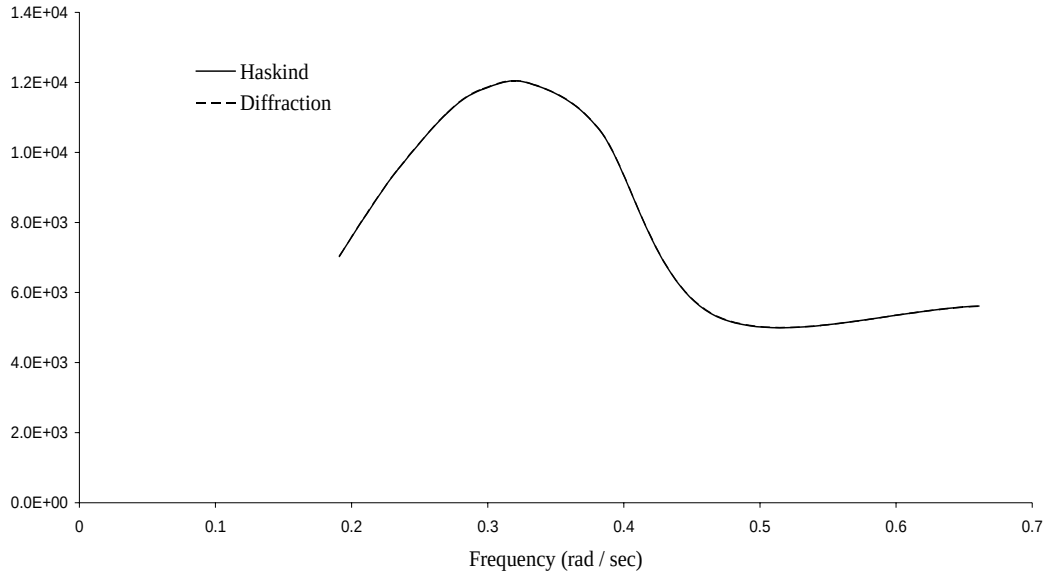

Figure 7.11: Surge wave excitation forces for the damaged Derbyshire scenario A (in head seas).

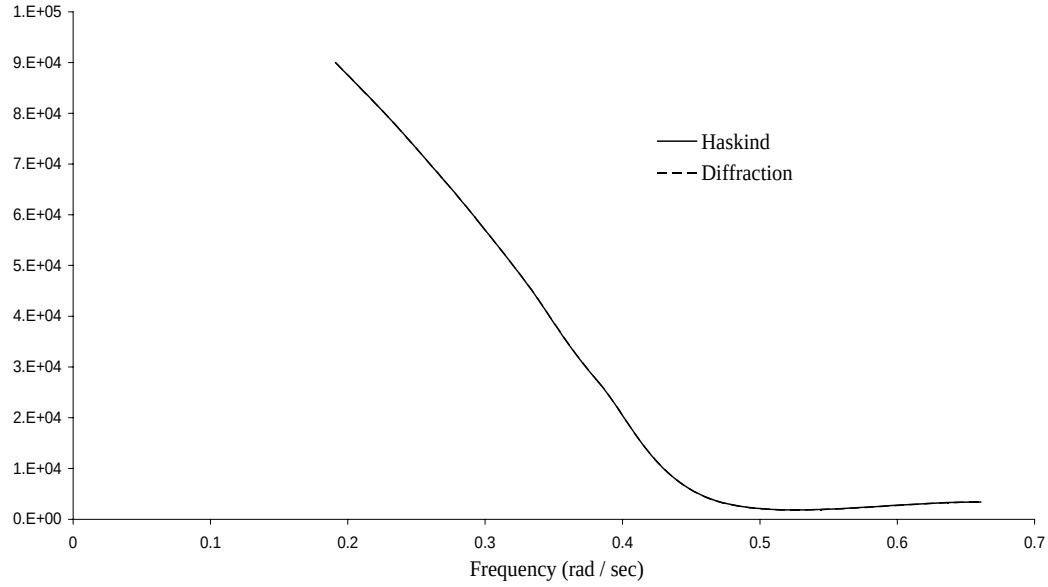

Figure 7.12: Heave wave excitation forces for the damaged Derbyshire scenario A (in head seas).

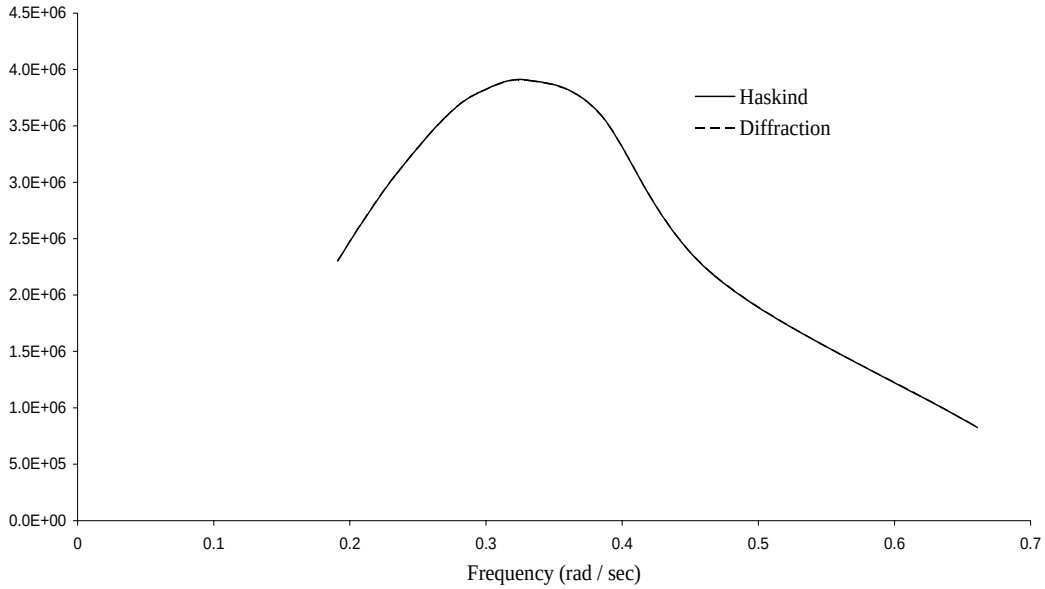

Figure 7.13: Pitch wave excitation moments for the damaged Derbyshire scenario A (in head seas).

Having established numerical stability of the fluid-structure interaction analysis, good equality of the majority of hydrodynamic cross-coupling coefficients and very good agreement of wave exciting loads calculated directly and indirectly (Haskind) the hydrodynamic data based on the discretisation predicted in Figures 7.1, 7.2 and 7.8 (and those not shown) are sufficient to undertake the motion analyses for each of the ten scenarios.

7.3 Discussion of Hydrodynamic Data for Intact and Damaged Ships

Given that four damage scenarios are to be investigated for each of the alternative intact Derbyshire hull forms the influence of all damage scenarios upon the hydrodynamic coefficients is presented next. The variation of the pure hydrodynamic added mass and fluid damping coefficients for the parent and optimised Derbyshire hull form for the

intact and damaged conditions is provided through Figures 7.14 to 7.19 and Figures 7.20 to 7.25 respectively.

There is no a priori theory that allows objective judgement of the correctness, or otherwise of these calculated pure hydrodynamic reactive coefficients. However, certain trends are expected in terms of the frequency dependence. As frequency tends to zero the fluid damping should tend to zero and if provided frequencies investigated are high enough added mass should tend to a constant (see, for example, Lewis (1989)).

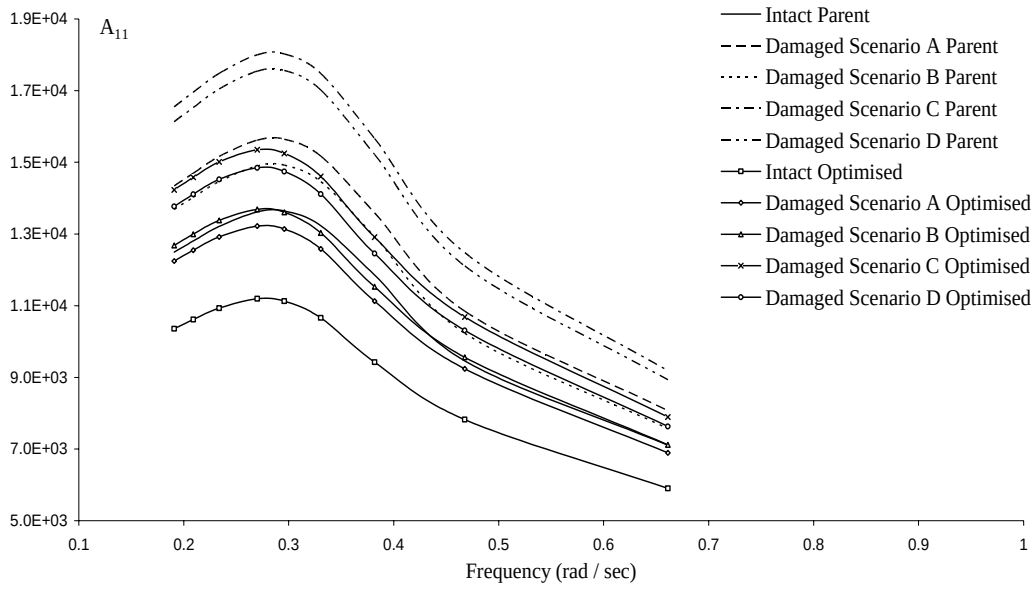

Figure 7.14: Pure surge added mass coefficient for intact and damaged hull forms.

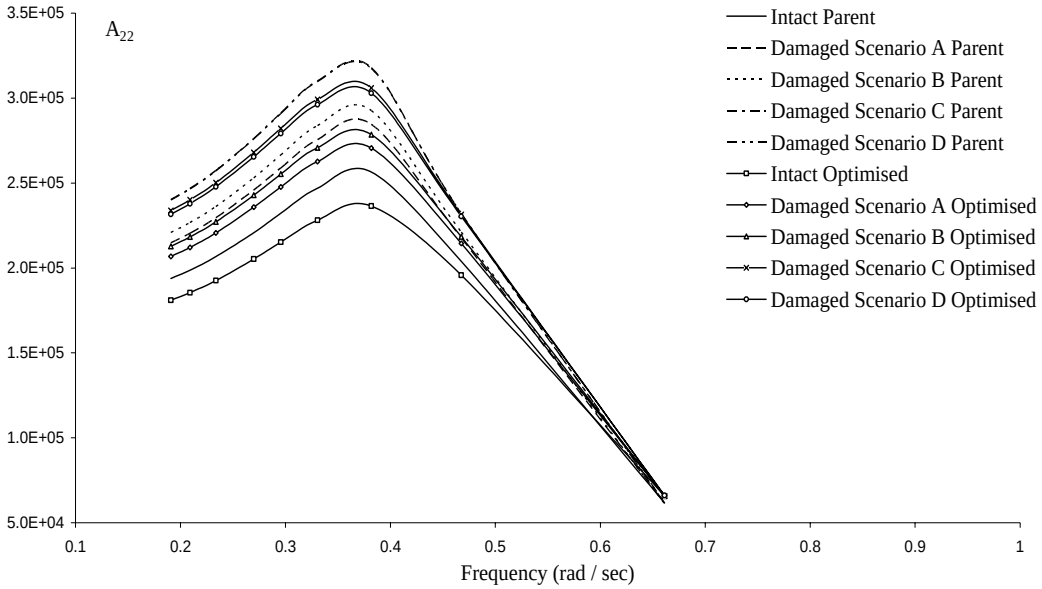

Figure 7.15: Pure sway added mass coefficient for intact and damaged hull forms.

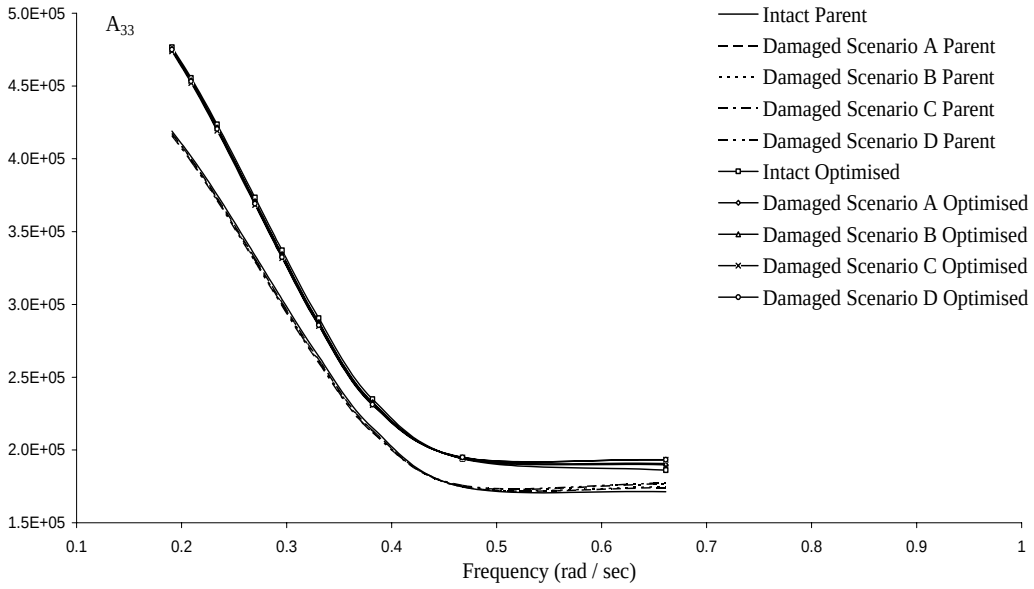

Figure 7.16: Pure heave added mass coefficient for intact and damaged hull forms.

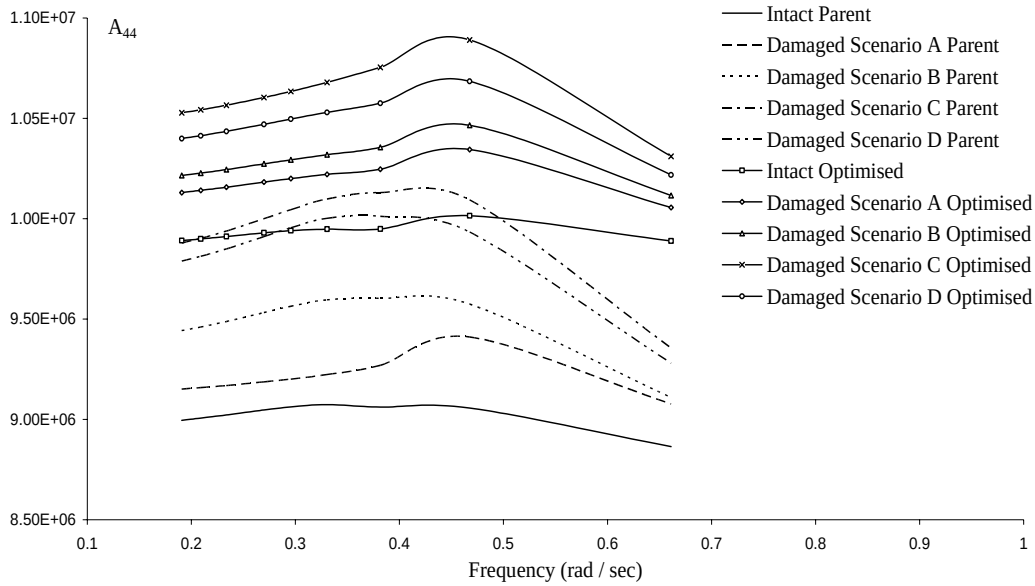

Figure 7.17: Pure roll added mass coefficient for intact and damaged hull forms.

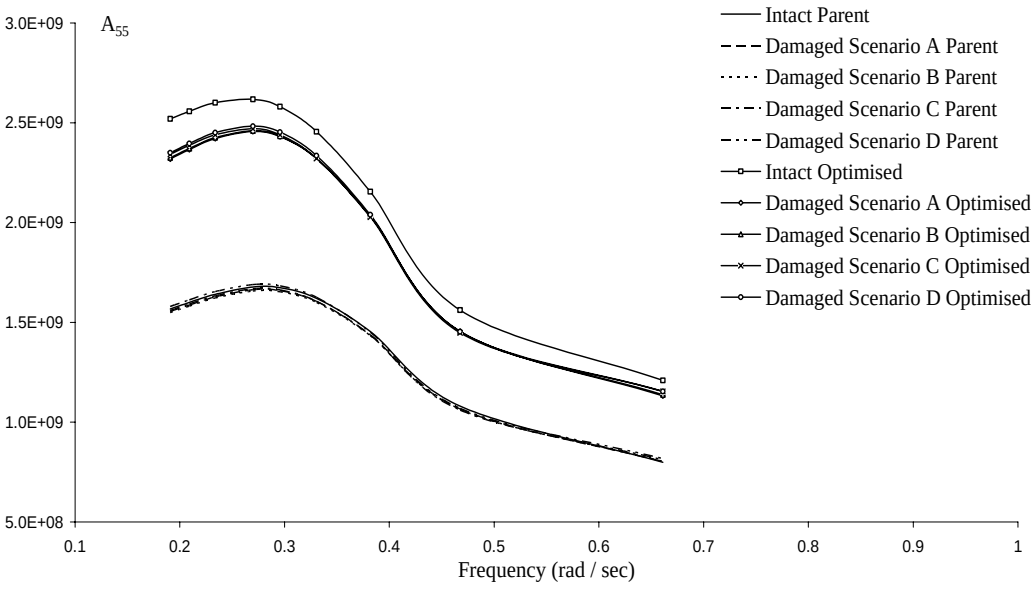

Figure 7.18: Pure pitch added mass coefficient for intact and damaged hull forms.

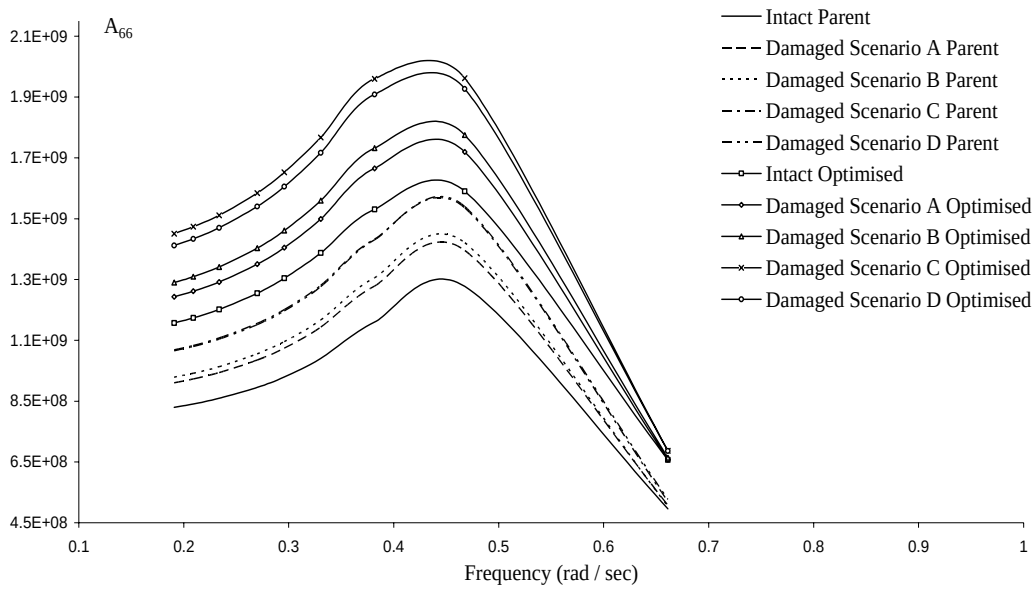

Figure 7.19: Pure yaw added mass coefficient for intact and damaged hull forms.

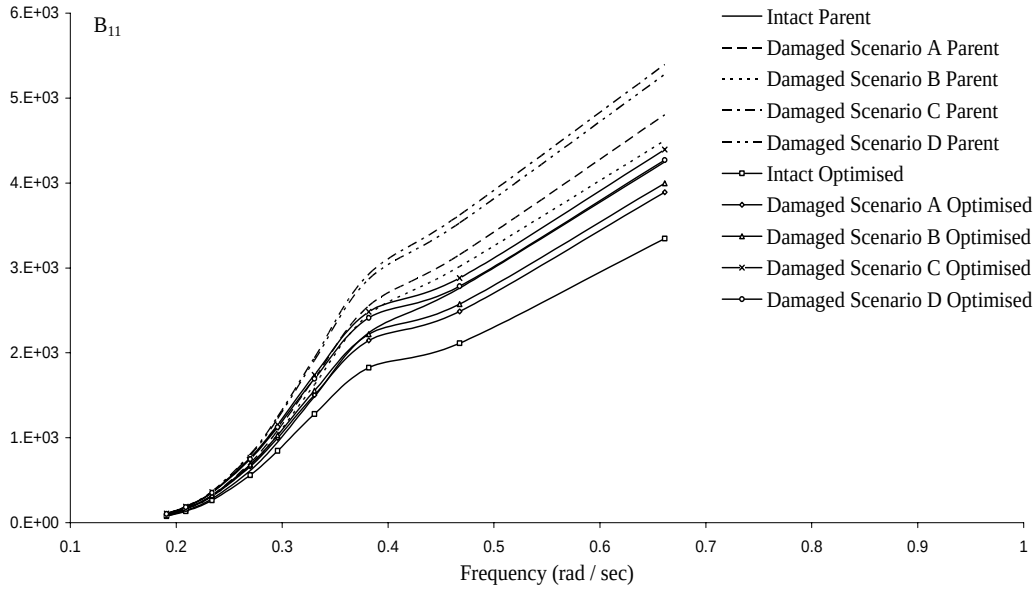

Figure 7.20: Pure surge fluid damping coefficient for intact and damaged hull forms.

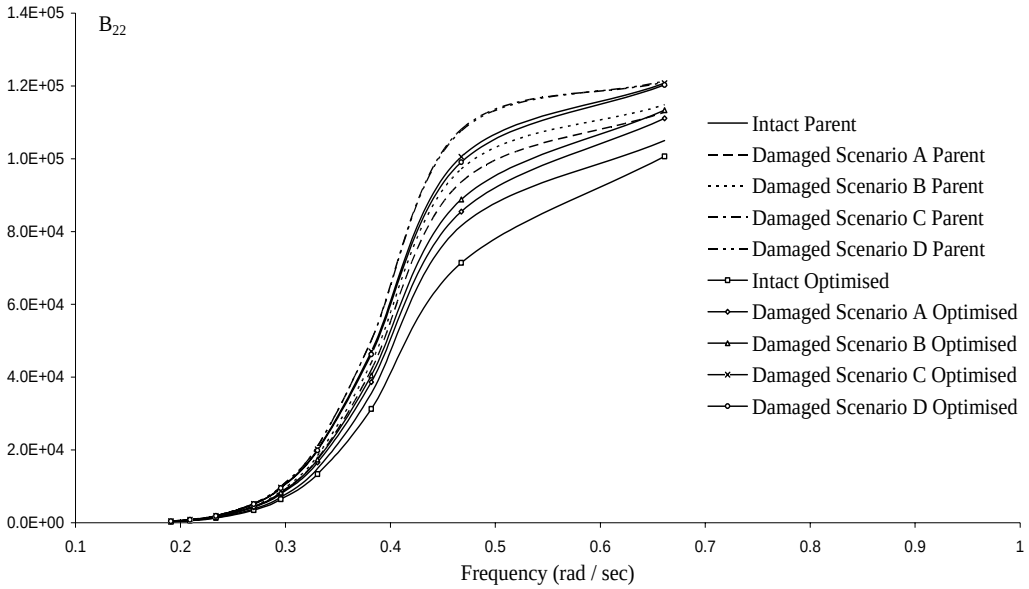

Figure 7.21: Pure sway fluid damping coefficient for intact and damaged hull forms.

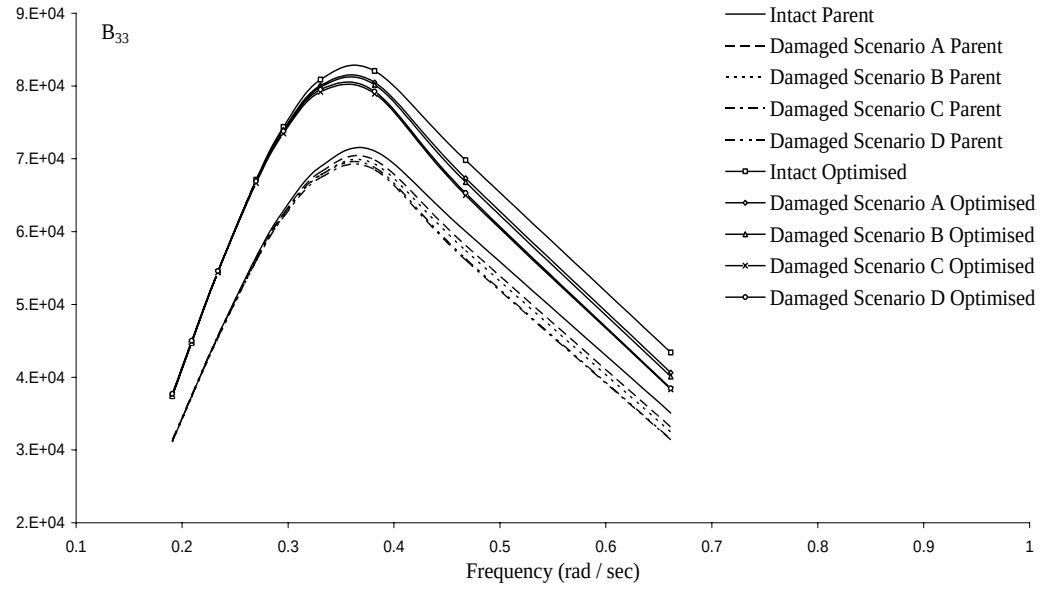

Figure 7.22: Pure heave fluid damping coefficient for intact and damaged hull forms.

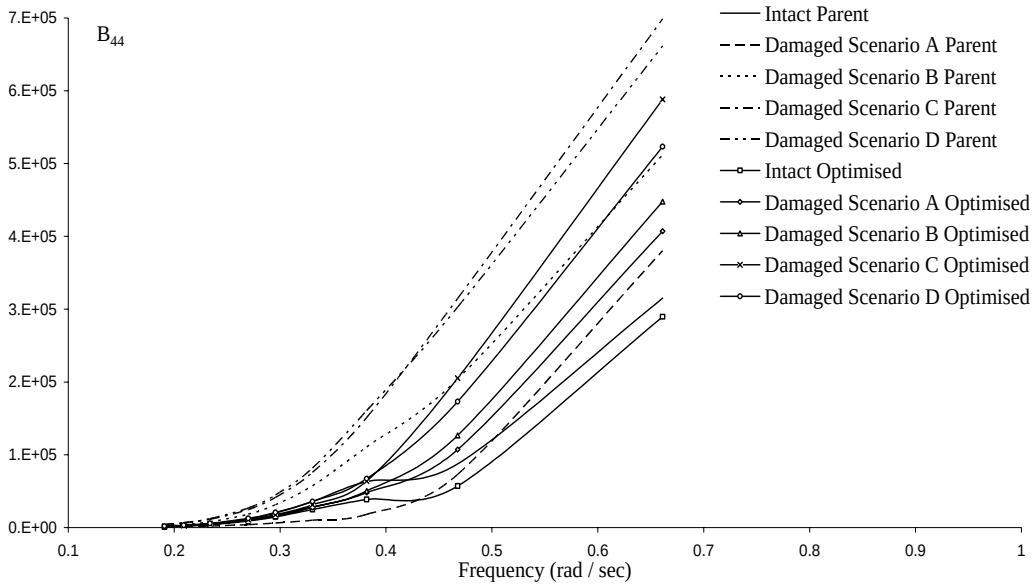

Figure 7.23: Pure roll fluid damping coefficient for intact and damaged hull forms.

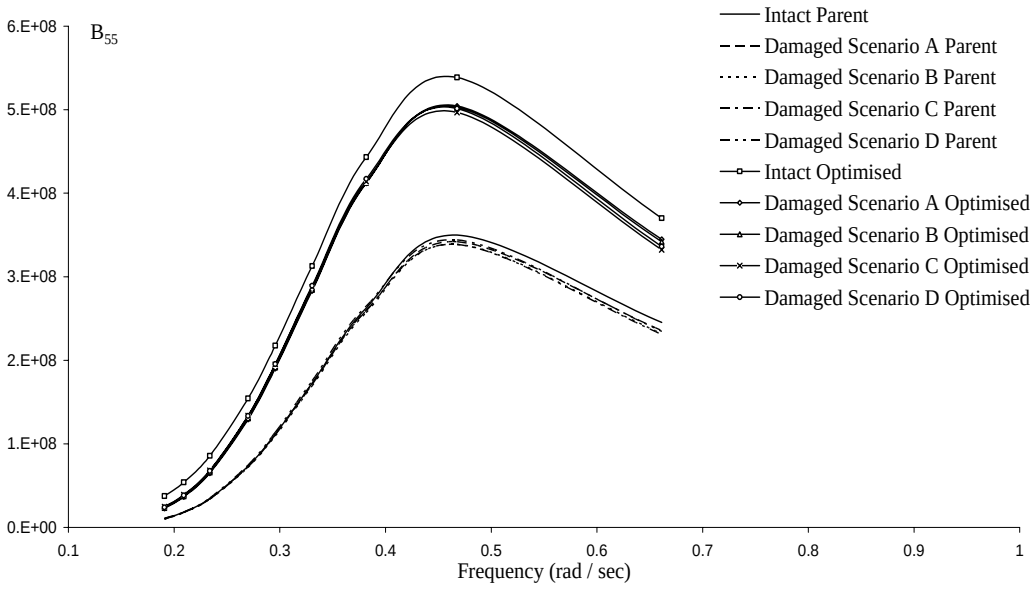

Figure 7.24: Pure pitch fluid damping coefficient for intact and damaged hull forms.

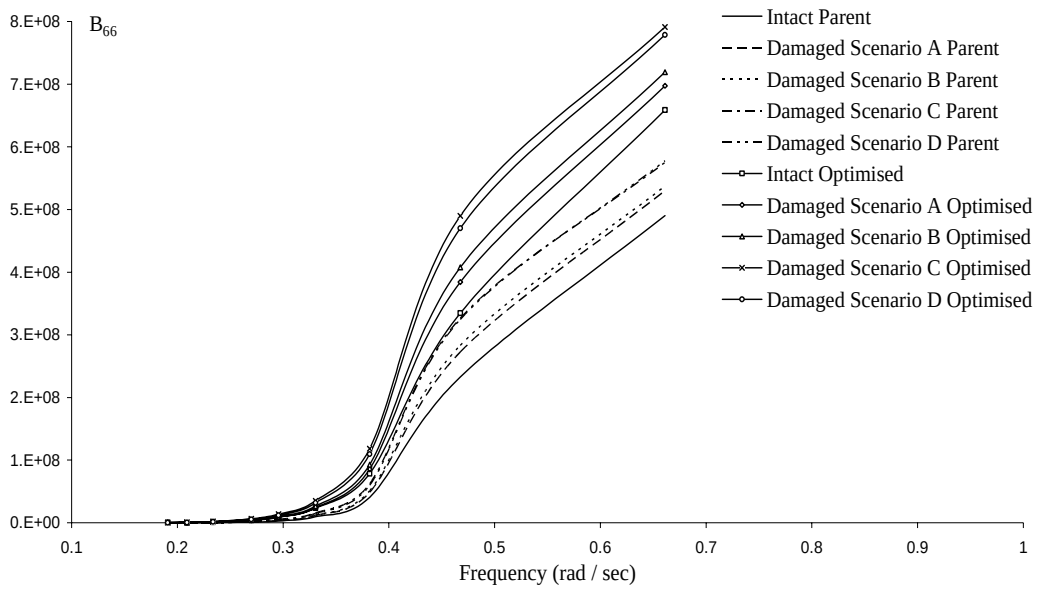

Figure 7.25: Pure yaw fluid damping coefficient for intact and damaged hull forms.

Since relative vertical motion (see Chapter 8) is determined from the heave, roll and pitch motions the pure hydrodynamic reactive coefficients associated with these degrees of freedom are commented first.

Figures 7.16 & 7.22 indicate that it is the pure heave fluid damping that is sensitive to the optimisation and damage changes. The heave added mass increases due to the optimisation but is generally insensitive to change associated with damage. Vassalos & Jasionowski (2002) observed similar insensitivities in heave added mass in their investigation.

For pure roll, Figures 7.17 & 7.23 demonstrate that roll added inertia is more sensitive to hull form geometry changes than wave frequency, whereas fluid damping is sensitive to both geometry and incident wave frequency variation. The damping almost monotonically increases after an initial slow variation with wave frequency for each geometric form. In the Vassalos & Jasionowski (2002) study the roll hydrodynamic coefficients (unlike heave) also showed some dependency on the damaged vessel's

attitude. In this study the pure roll (as well as pure surge, sway and yaw) added and fluid damping coefficients increase for the optimised hull as one considers damage case A and then B, and then damage case D with further increases for case C. Here the differences in parallel sinkage, trim and heel (although small) are apparently sufficient to generate a measurable difference.

For pure pitch, Figures 7.18 & 7.24, the pitch fluid damping (like heave) increase when the structure is optimised with maximum increases for intact case. The increases in pure pitch added inertia are more significant than the heave added mass changes.

When the structure is optimised B/T increases from 2.45 to 2.69. As Lewis (1989) points out a structure with the same cross sectional area but of beamier form will generate more fluid disturbance than a narrow section. Hence it is the B/T increases that it is thought to increase the pure vertical motion added mass hydrodynamic coefficients as a result of optimisation. B/T increases is also considered the underpinning reason for reduced surge and sway added mass coefficients as the structure is optimised (Newman (1977)).

The sensitivities of the hydrodynamic yaw coefficients, Figures 7.19 & 7.25, are quite worked due to optimisation and different damage scenarios.

The cross-coupled added mass and fluid damping coefficients for the intact and damaged parent and optimised Derbyshire hull forms are plotted in Figures 7.26 to 7.31 and Figures 7.32 to 7.37 respectively to indicate the sensitivity of the various coefficients to optimisation and damage. The hydrodynamic coefficients plotted correspond to those that are non-zero in the intact case.

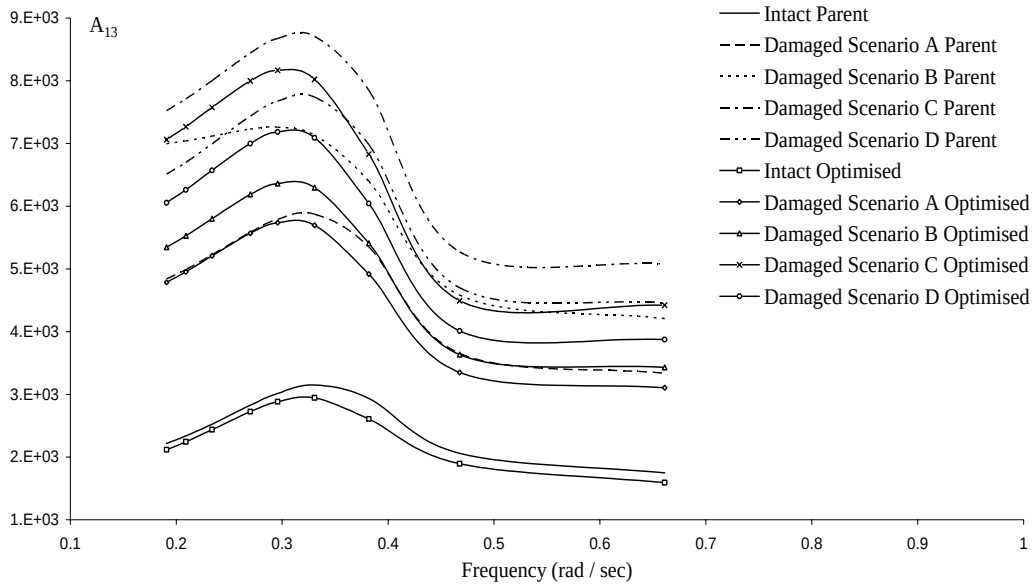

Figure 7.26: Heave induced surge added mass for the intact and damaged hull forms.

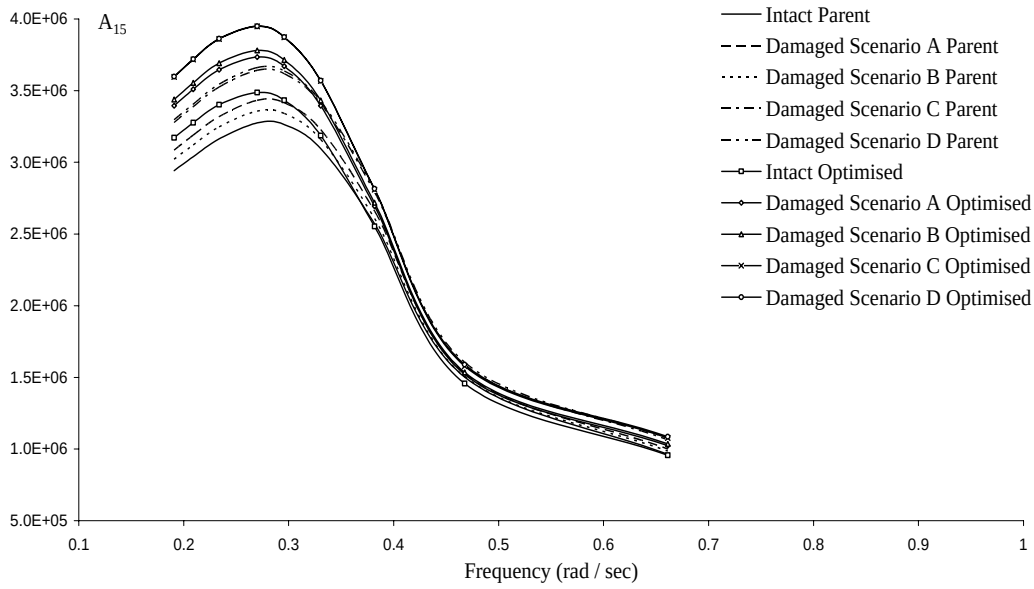

Figure 7.27: Pitch induced surge added mass for the intact and damaged hull forms.

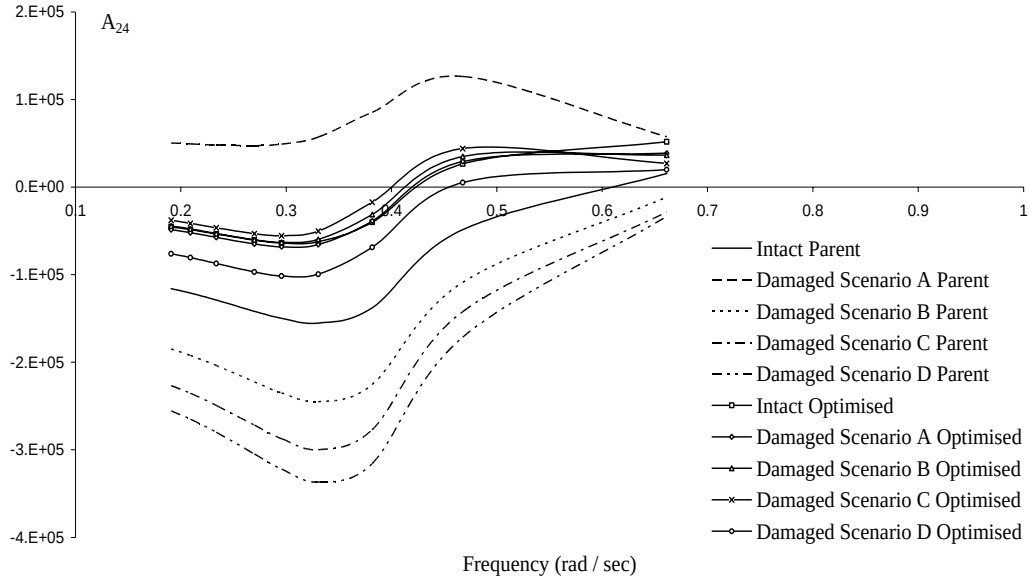

Figure 7.28: Roll induced sway added mass for the intact and damaged hull forms.

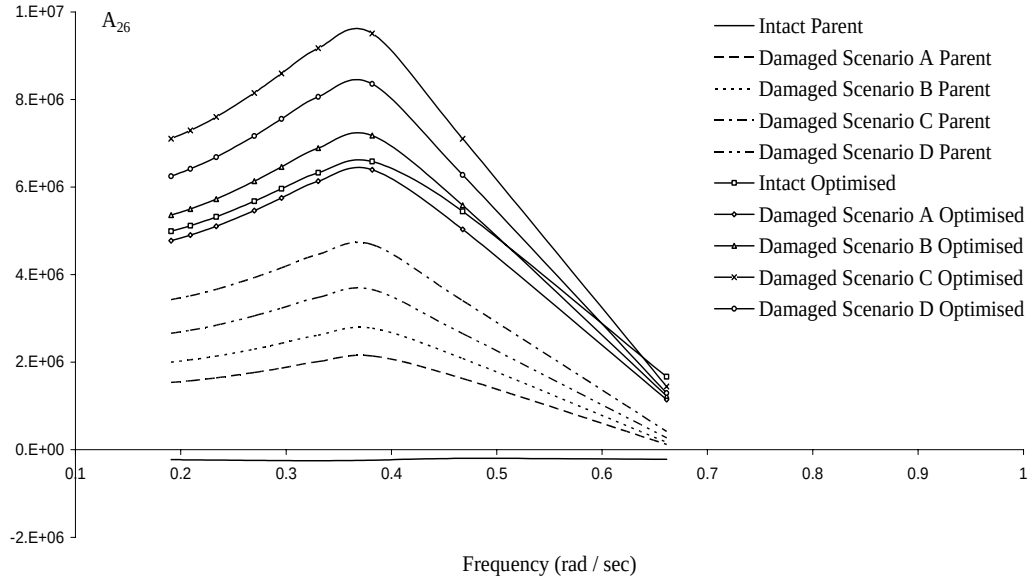

Figure 7.29: Yaw induced sway added mass for the intact and damaged hull forms.

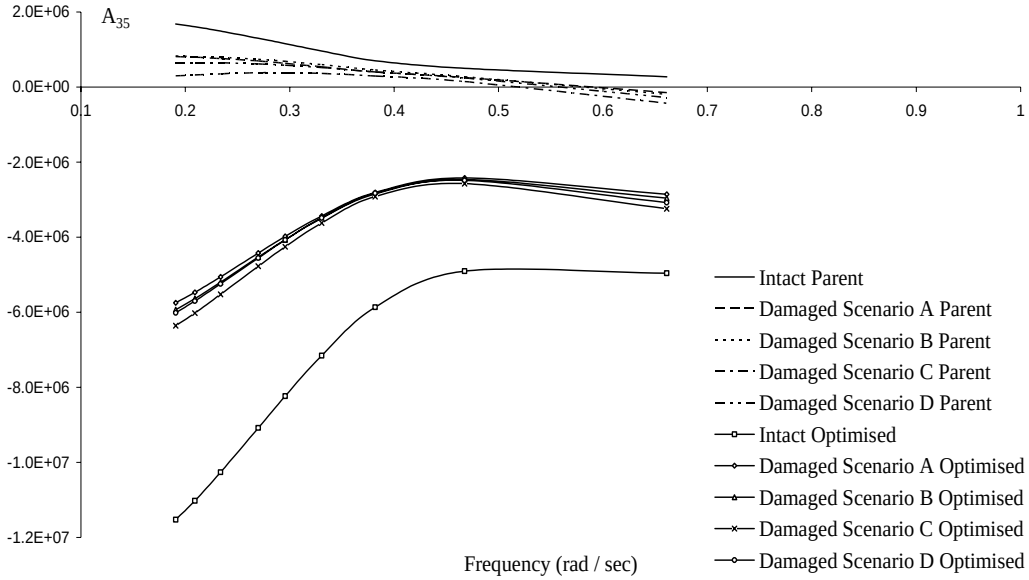

Figure 7.30: Pitch induced heave added mass for the intact and damaged hull forms.

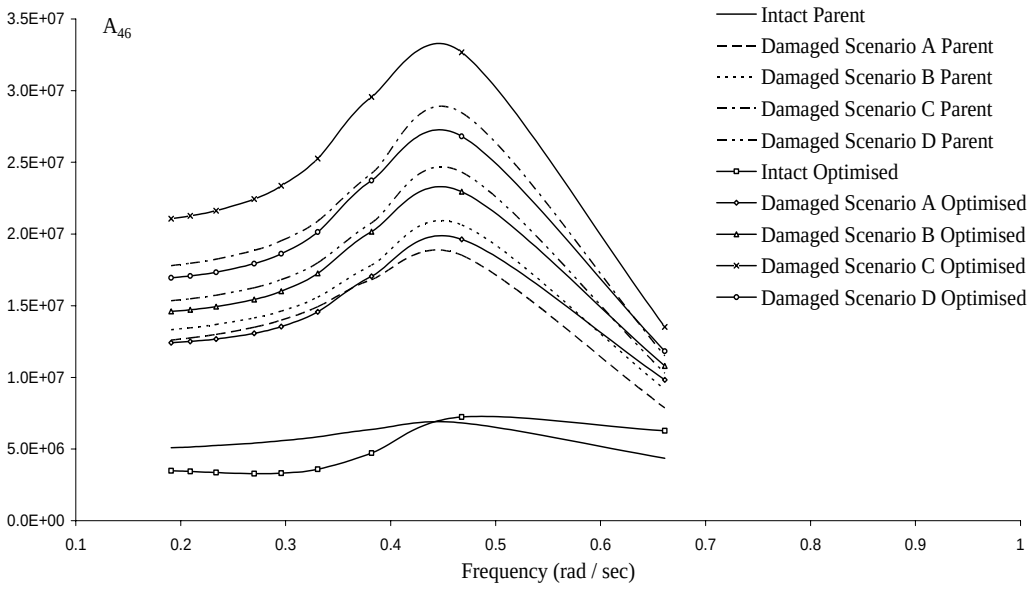

Figure 7.31: Yaw induced roll added mass for the intact and damaged hull forms.

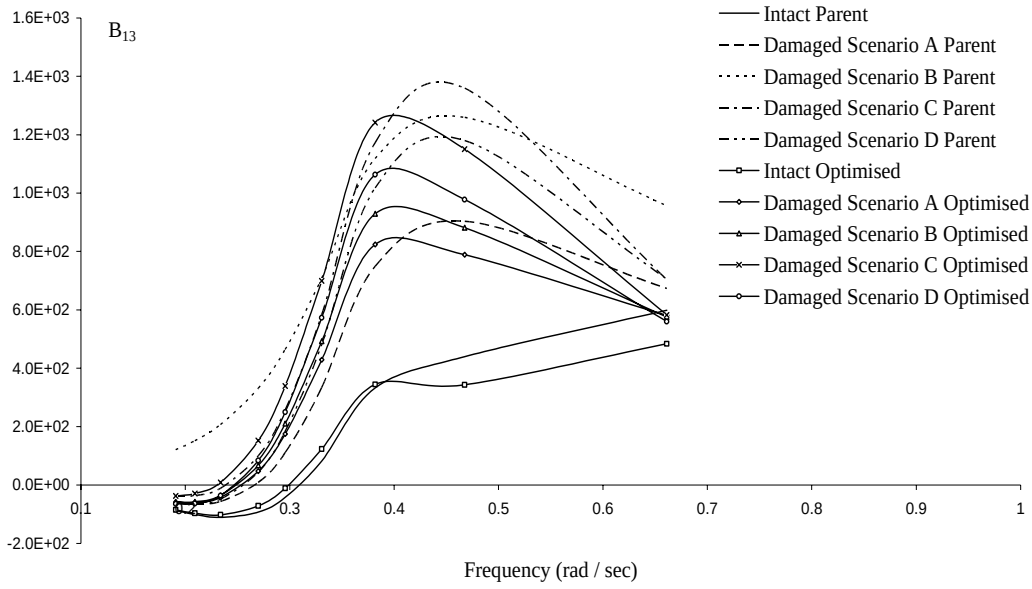

Figure 7.32: Heave induced surge fluid damping for the intact and damaged hull forms.

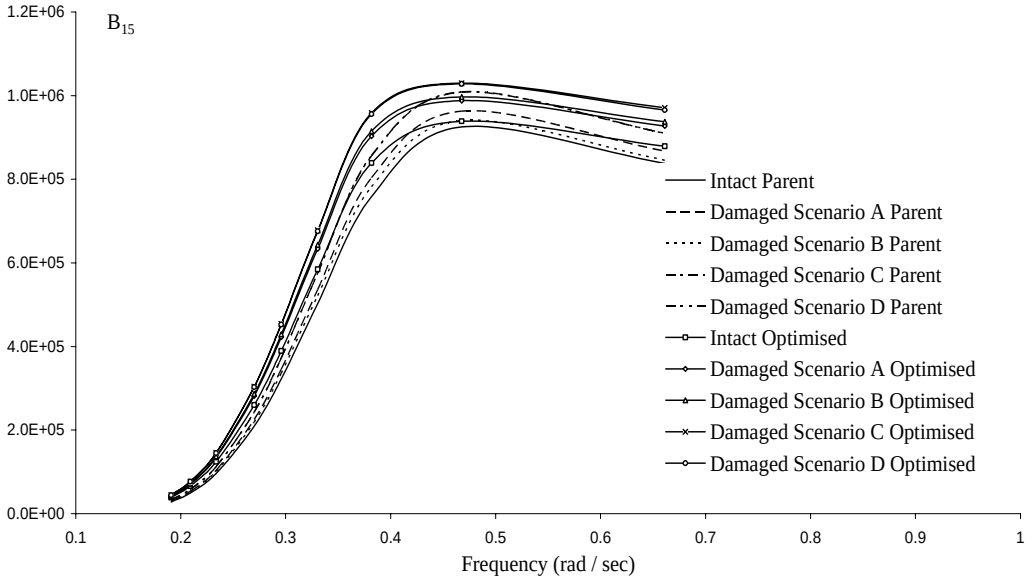

Figure 7.33: Pitch induced surge fluid damping for the intact and damaged hull forms.

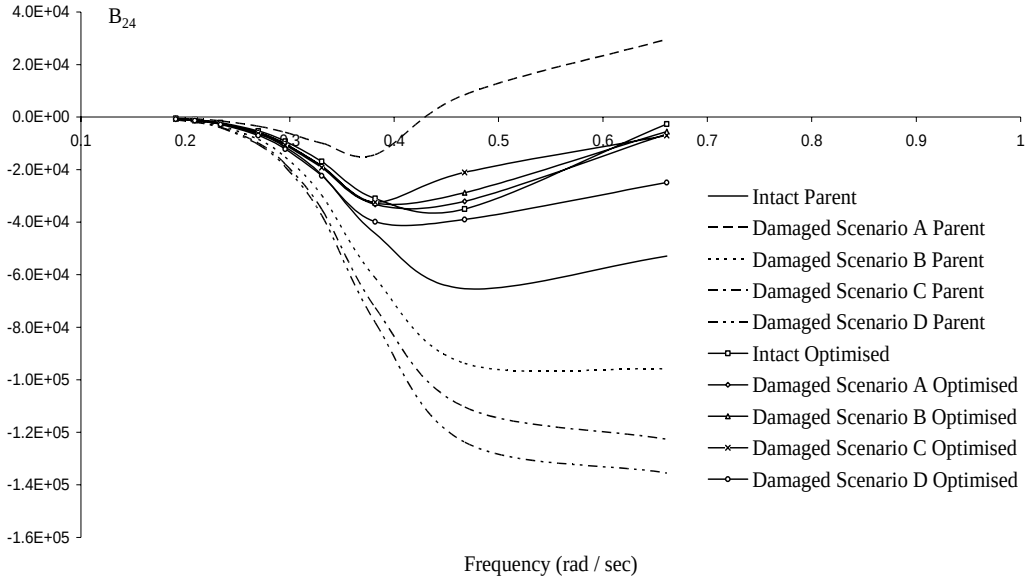

Figure 7.34: Roll induced sway fluid damping for the intact and damaged hull forms.

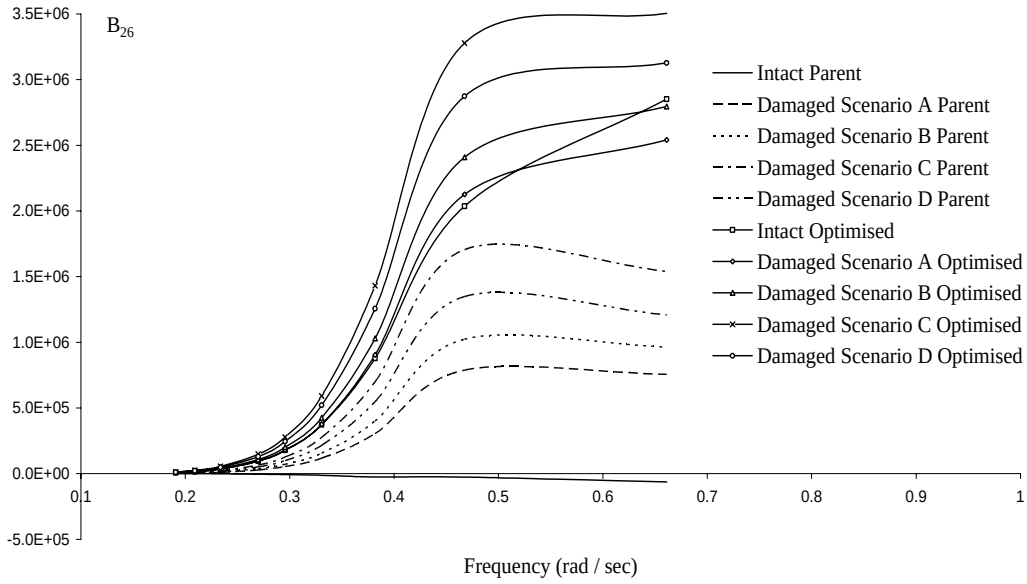

Figure 7.35: Yaw induced sway fluid damping for the intact and damaged hull forms.

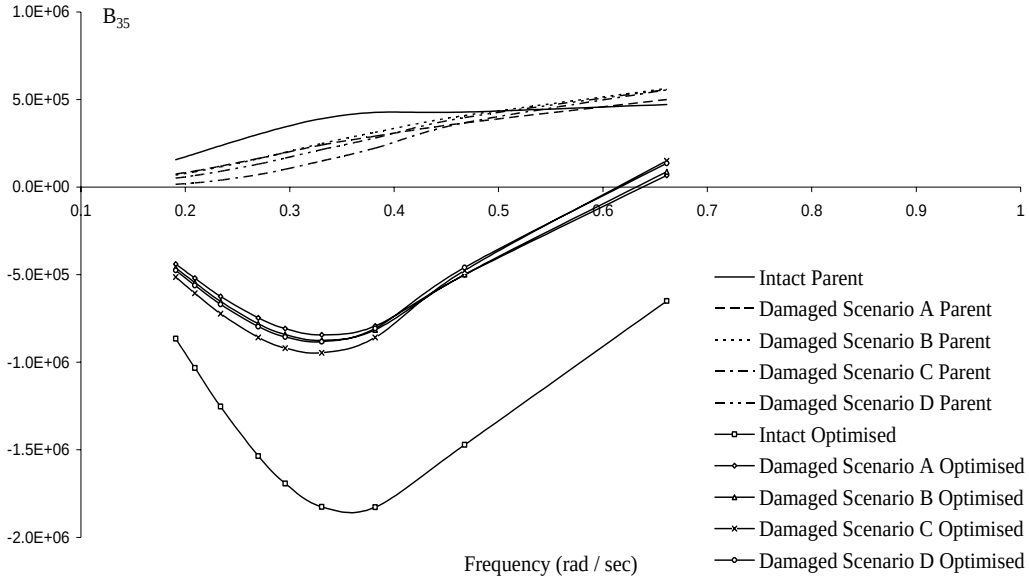

Figure 7.36: Pitch induced heave fluid damping for the intact and damaged hull forms.

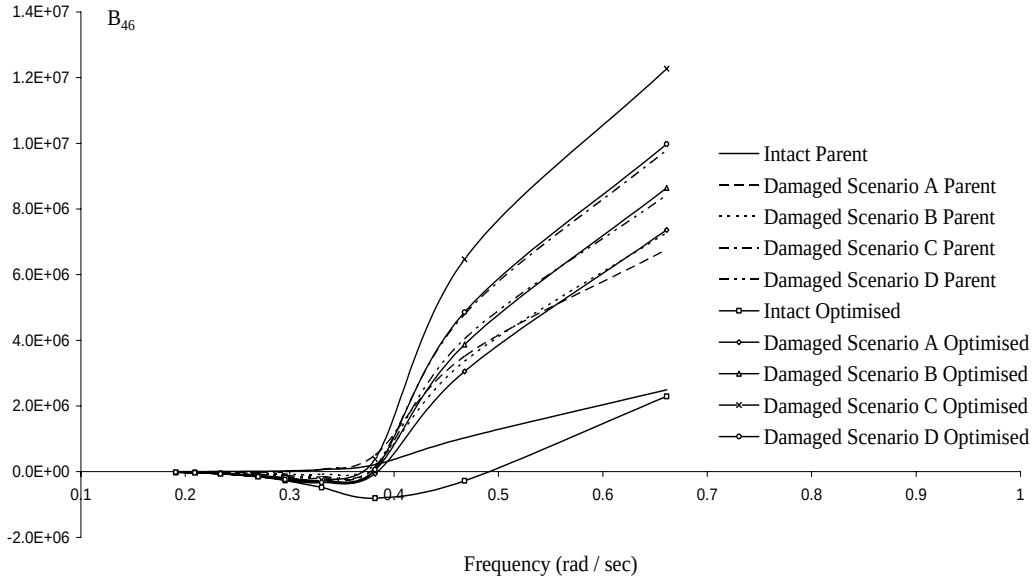

Figure 7.37: Yaw induced roll fluid damping for the intact and damaged hull forms.

Figures 7.26 & 7.27 provide the heave and pitch induced surge added mass and Figures 7.32 & 7.33 present the corresponding fluid damping. The heave induced surge

coefficients are significantly more sensitive to optimisation and damage changes than the pitch induced surge coefficients. The intact and damaged heave induced surge added mass and fluid damping coefficients are quite distinct with the intact values lower.

The roll and yaw induced sway added mass and fluid damping coefficients of Figures 7.28 & 7.29 and Figures 7.34 & 7.35 are well spread out. Apart from the largest predicted values for the parent Derbyshire hull form for damage scenario A the roll induced sway results partitioned into the lowest set of values for the damaged non-optimised hull form, the intact parent and the damaged optimised scenario D values and then the intact optimised and the damaged optimised scenarios A, B & C hull form values. For the yaw induced sway coefficients there is a different but common pattern. Starting with the lowest values for the intact parent Derbyshire hull form the next set are the damaged parent hull form followed by the optimised intact and damaged hull form values.

The pitch induced heave coefficient values in Figures 7.30 & 7.36 are quite distinct again. In each case there are three distinct groupings of results. The lowest values are associated with the intact optimised hull form. Next the damaged optimised hull form values form a narrow tight band of variation with the third set form by the parent hull form both intact and damaged.

Finally, there are the yaw induced roll coefficients of Figures 7.31 & 7.37 which divide into the intact ship values and the damaged ship values. For the added mass there are five pairs of curves. The lowest values are associated with the intact parent and optimised hull forms, the second pair is formed of the parent and optimised hull form values of Scenario A, the third pair is formed of the parent and optimised hull form values of Scenario B, the fourth pair is the parent and optimised hull form values of Scenario D and finally the fifth pair is the parent and optimised hull form values of Scenario C. For the fluid damping curves the order of the grouping is similar with few exceptions.

In general terms it appears that:

- The shape of the added mass curves is similar in trend for intact and damaged hull forms.

- Apart from a few exceptions the fluid damping coefficients increase as a consequence of optimisation.

- For added mass the heave induced surge value decrease as result of optimisation, whereas they increase for the pitch-surge, yaw-sway and pitch-heave added masses.

- Generally added mass coefficient increases with damage are associated with moving from scenario A to scenario B, then B to D and finally D to C.

Prior to undertaking the formulation and solution of the relative vertical motion set out in Chapter 8 and Appendix I completeness requires provision of the various hydrostatic restoration coefficients. Data for each of the 10 scenarios to be investigated are provided in Tables 7.1 to 7.10.

Table 7.1: Hydrostatic coefficients for the intact case for the parent Derbyshire.

Hydrostatic Coefficients	Heave	Roll	Pitch
Heave	1.16×10^5	0.00	5.27×10^5
Roll	0.00	1.36×10^7	0.00
Pitch	5.27×10^5	0.00	7.09×10^8

Table 7.2: Hydrostatic coefficients for the damage case scenario A for the parent Derbyshire.

Hydrostatic Coefficients	Heave	Roll	Pitch
Heave	$1.16x10^{5}$	$-1.17x10^{4}$	$2.24x10^{5}$
Roll	$-1.17x10^{4}$	$1.22x10^{7}$	$-9.27x10^{4}$
Pitch	$2.24x10^{5}$	$-9.43x10^{4}$	$7.10x10^{8}$

Table 7.3: Hydrostatic coefficients for the damage case scenario B for the parent Derbyshire.

Hydrostatic Coefficients	Heave	Roll	Pitch
Heave	$1.16x10^{5}$	$-1.56x10^{4}$	$2.32x10^{5}$
Roll	$-1.56x10^{4}$	$1.73x10^{7}$	$-1.05x10^{5}$
Pitch	$2.32x10^{5}$	$-9.27x10^{4}$	$7.09x10^{8}$

Table 7.4: Hydrostatic coefficients for the damage case scenario C for the parent Derbyshire.

Hydrostatic Coefficients	Heave	Roll	Pitch
Heave	$1.16x10^{5}$	$-2.75x10^{4}$	$8.24x10^{3}$
Roll	$-2.75x10^{4}$	$1.97x10^{7}$	$-1.13x10^{5}$
Pitch	$8.24x10^{3}$	$-1.20x10^{5}$	$7.23x10^{8}$

Table 7.5: Hydrostatic coefficients for the damage case scenario D for the parent Derbyshire.

Hydrostatic Coefficients	Heave	Roll	Pitch
Heave	$1.17x10^{5}$	$-2.71x10^{4}$	$1.34x10^{5}$
Roll	$-2.71x10^{4}$	$2.00x10^{7}$	$-8.12x10^{4}$
Pitch	$1.34x10^{5}$	$-9.21x10^{4}$	$7.29x10^{8}$

Table 7.6: Hydrostatic coefficients for the intact case for the optimised Derbyshire.

Hydrostatic Coefficients	Heave	Roll	Pitch
Heave	$1.27x10^{5}$	0.00	$-3.00x10^{6}$
Roll	0.00	$1.05x10^{7}$	0.00
Pitch	$-3.00x10^{6}$	0.00	$1.01x10^{9}$

Table 7.7: Hydrostatic coefficients for the damage case scenario A for the optimised Derbyshire.

Hydrostatic Coefficients	Heave	Roll	Pitch
Heave	$1.28x10^{5}$	$-1.19x10^{4}$	$-1.55x10^{6}$
Roll	$-1.19x10^{4}$	$1.28x10^{7}$	$6.73x10^{4}$
Pitch	$-1.55x10^{6}$	$6.17x10^{4}$	$9.69x10^{8}$

Table 7.8: Hydrostatic coefficients for the damage case scenario B for the optimised Derbyshire.

Hydrostatic Coefficients	Heave	Roll	Pitch
Heave	$1.28x10^{5}$	$-1.22x10^{4}$	$-1.63x10^{6}$
Roll	$-1.22x10^{4}$	$1.33x10^{7}$	$4.81x10^{4}$
Pitch	$-1.63x10^{6}$	$4.13x10^{4}$	$9.74x10^{8}$

Table 7.9: Hydrostatic coefficients for the damage case scenario C for the optimised Derbyshire.

Hydrostatic Coefficients	Heave	Roll	Pitch
Heave	$1.28x10^{5}$	$-1.70x10^{4}$	$-1.81x10^{6}$
Roll	$-1.70x10^{4}$	$1.51x10^{7}$	$1.36x10^{5}$
Pitch	$-1.81x10^{6}$	$1.27x10^{5}$	$9.88x10^{8}$

Table 7.10: Hydrostatic coefficients for the damage case scenario D for the optimised Derbyshire.

Hydrostatic Coefficients	Heave	Roll	Pitch
Heave	1.29×10^{5}	-1.70×10^{4}	-1.68×10^{6}
Roll	-1.70×10^{4}	1.54×10^{7}	1.39×10^{5}
Pitch	-1.68×10^{6}	1.28×10^{5}	9.90×10^{8}

As expected cross-coupling of the restoration terms, in particular for the heave-roll and roll-pitch hydrostatic coefficients occurs when the structure is damaged (see Tables 7.2-7.5 and Tables 7.7-7.10) and does not occur when the structure is intact. Irrespective of geometric characteristics the cross-terms should be symmetric. In general the cross-terms agree quite well, but significant figures are being lost for those terms one or two magnitudes smaller.

While the hydrostatic restoration coefficients in pure heave do not vary so much the other coefficients change in magnitude from one case to another.

7.4 Summary

Having argued that the numerical stability of the fluid-structure interaction is more than satisfactory and noted that for some degrees of freedom hydrodynamic coefficients are slightly sensitive to geometric and damage changes the next stage is to provide relative motion responses to ascertain whether the optimised damaged ships have less pleasing motion characteristics than the parent damaged hull forms.

8. RELATIVE VERTICAL MOTION ANALYSIS OF INTACT AND DAMAGED SHIPS

With the hydrodynamic, hydrostatic and mass-inertia details for all ten scenarios available the motion equations formulated in Chapter 5 may be solved. The components of the motion amplitudes in each case for each degree of freedom have real and imaginary parts. Whilst some typical transfer functions are presented it is more meaningful to consider vector relationships such as relative vertical motion or accelerations as they combine both the amplitude and phase data determined. The transfer functions merely define individual amplitude envelops, whereas the other cited qualities provide measures of what a human being or machinery will actual experience on board of the ship.

The significance of the scalar quantity α of Equation (7.2) will be highlighted prior to presentation of the motion results. The determination of the different motion qualities and the selection of their location are addressed next.

8.1 Motion Dependent Qualities of Engineering Interest

Each degree of freedom is described as

$$\eta_j = \eta_{ja}\, \mathrm{e}^{-i\omega t} \equiv \left(\eta_{\mathrm{jr}} + i\eta_{ji}\right) e^{-i\omega t}, \tag{8.1}$$

with subscripts r and i denoting real and imaginary parts.

To determine the resultant vertical motion at some generic point (z,x,y) defined relative to origin located at LCF of ship, the positive sign convention indicated in Figure 5.1 is

used. That is, heave is positive upwards, pitch is positive bow down and roll is positive to starboard. The derivation of the Equation (8.2) is given in Appendix I.

The positive sign convention defined in Appendix I implies that

$$S_V = S_{Vr} + iS_{Vi} = \left(\eta_{3\mathrm{r}} + i\eta_{3i}\right) - l_p \,\mathrm{sgn}(z)\left(\eta_{5\mathrm{r}} + i\eta_{5i}\right) + l_r \,\mathrm{sgn}(x)\left(\eta_{4\mathrm{r}} + i\eta_{4i}\right), \qquad (8.2)$$

where (z,x) is projected coordinates of selected point in the z-x plane.

8.2 Selection of Points Investigated for Relative Vertical Displacement

When the ship is damaged the ship's crew and passengers (if appropriate) will move to the deck and muster at the appropriate lifeboat stations. Therefore, in general the points of interest for determining and comparing the relative vertical motion lie on the perimeter of the deck. In this study the points designated A, B, C, D, E, F & G of Figure 8.1 will be investigated.

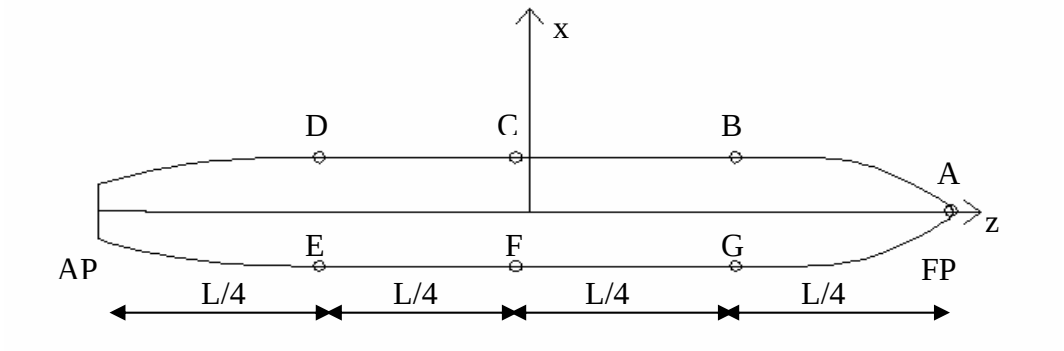

Figure 8.1: Relative positions of the points of interest for the parent Derbyshire for investigating vertical displacement.

Solution of the diffraction problem and hence specification of wave excitation loads requires explicit specification of the incident wave velocity potential. In Chapter 7 the incident wave velocity potential was defined as

$$\phi_W(z,x,y) = \alpha \frac{ag}{\omega} \frac{\cosh k(y+d)}{\cosh(kd)} e^{ik(z\cos\beta + x\sin\beta)}. \tag{8.3}$$

The parameter α is set to different values within different computer programmes. Consequently it is a constant source of concern when comparing independently determined motion details, since α influences the associated phase relationship between the ship motions and the incident wave.

Irrespective of which free-surface boundary condition is selected it may be readily shown that the incident wave free surface profile associated with the defined velocity potential is given by

$$\zeta(z,x,t) = i\alpha a e^{ik(z\cos\beta + x\sin\beta)} e^{-i\omega t} = \zeta_a(z,x) e^{-i\omega t} \tag{8.4}$$

where β defines the wave direction.

As a consequence of the fluid-structure interactions the actual resulting wave profile should include the contributions of each of the radiation wave systems generated and the diffraction wave system for the wave direction of interest. This is not, however, normal practice in much of ship motion calculations and hence (in common with observed practice) the free-surface profile will be simply equated to the incident free-surface profile.

In the Matthew Diffraction Suite, used in the earlier three-dimensional hydrodynamic analysis, $\alpha = 1$. In the Optistanbul Suite a different description for α is used and hence

there will not be a one-to-one correspondent because of different initial phase selection and differences of two-dimensional versus three-dimensional calculations.

The time-independent relative vertical displacement is here defined as

$$RVM\left(z,x\right)=S_V\left(z,x\right)-\zeta_a\left(z,x\right). \tag{8.5}$$

Therefore at location (z,x) it follows that

$$\begin{aligned} RVM\left(z,x\right)=&\left(\eta_{3\mathrm{r}}+i\eta_{3i}\right)-l_p\,\mathrm{sgn}(z)\left(\eta_{5\mathrm{r}}+i\eta_{5i}\right)+l_r\,\mathrm{sgn}(x)\left(\eta_{4\mathrm{r}}+i\eta_{4i}\right)\\ &+a\left[\sin\left(kz\cos\beta+kx\sin\beta\right)-i\cos\left(kz\cos\beta+kx\sin\beta\right)\right]. \end{aligned} \tag{8.6}$$

Furthermore, without loss of generality, $a=1$ is assumed, because of the linearity of the motion equations and the linearity of the fluid-structure interaction analysis used. Setting $a=1$ in Equation (8.6) is also equivalent to treating $RVM\left(z,x\right)$ as a non-dimensional relative vertical motion, that is, $RVM\left(z,x\right)/a$.

The changes in the coordinates of the points A to G, originally defined on the parent hull form of the Derbyshire, are initially a consequence of the hull optimisation undertaken. Thereafter the points take up new positions as a consequence of damage scenarios A to D being applied to the parent and optimised Derbyshire hull forms. The equivalent positions of the selected points are defined in Tables 8.1 to 8.3.

Table 8.1: Location of the points of interest on intact hull forms.

Point	Intact Derbyshire	Intact Derbyshire Optimised
A	(140.102,0.000,0.000)	(168.296,0.000,0.000)
B	(69.617,22.098,7.024)	(90.763,21.995,8.654)
C	(-0.868,22.098,7.024)	(13.229,21.995,8.654)
D	(-71.353,22.098,7.024)	(-64.304,21.995,8.654)
E	(-71.353,-22.098,7.024)	(-64.304,-21.995,8.654)
F	(-0.868,-22.098,7.024)	(13.229,-21.995,8.654)
G	(69.617,-22.098,7.024)	(90.763,-21.995,8.654)

Table 8.2: Location of the points of interest for the damaged parent Derbyshire hull form.

Point	Case A	Case B	Case C	Case D
A	(140.065,0.073,-3.393)	(140.046,0.093,-4.156)	(139.962,0.230,-6.571)	(140.004,0.196,-5.625)
B	(69.708,21.990,5.286)	(69.722,21.995,4.827)	(69.745,21.989,3.521)	(69.722,21.973,3.971)
C	(-0.767,21.965,6.471)	(-0.747,21.962,6.293)	(-0.703,21.908,5.826)	(-0.740,21.910,5.778)
D	(-71.242,21.939,7.657)	(-71.217,21.929,7.759)	(-71.150,21.828,8.131)	(-71.201,21.847,7.585)
E	(-71.242,-22.247,6.713)	(-71.217,-22.256,6.766)	(-71.150,-22.342,6.588)	(-71.201,-22.323,6.042)
F	(-0.767,-22.221,5.527)	(-0.747,-22.223,5.300)	(-0.703,-22.261,4.283)	(-0.740,-22.259,4.235)
G	(69.708,-22.196,4.342)	(69.722,-22.190,3.834)	(69.745,-22.181,1.979)	(69.722,-22.196,2.428)

Table 8.3: Location of the equivalent points of interest for the damaged optimised Derbyshire hull form.

Point	Case A	Case B	Case C	Case D
A	(168.267,0.070,-3.276)	(168.251,0.090,-4.066)	(168.186,0.167,-6.363)	(168.219,0.142,-5.420)
B	(90.861,21.852,6.921)	(90.880,21.859,6.423)	(90.915,21.873,4.958)	(90.887,21.860,5.449)
C	(13.335,21.829,7.998)	(13.358,21.829,7.776)	(13.410,21.818,7.056)	(13.371,21.817,7.094)
D	(-64.191,21.806,9.075)	(-64.163,21.799,9.129)	(-64.096,21.763,9.154)	(-64.146,21.774,8.739)
E	(-64.191,-22.174,8.136)	(-64.163,-22.181,8.157)	(-64.096,-22.212,8.002)	(-64.146,-22.201,7.588)
F	(13.335,-22.151,7.059)	(13.358,-22.151,6.805)	(13.410,-22.157,5.904)	(13.371,-22.158,5.943)
G	(90.861,-22.128,5.982)	(90.880,-22.121,5.452)	(90.915,-22.102,3.807)	(90.887,-22.115,4.298)

In subsequent calculations of RVM using Equation (8.6), with $a = 1$, the bow point A (initially located at the undisturbed free surface) and the deck points B & G, C & F and D & E will essentially be analysed as four distinct cases. Point A is basically the selected point considered in the optimisation of the relative bow motion.

8.3 Comparison of Relative Vertical Motion for the Selected Points

Optimisation of the Derbyshire was undertaken subject to improving the relative bow motion without increasing calm water resistance. That is, the relative vertical motion at point A, where A is the intersection of the undisturbed free surface and the longitudinal profile of the parent ship. The other points are located on the first deck, in this case the bulkhead deck.

The basic heave, roll and pitch motions will change as each damage scenario is investigated. The heave, roll and pitch transfer functions are presented in Figures 8.2 to 8.4. To compare results for the same relative wavelength the incident wave wavelength for the parent Derbyshire (intact or damaged) is scaled with respect to the parent hull length of Table 6.4. Similarly for the optimised Derbyshire (intact or damaged) the incident wave wavelength is scaled with respect to the optimised hull length provided in Table 6.4.

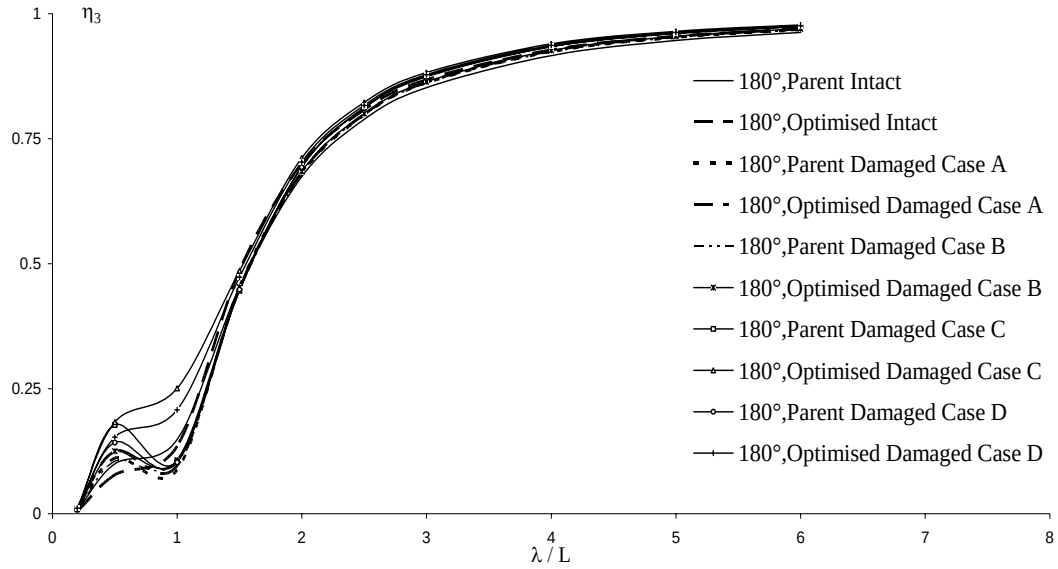

Figure 8.2: Heave motion for the intact and damaged parent and optimised hull forms of Derbyshire.

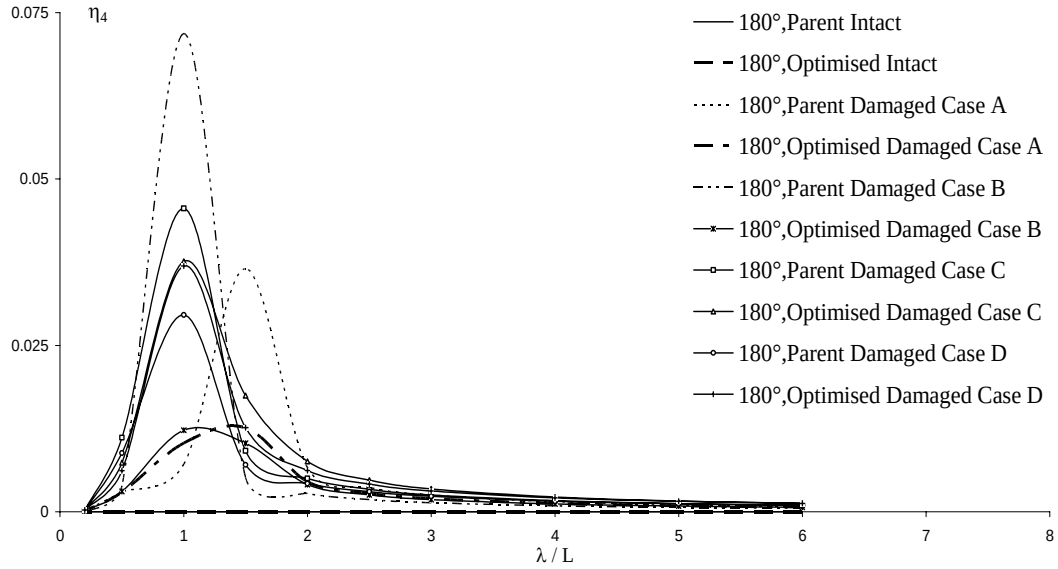

Figure 8.3: Roll motion for the intact and damaged parent and optimised hull forms of Derbyshire.

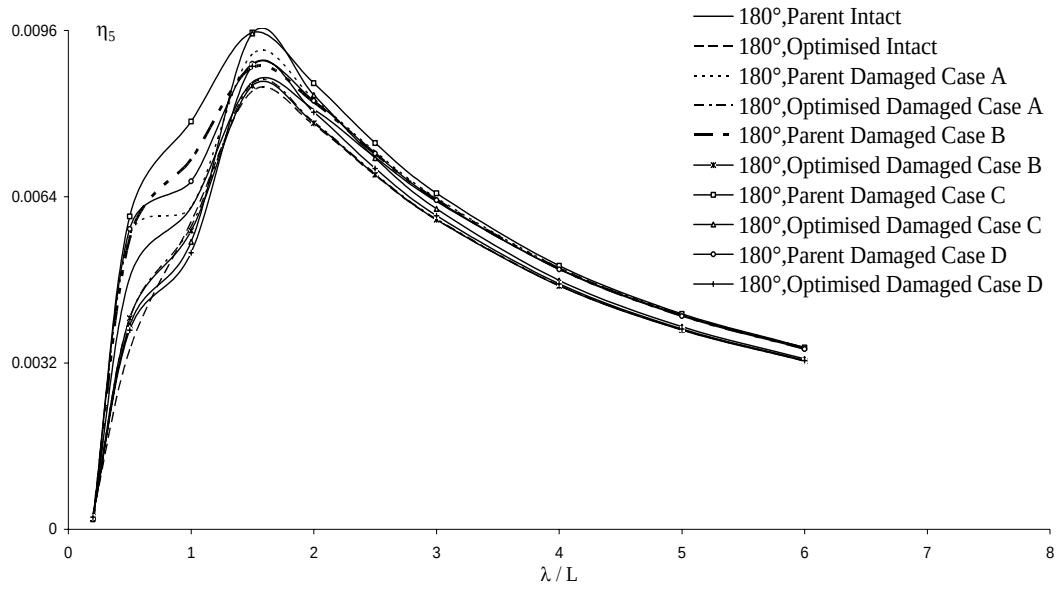

Figure 8.4: Pitch motion for the intact and damaged parent and optimised hull forms of Derbyshire.

It is worth noting that in the heave transfer functions peaks and troughs are associated with $\frac{\lambda}{L} \sim 0.5$ and $\frac{\lambda}{L} \sim 1$ respectively. The roll motion has some peak responses at $\frac{\lambda}{L} \sim 1$ and $\frac{\lambda}{L} \sim 1.5$, whereas pitch peaks generally occur for $\frac{\lambda}{L} \sim 1.5$.

For heave, roll and pitch the transfer functions for the parent hull represent an upper bound for the optimised hull transfer functions. For heave only the inseparable optimised hull form transfer functions for damage scenarios C & D exceed the parent values. Generally, for pitch the parent intact hull form exceeds all damage scenarios of the optimised hull form. The lower boundary pitch transfer function is provided by the intact optimised hull form.

For head seas (180°) the RVM for point A, for all intact and damaged scenarios, is presented in Figure 8.5.

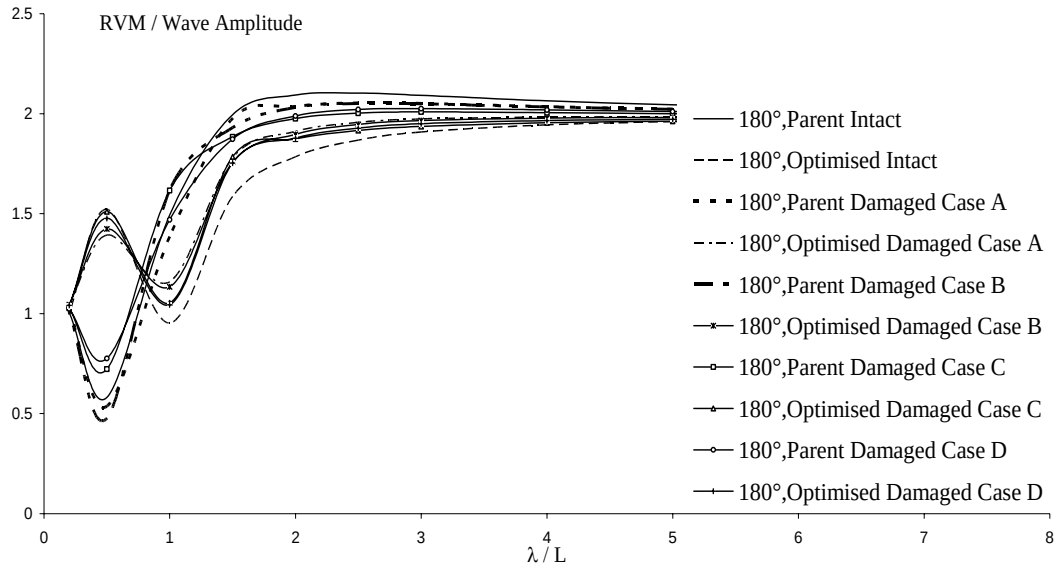

Figure 8.5: Relative vertical motion responses for the intact and damaged hull forms for point A (in head seas).

As might be expected from the resonant wavelengths observed in the pure motion transfer functions the relative vertical motion at point A exhibits peaks and troughs for the optimised hull form at $\frac{\lambda}{L} \sim 0.5$ and $\frac{\lambda}{L} \sim 1$ respectively, whereas the troughs associated with the parent hull form occur for $\frac{\lambda}{L} \sim 0.5$. At the longer wavelengths the RVM values for the damaged scenarios lie between an upper boundary formed by the intact parent RVM values and the lower boundary formed by the intact optimised RVM values. For intact parent hull form the resonant RVM values for damage scenarios C & D exceed the intact values and for damage scenarios A & B the resonant RVM values lie below the intact RVM values. For the intact optimised hull the resonant RVM values for all damage scenarios lie below the intact RVM values.

Corresponding results for the deck positions B & G, C & F and D & E are provided in Figures 8.6 to 8.11 for the same head sea wave heading.

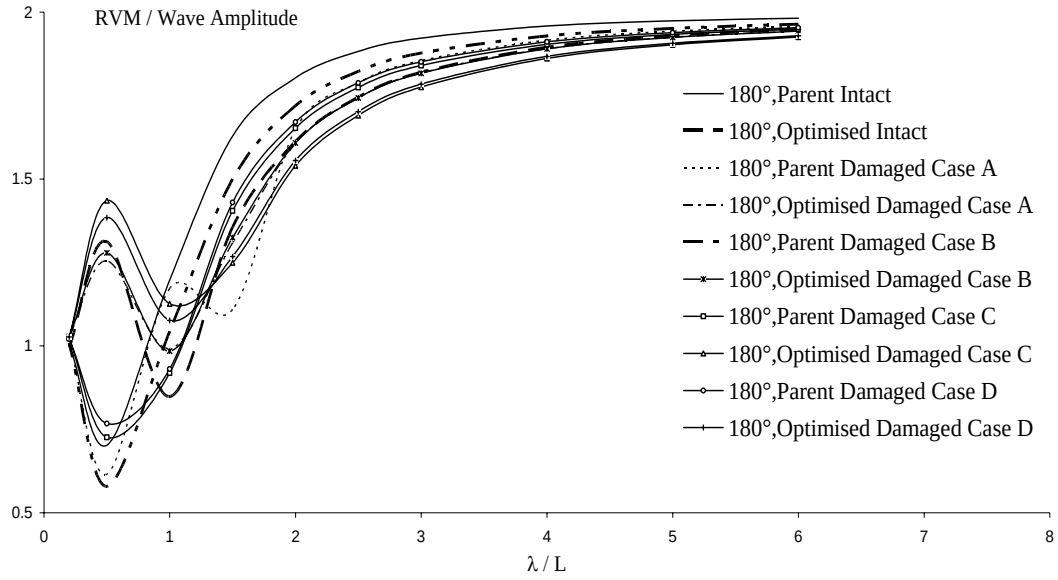

Figure 8.6: Relative vertical motion responses for the intact and damaged hull forms for point B (in head seas).

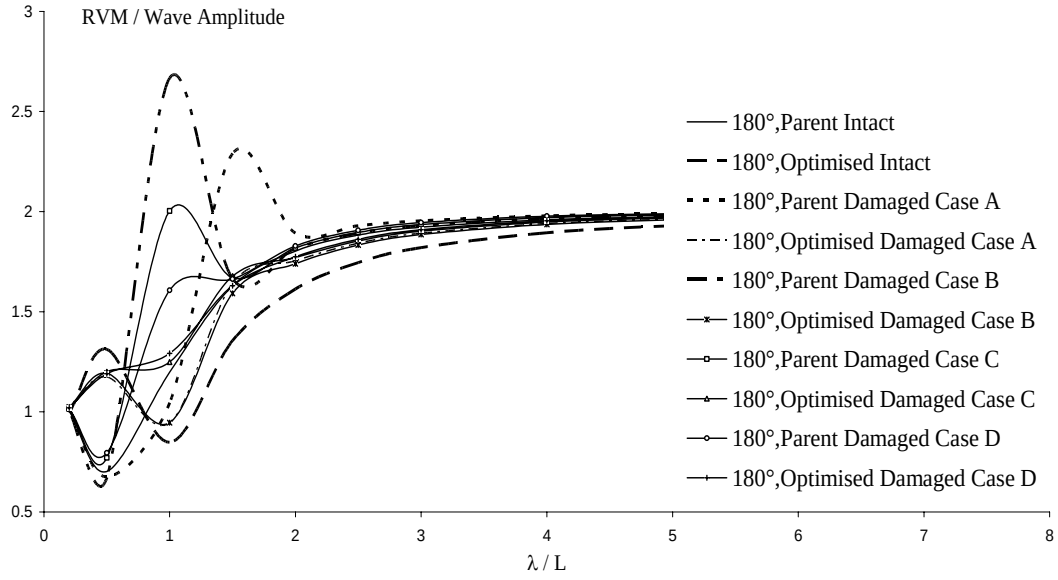

Figure 8.7: Relative vertical motion responses for the intact and damaged hull forms for point G (in head seas).

For $\frac{\lambda}{L} \sim 0.5$ the RVM characteristics for point B (Figure 8.6) are similar to those for point A (Figure 8.5), but at the troughs for $\frac{\lambda}{L} \sim 1$ there is greater separation of the low points for point B. Furthermore for damage scenario A imposed on the parent hull the behaviour is quite different with a peak and trough at $\frac{\lambda}{L} \sim 1$ and $\frac{\lambda}{L} \sim 1.5$ respectively. Ultimately all damage scenario RVM values are bounded above by the intact parent values and below by the damaged optimised case C RVM values. For shorter wavelengths, $\frac{\lambda}{L} < 1$, the optimised RVM values exceed those of the parent RVM values.

At point G (initially the image point of B for the intact case) strong resonances occur for the parent hull for damage scenarios A, B and C (Figure 8.7). Whilst damage scenario D does not lead to a resonance it too exceeds the intact parent RVM values. The peaks and troughs initially associated with damage scenarios C and D (for point B) for optimised hull have now significantly flattened out and the other peaks and troughs for the optimised hull form are less separated.

Since the heave and pitch contributions are essentially the same it appears that the roll influence (even for a 180° heading) is bringing about these changes. To understand fully why the significant differences between points B and G exist for the parent hull it is necessary to examine the intermediate calculations. For damage scenario B comparison of the intermediate calculations for points B and G yield the following observations:

- All contributions to the real and imaginary parts of RVM are negative for point G. Thus all contributions reinforce to create the larger RVM values for point G.

- The dominant contribution in the real part of RVM is the roll contribution and in the imaginary part of RVM it is the incident wave contribution.

- Whilst the roll levers for point B & G are comparable the positive roll contribution to RVM for point B leads to a significantly smaller real part of RVM.

- The smaller imaginary roll motion component means that it is primarily the incident wave and roll contributions that control the imaginary part of RVM.

- The roll motion is an order of magnitude larger than the pitch motion, whereas the pitch lever to roll lever is approximately 3 to 1. Therefore, the roll contribution is more significant than the pitch.

Inspection of the intermediate calculations for damage scenario C, for the parent hull, indicates that peak value is less than that for case B (at point G) because:

- Imaginary heave is now positive and larger.

- Imaginary pitch is a little larger.

- Imaginary roll is slightly smaller.

Otherwise the observations for case B (apart from above minor changes) apply to case C.

Figures 8.8 & 8.9 provide corresponding results for the pair of points C & F.

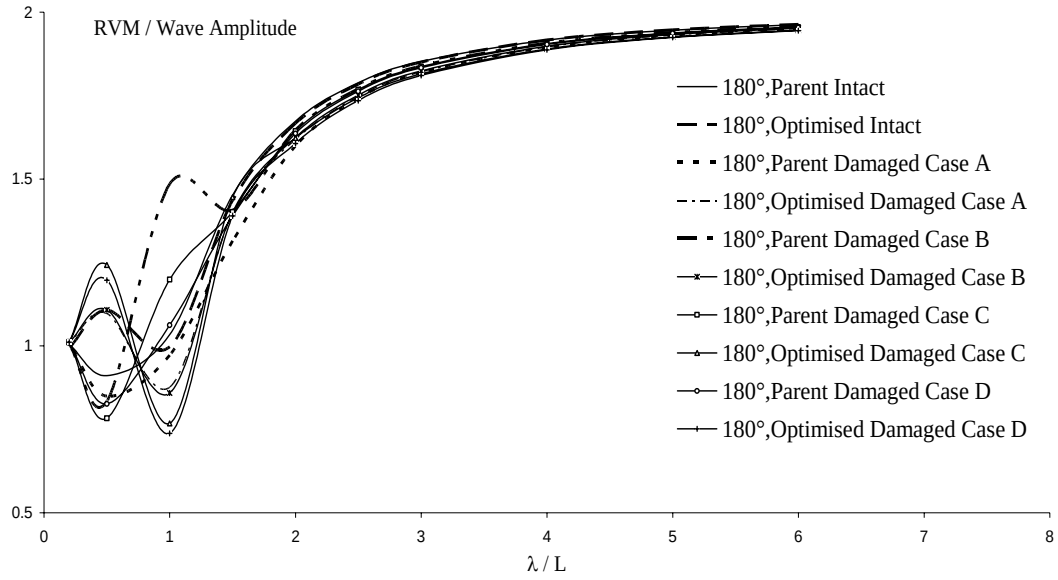

Figure 8.8: Relative vertical motion responses for the intact and damaged hull forms for point C (in head seas).

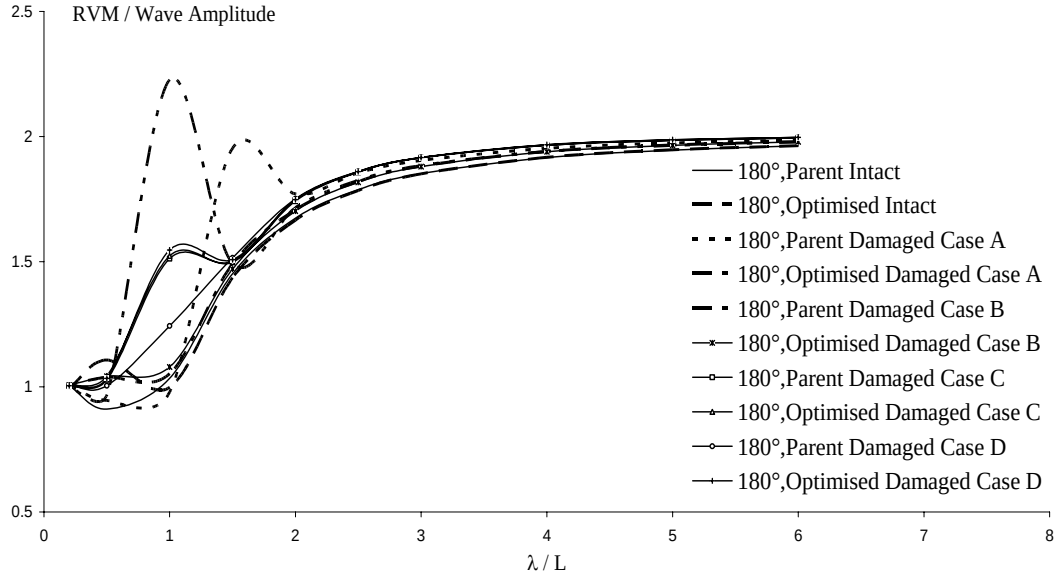

Figure 8.9: Relative vertical motion responses for the intact and damaged hull forms for point F (in head seas).

For points C & F there is a very small pitch lever (<1m aft of LCF) for the parent hull, but the roll levers for C & F are comparable with the roll levers for B & G. Hence for point C the peaks and troughs are still associated with $\frac{\lambda}{L} \sim 0.5$ and $\frac{\lambda}{L} \sim 1$. However, the differences are small. For the image point F the sign of the roll lever changes relative to C (as did G relative to B) and consequently the RVM values for the parent hull under damage scenarios B & A again loom large.

For point F the difference between intact parent and intact optimised hull forms remains negligible, but now forms the lower boundary of RVM values, whereas for point C it formed the upper boundary of RVM for $\frac{\lambda}{L} > 1$.

Next the location points D & E are addressed. The RVM values are presented in Figures 8.10 & 8.11.

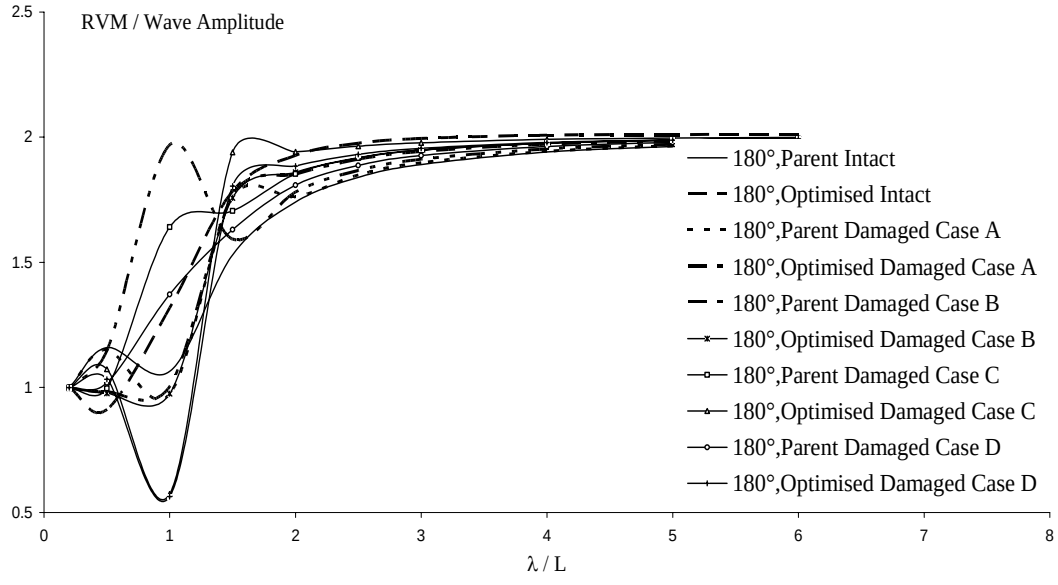

Figure 8.10: Relative vertical motion responses for the intact and damaged hull forms for point D (in head seas).

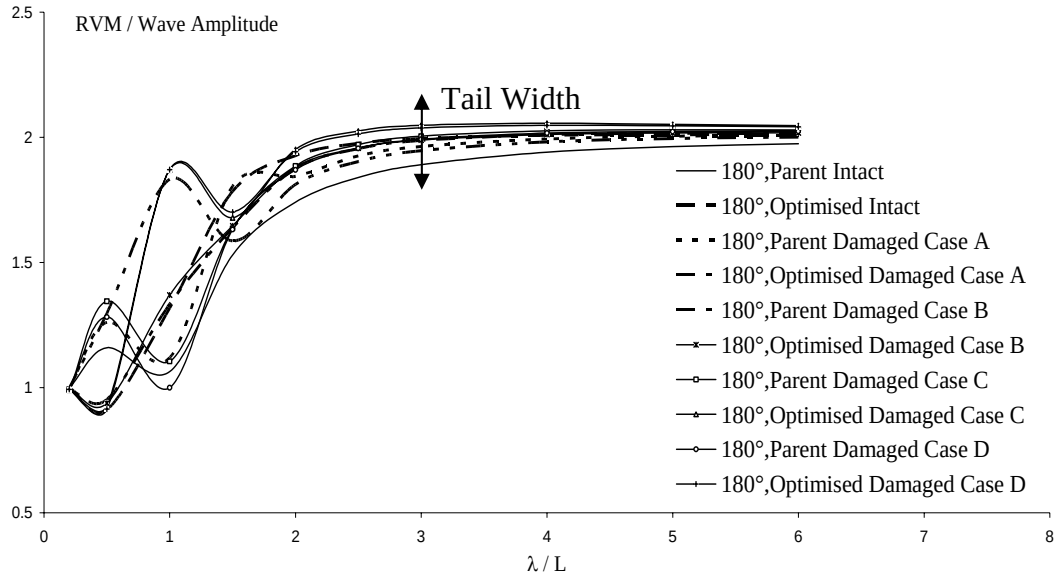

Figure 8.11: Relative vertical motion responses for the intact and damaged hull forms for point E (in head seas).

For points D & E the characteristics of the calculated RVM values change again because of the change in both the sign and size of the pitch associated levers (compared to points B & G). Whereas for point B the parent hull only exhibited various troughs for the intact and damaged hull forms, for point D damage scenarios B & C now exhibit peaks for $\frac{\lambda}{L} \sim 1$, a peak and a trough for $\frac{\lambda}{L} \sim 0.5$ and 1 respectively for damage scenario A. Thereafter, the parent RVM values are monotonically increasing.

The peak-trough pattern of the parent hull for damage scenario A for point D is now adopted by all parent hull form cases apart from damage case B for the image point E. The peak for damage case B is not quite comparable with the peaks for damage scenarios C & D for the optimised hull form for $\frac{\lambda}{L} \sim 1$. For the slightly increased tail width for point E (compared to that for points C & F) the intact parent RVM values form a lower boundary for points D and E, whereas the intact optimised RVM values

are centrally located with the tail for point E (exceeded by damage scenarios C & D for the optimised hull) and form an upper boundary for the tail of point D.

In addition to the results presented in Figures 8.5 to 8.11 additional results for points A, B, C, D, E, F and G are presented in Appendix J as Figures J.1 to J.10, J.11 to J.20, J.21 to J.30, J.31 to J.40, J.41 to J.50, J.51 to J.60 and J.61 to J.70 respectively for the different wave headings defined in Figure 8.12.

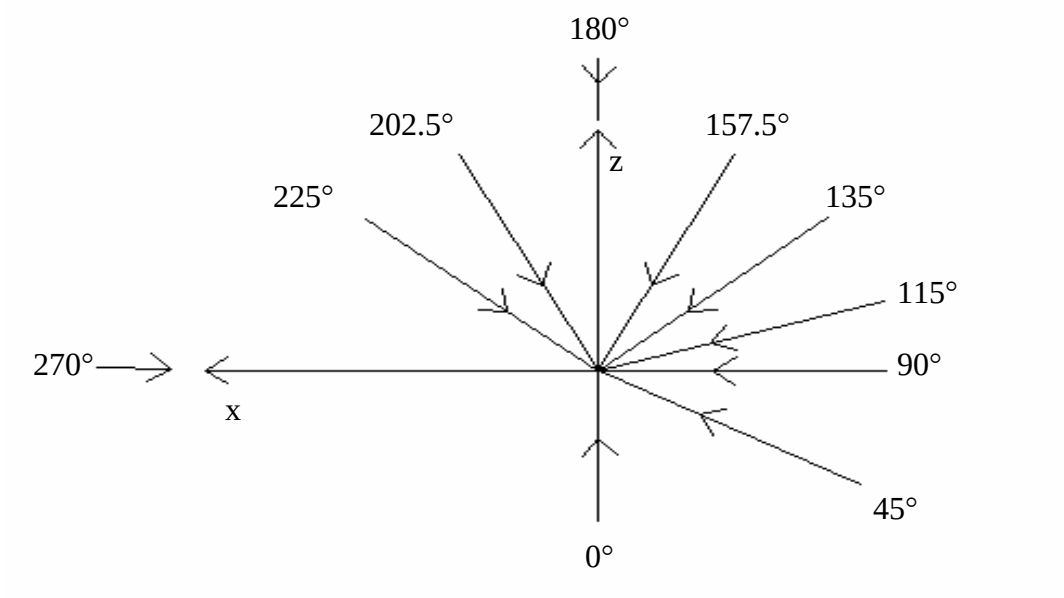

Figure 8.12: Definition of wave headings.

Figure 8.5, Figures 8.6 & 8.7, Figures 8.8 & 8.9 and Figures 8.10 & 8.11 are repeated in Appendix J (to provide complete set of results in one location) as Figure J.7, Figures J.17 & J.67, Figures J.27 & J.57 and Figures J.37 & J.47 respectively.

From the figures in Appendix J and those cited here it is noted that:

- All significant changes take place at the wavelengths $\frac{\lambda}{L} < 1.5$.

- Peak and troughs generally occur at $\frac{\lambda}{L}=0.5$, $\frac{\lambda}{L}=1$ and $\frac{\lambda}{L}=1.5$.

- For large $\frac{\lambda}{L}$ RVM values are asymptotic to 2.

The variation of the RVM characteristics with wave heading is quite different for each point. To illustrate this point the variation of RVM with wave heading for point A as presented in Figures J.1 to J.10 is considered.

For a following sea $\left(\beta=0^{\circ}\right)$ the intact parent and intact optimised hull form RVM values provided an upper and lower boundary for $\frac{\lambda}{L}>1$. The peaks at $\frac{\lambda}{L}\sim 0.5$ for the damaged parent hull exceed the intact parent hull values, which have no peak. The troughs at $\frac{\lambda}{L}\sim 1$ for the optimised hull for the damaged scenarios exceed the lower bound intact optimised RVM values.

For a quarter sea $\left(\beta=45^{\circ}\right)$ the intact parent and intact optimised hull form RVM values continue to provide the upper and lower boundary transfer functions.

For a beam sea $\left(\beta=90^{\circ}\right)$ the RVM values are peakier with the $\frac{\lambda}{L}\sim 0.5$ peaks, for the optimised hull, the damaged RVM values exceed the intact values. For the $\frac{\lambda}{L}\sim 1$ peaks the intact parent RVM values exceed all the damaged RVM values.

For a beam sea $\left(\beta=115^{\circ}\right)$ all the peaks occur at $\frac{\lambda}{L}\sim 0.5$ with parent damaged values forming the highest peaks and the parent intact value forming an upper boundary to the optimised damaged peaks. Thereafter the parent intact value forms upper boundary at

$\frac{\lambda}{L} > 1$. The intact optimised RVM values form a lower boundary for almost all $\frac{\lambda}{L}$ values.

For a bow sea $\left(\beta = 135^\circ\right)$ troughs return at $\frac{\lambda}{L} \sim 0.5$. One could suggest that the troughs that did not quite develop at $\beta = 45^\circ$ have developed for $\beta = 135^\circ$ otherwise the curves are quite similar.

For head seas $\left(\beta = 157.5^\circ, 180^\circ \text{and } 202.5^\circ\right)$ the trends are quite similar.

For a bow sea $\left(\beta = 225^\circ\right)$ the RVM transfer functions have troughs for the optimised hull form at $\frac{\lambda}{L} \sim 0.5$ and peaks for the parent hull form at $\frac{\lambda}{L} \sim 1$.

For a beam sea $\left(\beta = 270^\circ\right)$ the pattern is analogous to $\beta = 90^\circ$ except the peaks are generally larger.

For the other points B to G the richness of variation of RVM transfer functions with wave heading is not diminished. When companying B & G the damaged parent peaks again arise for reasons similar to these presented when discussing $\beta = 180^\circ$ previously.

Whilst the intact parent and intact optimised RVM values often provide upper and lower boundaries for RVM values associated with $\frac{\lambda}{L} > 1$ and 1.5, it is not the case that they form the upper or lower boundaries consistently. Hence it is difficult to state that damage of the optimised hull is less or more beneficial than damage of the parent hull.

8.4 Summary

Variation in magnitudes of RVM values for the selected points for different wave headings are discussed in this chapter. This analysis established:

- The results for the three-dimensional analysis of the RBM in head seas (RVM at point A) for the intact optimised hull and basis hull show that RBM is indeed better for optimised hull. Hence there is consistency of two-dimensional optimisation process and three-dimensional hydrodynamic analysis.

- All significant changes take place at the wavelengths $\frac{\lambda}{L} < 1.5$.

- Peak and troughs generally occur at $\frac{\lambda}{L} = 0.5$, $\frac{\lambda}{L} = 1$ and $\frac{\lambda}{L} = 1.5$.

- For large $\frac{\lambda}{L}$ RVM values are asymptotic to 2.

- The variation of the RVM characteristics with wave heading is quite different for each point.

In the following chapter a summary of the research highlighting the novel aspects of it is presented.

9. CONCLUSIONS AND FUTURE WORK

Within the literature, optimisation has been presented as a tool developed to assist designers to test and examine their initial conceptual design by considering variations of the selected hull form subject to permitted variations being within the control of the designers. Optimisation is rarely all embracing and hence the development of different optimisation tools considering different aspects of the complex and multi-tasked design process has been reviewed within the dissertation.

Whilst satisfaction of intact stability requirements has been built into existing alternative hull form optimisation packages seeking improved hydrodynamic hull forms (in terms of seakeeping, calm water resistance and added resistance) damage stability is not an automated feature. Depending upon knowledge of a particular ship type either a deterministic or a probabilistic approach to damage stability may be adopted. It was then argued that within the context of the hydrodynamic hull form optimisation techniques available their application to novel hull forms would exclude the probabilistic method. Including the deterministic damage stability analysis in the optimisation process would require facilitating a full three-dimensional description of the hull form and its internal subdivisions together with a fast and accurate method of determining sinkage, trim and heel with automated correct bulkhead subdivision. This task was considered too involved to include within the optimisation process, since the steps are quite involved when performing them outside the optimisation process and also require an objective function review of intermediate calculations performed, to be sure that damage stability is properly processed as well as required conditions being fulfilled. This is also the difficulty of building in an automatic selection of the most likely damage scenarios and hence specifying location and extent of damage. In this dissertation both MAIB and ‘Lutzen 2002’ databases have been accessed to identify the most likely damage for each ship type in terms of collisions and groundings. Prior to applying the identified damage extent to the selected bulk carrier Derbyshire the parent

hull was optimised for RBM in head seas subject to no increase in calm water resistance and then the new hydrostatic equilibrium positions determined for each hull form for each damage scenario. Hence, the fluid-structure interaction analysis for each situation for a representative selection of wave frequencies and wave directions were undertaken and the acceptance of the quality of the resulting hydrodynamic characteristics were justified prior to undertaking general motion analysis and resultant relative vertical motion at selected corresponding locations on each hull form. The overall approach is schematically presented in Figure 9.1.

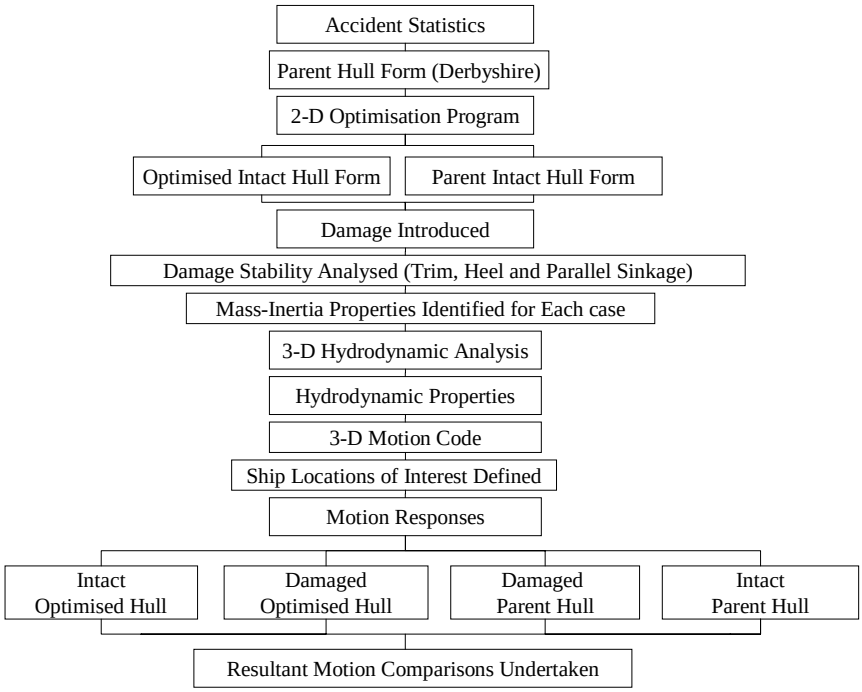

Figure 9.1: An overview of the dynamic analysis procedure.

9.1 Key Observation of Completed Research

- To compare the motions of a hull in its intact and damage condition, it will be necessary to determine the products of inertia for at least the damaged ship even

if the cross-products of inertia are assumed zero for the intact case. Since no public domain method was found to complete this task a new method of producing cross-products of inertia was developed.

- The determination of the cross-products of inertia is coupled to the assignment of the pure moments of inertia. The latter quantity is readily assigned for the intact case and here, since the trim and heel angles are not excessive, it is assumed that assignment of the moments of inertia in terms of radius of gyration can be dealt with similarly for both the intact and damaged ship.

- The changes in the amplitudes of the pure and cross-products of inertia for different damage scenarios are quite sensitive to the position of the damage and the resulting equilibrium angles.

- In the optimisation code the selected objective function is the peak value of the relative bow motion (RBM) in head seas. Usually, a reduction of the peak value of the objective function leads to a general reduction in the objective function amplitudes.

- Most of the intact stability properties are improved as the hull is optimised. This is occurred in this optimisation study where the constraint function was the calm water resistance and not the intact stability.

- The equilibrium angles evaluated for the optimised hull form are smaller than those associated with the parent hull form. This ought to be advantageous in terms of passenger and crew comfort.

- The damage scenarios carried out in this research represent all the damage cases possible according to the analysed damage statistics. One-compartment and two-compartment damages are investigated; since three-compartment damage is

highly unlikely based on this damage statistics three-compartment damage case is not analysed in this thesis.

- The advantage of using actual collected and recorded ship damage statistics is that only those parts of the ship that are known to be vulnerable to damage are investigated.

- The damage statistics indicate regions of ship where damage occurs and the extent of the damage. In generating the damage scenarios one has assumed (consistent with the statistics) that the damage may affect hold 2 alone and both hold 1 & hold 2 and hold 2 & hold 3 if damage occurred at interface of two holds. Since hold 2 contains no cargo it could be completely flooded and this was identified as the most extreme single hold damaged scenario (case A and case B). Hold 1 and 3 damaged in isolation was therefore not considered. Damaging hold 1& hold 2 and hold 2& hold 3 are treated as cases C & D.

- Since the grounding damage leads to greater changes in the trimming and heeling of the damaged ship, compared with data analysed for collisions, damage imposed on the ship is primarily concerned with the consequences of the ship grounding.

- Fore body of the optimised ship is more round-formed than the original ship. The lines of the aft body of the optimised ship are more V-shaped than the original ship. Such a hull form has better RBM characteristics at most headings and its resistance is decreased.

- The numerical modelling of the various ship fluid-structure interactions has been validated in this thesis through study of conditioning number, direct versus Haskind excitation loads and symmetry of hydrodynamic reactive cross-terms.

- The 10% change for L and B/T used leads to practical hull forms that confirms with intact stability. It is consistent with Hearn et al. (1994), Hearn et al. (1995b) and Hearn and Wright (1999) who noted that parameter increases beyond this percentage leads to impractical hull forms.

- In this dissertation Derbyshire was selected as a representative bulk carrier without any intention to understand or proffer reasons for its loss. Furthermore, it was thought that the official Derbyshire investigation would make available considerable technical detail in the public domain to allow proper modelling of the fluid-structure interactions and subsequent motion responses.

- The hydrodynamic analysis assumes regular harmonic waves in both the optimisation process and in the subsequent three-dimensional intact and damage hull form analysis. Given optimisation of peak value of selected response leads to general reduction in transfer function then seaway response for optimised hull will be better than parent hull for all sea-states. Responses in seaways are therefore not addressed explicitly.

- The origin of the coordinate reference system and the point about which motions are defined is the same point for the parent and optimised hull forms. Hence meaningful direct comparisons of intact and damaged ships are made possible.

- The structural responses of the parent and optimised ships are not examined. In a damaged state it is assumed that the outer shell of the ship allows water ingress in accordance with the damage statistics used.

- The change of length for the optimised ship necessitated a small change of bulkhead positions but no increase in the number of bulkheads, so that floodable length requirements are met by all hull forms analysed.

Having summarised the important points of the research completed the next task is to discuss the novel aspects of the research in greater detail.

9.2 Novel Aspects of Completed Research

The research is concerned with the behaviour of damaged ships and examination of the possibility that damaged optimised hydrodynamic hull forms exhibit more adverse seakeeping characteristics than the damaged non-optimised hull form.

The reason for addressing this problem was that different authors have demonstrated that seakeeping, calm water resistance and added resistance can be improved using optimisation techniques with automatic fulfilment of those IMO intact stability requirements included in the process. Since this situation appeared to present a 'win-win-win' situation, with little indication of disadvantages either being discussed or identified, it would be perverse if damaged optimised hull forms exhibited more extreme motions than the non-optimised damaged hull form.

To specify the cause and extent of damage any ship type might experience detailed analysis of damage statistics was considered a necessary first step. The MAIB damage statistics were found to be lacking in terms of number of accidents reported and the details recorded. Therefore another data base 'Lutzen 2002' was thoroughly interrogated and the damage statistics presented in this dissertation were generated by the author.

Having identified the ship types most often associated with the most common form of accidents 'collisions' and 'groundings' a suitable ship was required for investigation. Whilst a general cargo ship with collision or grounding damage was the obvious situation to analyse no ship with all the required details for a fluid-structure interaction

was available in the public domain. Consequently, Derbyshire a bulk carrier that has been in the public domain for some time was selected.

Whilst software capable of modelling external and internal fluid-structure interaction was readily available the subsequent motion analysis required provision of cross-products of inertia. There is no means of calculation in the public domain other than the classical text book method of integrating detailed mass distributions. Since the detail published (even for the Derbyshire) is insufficient a novel method of prediction was required, developed and implemented. Since the procedure is over specified consistency checks can be undertaken.

To ensure that the damaged ships represented likely feasible scenarios the damage statistics were used to generate different damage scenarios. To also ensure that damaged ships floated in new equilibrium position (rather than sink) floodable length requirements were fulfilled for each damage scenario. The basis Derbyshire hull and the optimised Derbyshire hull form fulfilled all IMO intact stability requirements.

As far as the author is aware (as a consequence of searching the literature) this is the first investigation of either a damaged basis hull or the damaged optimised hull form. The results for the three-dimensional analysis of the RBM in head seas for the intact optimised hull and basis hull show that RBM is indeed better for optimised hull. Hence there is consistency of optimisation process and three-dimensional analysis.

To extend the investigation of the behaviour of the intact and damaged hull forms six other points on the ship (B to G) were investigated to try and appreciate how heave, roll and pitch affected relative vertical motion. The results of such analysis were discussed in Chapter 8. Prior to undertaking such motion studies the quality and appropriateness of the hydrodynamic fluid-structure interaction analysis was demonstrated.

9.3 Recommendations for Future Work

- The quality of the external fluid-structure interaction of different intact and damaged forms of the Derbyshire has been demonstrated. An obvious extensions is to simultaneously analyse the internal free surfaces (modelled as massless flat plates with heave, roll and pitch degrees of freedom) and the external fluid-structure interaction. The complexity of the hydrodynamics can be addressed using the Matthew Diffraction Suite. The increased complexity of the motion response for scenarios A and B is provided in Appendix K. The extension to scenarios C and D follows the details provided in Appendix K with two rather than one massless plate.

- The damage statistics clearly relate to ships that survived the incurred damage. The statistics do not indicate how much more damage the ships could have experienced and remained afloat. Since the heel and trim angles due to the damage imposed are small one might argue that damage should be extended further (despite there being no statistics to support it) to examine how sensitive the motion responses are to larger heel and trim angles.

- Since in the stability analysis the equilibrium angles determined for each of the four different damage scenarios are small, the question of water on deck does not arise. If deck wetness did arise it could be readily included in the modelling of the wetted surfaces. The sloshing of ingressed water in the damaged holds would not be readily modelled by the massless flat plate model just proposed. To include sloshing a non-linear free surface model of the internal free surface would be required to form shape of internal free surface.

- For more extreme orientations of the ship analysis of sub-optimised (intermediate) hull forms should be performed to appreciate impact of different optimisation levels.

- Whilst specification of moments of inertia and products of inertia may not be attractive research topic knowledge of their specification is important when looking at damaged ships. Hence some further effort could be useful.

- Turan (1993) suggests that safety and commercial gain conflict. If practical procedures could be developed to include damage stability within available optimisation tools this conflict might be more readily resolved.

- In the optimisation process only primary parameters were investigated to permit LCF to remain invariant and hence make meaningful comparisons of intact and damaged ships motion responses. The cited optimisation tools indicate that improvements for secondary parameters are comparable with those for the primary parameters investigated. Therefore in the future research the secondary parameters should be investigated in the context of damage stability and motions of damaged optimised ships.

- The equilibrium angles of the damaged ships were small. Consequently their effect on the longitudinal and transverse mass distribution is neglected. However, for large equilibrium angles the relationship between the ship mass distribution and equilibrium angles needs to be investigated.

BIBLIOGRAPHY

Abkowitz, M.A., Vassilopoulos, L.A. and Sellars, F.H. (1966). Recent developments in seakeeping research and its application to design. *Trans. SNAME*, Vol. 74, pp. 194-259.

American Bureau of Shipping (1992). Rules for Building and Classing Steel Vessels. Parts 3.3 and 3.12: Hull Construction and Equipment.

Andrews, D. (1981). Creative ship design. *Trans. RINA*, Vol. 123, pp. 447-471.

Andrews, D. (1986). An integrated approach to ship synthesis. *Trans. RINA*, Vol. 128, pp. 73-102.

Andrews, D. (2003). A creative approach to ship architecture. *International Journal of Maritime Engineering*, Vol. 145(A3), pp. 69-92.

Aoki, M. (1971). Introduction to Optimization Techniques, Fundamentals and Applications of Nonlinear Programming. Section 4.7, pp. 152-155. *The Macmillan Company*, New York.

Bertram, V. (2000). Practical Ship Hydrodynamics. Section 1.4.1, pp. 9-14. *Butterworth-Heinemann*, Oxford.

Bertram, V. (2003). Optimistic, optimization in marine design. In *39th WEGEMT Summer School*, Berlin, Germany, 29-56.

Bird, H. and Browne, R.P. (1974). Damage stability model experiments. *Trans. RINA*, Vol. 116, pp. 69-91.

Bird, H. and Morrall, A. (1986). Research towards realistic stability criteria. In *Proceedings of the International Conference on the Safeship Project: Ship Stability & Safety*, London, UK.

Bishop, R.E.D., Price, W.G. and Tam, P.K.Y. (1977). The dynamical characteristics of some dry hulls. *Journal of Sound and Vibration*, Vol.54(1), pp. 29-38.

Bishop, R.E.D., Price, W.G. and Temarel, P. (1991). A theory on the loss of the MV Derbyshire. *Trans. RINA*, Vol.133, pp. 389-453.

Borlase, G.A. (2003). Research opportunities identified during the casualty analysis of the fishing vessel Arctic Rose. *Marine Technology*, Vol. 40(4), pp. 270-277.

Brook, A.K. (1988). The effect of motions in assessing intact ship stability. *Transactions of the North East Coast Institution of Engineers and Ship Builders (NECIES)*, Vol. 104(3), pp. 81-90.

Bureau Veritas (1986). Rules and Regulations for the Classification of Steel Ships of More Than 65m in Length. Part II, Section 4.6: Hull Structure, pp. 42-52.

Chan, H.S., Atlar, M. and Incecik, A. (2002). Large-amplitude motion responses of a Ro-Ro ship to regular oblique waves in intact and damaged conditions. *Journal of Marine Science and Technology*, Vol. 7(2), pp. 91-99.

Cramer, H. and Tellkamp, J. (2002). Towards the direct assessment of a ship's intact stability. In *Proceedings of the 6th International Ship Stability Workshop*, Webb Institute, pp. 1-7.

Cramer, H. and Tellkamp, J. (2003). Towards safety as performance criteria in ship design. In *Proceedings of the Passenger Ship Safety*, London, UK, pp. 17-25.

Dai, C., Hambric, S., Mulvihill, L., Tong, S.S. and Powell, D. (1994). A prototype marine propulsion design tool using artificial intelligence and numerical optimization techniques. *Trans. SNAME*, Vol. 102, pp. 57-69.

Day, A.H. and Doctors, L.J. (1997). Design of fast ships for minimal resistance and motions. In *Proceedings of the 6th International Marine Design Conference, IMDC'97*, Newcastle, UK, pp. 569-583.

Department of Transport (1989). The Merchant Shipping Act 1984 mv Derbyshire. *Report of Court No.8075*.

Doctors, L.J. and Day, A.H. (1995). Hydrodynamically optimal hull forms for river ferries. In *Proceedings of the International Symposium on High Speed Vessels for Transport and Defence, RINA*, London, UK, Paper No: 5, pp.1-21.

Eames, M.C. and Drummond, T.G. (1977). Concept exploration–an approach to small warship design. *Trans. RINA*, Vol. 119, pp. 29-54.

Fach, K. (2004). Corrosion and damages on high speed craft. In *Proceedings of the 4th International Conference on High-Performance Marine Vehicles*, Rome, Italy, pp. 295-303.

Faltinsen, O.M. (1978). A numerical nonlinear method of sloshing in tanks with two-dimensional flow. *Journal of Ship Research*, Vol. 22(3), pp. 193-202.

Faltinsen, O.M. (1990). Sea Loads on Ships and Offshore Structures. Chapter 3, pp. 37-68. *Cambridge University Press*, Cambridge.

Fisher, K.W. (1972). Economic optimisation procedures in preliminary ship design (applied to the Australian ore trade). *Trans. RINA*, Vol. 114, pp. 293-309.

Francescutto, A. (2004). Intact ship stability: the way ahead. *Marine Technology*, Vol. 41(1), pp. 31-37.

Frank, W. (1967). Oscillations of cylinders in or below the free surface of deep fluids. *NSRDC, Report 2375*, DTRC, Bethesda, MD.

Friis, A.M., Andersen, P. and Jensen, J.J. (2002). Ship Design. Part 1, Chapter 6, pp. 70-77. *Section of Maritime Engineering, Department of Mechanical Engineering, Technical University of Denmark*, Denmark.

Friis, A.M., Andersen, P. and Jensen, J.J. (2002). Ship Design. Chapter 11, pp. 171-176. *Section of Maritime Engineering, Department of Mechanical Engineering, Technical University of Denmark*, Denmark.

Furukawa, Y. and Hearn, G.E. (2000). Objective function development, using design charts, to reflect ship seakeeping, resistance, and manoeuvrability influences. In *Proceedings of the Design for Excellence Engineering Design Conference*, Brunel University, UK, pp. 571-584.

Ghani, M.P.A. (2003). Design Aspects of Catamarans Operating at High Speed in Shallow Water. *PhD Thesis*, The University of Southampton, U.K.

Gilfillan, A.W. (1969). The economic design of bulk cargo carriers. *Trans. RINA*, Vol. 111, pp. 113-140.

Greenberg, M. D. (1998). Advanced Engineering Mathematics, second edition. Section 8.3, pp. 396-397. *Prentice-Hall International*, London.

Greenberg, M. D. (1998). Advanced Engineering Mathematics, second edition. Section 10.6.3, pp. 517-518. *Prentice-Hall International*, London.

Grochowalski, S., Hsiung, C.C., Huang, Z.J. and Cong, L.Z. (1998). Theoretical modeling of ship motions and capsizing in large and steep waves. *Trans. SNAME*, Vol. 106, pp. 241-267.

Hasegawa, K., Ishibashi, K. and Yasuda, Y. (2000). Modeling and computer animation of damage stability. In *Proceedings of the 7th International Conference on Stability of Ships and Ocean Vehicles (STAB 2000),* Launceston, Tasmania, Australia, pp. 242-249.

Haskind, M.D. (1954). Approximate methods of determination of hydrodynamic characteristics of ship oscillations. *Izvestiya Akad. Naut. SSSR. Otd. Tech. Naut.,* No. 11.

Hearn, G.E. (1978). Diffraction Suite MATTHEW November 1981 Release.

Hearn, G.E. and Donati, E. (1981). Sea keeping theories-applying some choice. *Transactions of the North East Coast Institution of Engineers and Ship Builders (NECIES),* Vol. 97,pp. 53-72.

Hearn, G.E., Hills, W. and Colton, P. (1988). Incorporating a seakeeping capability in a computer aided preliminary design system. In *Proceedings of the 13th Ship Technology and Research (Star) Symposium*, Pittsburgh, Pennsylvania, pp. 179-194.

Hearn, G.E., Hills, W. and Sarioz, K. (1990). Making seakeeping analysis work for the designer – a new practical approach. In *Proceedings of 19th Scientific and Methodological Seminar on Ship Hydrodynamics* , Varna, Bulgaria, Vol. 2, pp. 69-1-69-8.

Hearn, G.E. (1991). Sea keeping theories: spoilt for choice? *Transactions of the North East Coast Institution of Engineers and Ship Builders (NECIES),* Vol. 107,pp. 45-66.

Hearn, G.E., Hills, W. and Sarioz, K. (1991). A hydrodynamic design methodology for conceptual ship design. In *Proceedings of 7th International Conference on Computer Applications in the Automisation of Shipyard Operation and Ship Design ICCAS'91*, Brazil, pp. 113-129.

Hearn, G.E., Hills, W. and Sarioz, K. (1992). Practical seakeeping for design: a ship shape approach. *Trans. RINA Spring Meetings*, UK, Vol. 134, pp. 225-244.

Hearn, G.E., Wright, P.N.H. and Hills, B. (1994). Seakeeping for design: the demands of multihulls in comparison to monohulls. In *Proceedings of the 8th International Conference on Computer Applications in Shipbuilding '94*, Vol. 2, pp. 11.125-11.144.

Hearn, G.E., Wright, P.N.H. and Hills, B. (1995a). Seakeeping for design: development and application of an inverse analysis design methodology to multihull forms. In *Proceedings of RINA International Conference on Seakeeping and Weather,* London, UK, Paper No: 13, pp. 1-15.

Hearn, G.E., Wright, P.N.H. and Hills, W. (1995b). Seakeeping for design: balancing the vertical and horizontal motions of a catamaran. In *Proceedings of the 3rd International Conference on Fast Sea Transportation, FAST'95*, Lubeck-Travemunde, Germany, Vol. 1, pp. 205-220.

Hearn, G.E., Wright, P.N.H. and Yaakob, O. (1995c). Seakeeping for design: identification of hydrodynamically optimal hull forms for large high speed catamarans. In *Proceedings of RINA International Symposium on High Speed Vessels for Transport and Defence*, London, UK, Paper No: 4, pp. 1-15.

Hearn, G.E. and Wright, P.N.H. (1997). Seakeeping for design: optimisation of motion responses and wave making resistance of catamarans via the application of a genetic

algorithm. In *Proceedings FAST'97, the Fourth International Conference on Fast Sea Transportation*, Sydney, Australia, Vol. 1, pp. 231-240.

Hearn, G.E. and Wright, P.N.H. (1998a). Optimal hull form design for seakeeping and resistance: a genetic algorithm based inverse method. In *Proceedings of Third Osaka Colloquium on Advanced CFD Applications to Ship Flow and Hull Form Design, OC'98*, Osaka, Japan, pp. 499-514.

Hearn, G.E. and Wright, P.N.H. (1998b). Michell wave resistance characteristics resulting from the optimisation of a catamaran hull form via genetic algorithms. In *Proceedings of the Third Biennial Engineering Mathematics and Applications Conference and Michell Centenary Symposium, EMAC'98*, Adelaide, South Australia, pp. 253-256.

Hearn, G.E. and Wright, P.N.H. (1999). Design for optimal hydrodynamic operation of large container ships. In *Proceedings of the International Conference on Design and Operation of Container Ships*, London, UK, Paper No: 5, pp. 1-13.

Hearn, G.E., Furukawa, Y. and Kijima, K. (2000). Development of a design support methodology to resolve seakeeping, resistance and manoeuvrability conflicts. *Trans. of the West-Japan Society of Naval Architects*, Vol. 100, pp. 1-16.

Hoffman, D. and Zielinski, T. (1977). The use of conformal mapping techniques for hull surface definition. In *Proceedings of the SNAME Computer-Aided Hull Surface Definition Symposium*, Annapolis, USA, pp. 159-174.

Holden, C.M.E., Davies, R. and Keane, A.J. (2002). Optimization methodologies in conceptual design. In *Proceedings of the 9th AIAA/ISSMO Symposium on Multidisciplinary Analysis and Optimization*, Atlanta, USA, pp. 1-11.

Holtrop, J. and Mennen, G.G.J. (1982). An approximate power prediction method. In *International Shipbuilding Progress*, Vol. 29, pp. 166-170.

Holtrop, J. (1984). A statistical re-analysis of resistance and propulsion data. In *International Shipbuilding Progress*, Vol. 31, pp. 272-276.

Hooke, R. and Jeeves, T.A. (1961). "Direct search" solution of numerical and statistical problems. *Journal of the Association for Computing Machinery*, Vol. 8, pp. 212-229.

Housner, G.W. and Hudson, D.E. (1966). Applied Mechanics Dynamics, second edition. Volume II. Sections 7.3 and 7.4, pp. 188-191. *D. Van Nostrand Company*, New Jersey.

Huang, Z. J. and Hsiung, C.C. (1997). Nonlinear shallow-water flow on deck coupled with ship motion. In *Proceedings of the 21st Symposium on Naval Hydrodynamics*, Trondheim, Norway, pp. 220-234.

Huang, J., Cong, L., Grochowalski, S., Hsiung, C.C. (1998). Capsize analysis for ships with water shipping on and off the deck. In *Proceedings of the 22nd Symposium on Naval Hydrodynamics*, Washington, USA, pp. 376-389.

Hudson, D.A. (1999). A Validation Study on Mathematical Models of Speed and Frequency Dependence in Seakeeping of High Speed Craft. *PhD Thesis*, The University of Southampton, U.K.

Ikeda, Y. and Ma, Y. (2000). An experimental study on large roll motion in intermediate stage of flooding due to sudden ingress water. In *Proceedings of the 7th International Conference on Stability of Ships and Ocean Vehicles*, Launceston, Australia, pp. 270-285.

IMCO (1960). SOLAS 1960. International conference on safety of life at sea.

IMO (1971). Resolution A.265 (VIII): Regulation on subdivision and stability of passenger ships.

IMO (1993). Resolution A.751 (18). Interim standards for ship manoeuvrability.

IMO (1997). SOLAS Consolidated Edition 1997.

IMO (2002a). SLF 45/3/3: Investigations and proposed formulations for the factor “s”: the probability of survival after flooding.

IMO (2002b). SLF 45/3/5: Investigations and proposed formulations for the factors “p”, “r” and “v”: the probability of damage to a particular compartment or compartments.

Insel, M. and Molland, A.F. (1992). An investigation into the resistance components of high speed displacement catamarans. *Trans. RINA*, Vol. 134, pp. 1-20.

Janson, C. E. and Larsson, L. (1996). A method for the optimization of ship hulls from a resistance point of view. In *Proceedings of the 21st Symposium on Naval Hydrodynamics*, Trondheim, Norway, pp. 680-696.

Keane, A.J. (1988). A computer based method for hull form concept design: applications to stability analyses. *Trans. RINA*, Vol. 130 (A), pp. 61-75.

Keane, A.J., Price, W.G. and Schachter, R.D. (1991). Optimization techniques in ship concept design. *Trans. RINA*, Vol. 133, pp. 123-139.

Keane, A.J. and Robinson, G.M. (1999). Experiences with optimizers in design. In *Proceedings of the 14th International Symposium on Air Breathing Engines, ISABE '99*, Florence, Italy.

Kerczek, V.C. and Tuck, E.O. (1969). The representation of ship hulls by conformal mapping functions. In *Journal Ship Research*, Vol. 13, pp. 284-298.

Kim, Y. (2001). Coupled analysis of ship motions and sloshing flows. In *Proceedings of the 16th International Workshop on Water Waves and Floating Bodies*, Hiroshima, Japan, pp. 1-4.

Kobylinski, L.K. and Kastner, S. (2003). Stability and Safety of Ships. Volume I: Regulation and Operation. Section 1.1, pp. 3-10. *Elsevier Ocean Engineering Book Series*, Oxford.

Kowalik, J. and Osborne, M.R. (1968). Methods for Unconstrained Optimization Problems. Section 2.4, pp. 21-22. *American Elsevier Pub. Co.*, New York.

Kristensen, H.O. (2002). Design considerations of passenger ships with respect to damage stability requirements. In *DCAMM–course, Stability of Ships*, Lyngby, Denmark, pp. 1-22.

Kruger, C.J.C. (2004). Constrained cubic spline interpolation. Lecture notes.

Lackenby, H. (1950). On the systematic geometrical variation of ship forms. *Trans. INA*, Vol. 92, pp. 289-316.

Landweber, L. and Macagno, M. (1959). Added mass of a three-parameter family of two-dimensional forces oscillating in a free surface. *Journal of Ship Research*, pp. 36-48.

Lewis, E.V. (1959). Increasing the sea speed of merchant ships. *Trans. SNAME*, Vol. 67, pp. 757-772.

Lewis, E.V. (1988). Principles of Naval Architecture. Volume I: Stability and Strength. Sections 3.3 and 3.4, pp. 149-176. *Sname,* New Jersey, USA.

Lewis, E.V. (1988). Principles of Naval Architecture. Volume I: Stability and Strength. Section 3.6, pp. 178-180. *Sname,* New Jersey, USA.

Lewis, E.V. (1989). Principles of Naval Architecture. Volume III: Motions in Waves and Controllability. Section 8.3, pp. 41-83. *Sname,* New Jersey, USA.

Lewis, E.V. (1989). Principles of Naval Architecture. Volume III: Motions in Waves and Controllability. Section 8.5, pp. 109-112. *Sname,* New Jersey, USA.

Liu, D., Hughes, O. and Mahowald, J. (1981). Applications of a computer-aided, optimal preliminary ship structural design method. *Trans. SNAME*, Vol. 89, pp. 275-294.

Lloyd, A.R.J.M. (1991). The seakeeping design package (SDP). In *RINA Spring Meetings,* London, UK and (1992) *Trans. RINA*, Vol. 134, pp. 161-180.

Lloyd, A.R.J.M. (1998). Seakeeping: Ship Behaviour in Rough Weather. Section 3.3, pp. 71-77. *A.R.J.M. Lloyd*, UK.

Lloyd, A.R.J.M. (1998). Seakeeping: Ship Behaviour in Rough Weather. Chapter 8, pp. 152-164. *A.R.J.M. Lloyd*, UK.

Lloyd, A.R.J.M. (1998). Seakeeping: Ship Behaviour in Rough Weather. Chapter 15, pp. 303-314. *A.R.J.M. Lloyd,* UK.

Lloyd's Register (2003). Rules and regulations for the classification of ships. Part 3, Section 3.4, pp. 8-10.

Lunde, J.K. (1951). On the linearized theory of wave resistance for displacement ships in steady and accelerated motion. *Trans. SNAME*, Vol. 59, pp. 25-85.

Lutzen, M. (2002). Discussions on damage statistics. Private communication.

Lyon, T.D. and Mistree, F. (1985). A computer-based method for the preliminary design of ships. *Journal of Ship Research*, Vol. 29, pp. 251-269.

MAIB (1999). Marine Accident Investigation Branch MGN 115 (M+F): Accident reporting and investigation.

MAIB (2000). Marine Accident Investigation Branch Annual Report 2000.

MAIB (2001). Marine Accident Investigation Branch Annual Report 2001.

MAIB (2002). Marine Accident Investigation Branch Annual Report 2002.

Mandel, P. and Leopold, R. (1966). Optimization methods applied to ship design. *Trans. SNAME*, Vol. 74, pp. 477-521.

MCA (1999). MSN 1715 (M): Subdivision and damage stability of cargo ships of 80m in length and over.

Michell, J.H. (1898). The wave resistance of a ship, *Philosophical Magazine*, Series 5, Vol. 45, pp. 106-123.

Middleton, E.H. and Numata, E. (1970). Tests of a damaged stability model in waves. *Trans. SNAME*, Vol. 7, pp. 1-14.

Molland, A.F., Wellicome, J.F. and Couser, P.R. (1996). Resistance experiments on a systematic series of high speed displacement catamaran forms: variation of length-displacement ratio and breadth-draught ratio. *Trans. RINA*, Vol. 138, pp. 55-71.

Molland, A.F. and Karayannis, T. (1997). Development of a concept exploration and assessment model for advanced fast marine vehicles. In *Proceedings of the Sixth International Marine Design Conference*, Newcastle, UK, Vol.1, pp. 249-265.

Molland, A.F. and Lee, A.R. (1997). An investigation into the effect of prismatic coefficient on catamaran resistance. *Trans. RINA*, Vol. 139, pp. 157-165.

Molland, A.F., Wellicome, J.F., Temarel, P., Cic, J. and Taunton, D.J. (2001). Experimental investigation of the seakeeping characteristics of fast displacement catamarans in head and oblique seas. *Trans. RINA*, Vol. 143, pp. 79-98.

Murphy, R.D., Sabat, D.J. and Taylor, R.J. (1965). Least cost ship characteristics by computer techniques. *Marine Technology*, Vol. 2, pp. 174-202.

Newman, J.N. (1977). Marine Hydrodynamics. Sections 6.17 and 6.18, pp. 295-307. *The MIT Press*, Massachusetts.

Newman, J.N. (1978). The theory of ship motions. *Advances in Applied Mechanics*, Vol. 18, pp. 221-283.

Nowacki, H., Brusis, F. and Swift, P.M. (1970). Tanker preliminary design–an optimization problem with constraints. *Trans. SNAME*, Vol. 78, pp. 357-390.

Odabasi, A.Y. and Hearn, G.E. (1978). Sea keeping theories: what is the choice? *British Ship Research Association*, pp. 53-84.

Paik, J.K. and Faulkner, D. (2003). Reassessment of the M.V. Derbyshire sinking with the focus on hull-girder collapse. *Marine Technology*, Vol. 40(4), pp. 258-269.

Palazzi, L. and Kat, J.D. (2004). Model experiments and simulations of a damaged ship with air flow taken into account. *Marine Technology*, Vol. 41(1), pp. 38-44.

Pawlowski, M. (1999). The new damage stability criteria (in English and Polish). *Raport Techniczny Nr.35/99.*

Pawlowski, M., Vassalos, D., Cabaj, D., Tuzcu, C. and Konovessis, D. (2004). Floodable length curves based on probability of survival. In *Proceedings of the 4th International Conference on High-Performance Marine Vehicles*, Rome, Italy, pp. 192-199.

Peach, R.W. and Brook, A.K. (1987). The radii of gyration of merchant ships. *Transactions of the North East Coast Institution of Engineers and Ship Builders (NECIES)*, Berlin, Vol. 103(3), pp. 115-117.

Pelaez, J.G., Papanikolaou, A. and Gonzalez, V. (2000). Numerical and experimental study on the seakeeping performance of a fast round-bilge monohull. In *Proceedings of the 4th International Osaka Colloquium on Seakeeping Performance of Ships*, Osaka, Japan, pp. 1-10.

Ravn, E.S. (2002). Decision and optimization methods. In *DCAMM–course, Stability of Ships*, Lyngby, Denmark, pp. 1-13.

Robson, B.L. (1988). Systematic series of high speed displacement hull forms for naval combatants. *Trans. RINA*, Vol. 130, pp. 241-259.

Rognebakke, O.F. and Faltinsen, O.M. (2001). Effect of sloshing on ship motions. In *Proceedings of the 16th International Workshop on Water Waves and Floating Bodies*, Hiroshima, Japan, pp. 1-4.

Rusas, S. (2002). Stability of ships: probability of survival. In *DCAMM–course, Stability of Ships*, Lyngby, Denmark, pp. 1-13.

Salvesen, N., Tuck, E.O. and Faltinsen, O. (1970). Ship motions and sea loads. *Trans. SNAME*, Vol. 78, pp. 250-287.

Sarioz, K., Hearn, G.E. and Hills, B. (1992). Practical seakeeping for design: an optimised approach. In *Proceedings of PRADS '92*, Vol. 1, pp. 1.233-1.246.

Sarioz, K. (1993). A Hydrodynamic Hull Form Design Procedure in Conceptual and Preliminary Ship Design. *PhD Thesis*, The University of Newcastle upon Tyne, U.K.

Saydan, D. (1999). The analysis of irregular waves at time and frequency domain (in Turkish). *Final Year Project*, Faculty of Naval Architecture and Ocean Engineering, Technical University of Istanbul.

Saydan, D. (2003). Manual for Motion Code, School of Engineering Sciences, University of Southampton, UK.

Saydan, D. and Hearn G.E. (2004). Damage stability as a safety criterion for optimisation tools. In *Proceedings of the 4th International Conference on High-Performance Marine Vehicles*, Rome, Italy, pp. 177-191.

Saydan, D. (2004). Manual for Equilibrium Search Code, School of Engineering Sciences, University of Southampton, UK.

Schey, J.A. (1977). Introduction to Manufacturing Processes. Section 1.4, pp. 8-11. *McGraw-Hill*, New York.

Schneekluth, H. and Bertram, V. (1998). Ship Design for Efficiency and Economy. Section 1.2, pp. 5-13. *Butterworth Heinemann*, Oxford.

Schneekluth, H. and Bertram, V. (1998). Ship Design for Efficiency and Economy. Chapter 3, pp. 85-111. *Butterworth Heinemann*, Oxford.

Schroter, C. and Juhl J.S. (2002). Survivability after damage as observed from model tests. In *DCAMM – course, Stability of Ships*, Lyngby, Denmark, pp. 1-6.

Sen, P. (1992). Marine design: the multiple criteria approach. *Trans. RINA*, Vol. 134, pp. 261-276.

Sen, P., Birmingham, R., Cripps R.M. and Cain, C. (1997). A methodology for the integration of formal safety analysis into the design of lifeboats. In *Proceedings of the Sixth International Marine Design Conference*, Newcastle, UK, Vol. 1, pp. 313-327.

ShipShape (1992). Manual for Shipshape. Wolfson Unit for Marine Technology and Industrial Aerodynamics (WUMTIA), University of Southampton, UK.

Spouge, J.R. (2003). The safety of general cargo ships. *Trans. RINA International Journal of Maritime Engineering*, Vol. 145(A3), pp. 29-40.

Subramanian, V.A. and Kastner, S. (2000). Ship behaviour due to dynamic impact of water on deck. In *Proceedings of the 7th International Conference on Stability of Ships and Ocean Vehicles*, pp. 206-225.

Tagg, R. and Tuzcu, C. (2003). A performance-based assessment of the survival of damaged ships: final outcome of the EU research project HARDER. *Marine Technology*, Vol. 40(4), pp. 288-295.

Timman, R. and Newman, J.N. (1962). The coupled damping coefficients of a symmetric ship. *Journal of Ship Research*, Vol. 5(4), pp. 1-7.

Tuck, E.O. (1987). Wave resistance of thin ships and catamarans. *Report T8701*.

Tuck, E.O. and Lazauskas, L. (1998). Optimum hull spacing of a family of multihulls. *Ship Tech. Res.*, Vol. 45, pp. 180-195.

Turan, O. (1993). Dynamic Stability Assessment of Damaged Passenger Ships Using a Time Simulation Approach. *PhD Thesis*, The University of Strathclyde, Glasgow, U.K.

Turan, O. and Vassalos, D. (1994). Dynamic stability assessment of damaged passenger ships. *Trans. RINA*, Vol. 136, pp. 79-104.

Umeda, N., Kamo, T. and Ikeda, Y. (2004). Some remarks on theoretical modelling of damaged stability. *Marine Technology*, Vol. 41(1), pp. 45-49.

Vassalos, D., Pawlowski, M. and Turan, O. (1996). A theoretical investigation on the capsizal resistance of passenger/Ro-Ro vessels and proposal of survival criteria. *Final Report, Task 5, The Joint North West European R&D Project*, University of Strathclyde.

Vassalos, D., Letizia, L., Shaw, M. and MacPherson, C. (1998). An investigation on the flooding of damaged Ro-Ro ships. *Trans. RINA*, Vol. 140, pp. 273-289.

Vassalos, D., Guarin, L. and Jasionowski, A. (2001). Original tests on MV Derbyshire and the seakeeping investigation programme on the safety of bulk carriers. In *Proceedings of Glasgow Marine Fair and International Workshop on "Safety of Bulk Carriers"*, Glasgow, Scotland, UK, pp. 1-9.

Vassalos, D. and Jasionowski, A. (2002). Damaged ship hydrodynamics. In *Proceedings of the 6th International Ship Stability Workshop*, Webb Institute, pp. 1-13.

Veer, R.V. and Kat, J.O. (2000). Experimental and numerical investigation on progressive flooding and sloshing in complex compartment geometries. In *Proceedings of the 7th International Conference on Stability of Ships and Ocean Vehicles*, pp. 305-321.

Vossers, G., Swaan, W.A. and Rijken, H. (1960). Experiments with series 60 models in waves. *Trans. SNAME*, Vol. 68, pp. 364-450.

Walsh, G.R. (1975). Methods of Optimization. Section 3.3, pp. 76-79. *John Wiley & Sons*, London.

Watson, D.G.M. (1962). Estimating preliminary dimensions in ship design. *Trans. IESS*, Vol. 105, pp. 1-52.

Watson, D.G.M. and Gilfillan, A.W. (1977). Some ship design methods. *Trans. RINA*, Vol. 119, pp. 279-324.

Westlake, P.C. and Wilson, P.A. (2000). A new conformal mapping technique for ship sections. In *International Shipbuilding Progress*, Vol. 47(449), pp. 5-22.

Westlake, P.C., Wilson, P.A. and Bailey, P.A. (2000). Time domain simulations of ship motions. *Trans. RINA*, Vol. 142, pp. 268-288.

Wilson, P.A. (1986). A seakeeping analysis of a family of merchant ships. In *Proceedings of the International Conference on Computer Aided Design, Manufacture and Operation in the Marine and Offshore Industries*, Washington D.C., USA, pp. 237-253.

Wolfson (2001a). Wolfson Unit Hydrostatics and Stability Program 2001 Release.

Wolfson (2001b). Wolfson Unit Floodable Length Program 2001 Release.

Woodburn, P., Gallagher, P. and Letezia, L. (2002). Fundamentals of damaged ship survivability . *Trans. RINA*, Vol. 144, pp. 1-17.

Wright, P.N.H. (2004). The Preliminary Design of Catamarans for Seakeeping and Resistance. *PhD Thesis*, The University of Newcastle upon Tyne, U.K.

APPENDIX A – HOOKE – JEEVES ALGORITHM

The Hooke-Jeeves method based optimisation process has two main steps designated ‘exploratory’ and ‘pattern’. The exploratory move tries to understand the local behaviour of the objective function. The pattern move seeks to confirm, or otherwise, the existence of some advantage in adopting the variation of the point suggested by the exploratory move. The pattern move is always followed by a sequence of exploratory moves, so that an improved direction of search can be found and another patter move can be followed in that direction.

Thus if the problem of minimizing $g(x)$ is considered, the exploratory move starts with an initial base point, b_1, from,

$$b := (b_1, b_2 .....b_n) \tag{A.1}$$

together with step lengths,

$$HJ := (HJ_1, HJ_2 .....HJ_n) \tag{A.2}$$

for the respective variables,

$$x := (x_1, x_2 .....x_n). \tag{A.3}$$

After the determination of $g(b_1)$, the evaluation of $g(b_1 + HJ_1)$ is carried out. If the $g(b_1 + HJ_1) < g(b_1)$, the new base point will be ‘$b_1 + HJ_1$’ instead of ‘b_1’; otherwise $g(b_1 - HJ_1)$ will be evaluated. If the $g(b_1 - HJ_1) < g(b_1)$, the new base point will be ‘$b_1 - HJ_1$’ instead of ‘b_1’. If none of these moves is a success, the original point will be retained. The cited procedure has to be carried out for all variables in turn, finally arriving at a new base point after $2n+1$ function evaluations at most. If $b_2 = b_1$, the step lengths for each variable has to be halved and the exploratory move has to be repeated.

The analysis finishes when the step length is reduced below predetermined limits. If $b_2 \neq b_1$, a pattern move will be carried out from 'b_2'.

The pattern move starts from the new base point 'b_2' in the direction '$b_2 - b_1$' since exploratory move indicates a decrease in the value of $g(x)$ in this direction. Therefore, a move from 'b_2' to '$2b_2 - b_1$' will be analysed and new exploratory moves will be carried out about '$2b_2 - b_1$'. If the pattern and exploratory moves about '$2b_2 - b_1$' represents a lowest function value which is lower than $g(b_2)$, then a new base point 'b_3' has been found. In this case, next pattern move will be from 'b_3' to '$2b_3 - b_2$'. Otherwise, the pattern move from 'b_2' is terminated and a new exploratory move about 'b_2' will be initiated.

APPENDIX B - BOUNDARY VALUE PROBLEM

As it is mentioned earlier in the dissertation the unknown diffraction & radiation velocity potentials are determined using Green's second identity to convert the partial differential equation formula presented into an equivalent Fredholm formulation boundary integral. The fluid and structural boundaries in seakeeping fluid-structure interaction formulations are the free surface, the wetted surface of the vessel, the sea-bed and the artificial cylindrical radiation boundary linking sea-bed and free surface. The boundary condition on this last boundary (which ultimately tends to infinity) is often referred to as the Sommerfield radiation condition. The radiation condition is necessary because the governing partial differential equation is Laplace's equation, which includes the conditions of an incompressible fluid subject to irrotational flow, and being an elliptic partial differential equation a closed boundary is required.

The Sommerfield radiation condition implies that the energy associated with the disturbance of the fluid caused by the motion of the vessel must vanish at infinity.

The sea-bed condition assumes that the sea-bed is a rigid horizontal, flat and impermeable boundary. Since there is no flow across this boundary

$$\frac{\partial \phi_W}{\partial n} = 0 \text{ and } \frac{\partial \phi_D}{\partial n} = 0 \text{ on the seabed.} \tag{B.1}$$

Here ϕ_W describes the incident wave potential and ϕ_D is the diffraction potential, resulting from the interaction of the incident wave and the structure(s) being investigated.

On the wetted surface of the structure the fluid velocity normal to the body surface must be identical to normal velocity of the structure. One can either view this as requiring continuity of velocity across the wetted surface or impermeability of the wetted surface and thus

$$\frac{\partial}{\partial n}\left(\phi_W + \phi_D\right) = 0 \text{ on } S_W \tag{B.2}$$

and

$$\frac{\partial \phi_j}{\partial n} = v_{jn} \text{ on } S_W \tag{B.3}$$

Here ϕ_j is the time-independent radiation potential arising from the structure moving in the jth mode of motion and v_{jn} denotes the normal velocity component of the structure moving in the jth mode of motion.

On the free surface continuity of velocity and pressure can be shown to be satisfied using the linearised composite free surface condition

$$\frac{\partial \phi}{\partial Y} - \frac{\omega^2}{g}\phi = 0\,. \tag{B.4}$$

The time independent velocity potential ϕ representing either the radiation potential ϕ_j or the diffraction potential ϕ_D with the time dependence satisfying

$$\Phi\left(Z, X, Y, t\right) = \phi\left(Z, X, Y\right)e^{-i\omega t}\,. \tag{B.5}$$

The resultant fluid flow is described by

$$\phi = \phi_W + \phi_D + \sum_{i=1}^{6}\phi_j\,, \tag{B.6}$$

since the governing equations are linear and superposition may be applied.

The details of the theory can be found in many text, see for example Odabasi and Hearn (1978), Newman (1978) and Hudson (1999).

APPENDIX C - NUMERICAL APPLICATION OF THE NEW METHOD TO DETERMINE THE MASS MOMENT OF INERTIA FOR PARENT DERBYSHIRE AND FOR A TANKER HULL FORM

Here the pure and product moment of inertia equations already provided in Chapter 5 are applied to the parent Derbyshire and a tanker hull form.

Firstly, calculations are carried out for the parent Derbyshire. Hence, the magnitudes of four point masses and their longitudinal positions already provided in Table 6.2 (with more decimal points) are used to determine the vertical and horizontal positions of the four point masses.

From Equation (5.38) the coordinate X_P can be determined assuming $k_{YY} = 0.225L$.

$$M_A\left(Z_A^2 + X_P^2\right) + M_F\left(Z_F^2 + X_P^2\right) = \left(M_A + M_F\right) \times k_{YY}^2 \tag{5.38}$$

$$94686.56 \times \left(64.05667^2 + X_P^2\right) + 104793.6 \times \left(57.87859^2 + X_P^2\right) = \left(199480.16\right) \times \left(0.225 \times 281.94\right)^2 \tag{C.1}$$

Therefore, X_P equals to 17.79547617 and hence from Equation (5.30) it is clear that $X_S = -X_P$.

With X_S known, Equation (5.41) can be used to determine $Y_{AS} = Y_{FS}$, subject to the assumption that $k_{ZZ} = 0.41B$ together with the deduction made earlier from Equation (5.34).

$$M_A\left(X_S^2 + Y_{AS}^2\right) + M_F\left(X_S^2 + Y_{FS}^2\right) = M \times k_{ZZ}^2 . \tag{5.41}$$

$$94686.56 \times \left(17.79547617^2 + Y_{AS}^2\right) + 104793.6 \times \left(17.79547617^2 + Y_{FS}^2\right) = \left(199480.16\right) \times \left(0.41 \times 44.196\right)^2 \tag{C.2}$$

Therefore, Y_{AS} and Y_{FS} equal to 3.41579.

Finally, to check consistency of assumed radii of gyration $Y_{AS} = Y_{FS}$ is re-determined using Equation (5.45)

$$M_A\left(Z_A^2 + Y_{AS}^2\right) + M_F\left(Z_F^2 + Y_{FS}^2\right) = M \times k_{XX}^2 . \tag{5.45}$$

$$94686.56\times\left(64.05667^2 + Y_{AS}^2\right) + 104793.6\times\left(57.87859^2 + Y_{FS}^2\right) = \left(199480.16\right)\times\left(0.216305098\times 281.94\right)^2 \tag{C.3}$$

This results in $Y_{AS} = Y_{FS}$ equal to 3.41579.

Second example is a tanker hull form with 216m of length and 32.2m of beam. The magnitudes of four point masses and their longitudinal positions are provided in Table C.1. For more details related to the tanker hull form see Bishop et al. (1977).

Table C.1: The four masses and their longitudinal positions for the tanker hull form.

M_A	35656.6 tonnes
M_F	39255.01 tonnes
Z_A from LCG	46.795 metres
Z_F from LCG	42.506 metres
$M_{AP} = M_{AS}$	17828.3 tonnes
$M_{FP} = M_{FS}$	19627.505 tonnes

Again from Equation (5.38) the coordinate X_P can be determined assuming $k_{YY} = 0.215L$.

$$35656.6\times\left(46.795^2 + X_P^2\right) + 39255.01\times\left(42.506^2 + X_P^2\right) = \left(74911.61\right)\times\left(0.215\times 216\right)^2 \tag{C.4}$$

Therefore, X_P equals to 12.946 and hence from Equation (5.30) it is clear that $X_S = -X_P$.

With X_S known, Equation (5.41) can be used to determine $Y_{AS} = Y_{FS}$, subject to the assumption that $k_{ZZ} = 0.41B$ together with the deduction made earlier from Equation (5.34).

$$35656.6\times\left(12.946^2 + Y_{AS}^2\right) + 39255.01\times\left(12.946^2 + Y_{FS}^2\right) = \left(74911.61\right)\times\left(0.41\times 32.2\right)^2 \quad \text{(C.5)}$$

Therefore, Y_{AS} and Y_{FS} equal to 2.587.

Finally, to check consistency of assumed radii of gyration $Y_{AS} = Y_{FS}$ is re-determined using Equation (5.45)

$$35656.6\times\left(46.795^2 + Y_{AS}^2\right) + 39255.01\times\left(42.506^2 + Y_{FS}^2\right) = \left(74911.61\right)\times\left(0.2068\times 216\right)^2 \quad \text{(C.6)}$$

This results in $Y_{AS} = Y_{FS}$ equal to 2.587.

APPENDIX D - GENERAL ARRANGEMENT DRAWING OF THE DERBYSHIRE

M.V. LIVERPOOL BRIDGE
(Re-named M.V. DERBYSHIRE)
CAPACITY PLAN

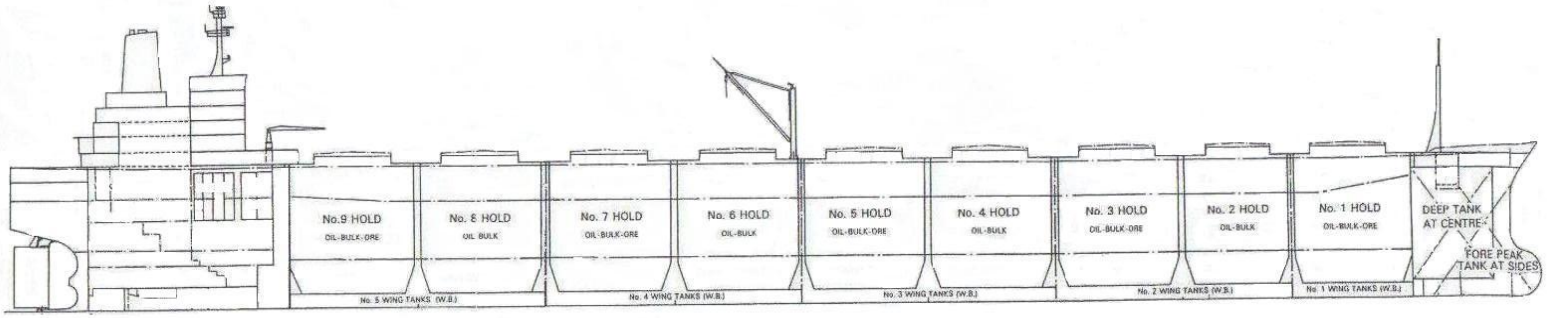

APPENDIX E – GENERAL APPRAISAL OF DAMAGE SCENARIOS FOR PARENT DERBYSHIRE

In Chapter 6 (Table 6.11) four distinct scenarios were defined based on one hold and two hold damage. The statistics of Chapter 3 suggest that more than two holds being simultaneously damaged is unlikely. Whilst this may be the case it was interesting to consider more damaged holds than is thought feasible to appreciate the attitude of the hull as a result of water ingress into the parent Derbyshire hull form. Table E.1 indicates the amount of parallel sinkage and trim angle achieved as the number of damaged compartments increases. Heel angles were not significant and hence there is no need to record them.

Table E.1: Different damage scenarios.

Holds Damaged	Parallel sinkage (m)	Trim (degrees)	Draught at AP (m)	Draught at FP (m)
2	1.243	1.192	16.262	22.128
1+2	1.992	1.875	15.319	24.549
1+2+Deep Tank	2.6471	2.7321	13.849	27.3
1+2+3+Deep Tank	3.5	3.2	13.541	29.3
1+2+3+4+Deep Tank	4.3534	3.4795	13.7	30.843
1+2+3+4+5+Deep Tank	5.2065	3.556	14.363	31.884

Depending on the number of damaged compartment the magnitude of parallel sinkage and trim angle vary. This change has also effect on the draught at AP and FP.

APPENDIX F - ITERATIVE METHOD FOR DETERMINATION OF EQUILIBRIUM TRIM AND HEEL ANGLES

The determination of the equilibrium trim and heel angles is very important for the accurate analysis of the static and dynamic properties of the damaged ship. The analysis method employed is applied to both the parent Derbyshire hull form and the optimised hull form.

The algorithm employed is summarised as follows:

- Determine parallel sinkage in accordance with structural mass losses and mass gains through water ingress.

- Apply 1° of trim (see Figure F.1) and determine whether ship orientation is one of hydrostatic equilibrium.

- Repeat second step until either the equilibrium achieved or trim angle just too large. In latter case reduce trim angle increment to 0.5° and apply from previous starting position. Reduce incremental trim angle as necessary until equilibrium established.

- Repeat procedures of step 2 and 3 for heel angle determination for given parallel sinkage and trim angle.

- Note trim and heel angles for equilibrium.

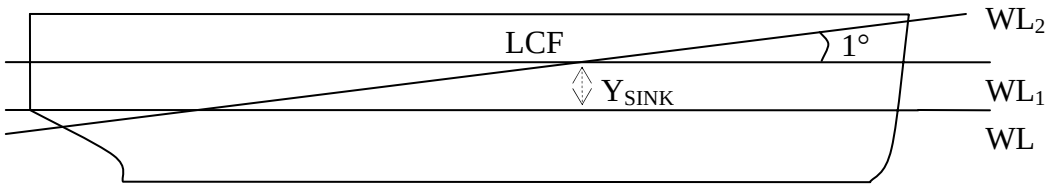

Figure F.1: Analysis of the equilibrium angles.

APPENDIX G – SENSITIVITY ANALYSIS OF THE PURE AND PRODUCT MOMENT OF INERTIAS TO THE EQUILIBRIUM ANGLES

Here, the effect of parallel sinkage, trim and heel angles on the pure and product moment of inertias is examined for the parent and optimised hull forms (see Table G.1 for the parent hull form and Table G.2. for the optimised hull form).

Table G.1: The pure and product moment of inertias belonging to the parent hull for different damage scenarios.

PARENT	INTACT	DAMAGED	CASE A	CASE B	CASE C	CASE D
I44	6.55E+07	I44	7.05E+07	7.04E+07	7.52E+07	7.57E+07
I45	0.00E+00	I45	2.23E+07	2.23E+07	5.23E+07	4.18E+07
I46	4.14E+07	I46	5.47E+05	3.62E+06	3.21E+06	-7.33E+05
I55	7.42E+08	I55	8.54E+08	8.53E+08	1.03E+09	9.25E+08
I56	0.00E+00	I56	-3.95E+06	-3.97E+06	-6.03E+06	-6.81E+06
I66	8.03E+08	I66	9.18E+08	9.18E+08	1.10E+09	9.94E+08

Table G.2: The pure and product moment of inertias belonging to the optimised hull for different damage scenarios.

OPTIMISED	INTACT	DAMAGED	CASE A	CASE B	CASE C	CASE D
I44	6.49E+07	I44	7.01E+07	7.00E+07	7.50E+07	7.54E+07
I45	0.00E+00	I45	2.81E+07	2.80E+07	6.49E+07	5.36E+07
I46	2.36E+07	I46	-1.09E+06	2.36E+06	4.32E+06	-1.26E+06
I55	8.80E+08	I55	1.06E+09	1.06E+09	1.33E+09	1.18E+09
I56	0.00E+00	I56	-3.61E+06	-3.53E+06	-4.47E+06	-5.21E+06
I66	9.44E+08	I66	1.12E+09	1.12E+09	1.40E+09	1.25E+09

The four product of inertias namely I_{45} and I_{56} are zero valued for the intact case. However, this is not the case when the ship is damaged. Usually the pure and product moment of inertias remain the same for damage case A and B, I_{46} differs for these two damage scenarios.

APPENDIX H – HYDRODYNAMIC COEFFICIENT PLOTS FOR THE INTACT DERBYSHIRE AND FOR THE DAMAGED DERBYSHIRE (SCENARIO A)

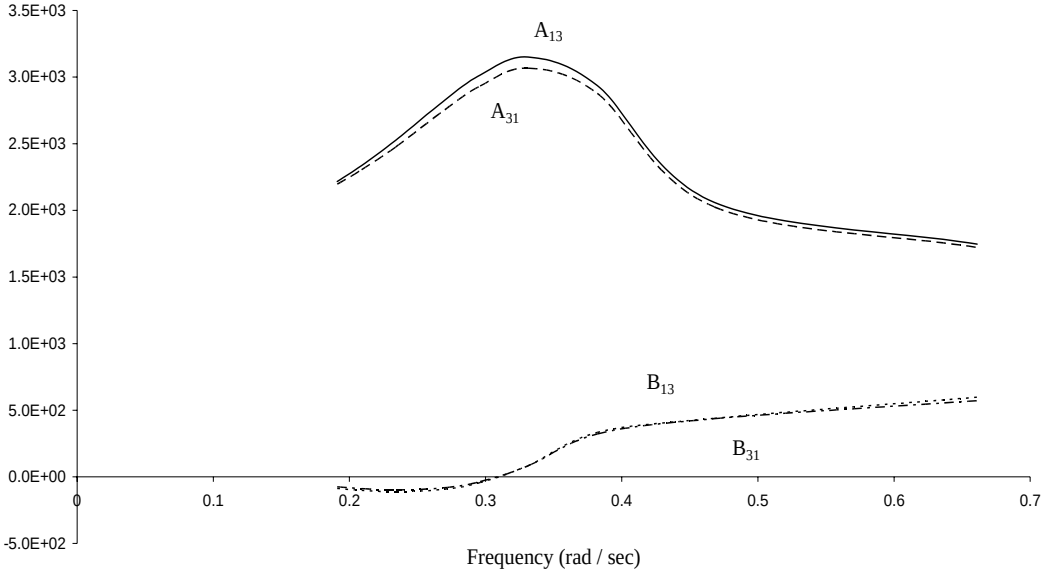

Figure H.1: Surge-heave and heave-surge added mass and fluid damping coefficients for the intact Derbyshire.

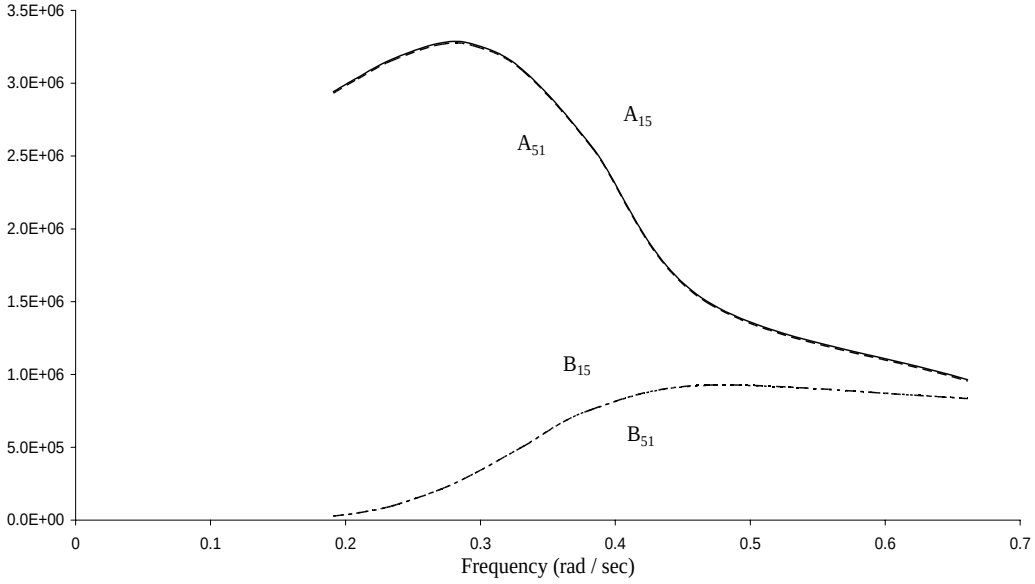

Figure H.2: Surge-pitch and pitch-surge added mass and fluid damping coefficients for the intact Derbyshire.

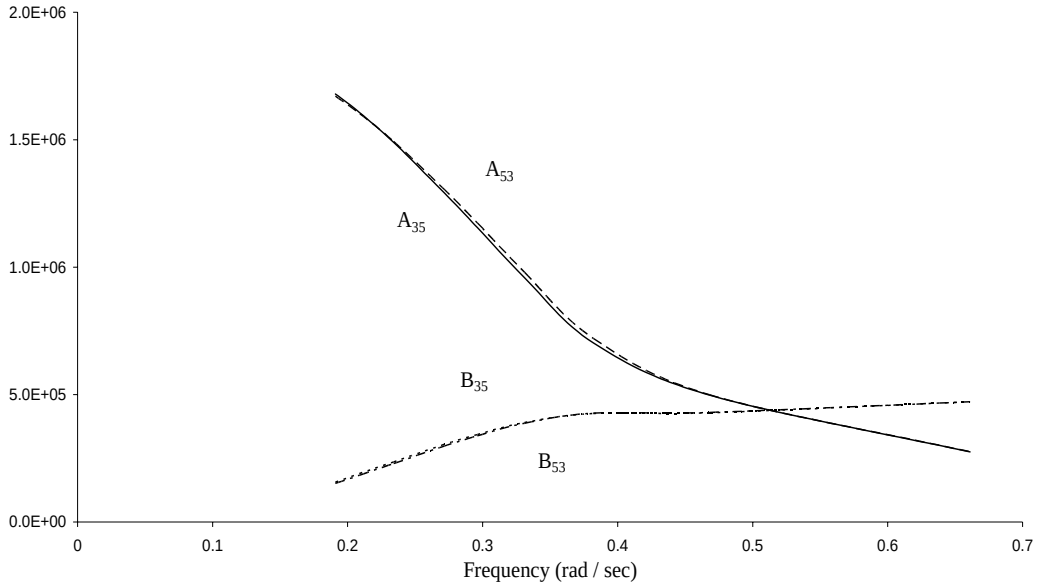

Figure H.3: Heave-pitch and pitch-heave added mass and fluid damping coefficients of for the intact Derbyshire.

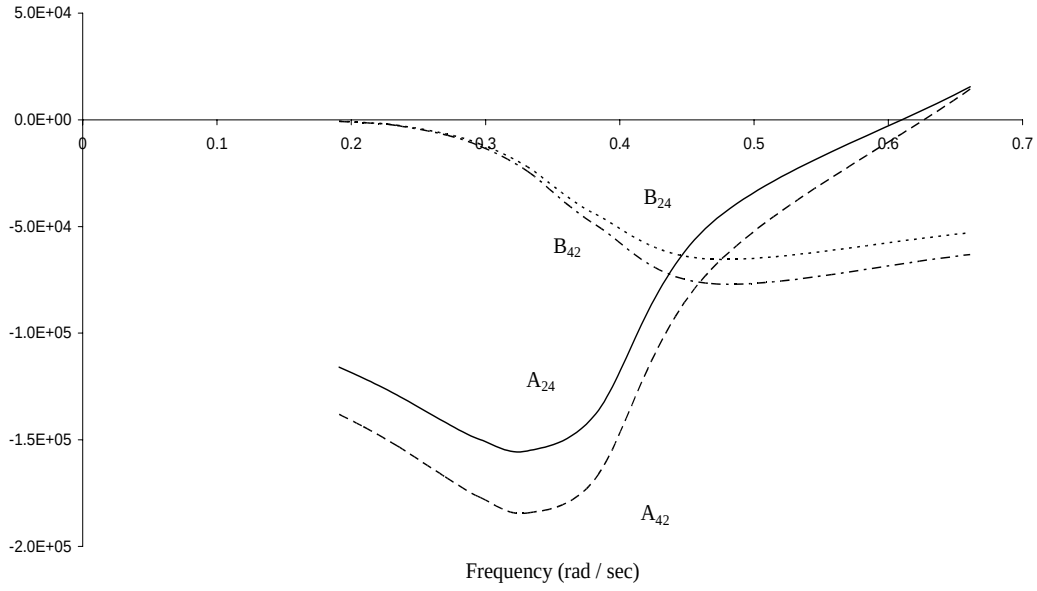

Figure H.4: Sway-roll and roll-sway added mass and fluid damping coefficients for the intact Derbyshire.

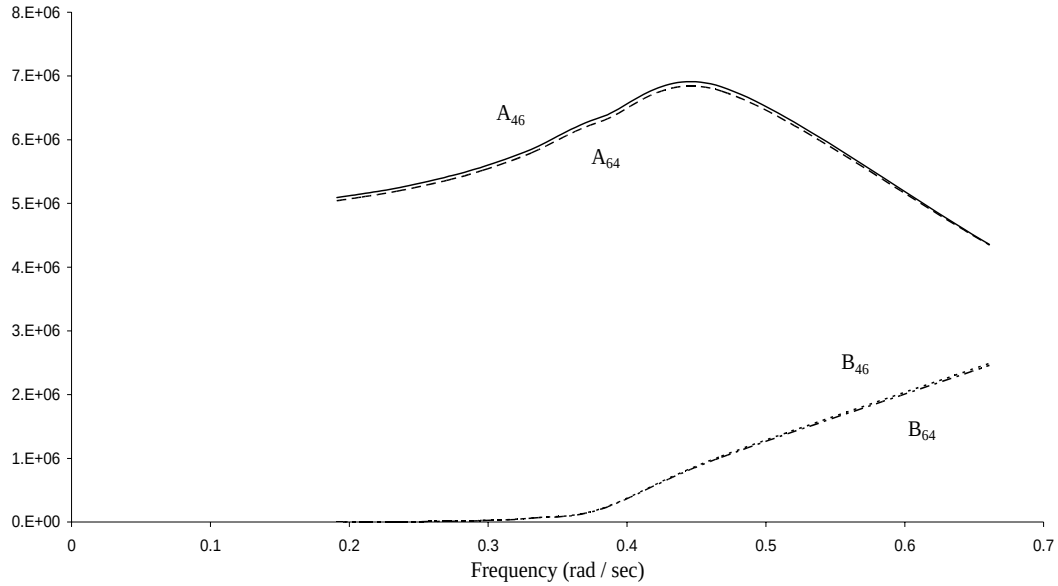

Figure H.5: Roll-yaw and yaw-roll added mass and fluid damping coefficients for the intact Derbyshire.

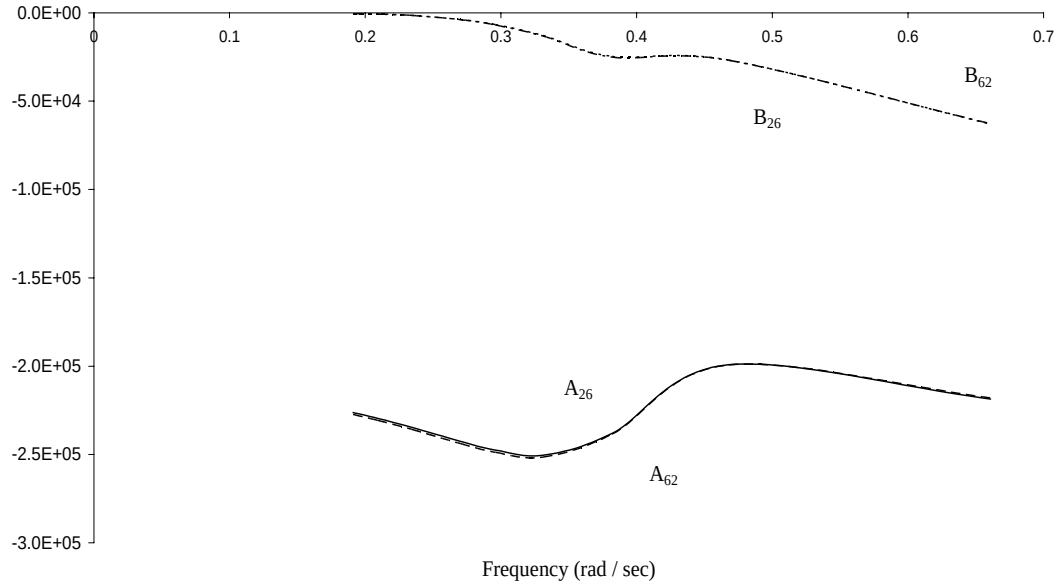

Figure H.6: Sway-yaw and yaw-sway added mass and fluid damping coefficients for the intact Derbyshire.

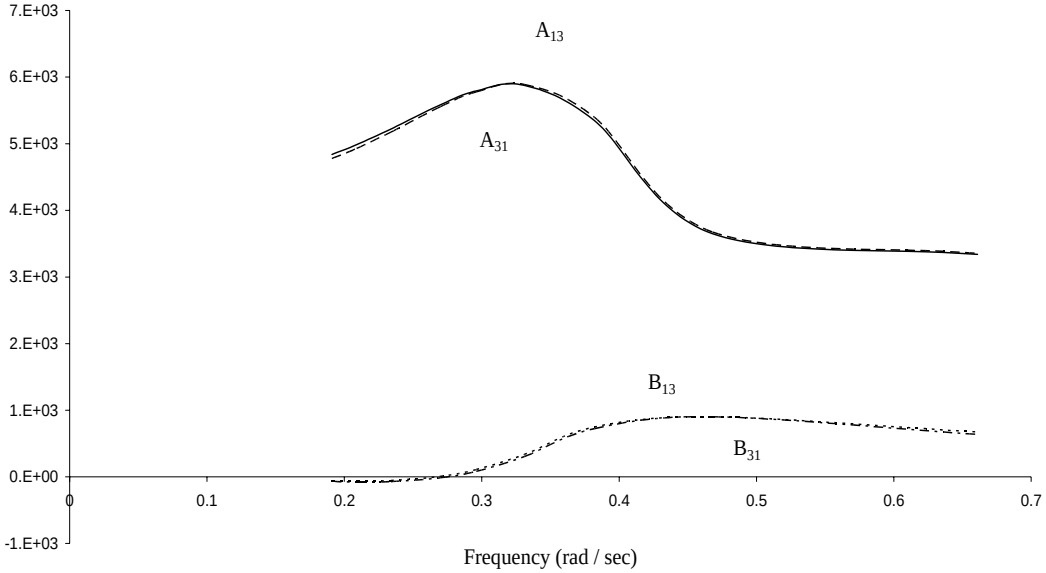

Figure H.7: Surge-heave and heave-surge added mass and fluid damping coefficient for the damaged Derbyshire (scenario A).

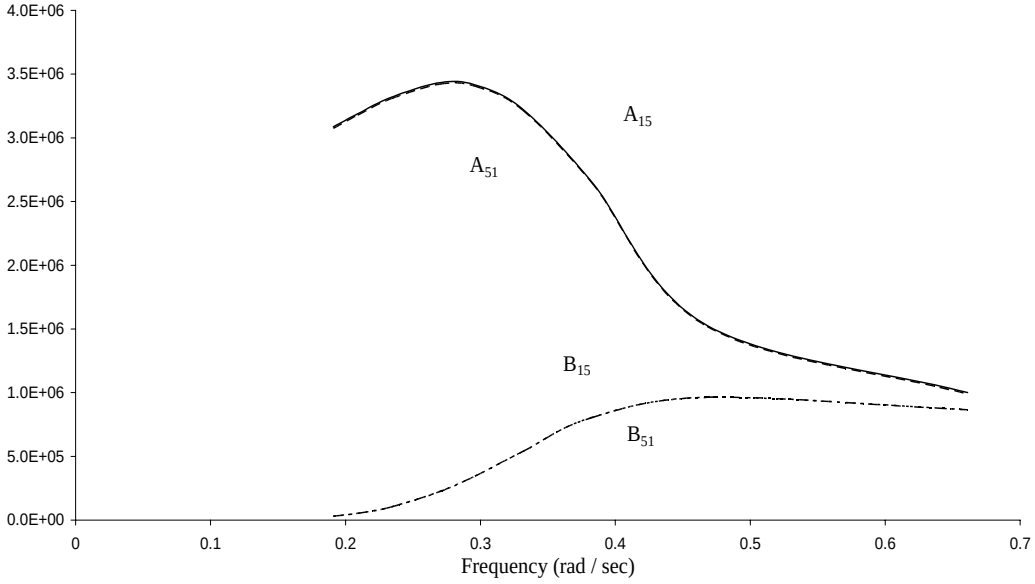

Figure H.8: Surge-pitch and pitch-surge added mass and fluid damping coefficient for the damaged Derbyshire (scenario A).

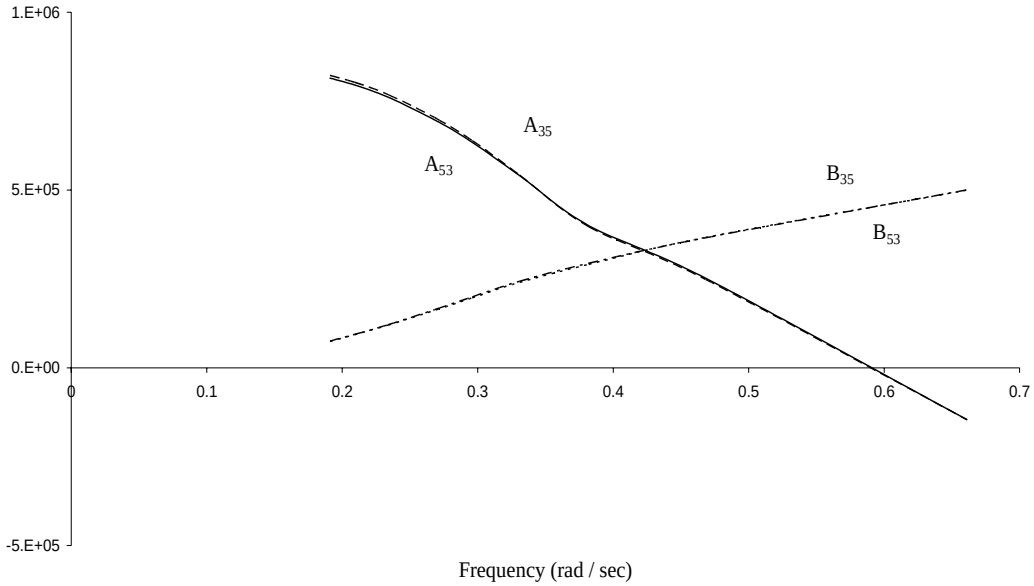

Figure H.9: Heave-pitch and pitch-heave added mass and fluid damping coefficient for the damaged Derbyshire (scenario A).

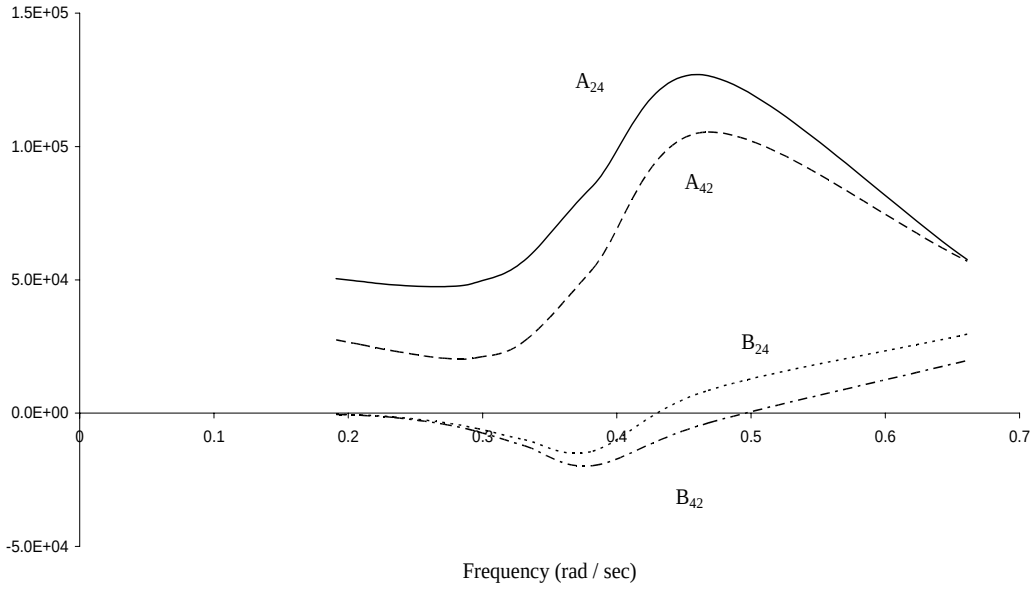

Figure H.10: Sway-roll and roll-sway added mass and fluid damping coefficient for the damaged Derbyshire (scenario A).

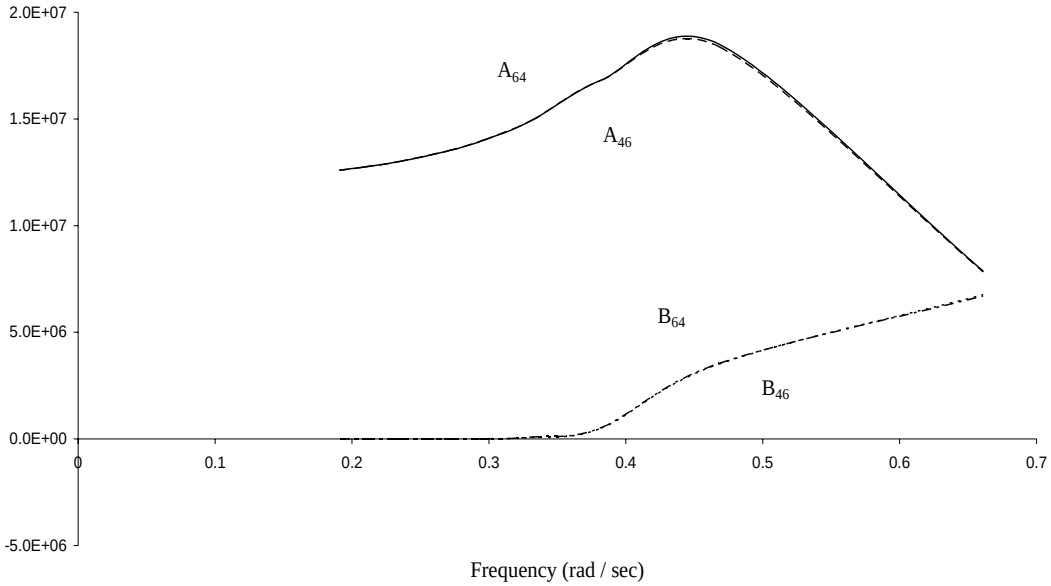

Figure H.11: Roll-yaw and yaw-roll added mass and fluid damping coefficient for the damaged Derbyshire (scenario A).

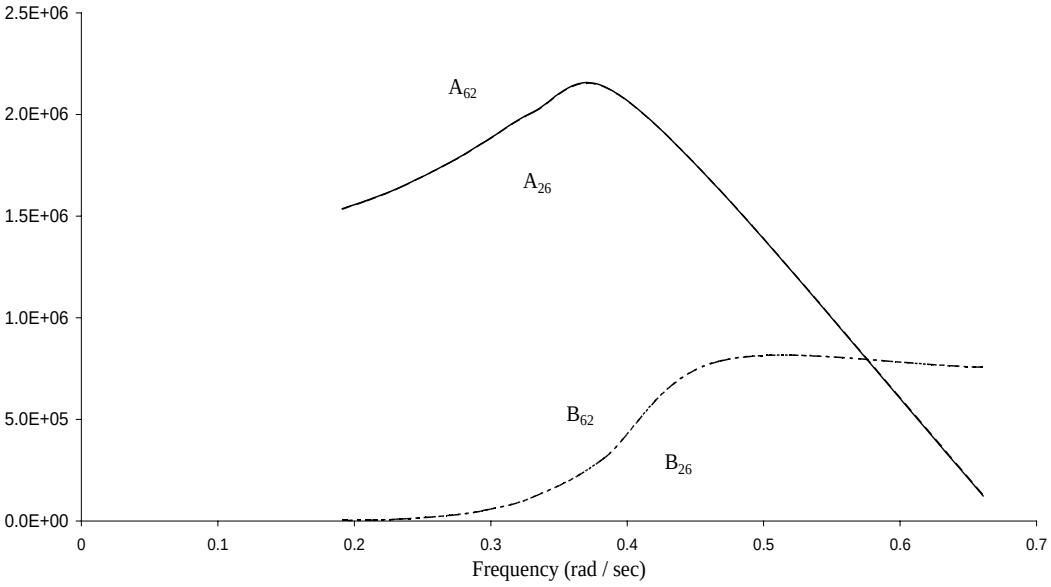

Figure H.12: Sway-yaw and yaw-sway added mass and fluid damping coefficient for the damaged Derbyshire (scenario A).

APPENDIX I – THEORY BEHIND THE RELATIVE VERTICAL MOTION

The resultant vertical displacement at (z,x,y) relative to the origin (z_0,x_0,y_0) at LCF is dependent upon the pitch and roll levers l'_p and l'_r defined as

$$l'_p = \sqrt{(z - z_0)^2 + (y - y_0)^2} \tag{I.1}$$

and

$$l'_r = \sqrt{(x - x_0)^2 + (y - y_0)^2}\,. \tag{I.2}$$

Depending on the actual location of (z,x,y), relative to (z_0,x_0,y_0), the resultant vertical motion requires adding/subtracting the vertical resolved components of the pitch and roll displacements as defined in Figures I.1(a) & I.1(b) to the vertical heave motion.

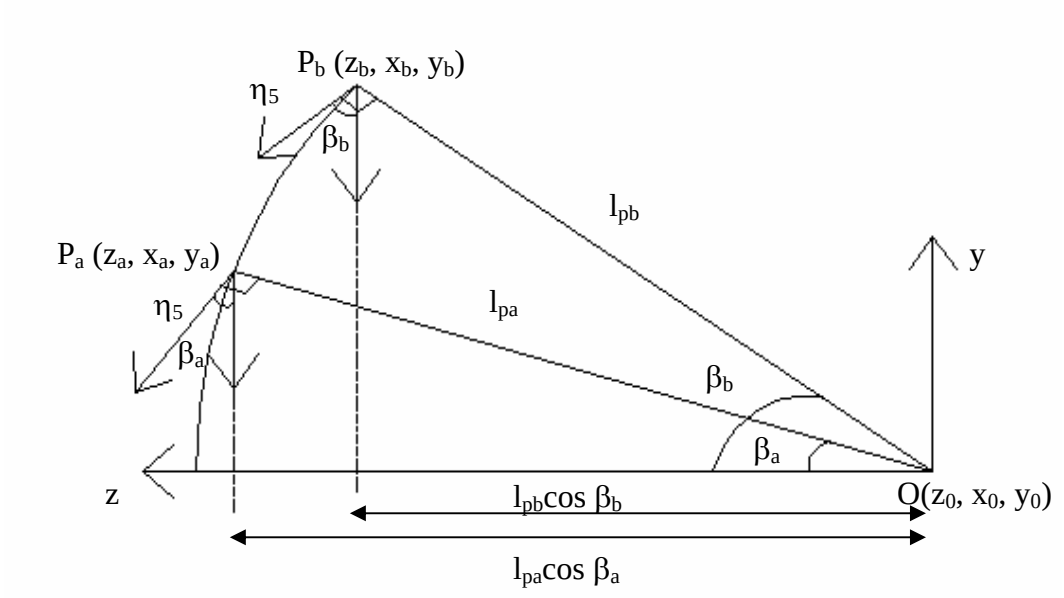

Figure I.1(a): Pitch and associated vertical displacement.

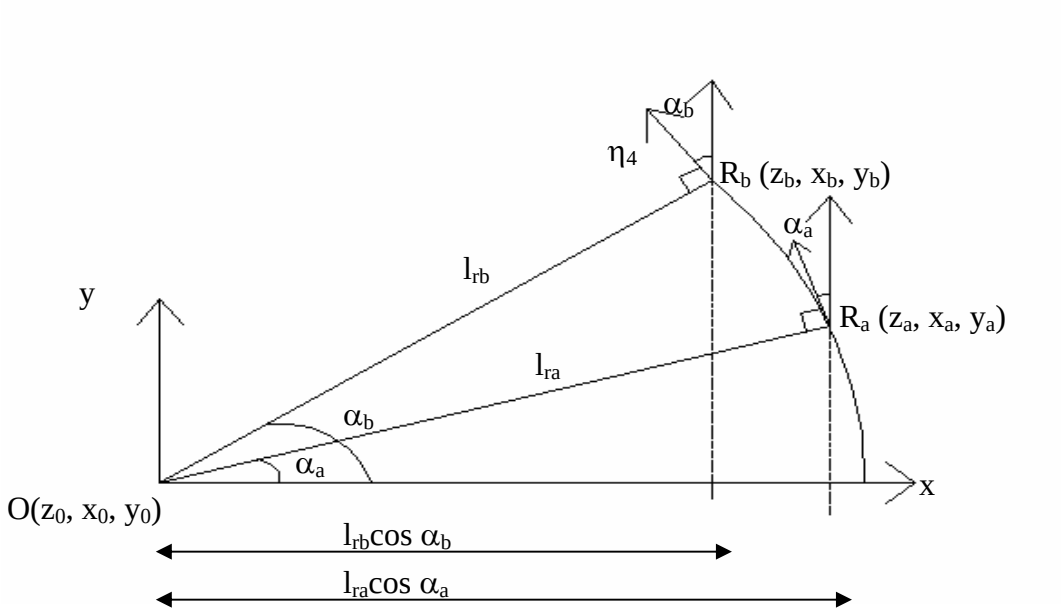

Figure I.1(b): Roll and associated vertical displacement.

From Figures I.1(a) & I.1(b) the following general observations may be made:

- Tangential displacement is lever multiplied by roll or pitch amplitude.

- Vertical displacement is tangential displacement multiplied by cosine of angle subtended by point of interest and horizontal.

- Vertical displacement is equivalent to projected lever in z-x plane multiplied by roll or pitch amplitude.

- Projected levers in z-x plane is simply

$$l_p = \sqrt{\left(z - z_0\right)^2} \tag{I.3}$$

and

$$l_r = \sqrt{\left(x - x_0\right)^2} \ . \tag{I.4}$$

- Vertical displacement is explicitly independent of vertical position of point of interest, but is implicitly dependent on vertical coordinate through variation of (z,x) on wetted surface. As point of interest moves from undisturbed free surface to points on selected deck x increases in magnitude and its amplitude becomes the half beam.

That is, the vertical displacement, $S_V(z,x)$, may be written as

$$S_V(z,x) = \eta_3 - l_p \,\mathrm{sgn}(z)\eta_5 + l_r \,\mathrm{sgn}(x)\eta_4 \tag{I.5}$$

where

$$\mathrm{sgn}(z) = \begin{cases} +1 \text{ if } z \text{ positive} \\ -1 \text{ if } z \text{ negative} \end{cases} \tag{I.6}$$

and

$$\mathrm{sgn}(x) = \begin{cases} +1 \text{ if } x \text{ positive} \\ -1 \text{ if } x \text{ negative} \end{cases} . \tag{I.7}$$

APPENDIX J – RELATIVE VERTICAL MOTION FOR DIFFERENT SELECTED POINTS ALONG THE SHIP

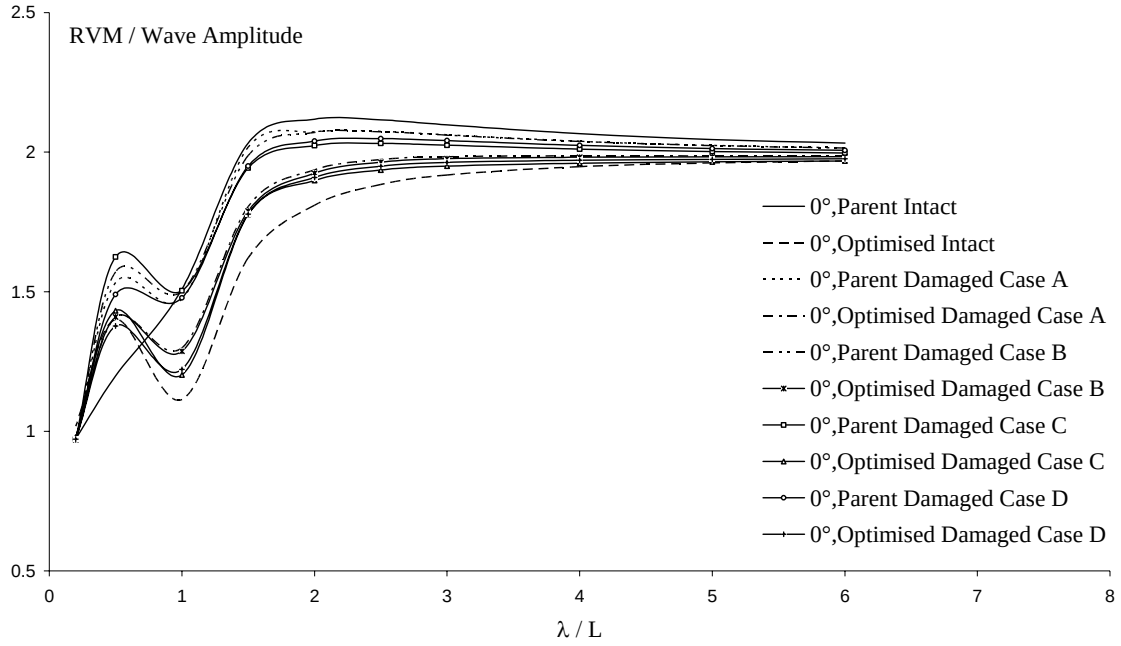

Figure J.1: Relative vertical motion responses for the intact and damaged hull forms for point A (in following seas).

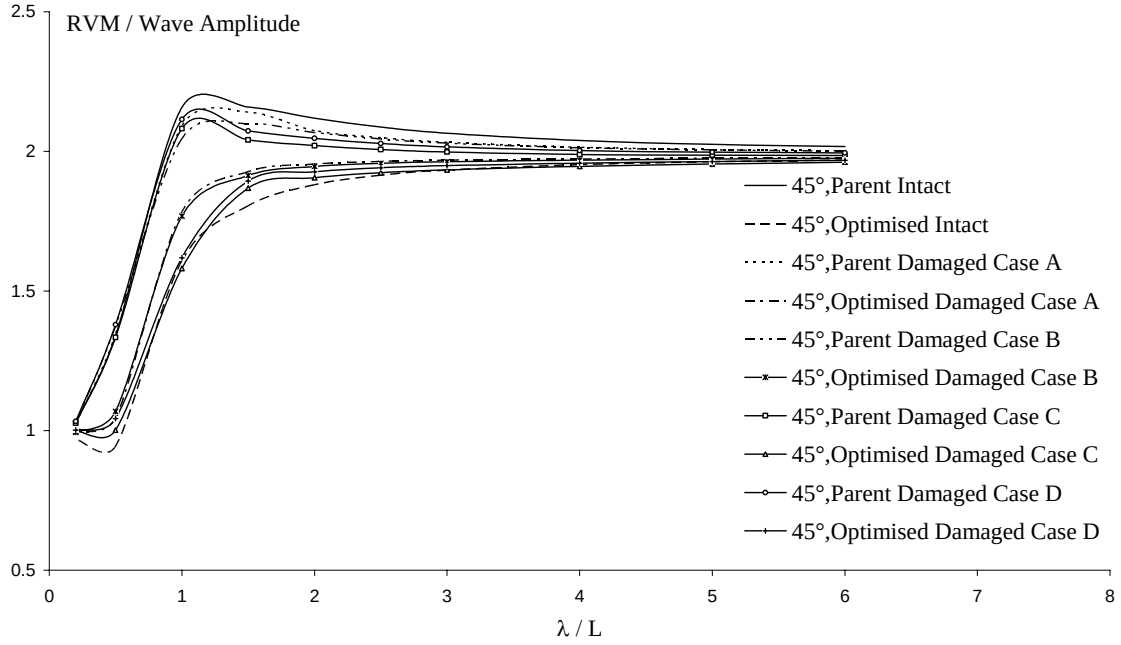

Figure J.2: Relative vertical motion responses for the intact and damaged hull forms for point A (in quartering seas).

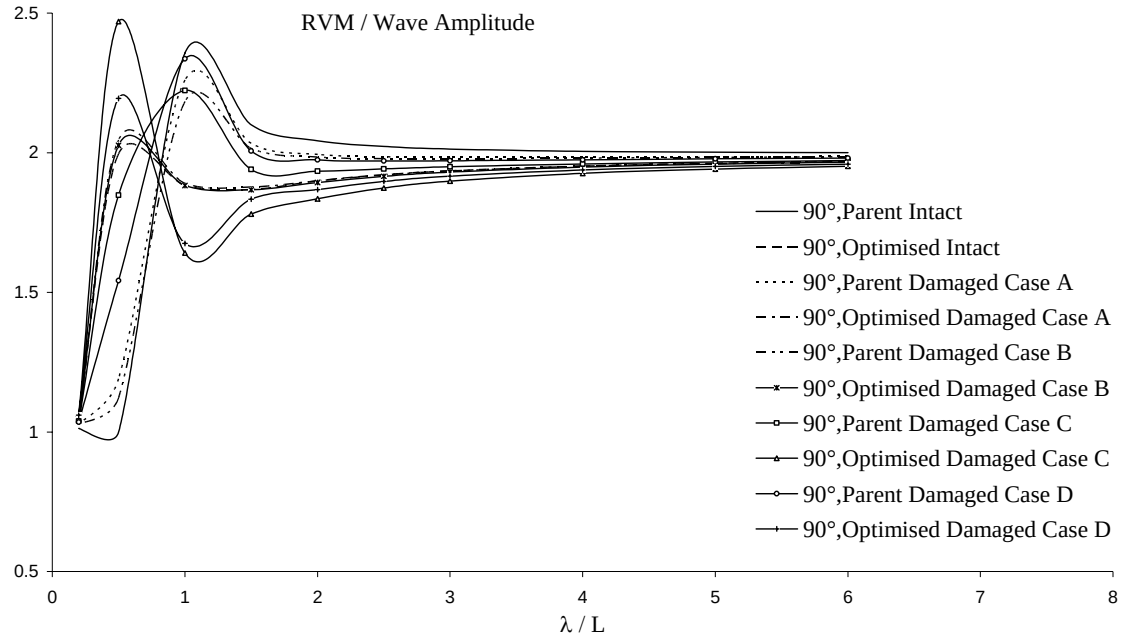

Figure J.3: Relative vertical motion responses for the intact and damaged hull forms for point A (in beam seas).

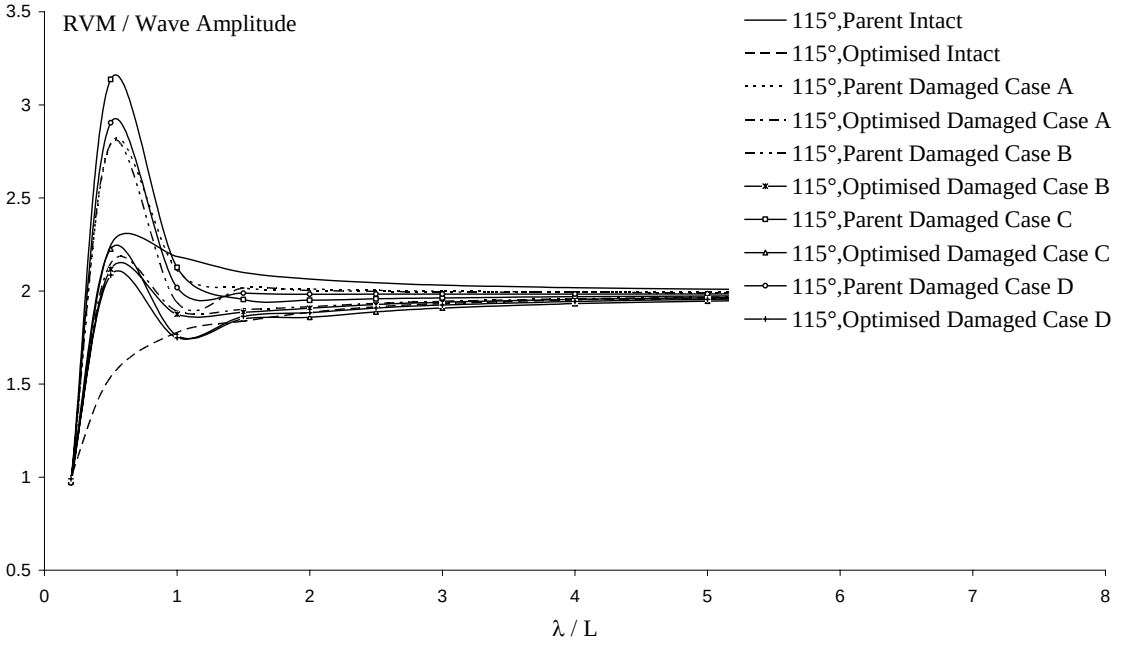

Figure J.4: Relative vertical motion responses for the intact and damaged hull forms for point A (in beam seas).

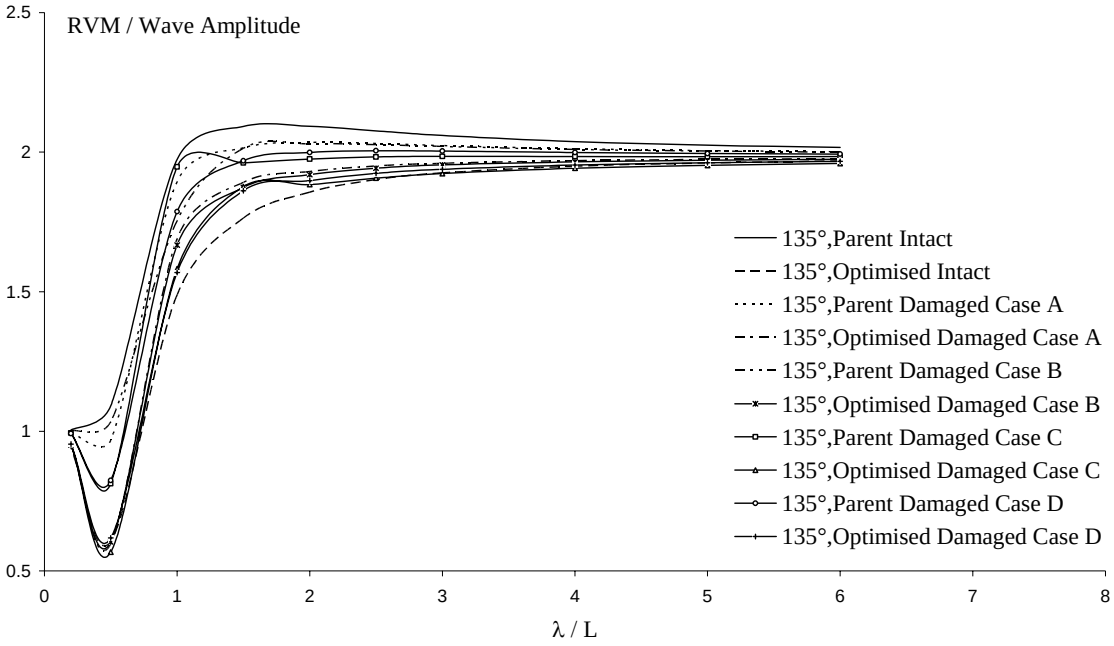

Figure J.5: Relative vertical motion responses for the intact and damaged hull forms for point A (in bow seas).

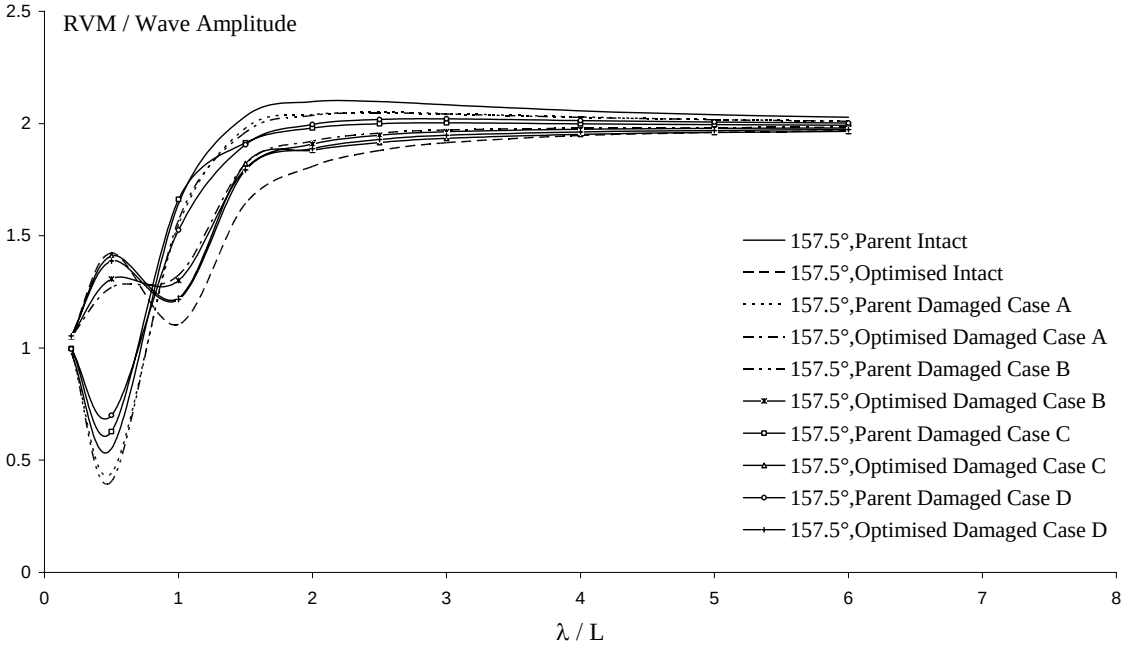

Figure J.6: Relative vertical motion responses for the intact and damaged hull forms for point A (in head seas).

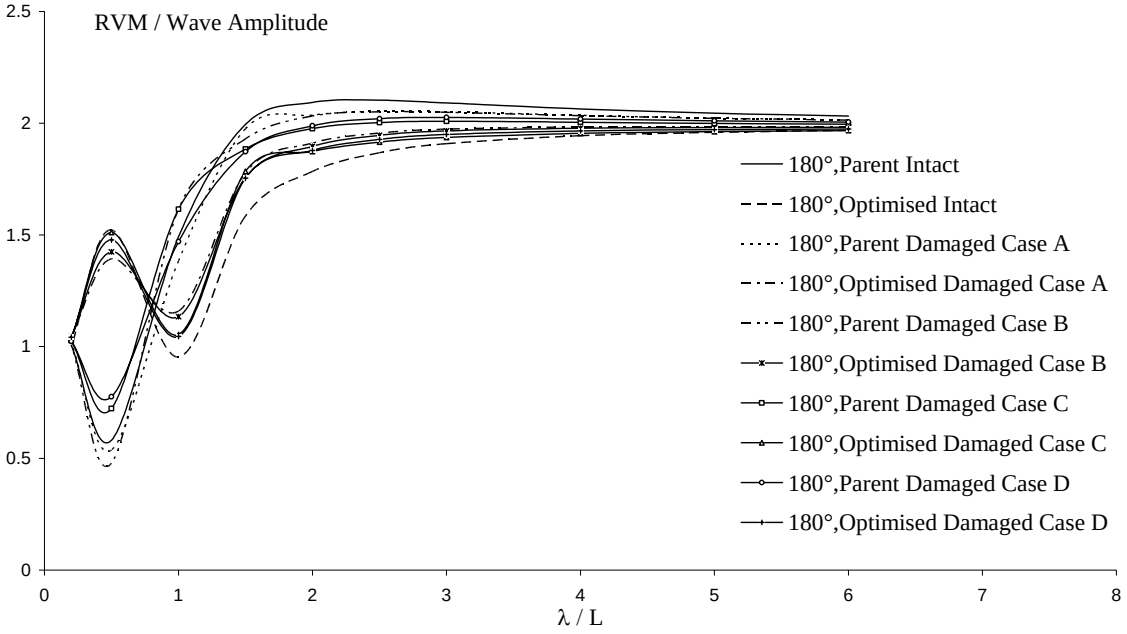

Figure J.7: Relative vertical motion responses for the intact and damaged hull forms for point A (in head seas).

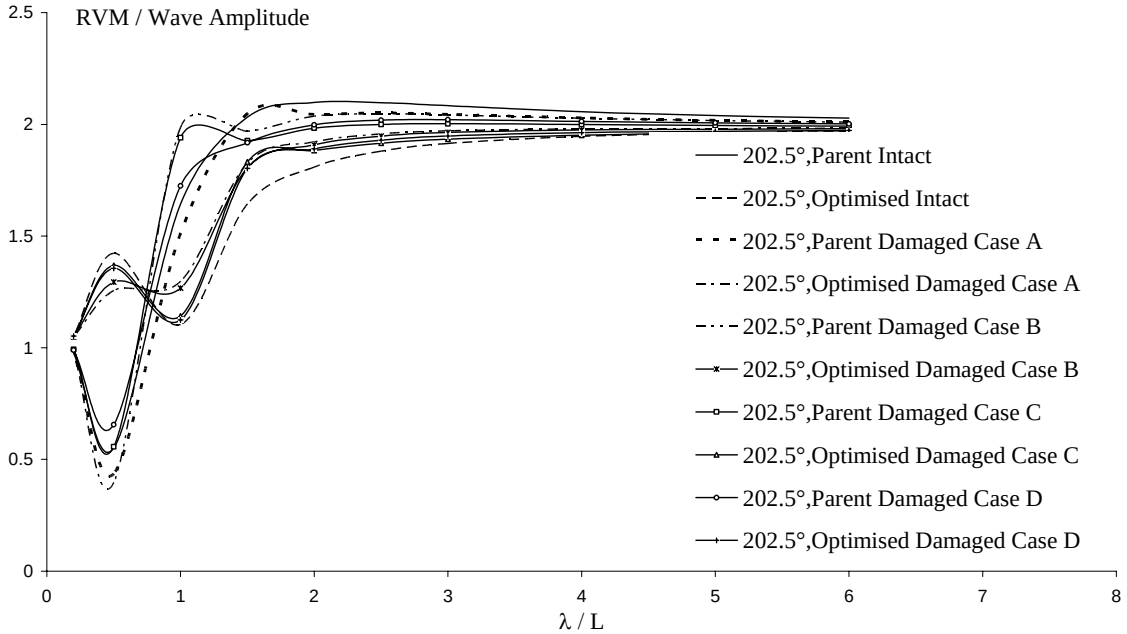

Figure J.8: Relative vertical motion responses for the intact and damaged hull forms for point A (in head seas).

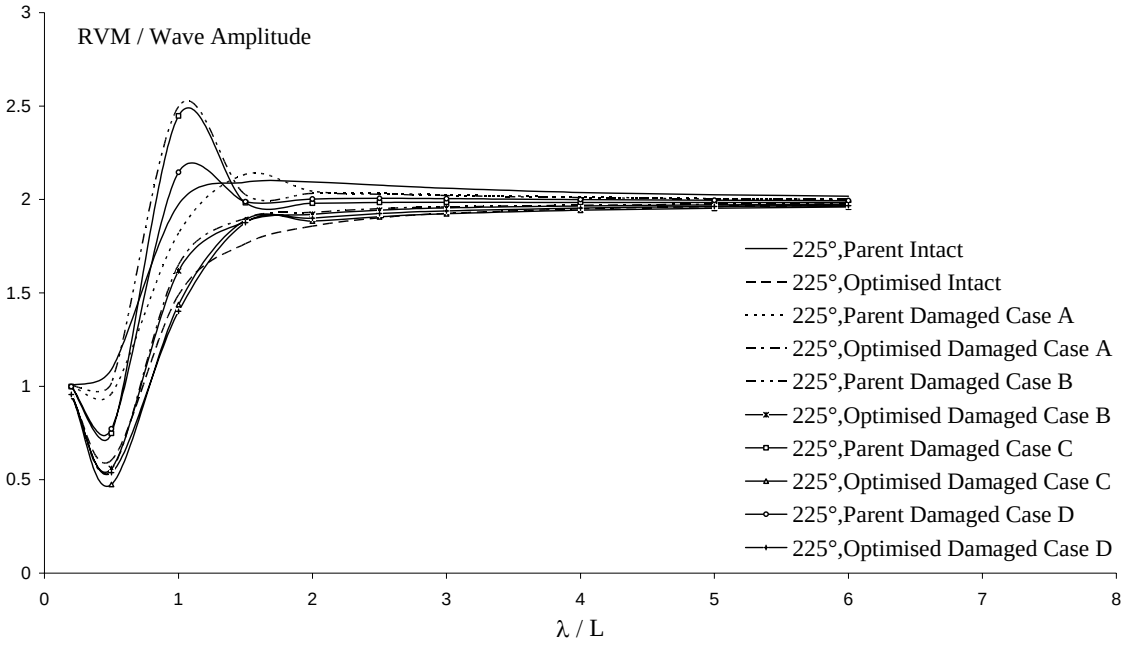

Figure J.9: Relative vertical motion responses for the intact and damaged hull forms for point A (in bow seas).

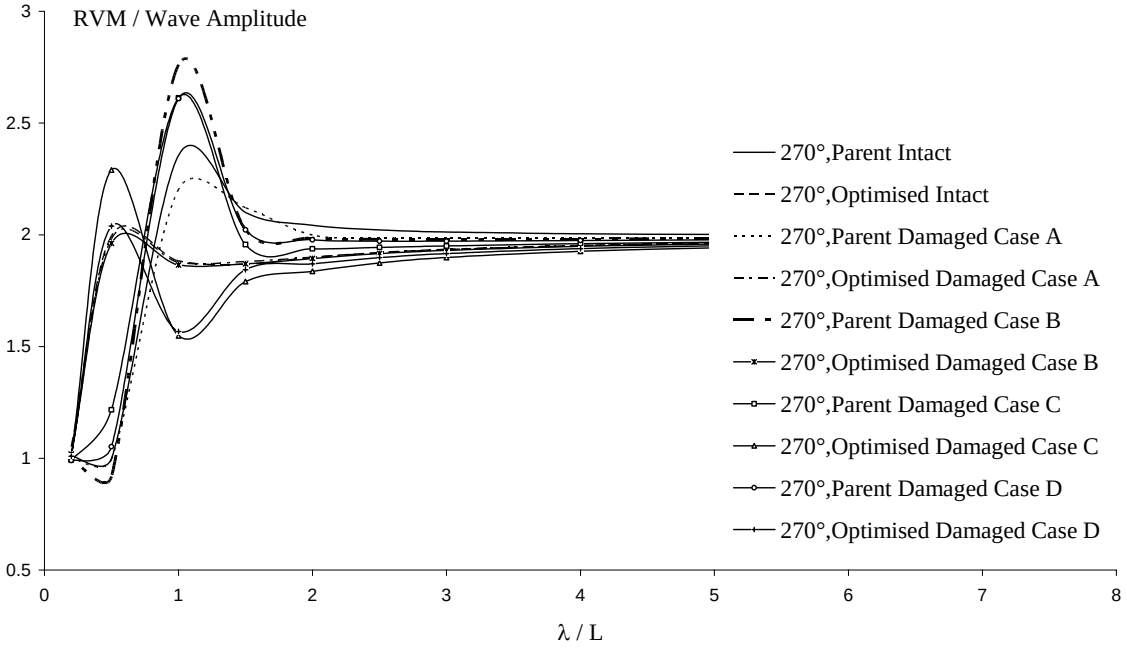

Figure J.10: Relative vertical motion responses for the intact and damaged hull forms for point A (in beam seas).

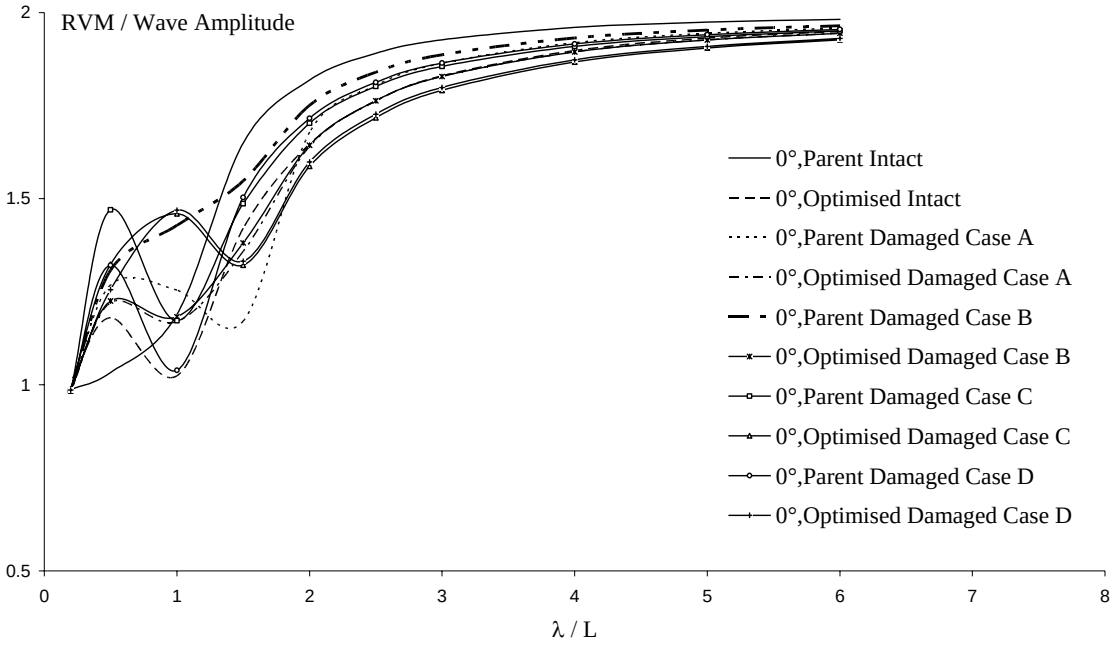

Figure J.11: Relative vertical motion responses for the intact and damaged hull forms for point B (in following seas).

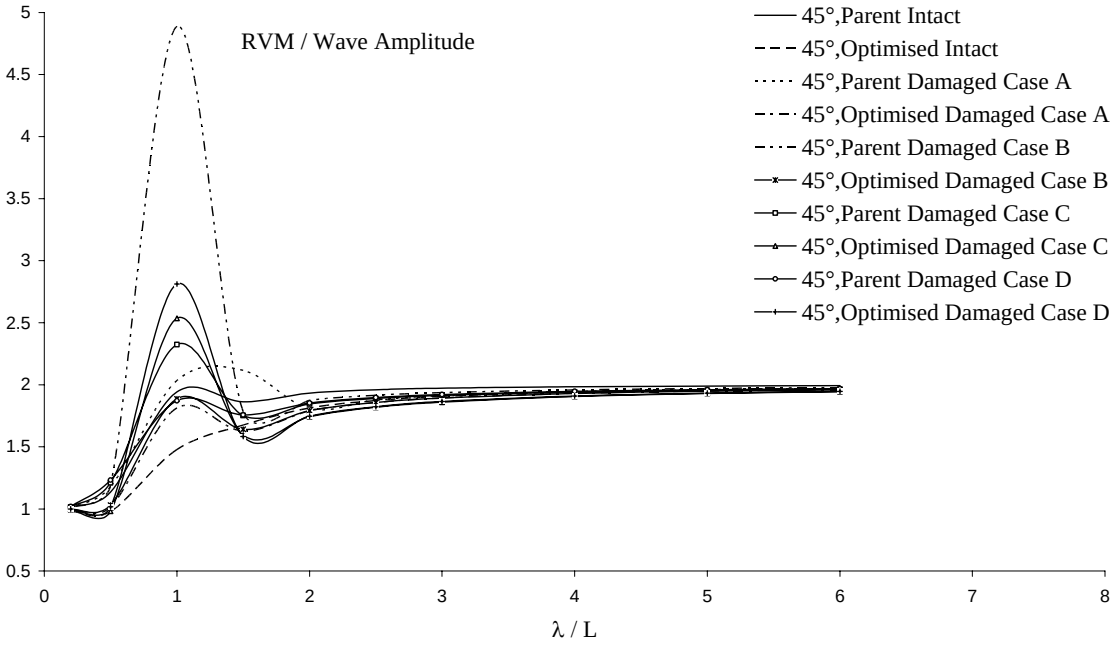

Figure J.12: Relative vertical motion responses for the intact and damaged hull forms for point B (in quartering seas).

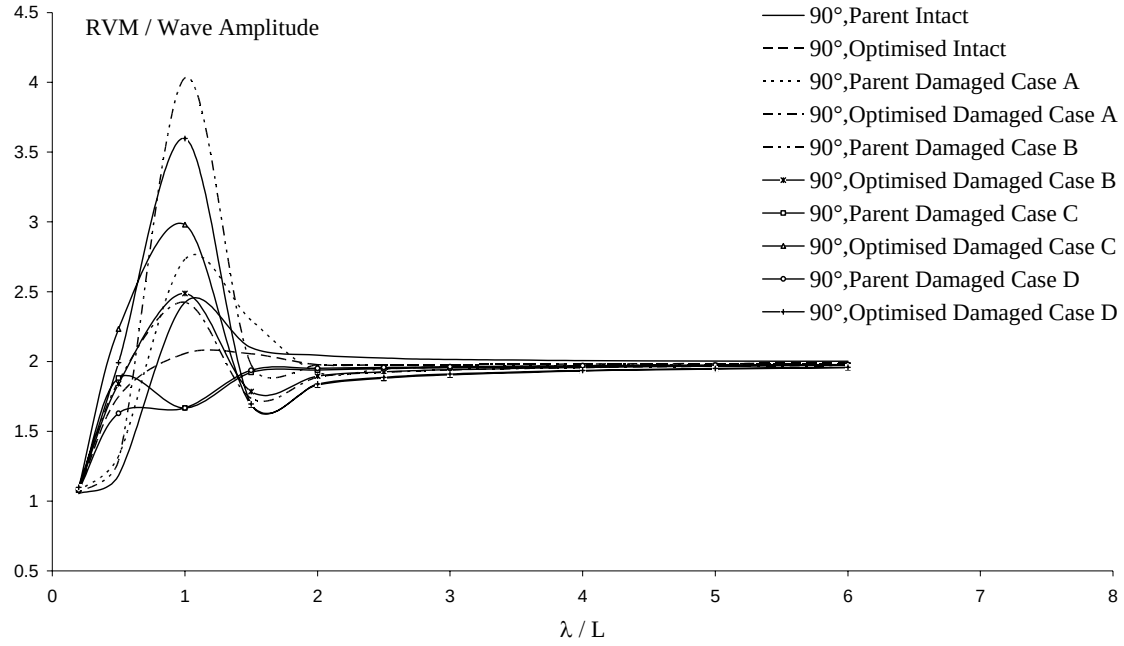

Figure J.13: Relative vertical motion responses for the intact and damaged hull forms for point B (in beam seas).

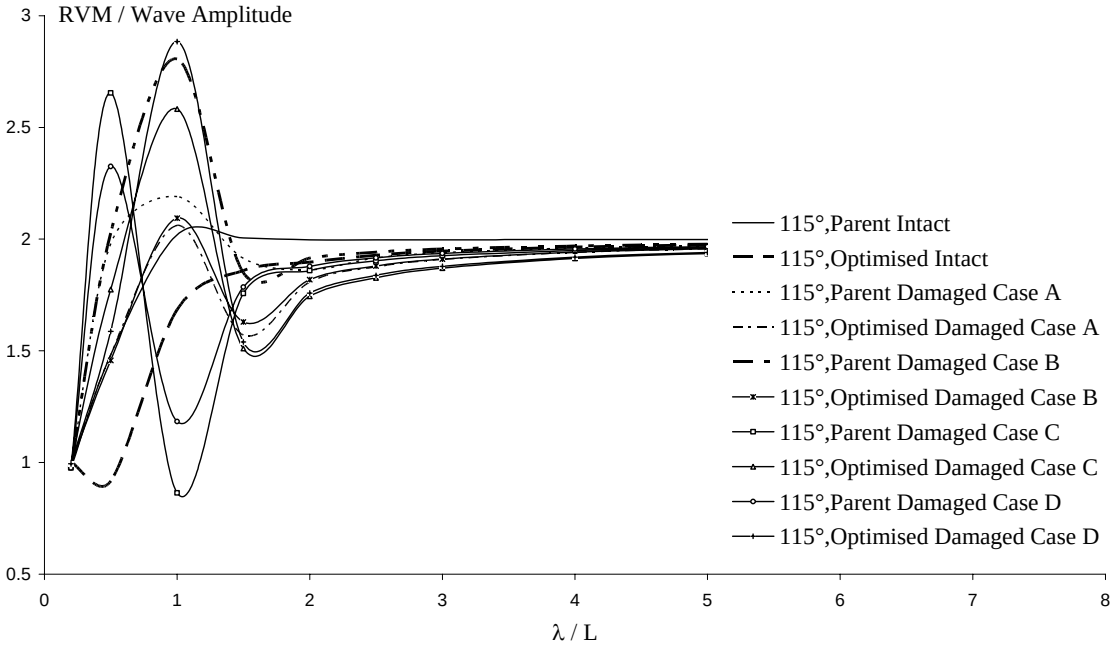

Figure J.14: Relative vertical motion responses for the intact and damaged hull forms for point B (in beam seas).

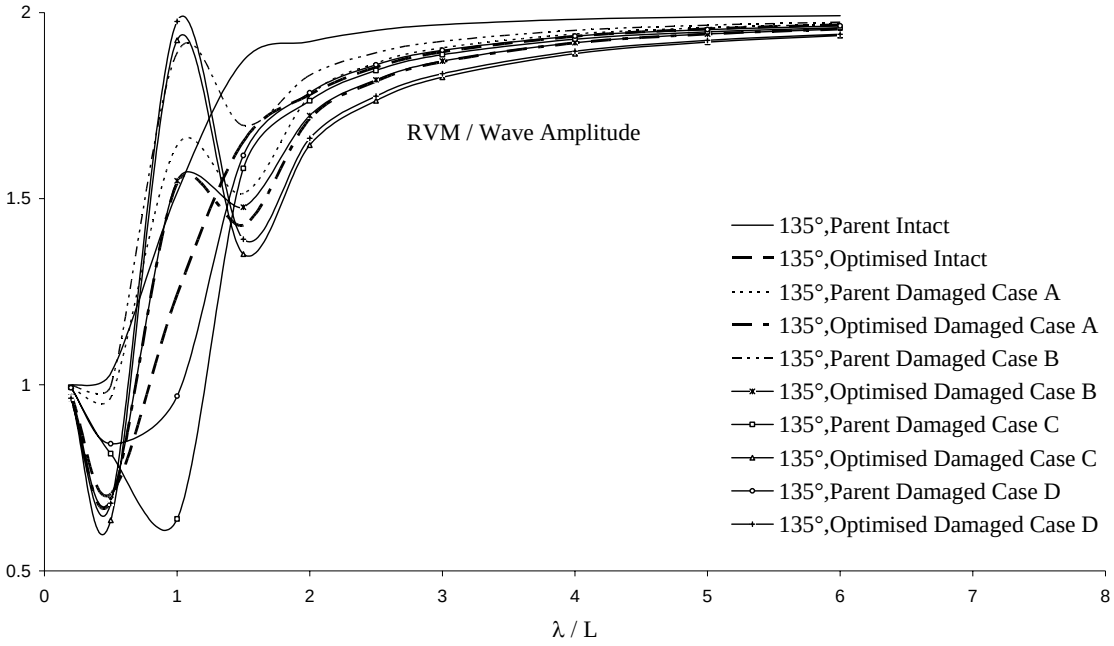

Figure J.15: Relative vertical motion responses for the intact and damaged hull forms for point B (in bow seas).

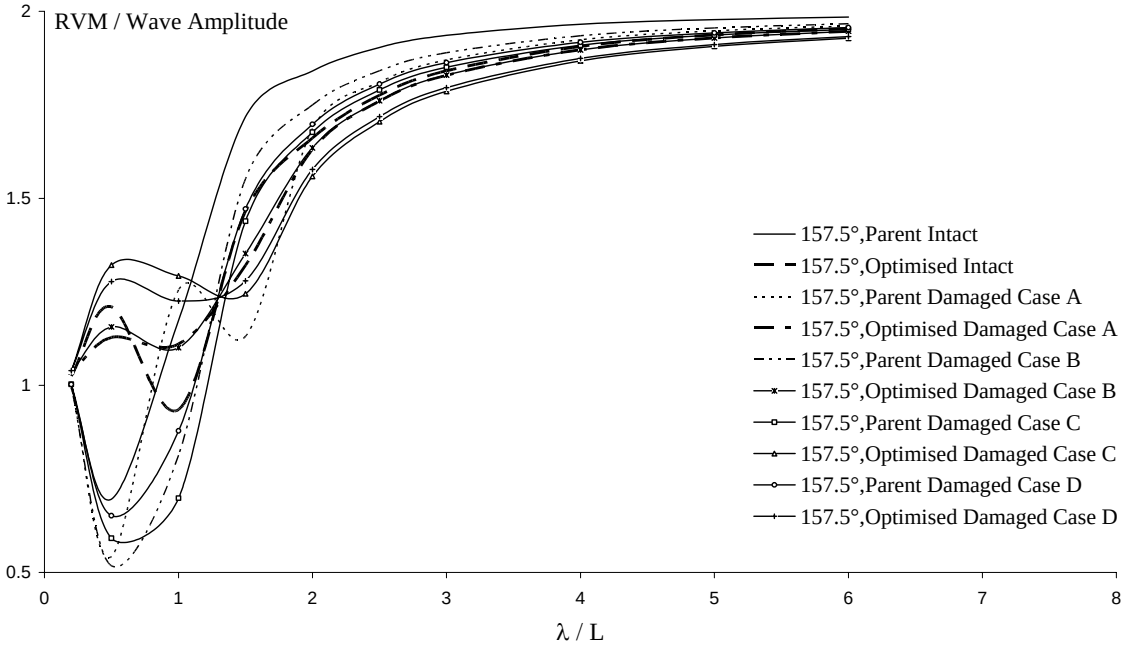

Figure J.16: Relative vertical motion responses for the intact and damaged hull forms for point B (in head seas).

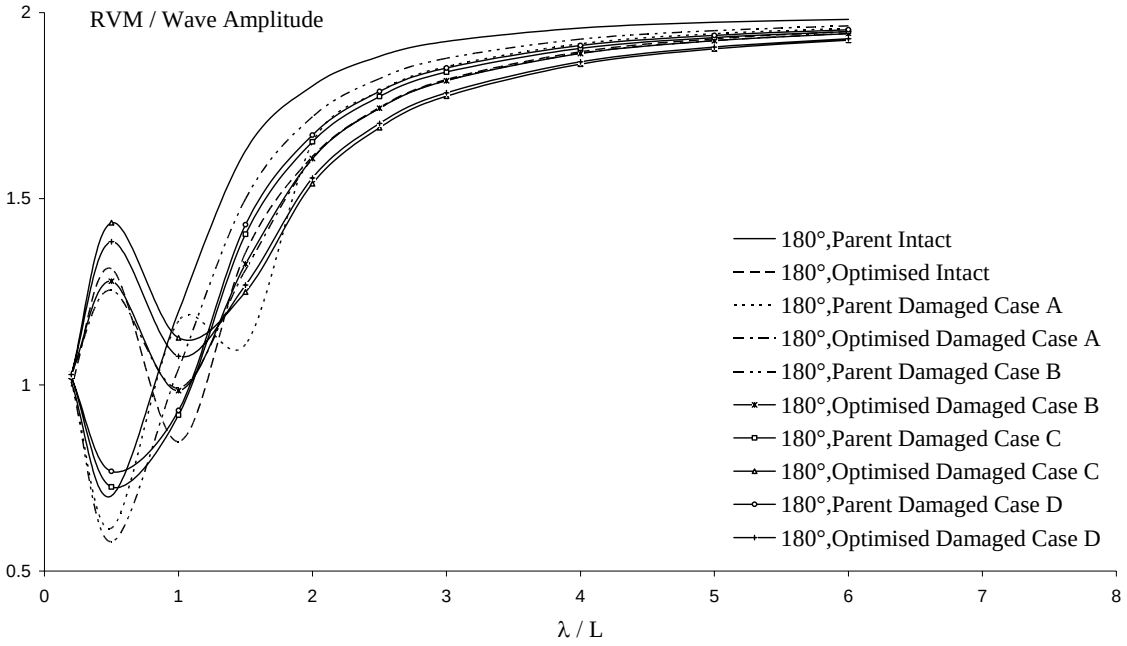

Figure J.17: Relative vertical motion responses for the intact and damaged hull forms for point B (in head seas).

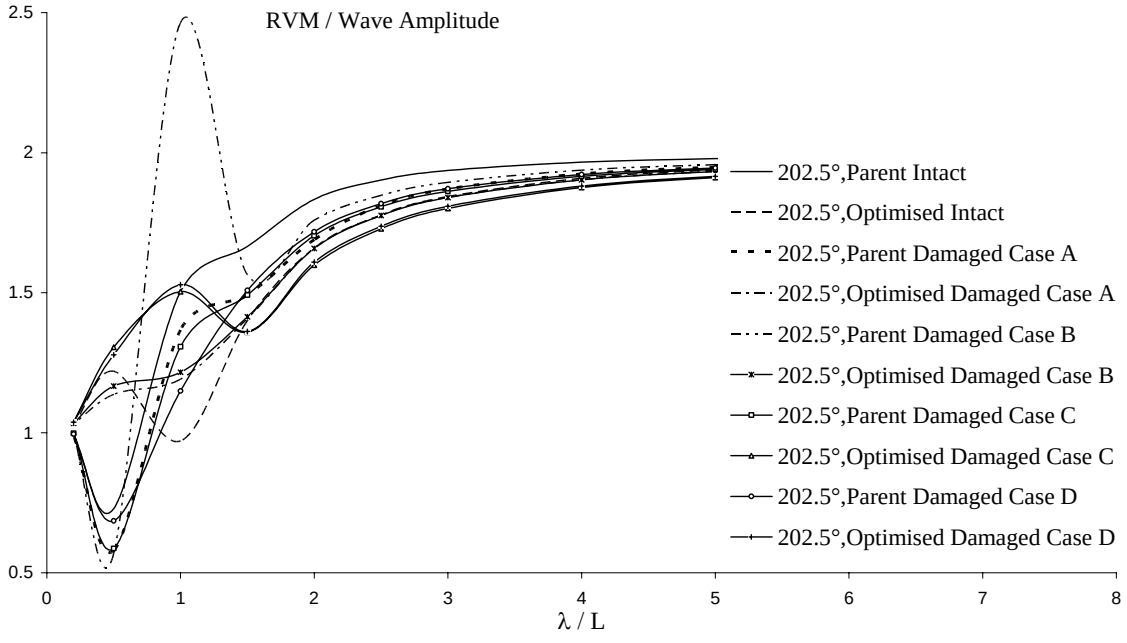

Figure J.18: Relative vertical motion responses for the intact and damaged hull forms for point B (in head seas).

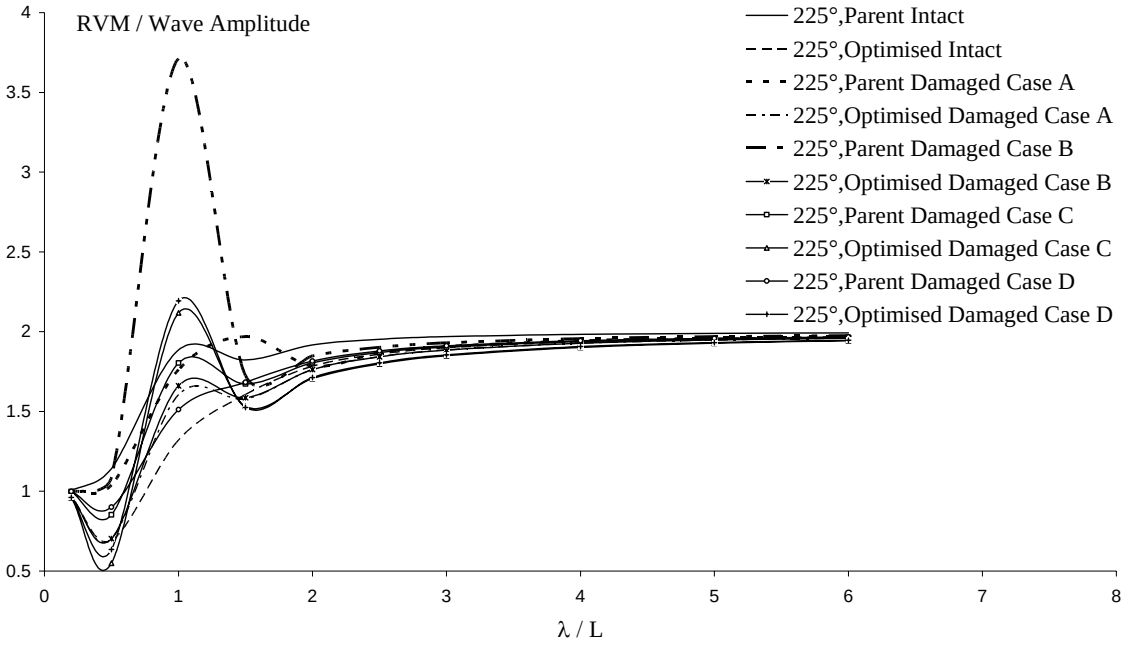

Figure J.19: Relative vertical motion responses for the intact and damaged hull forms for point B (in bow seas).

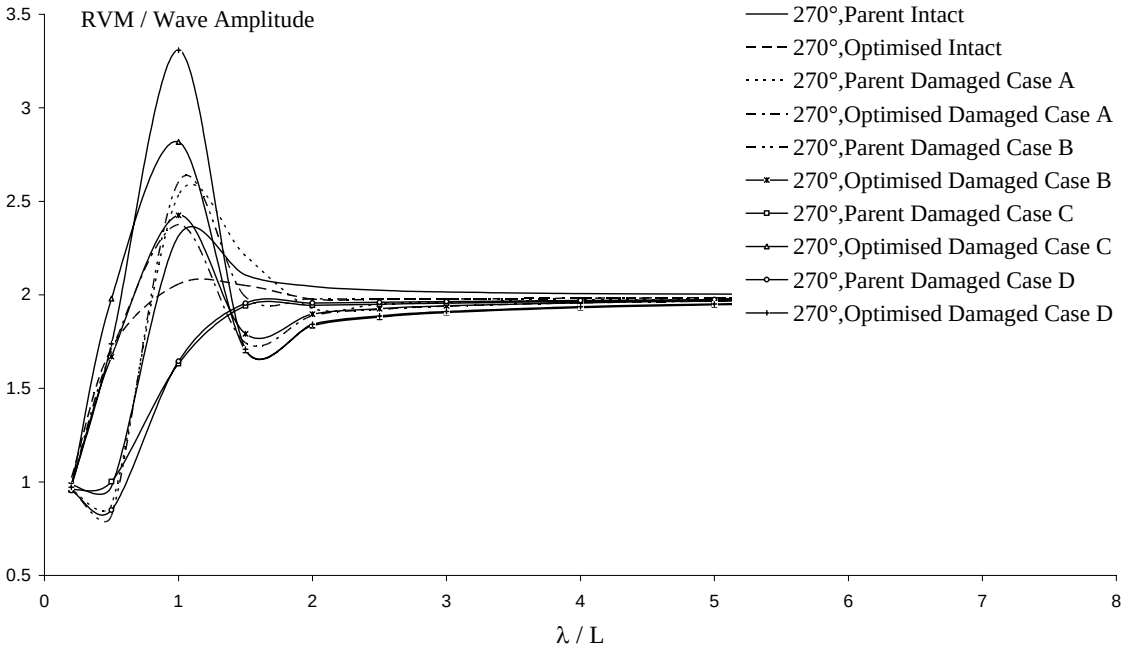

Figure J.20: Relative vertical motion responses for the intact and damaged hull forms for point B (in beam seas).

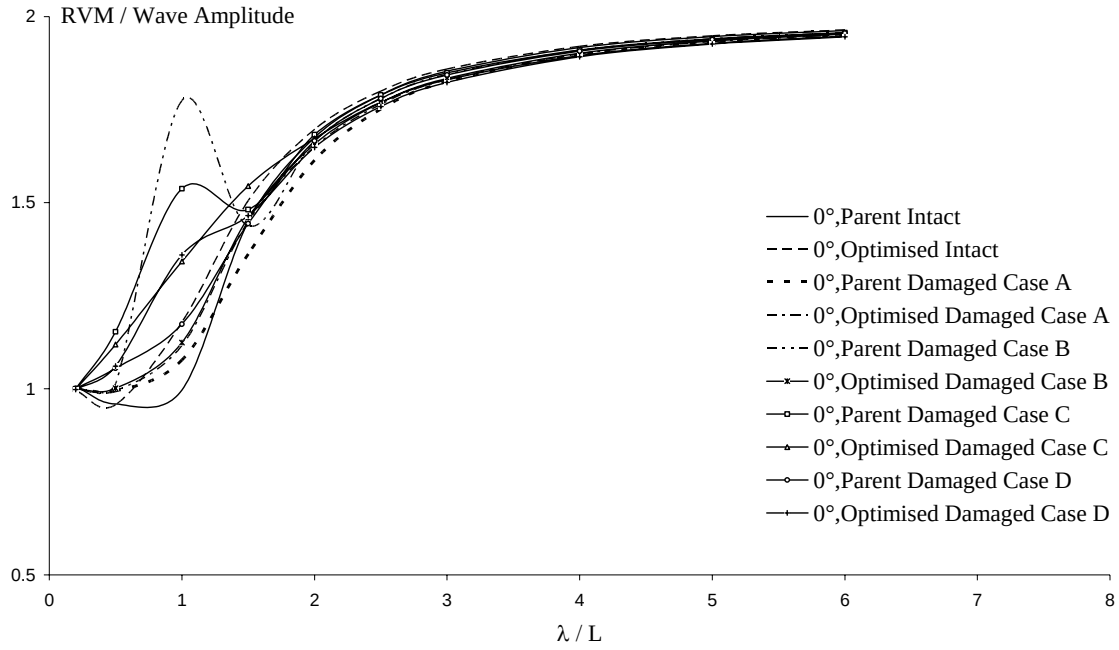

Figure J.21: Relative vertical motion responses for the intact and damaged hull forms for point C (in following seas).

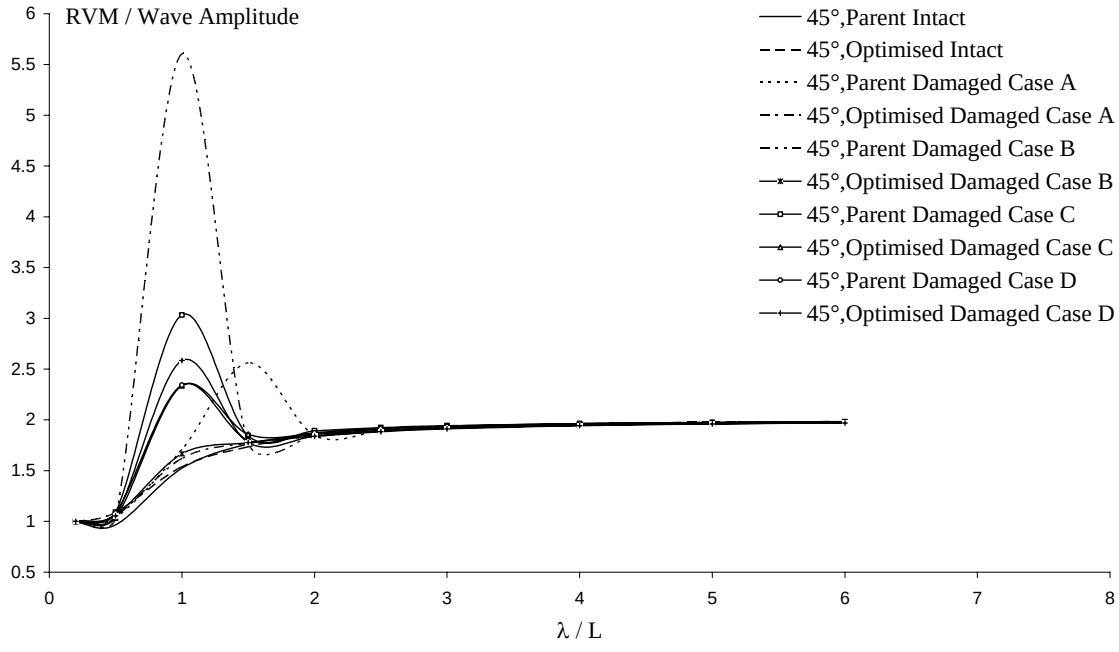

Figure J.22: Relative vertical motion responses for the intact and damaged hull forms for point C (in quartering seas).

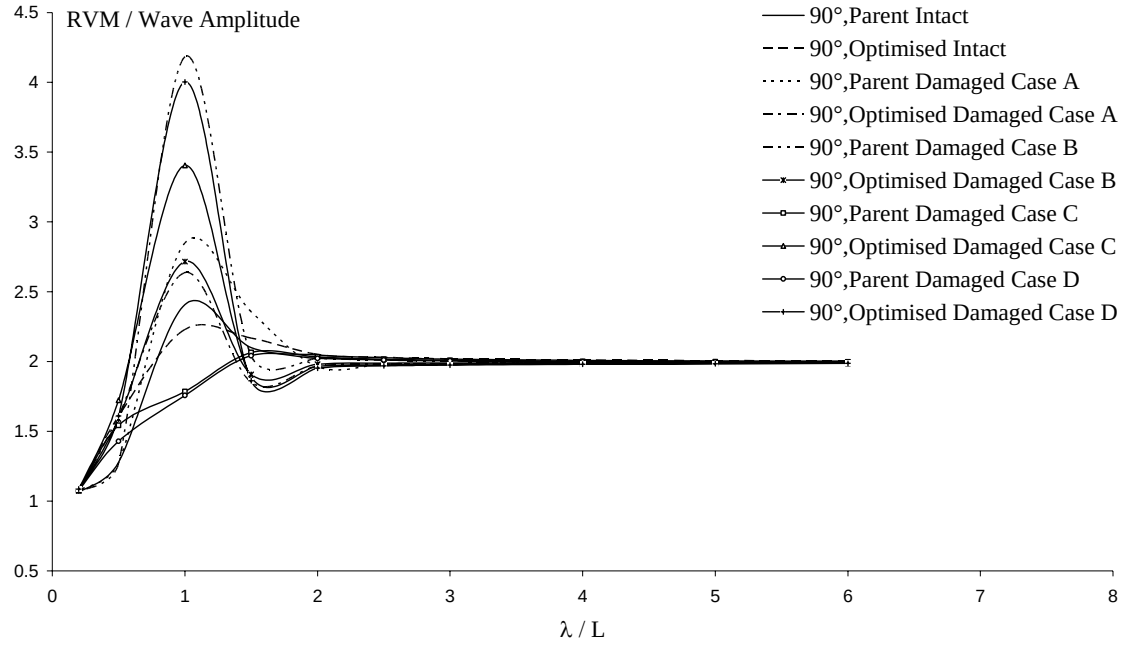

Figure J.23: Relative vertical motion responses for the intact and damaged hull forms for point C (in beam seas).

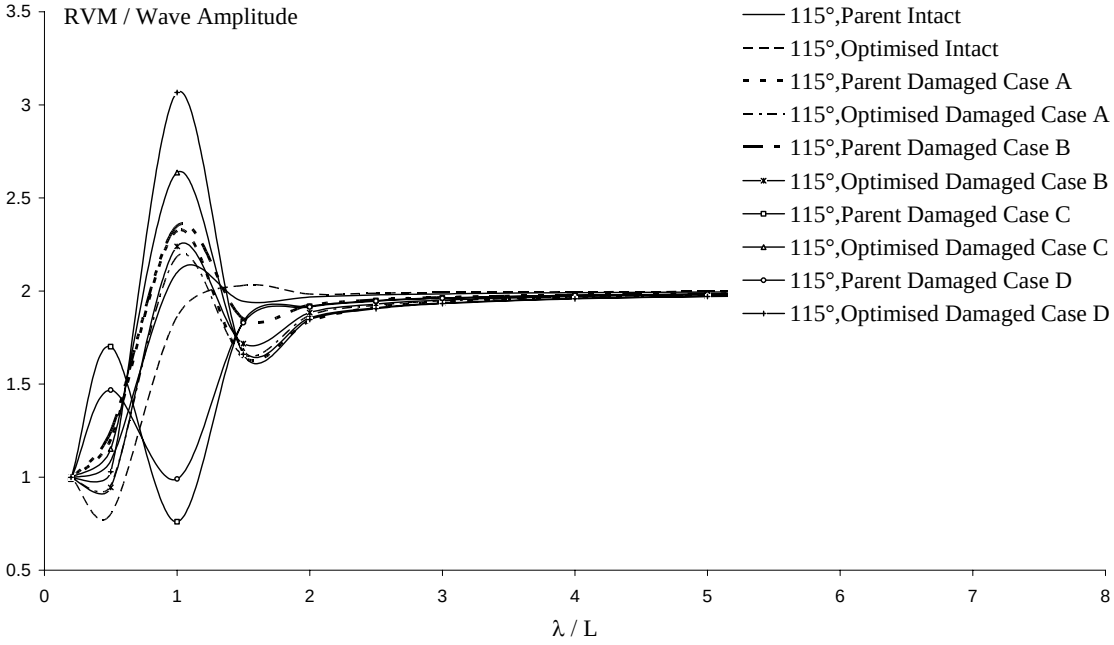

Figure J.24: Relative vertical motion responses for the intact and damaged hull forms for point C (in beam seas).

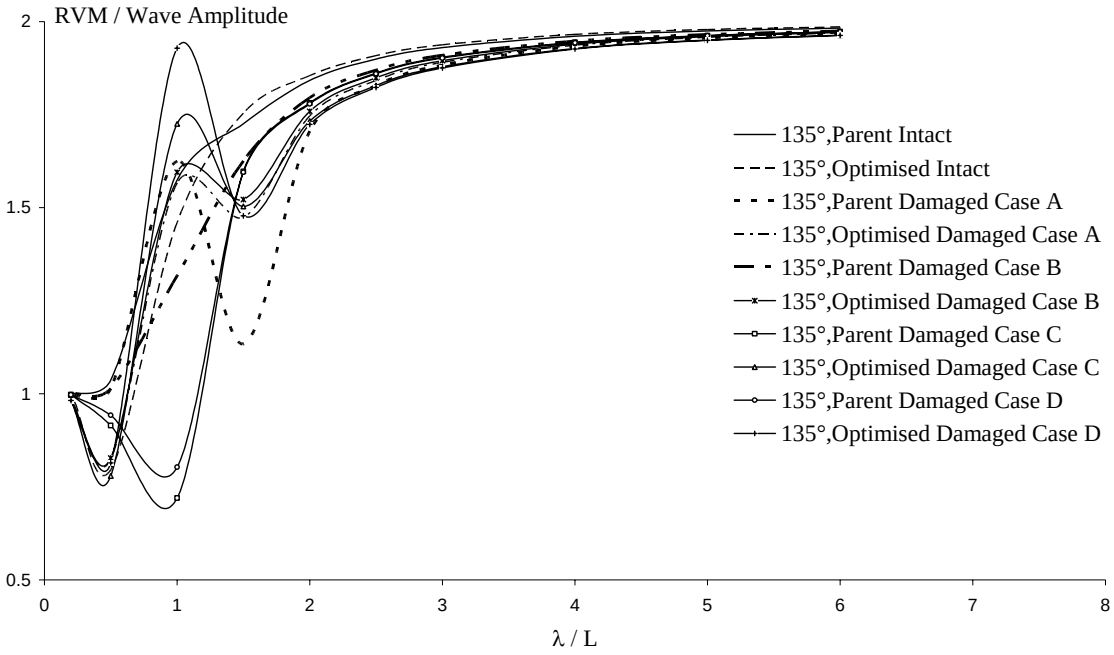

Figure J.25: Relative vertical motion responses for the intact and damaged hull forms for point C (in bow seas).

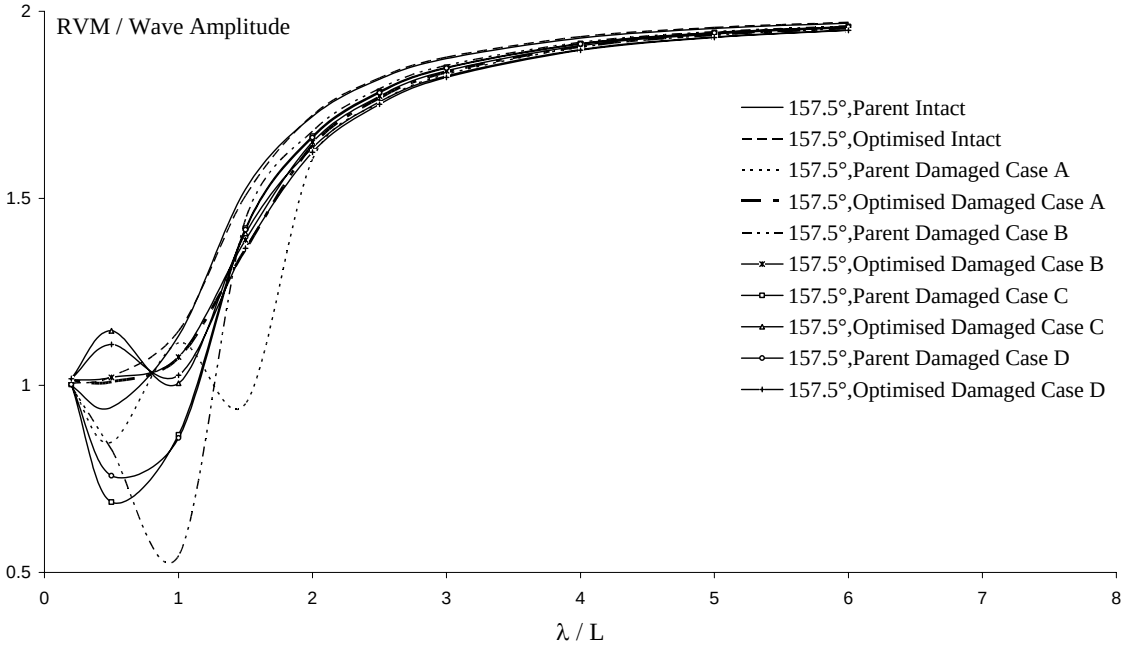

Figure J.26: Relative vertical motion responses for the intact and damaged hull forms for point C (in head seas).

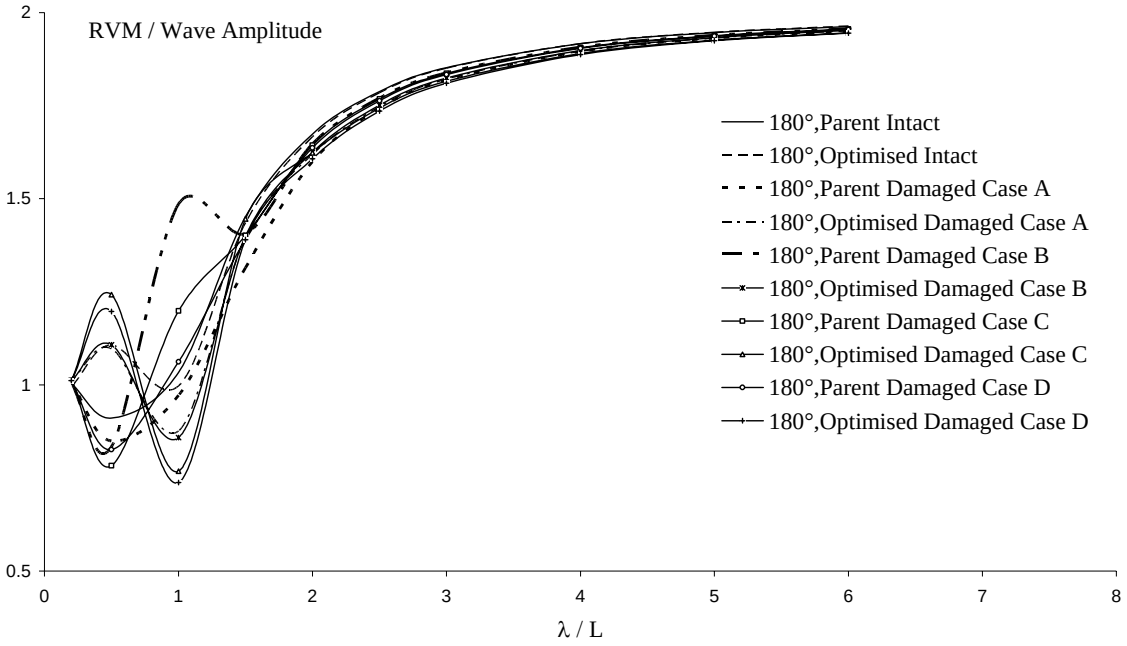

Figure J.27: Relative vertical motion responses for the intact and damaged hull forms for point C (in head seas).

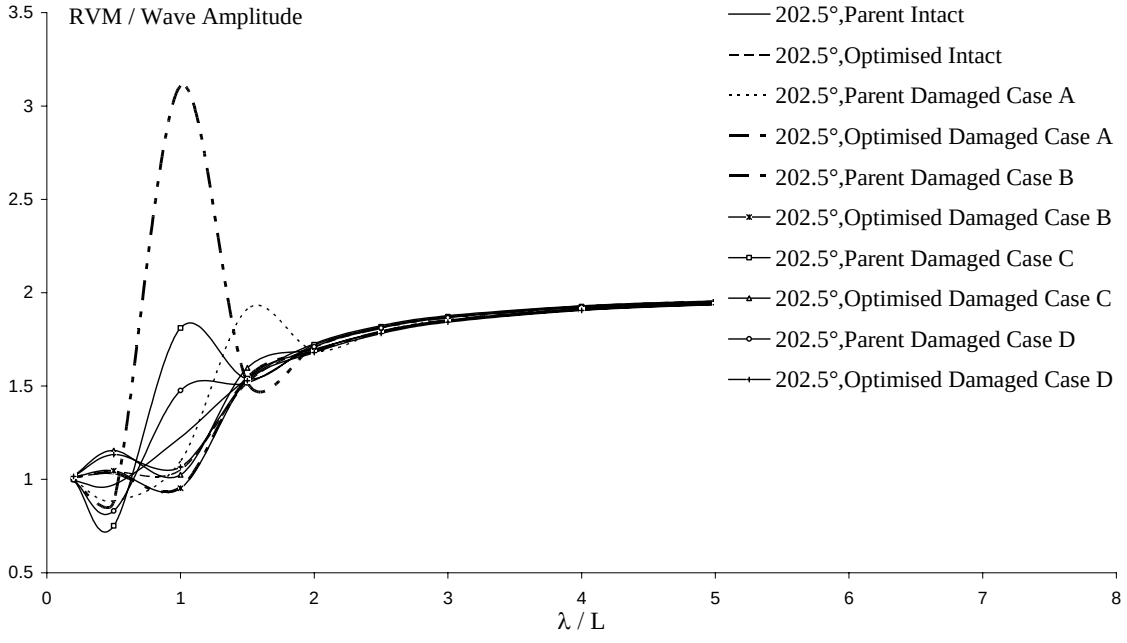

Figure J.28: Relative vertical motion responses for the intact and damaged hull forms for point C (in head seas).

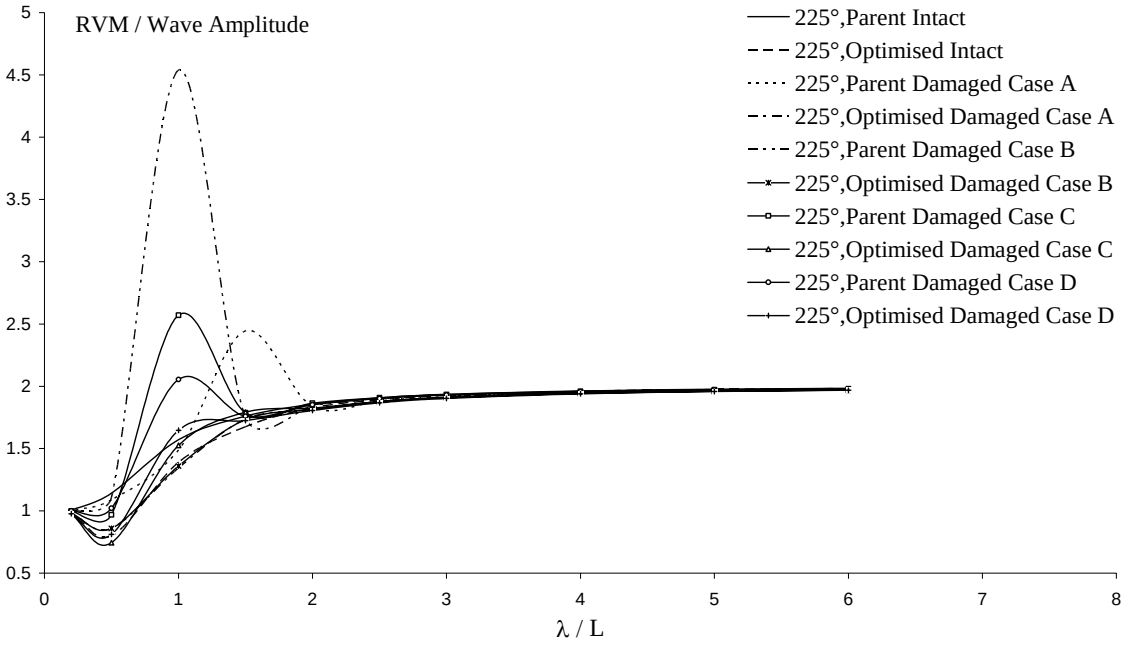

Figure J.29: Relative vertical motion responses for the intact and damaged hull forms for point C (in bow seas).

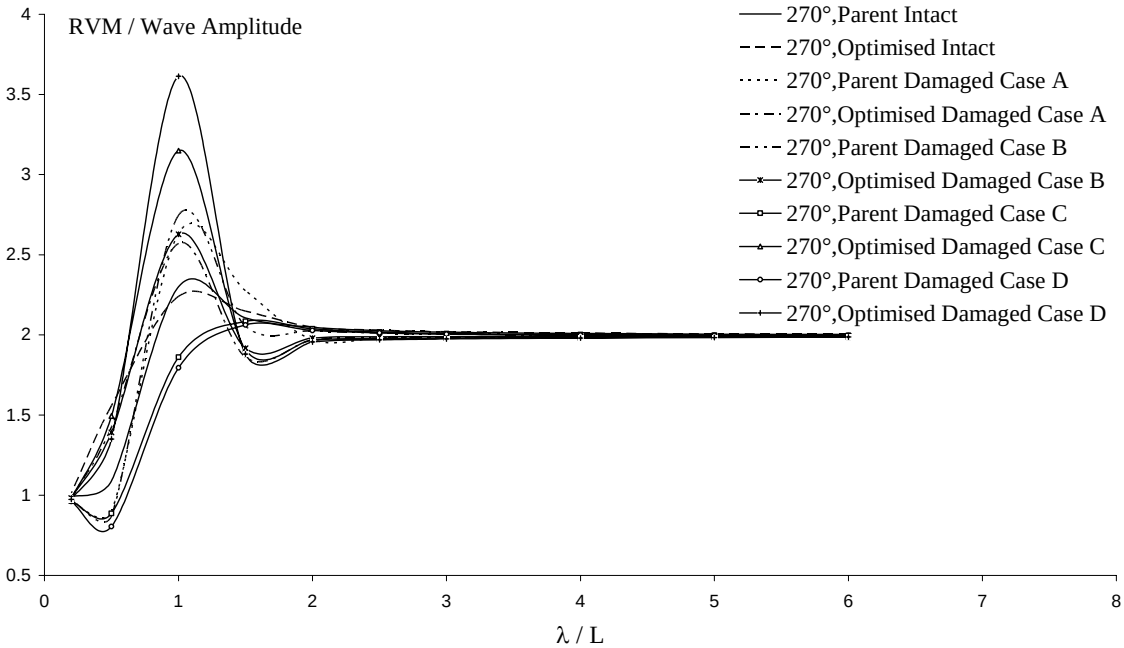

Figure J.30: Relative vertical motion responses for the intact and damaged hull forms for point C (in beam seas).

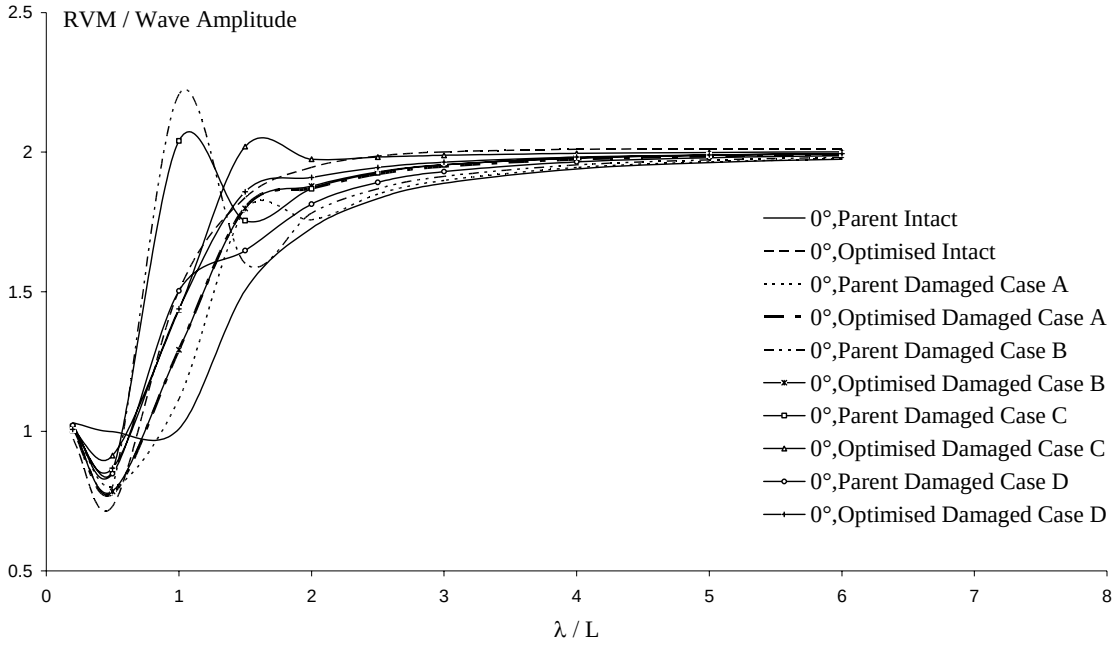

Figure J.31: Relative vertical motion responses for the intact and damaged hull forms for point D (in following seas).

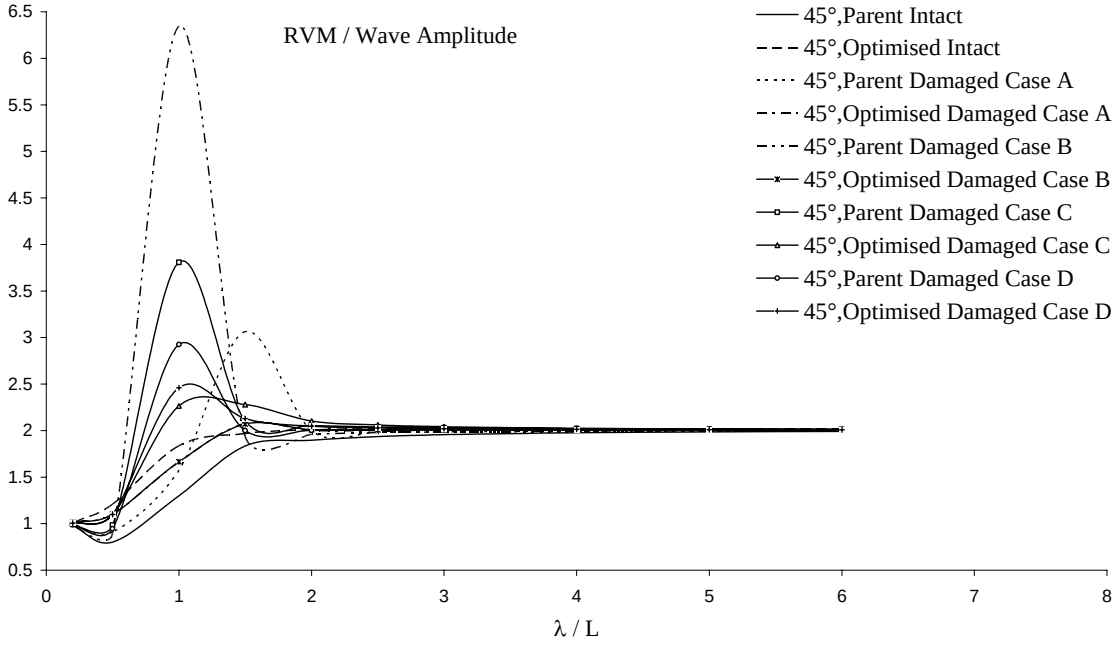

Figure J.32: Relative vertical motion responses for the intact and damaged hull forms for point D (in quartering seas).

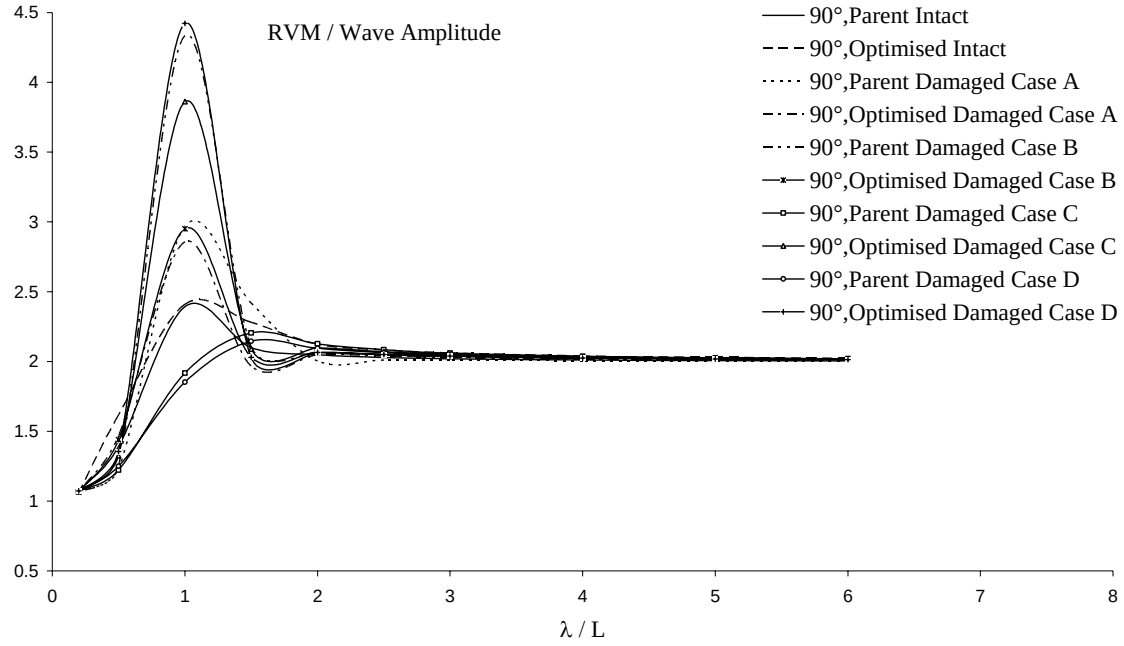

Figure J.33: Relative vertical motion responses for the intact and damaged hull forms for point D (in beam seas).

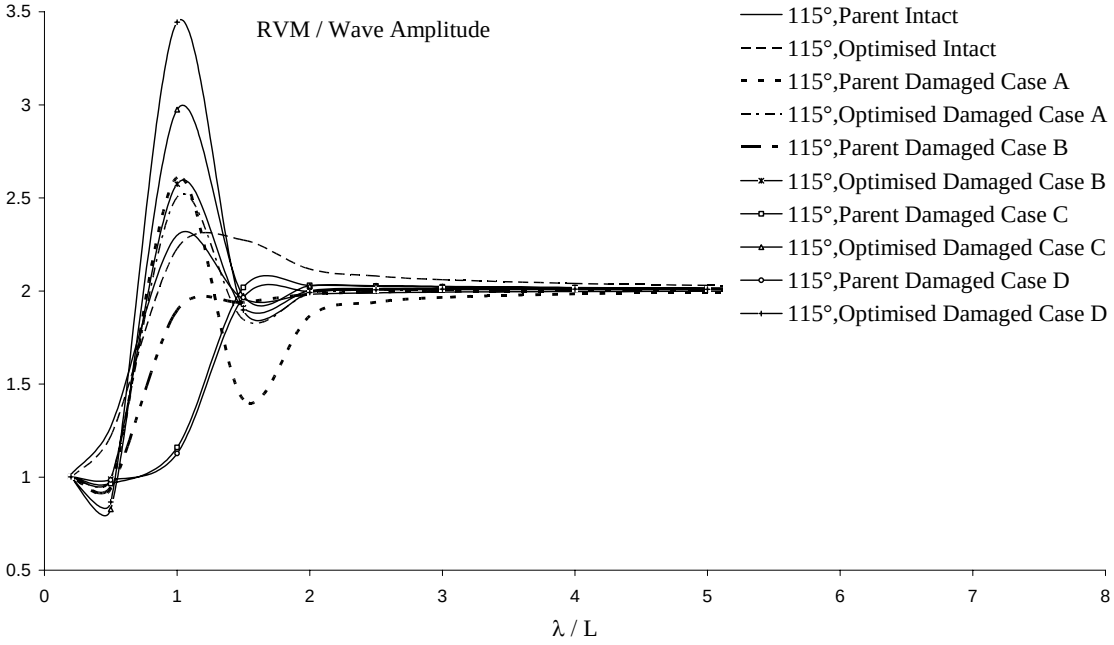

Figure J.34: Relative vertical motion responses for the intact and damaged hull forms for point D (in beam seas).

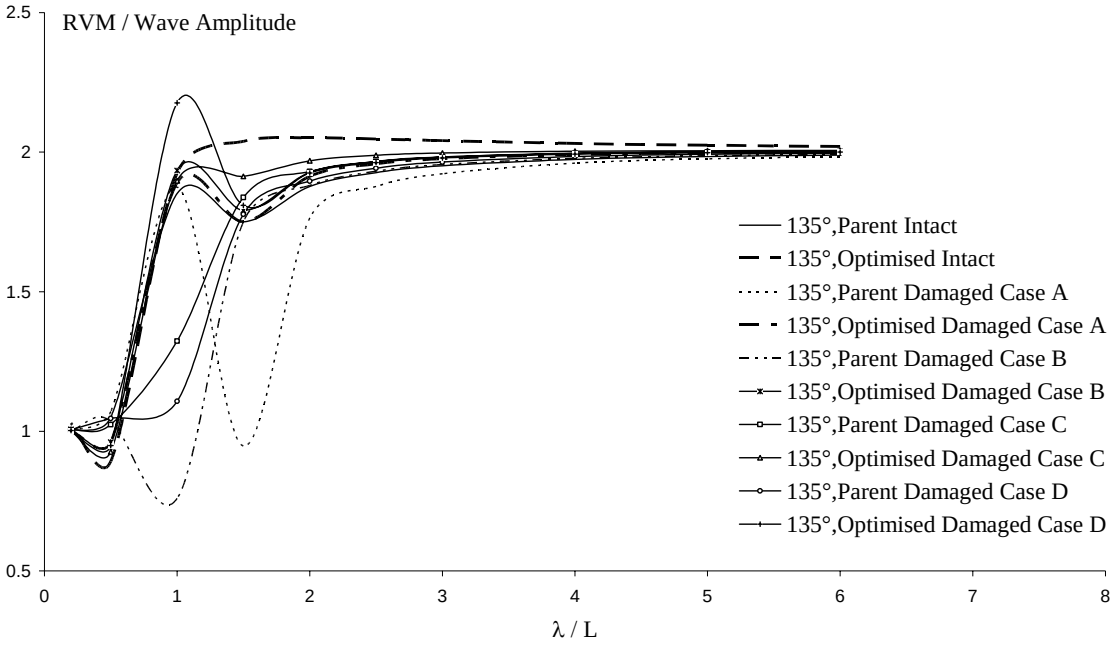

Figure J.35: Relative vertical motion responses for the intact and damaged hull forms for point D (in bow seas).

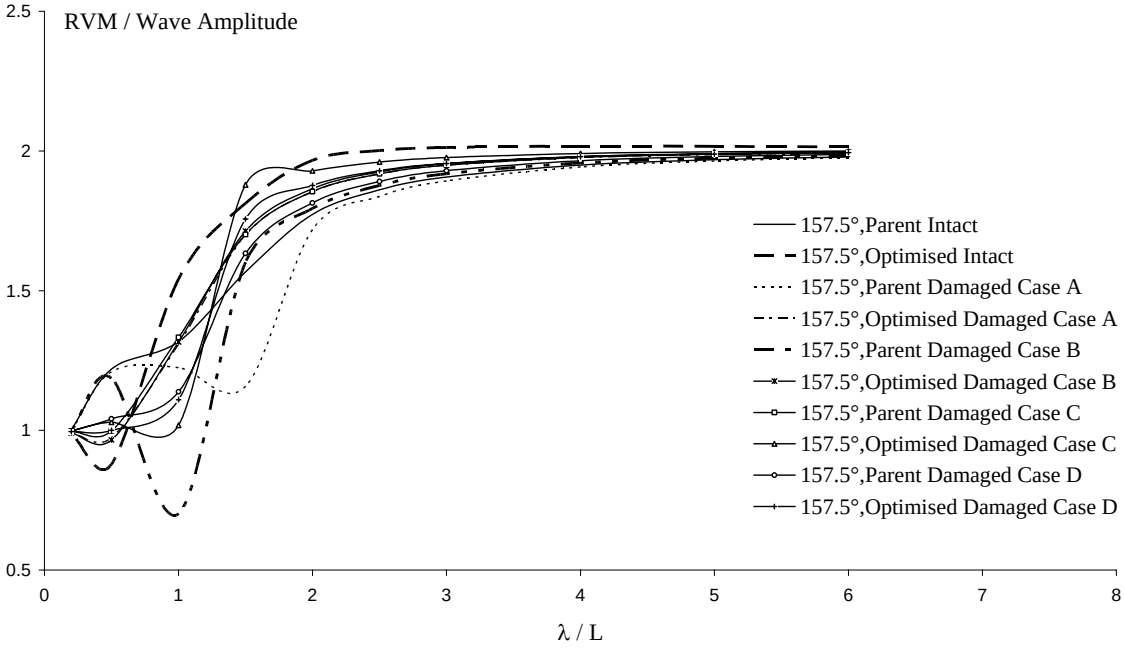

Figure J.36: Relative vertical motion responses for the intact and damaged hull forms for point D (in head seas).

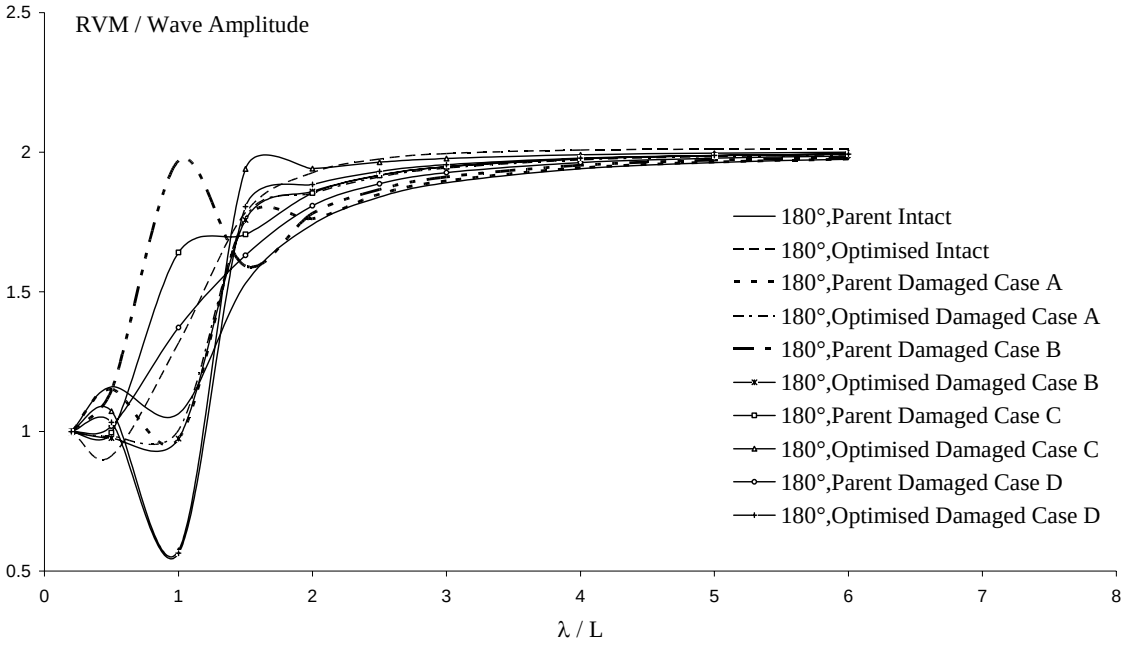

Figure J.37: Relative vertical motion responses for the intact and damaged hull forms for point D (in head seas).

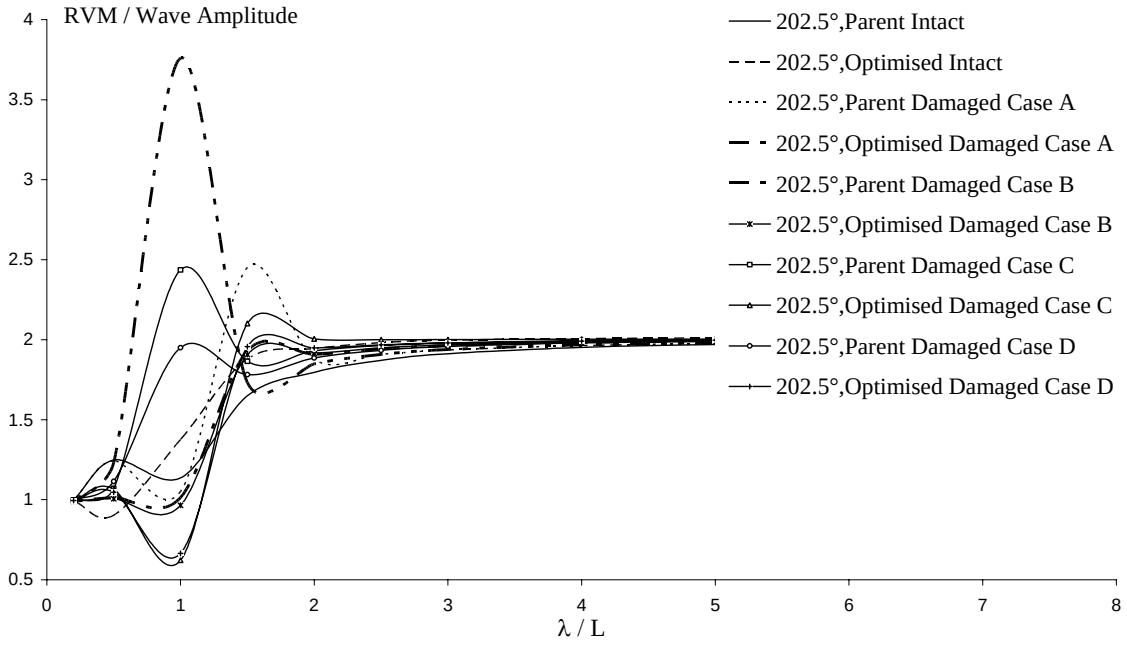

Figure J.38: Relative vertical motion responses for the intact and damaged hull forms for point D (in head seas).

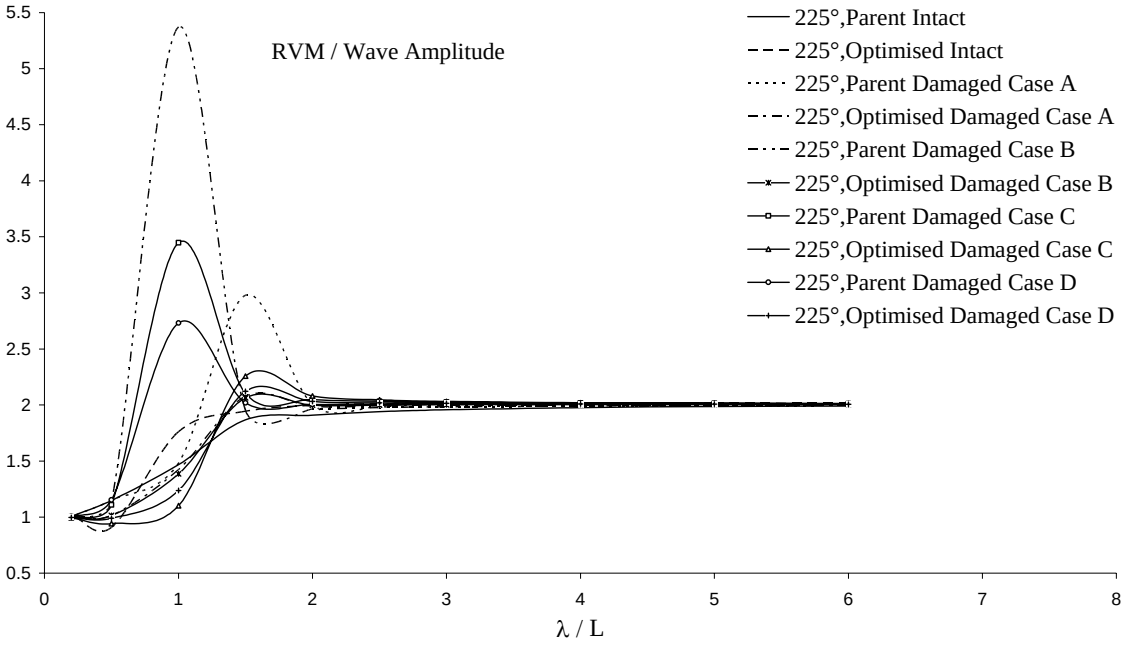

Figure J.39: Relative vertical motion responses for the intact and damaged hull forms for point D (in bow seas).

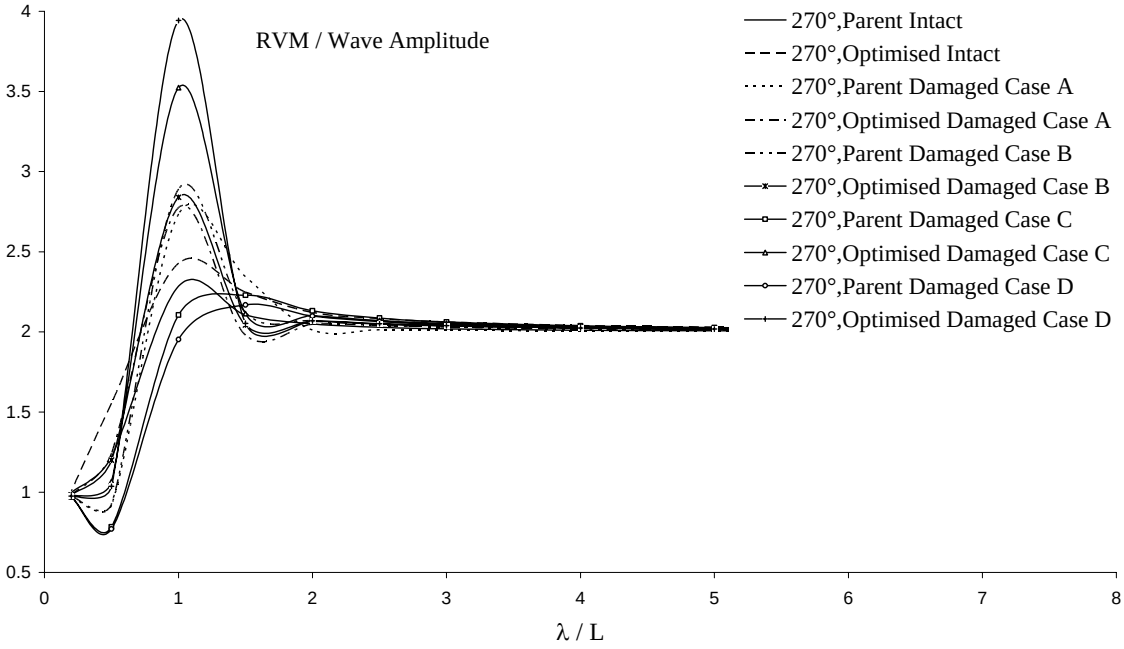

Figure J.40: Relative vertical motion responses for the intact and damaged hull forms for point D (in beam seas).

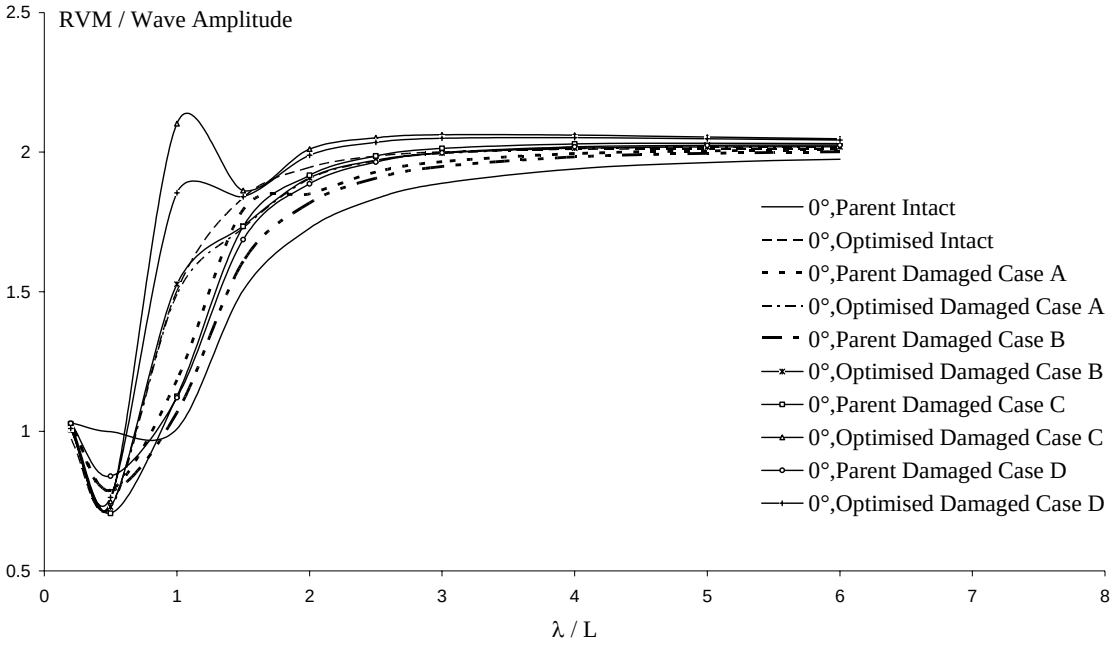

Figure J.41: Relative vertical motion responses for the intact and damaged hull forms for point E (in following seas).

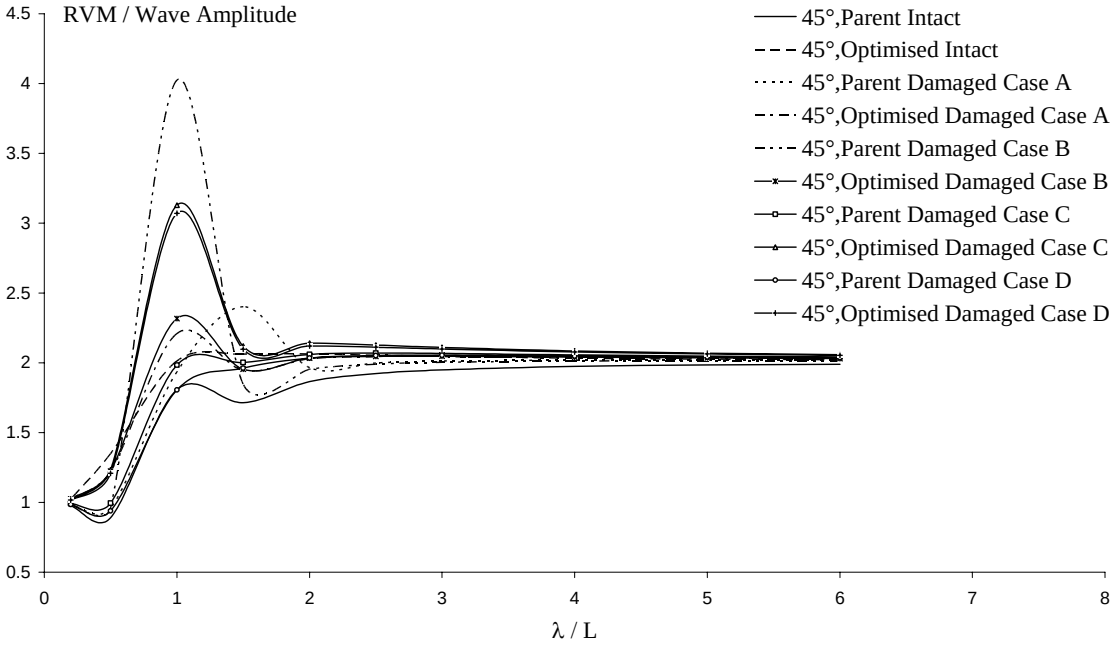

Figure J.42: Relative vertical motion responses for the intact and damaged hull forms for point E (in quartering seas).

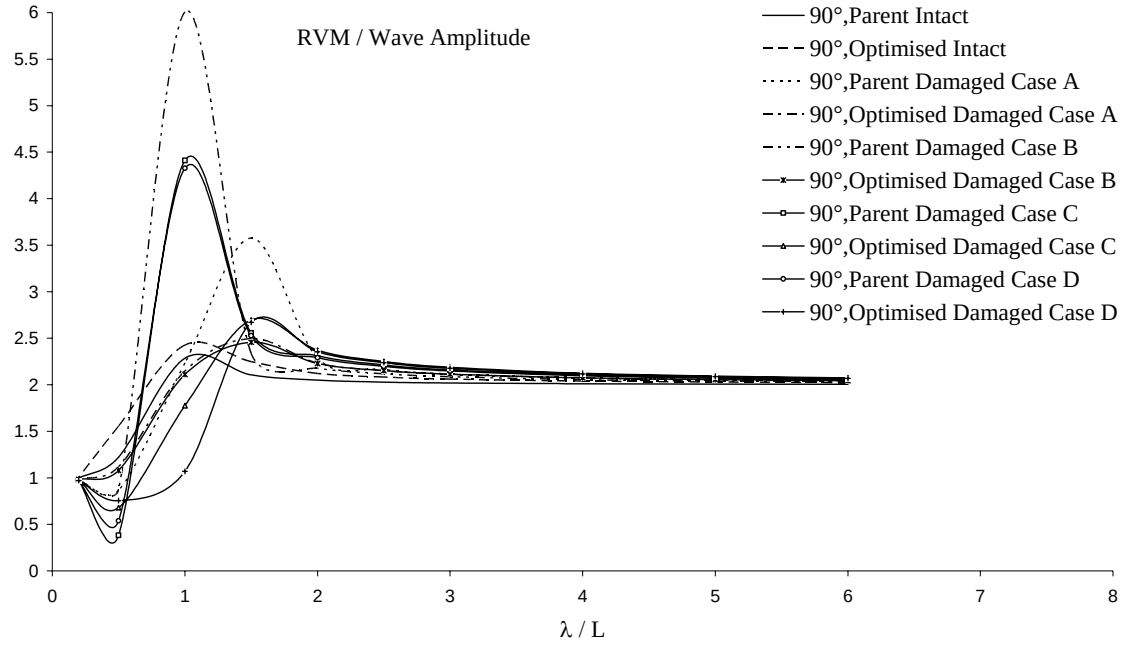

Figure J.43: Relative vertical motion responses for the intact and damaged hull forms for point E (in beam seas).

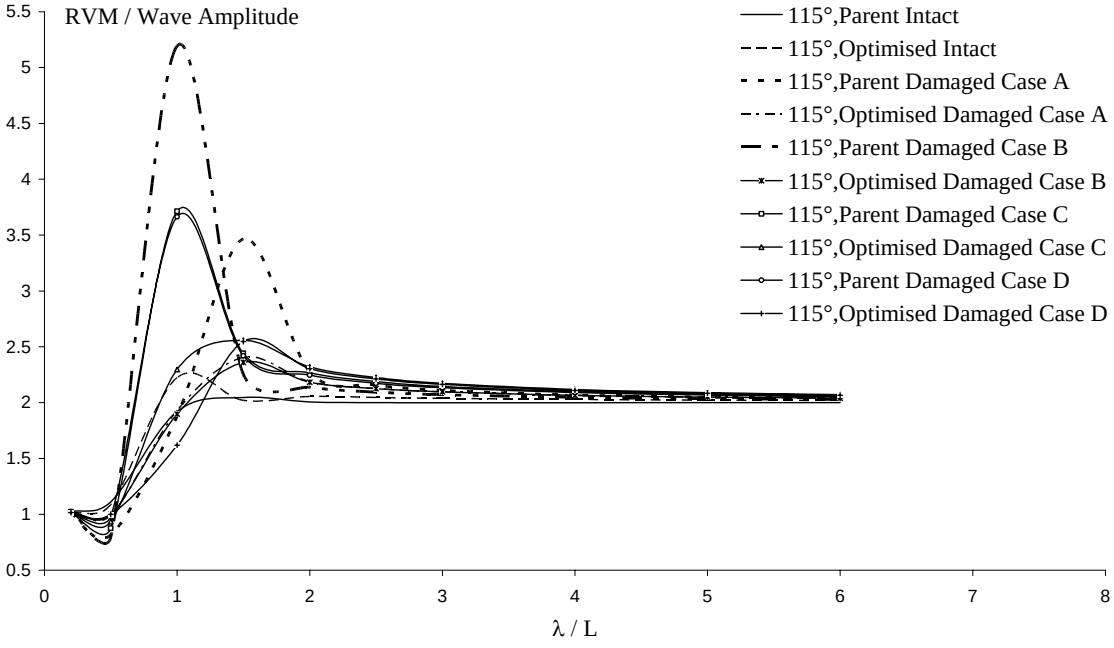

Figure J.44: Relative vertical motion responses for the intact and damaged hull forms for point E (in beam seas).

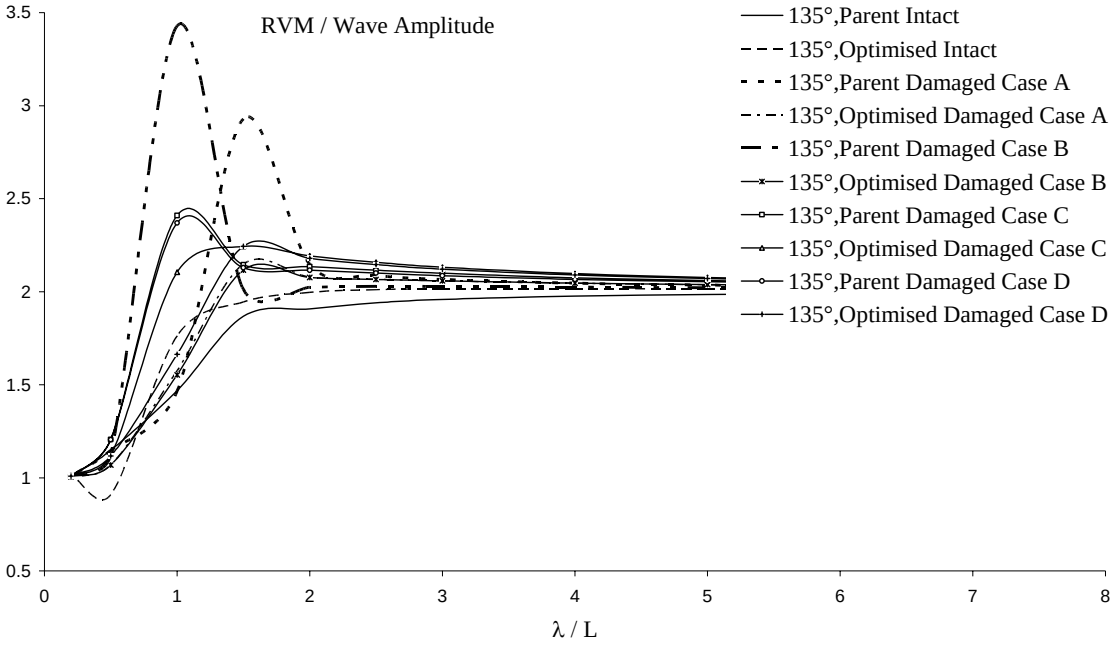

Figure J.45: Relative vertical motion responses for the intact and damaged hull forms for point E (in bow seas).

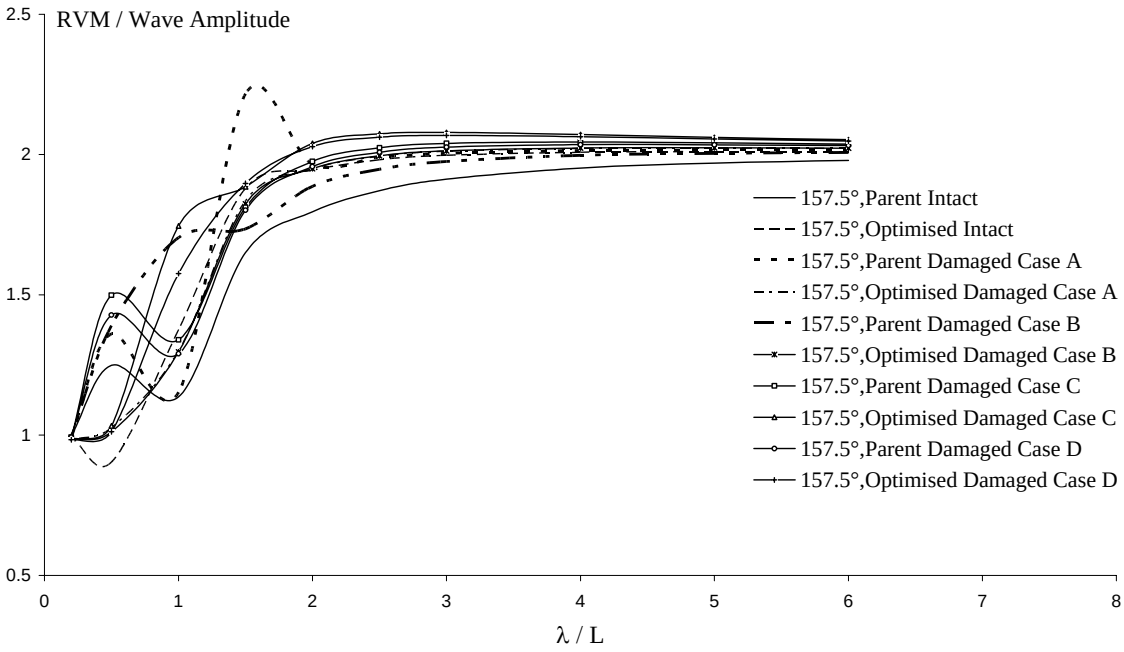

Figure J.46: Relative vertical motion responses for the intact and damaged hull forms for point E (in head seas).

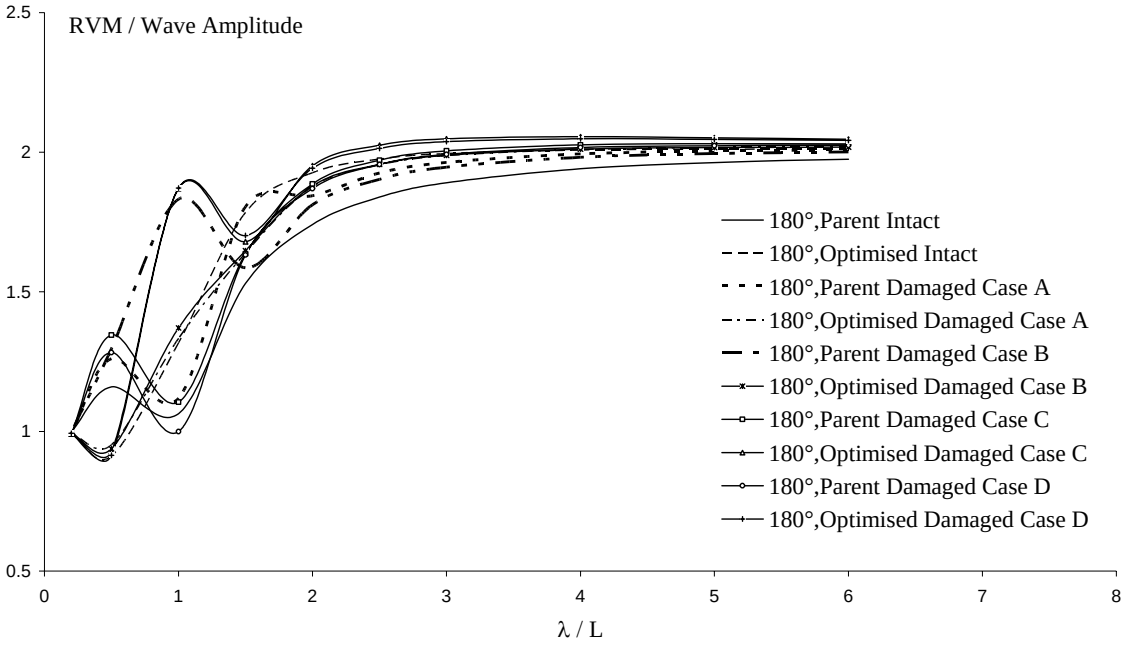

Figure J.47: Relative vertical motion responses for the intact and damaged hull forms for point E (in head seas).

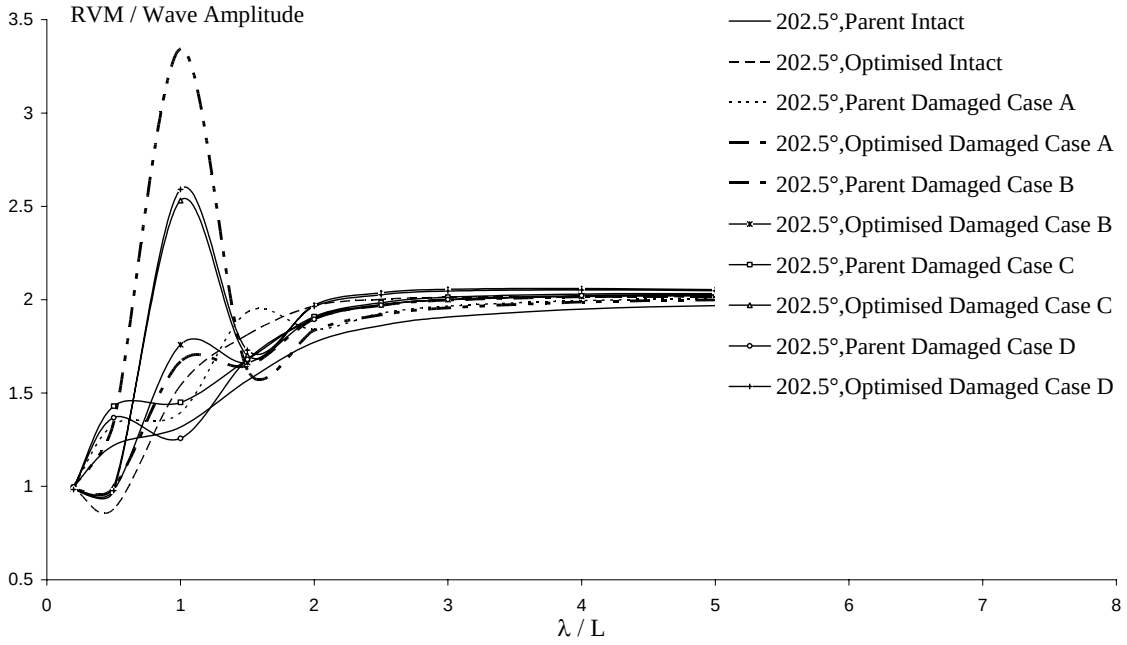

Figure J.48: Relative vertical motion responses for the intact and damaged hull forms for point E (in head seas).

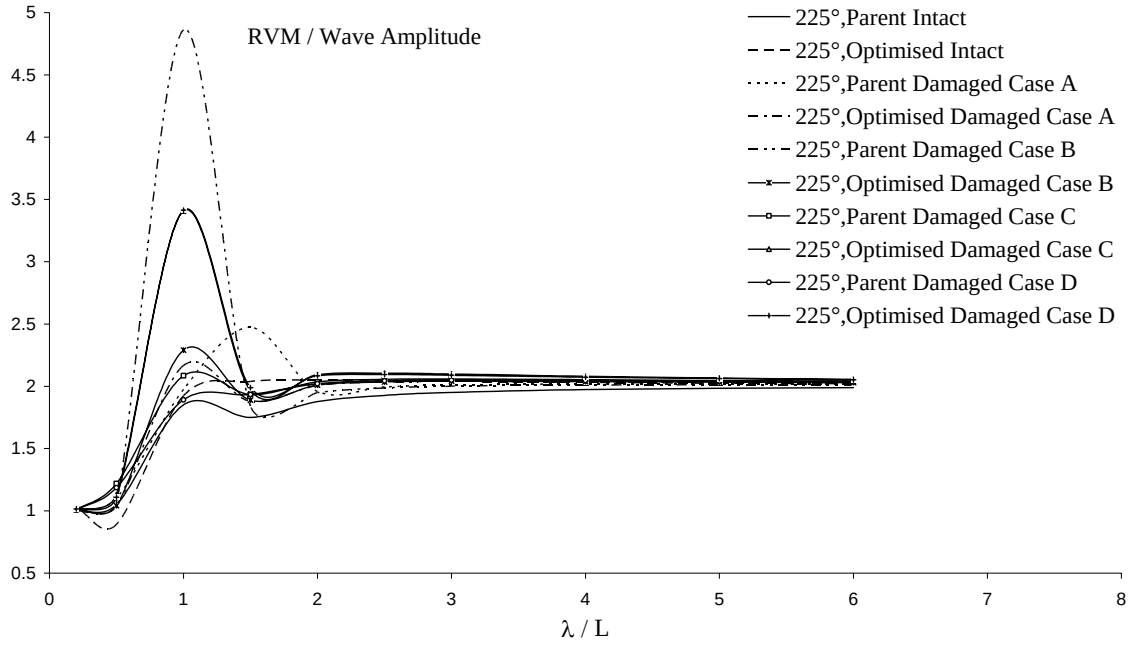

Figure J.49: Relative vertical motion responses for the intact and damaged hull forms for point E (in bow seas).

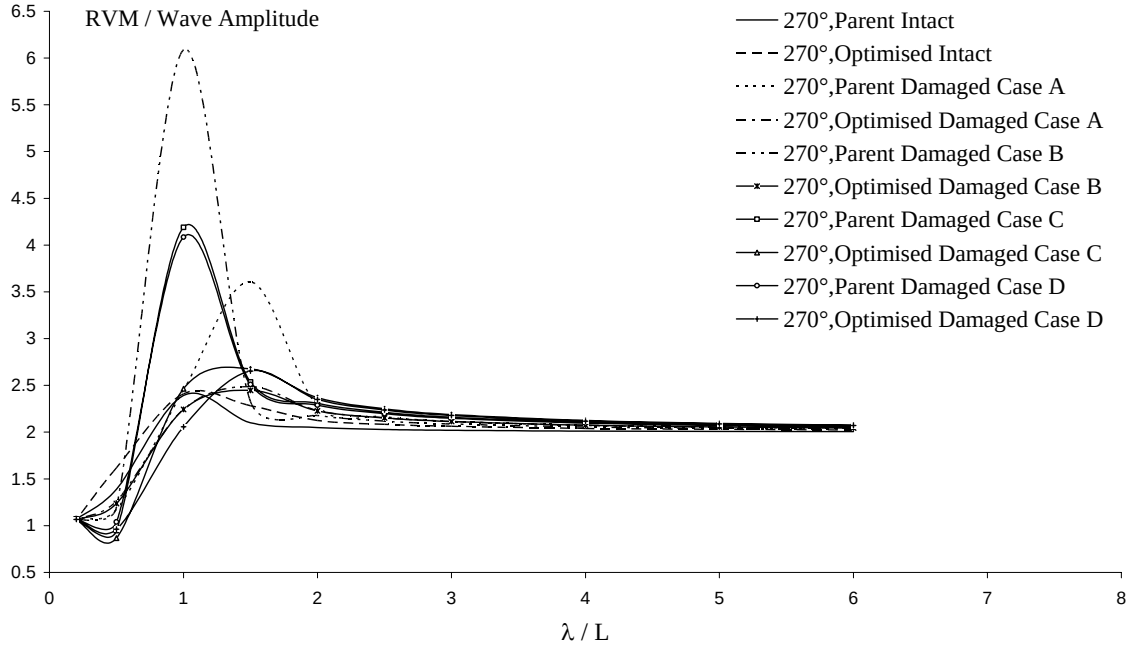

Figure J.50: Relative vertical motion responses for the intact and damaged hull forms for point E (in beam seas).

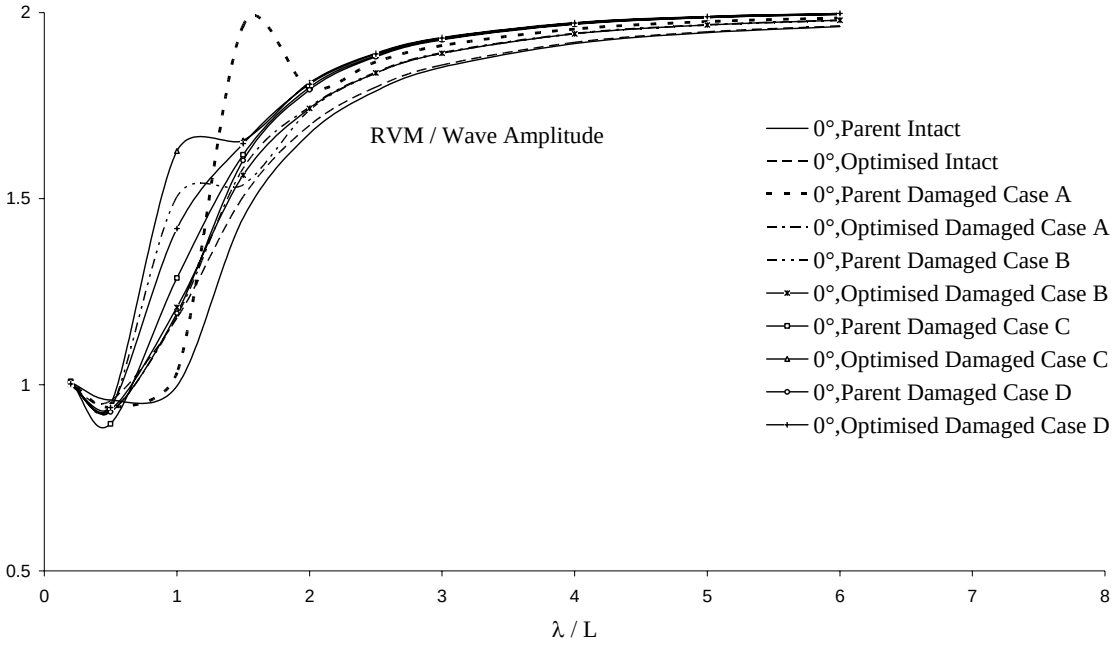

Figure J.51: Relative vertical motion responses for the intact and damaged hull forms for point F (in following seas).

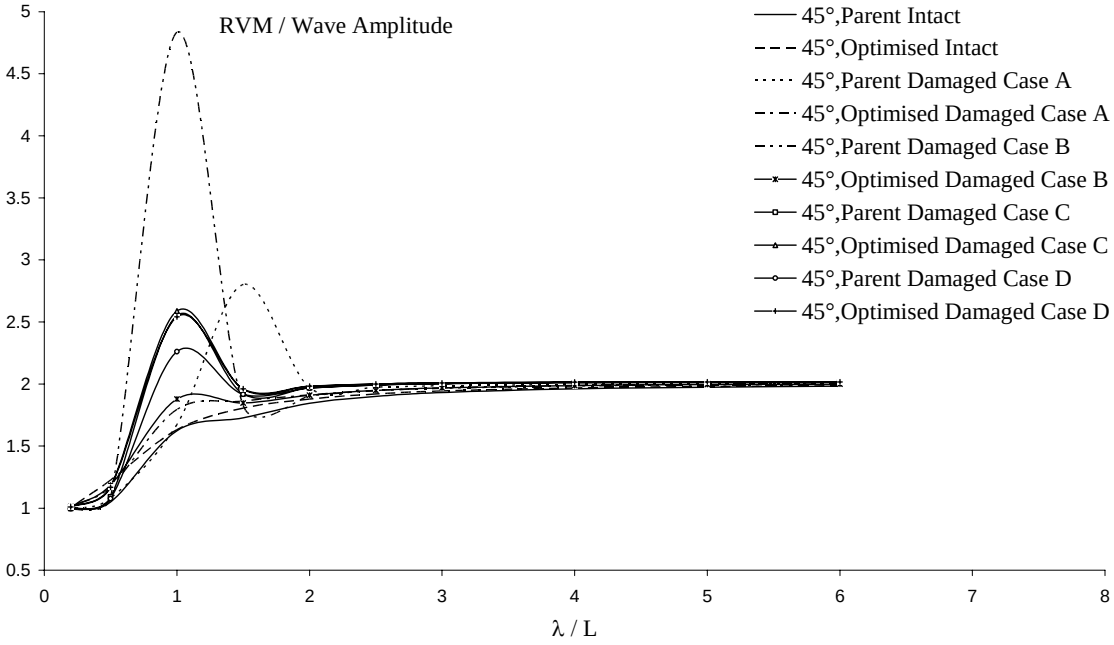

Figure J.52: Relative vertical motion responses for the intact and damaged hull forms for point F (in quartering seas).

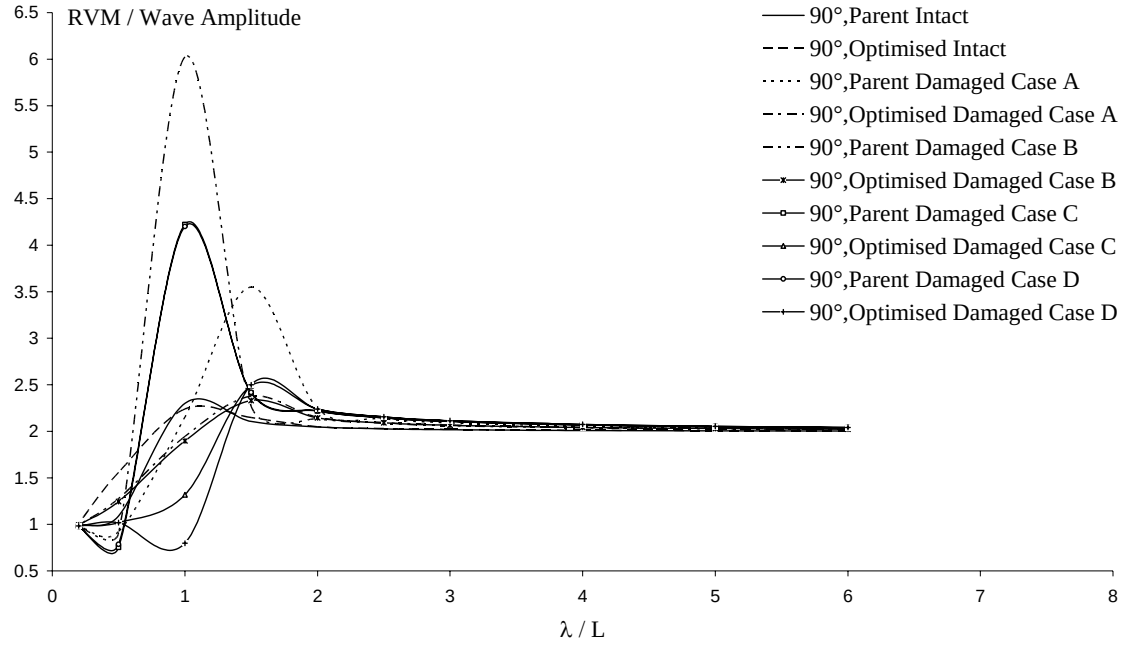

Figure J.53: Relative vertical motion responses for the intact and damaged hull forms for point F (in beam seas).

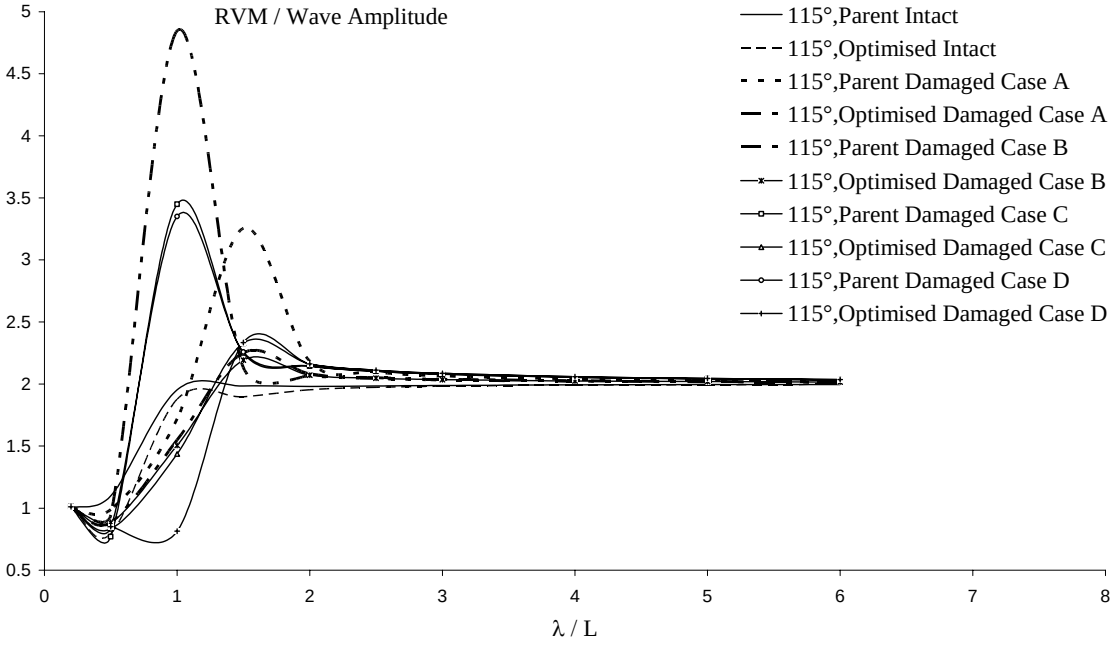

Figure J.54: Relative vertical motion responses for the intact and damaged hull forms for point F (in beam seas).

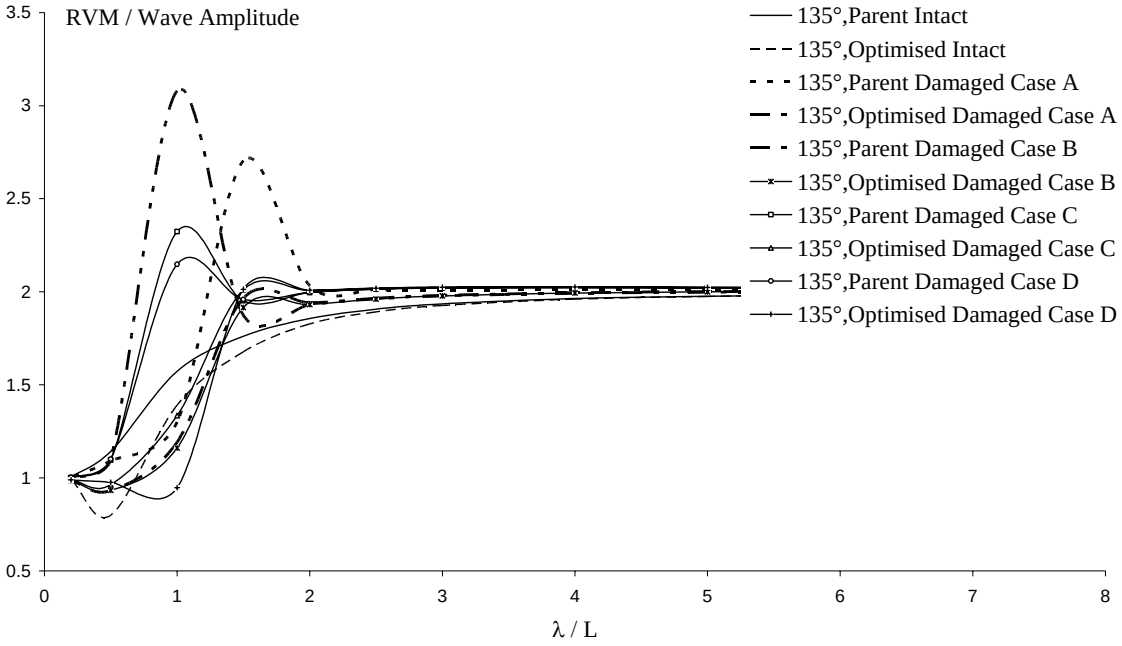

Figure J.55: Relative vertical motion responses for the intact and damaged hull forms for point F (in bow seas).

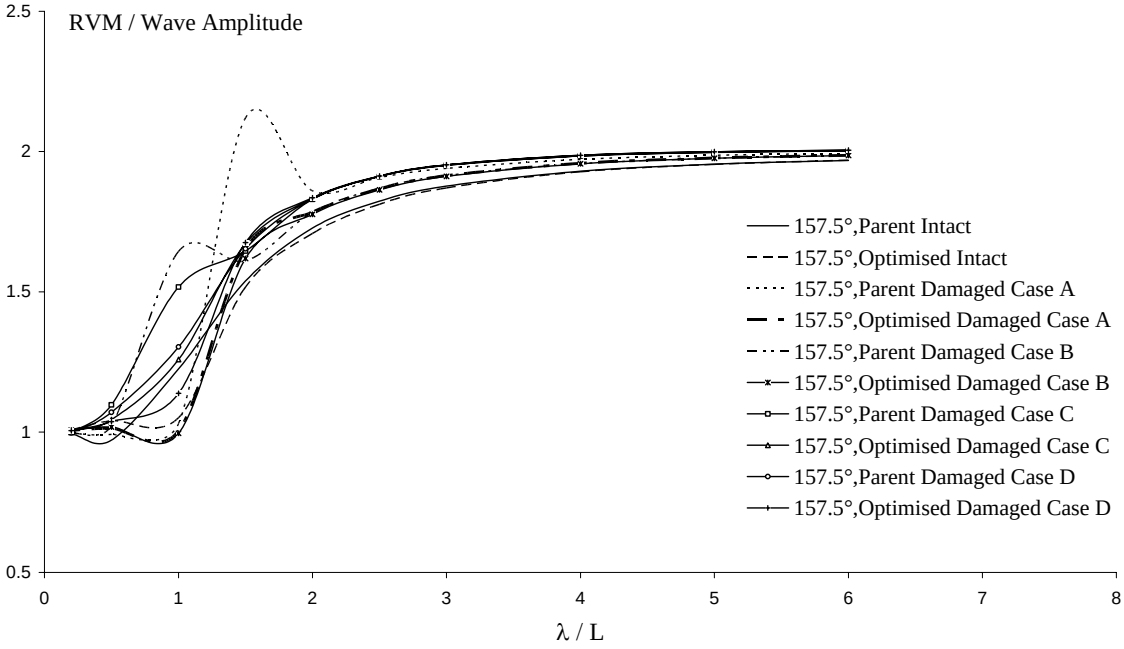

Figure J.56: Relative vertical motion responses for the intact and damaged hull forms for point F (in head seas).

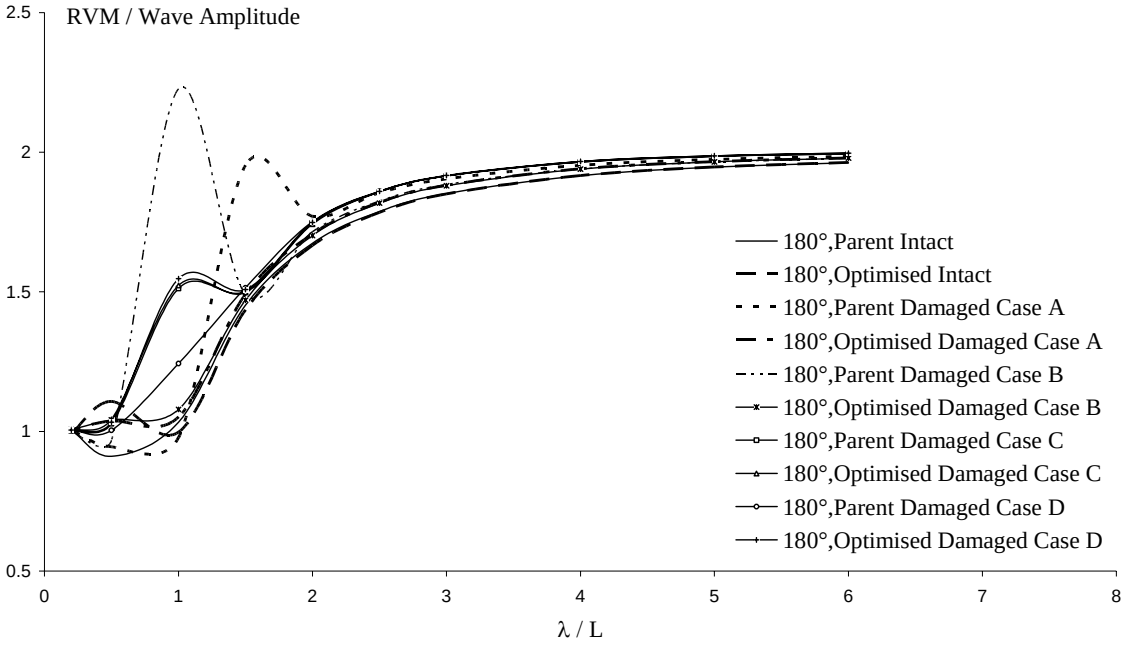

Figure J.57: Relative vertical motion responses for the intact and damaged hull forms for point F (in head seas).

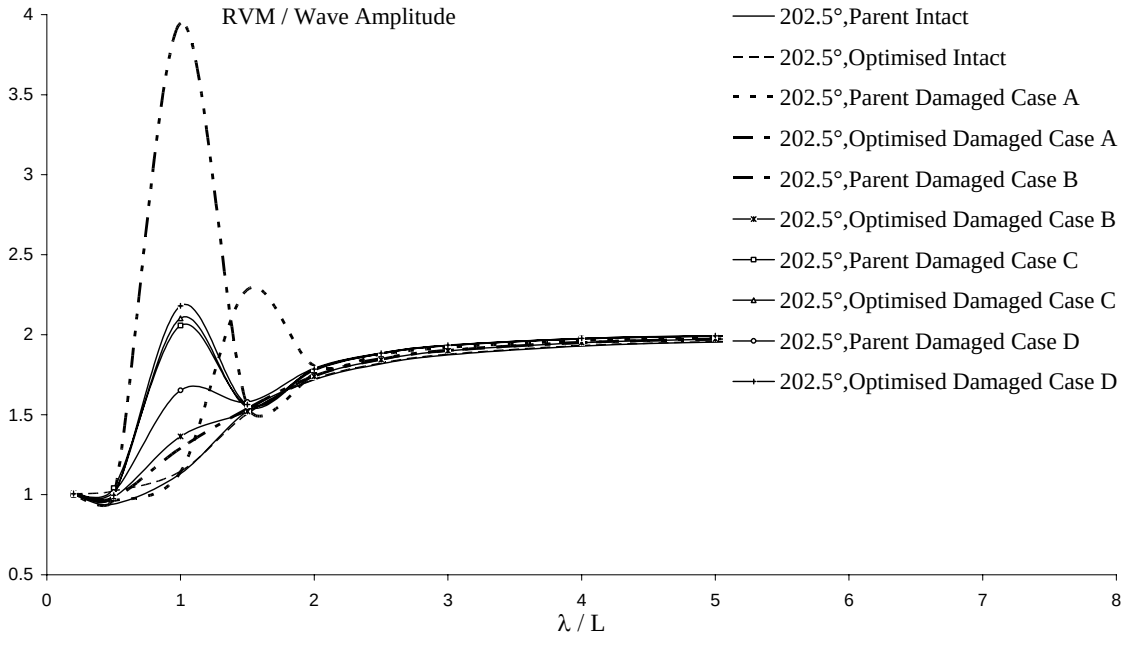

Figure J.58: Relative vertical motion responses for the intact and damaged hull forms for point F (in head seas).

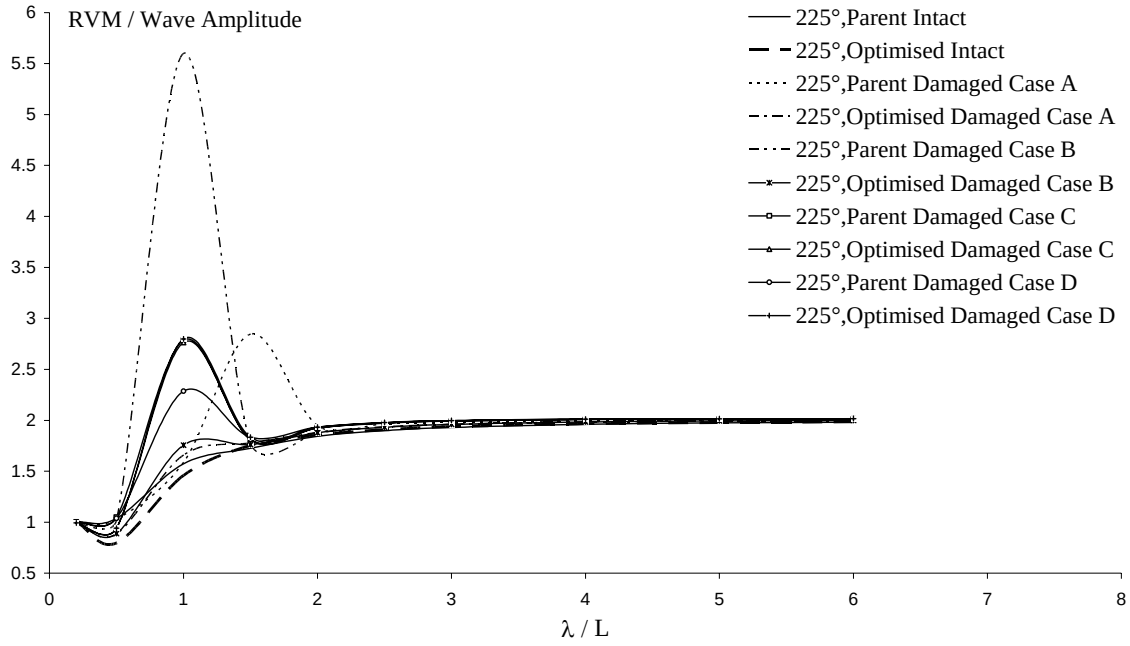

Figure J.59: Relative vertical motion responses for the intact and damaged hull forms for point F (in bow seas).

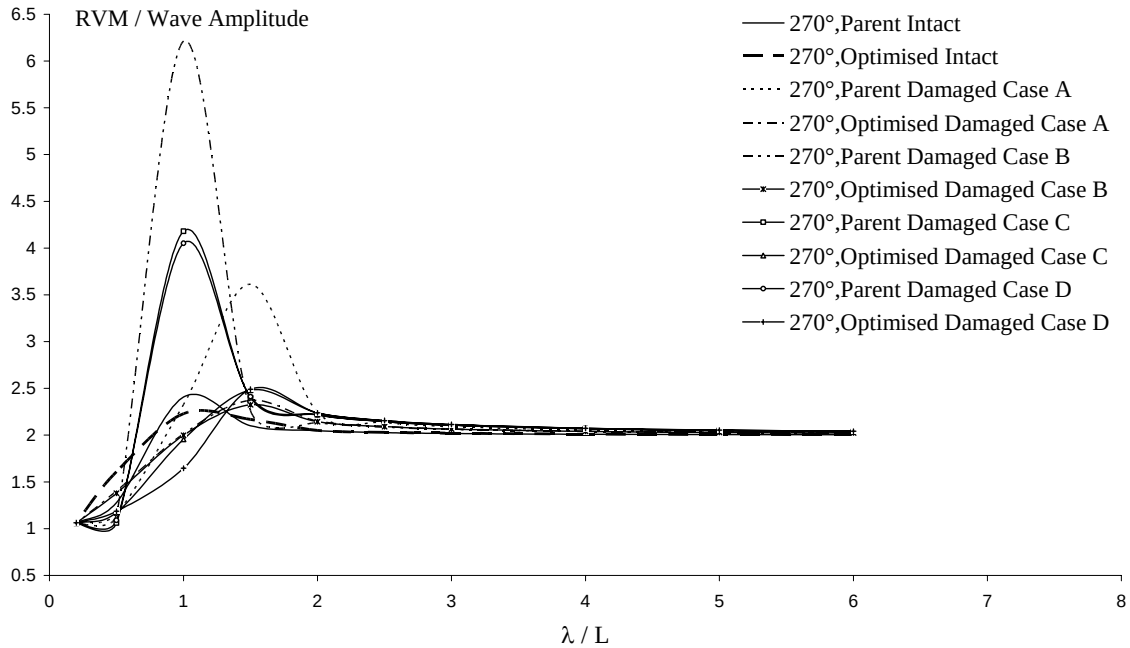

Figure J.60: Relative vertical motion responses for the intact and damaged hull forms for point F (in beam seas).

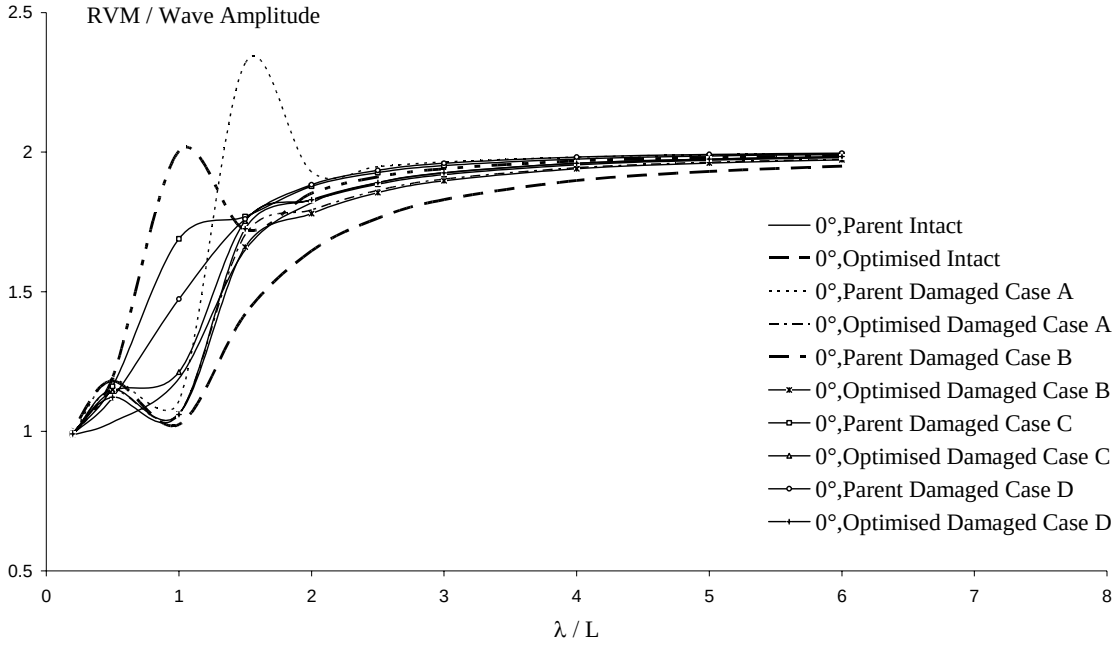

Figure J.61: Relative vertical motion responses for the intact and damaged hull forms for point G (in following seas).

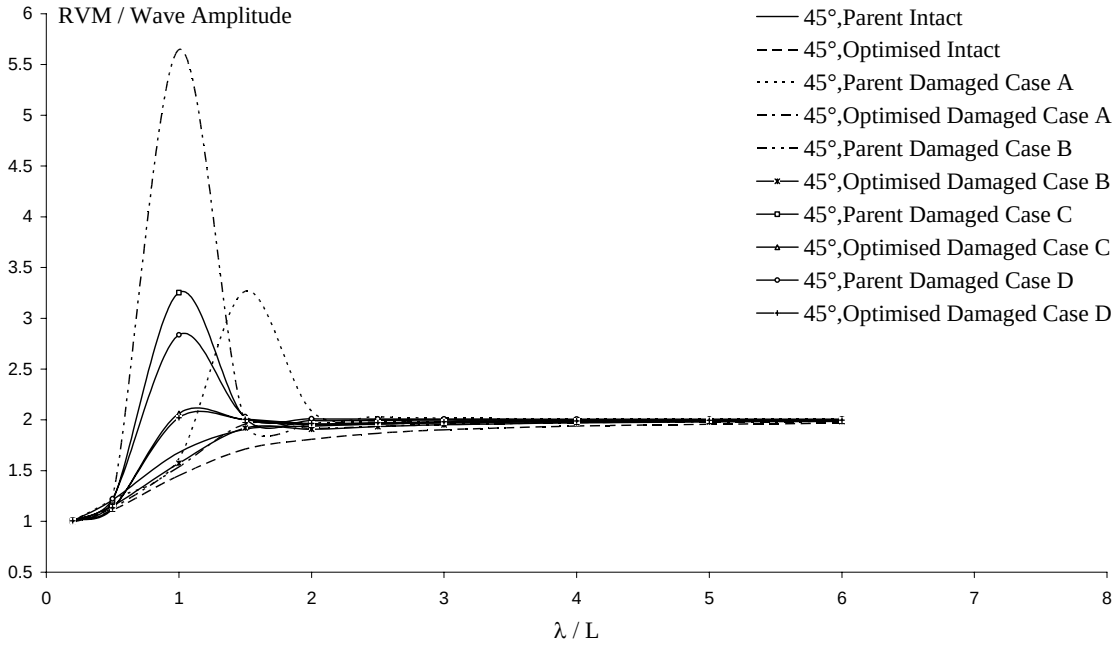

Figure J.62: Relative vertical motion responses for the intact and damaged hull forms for point G (in quartering seas).

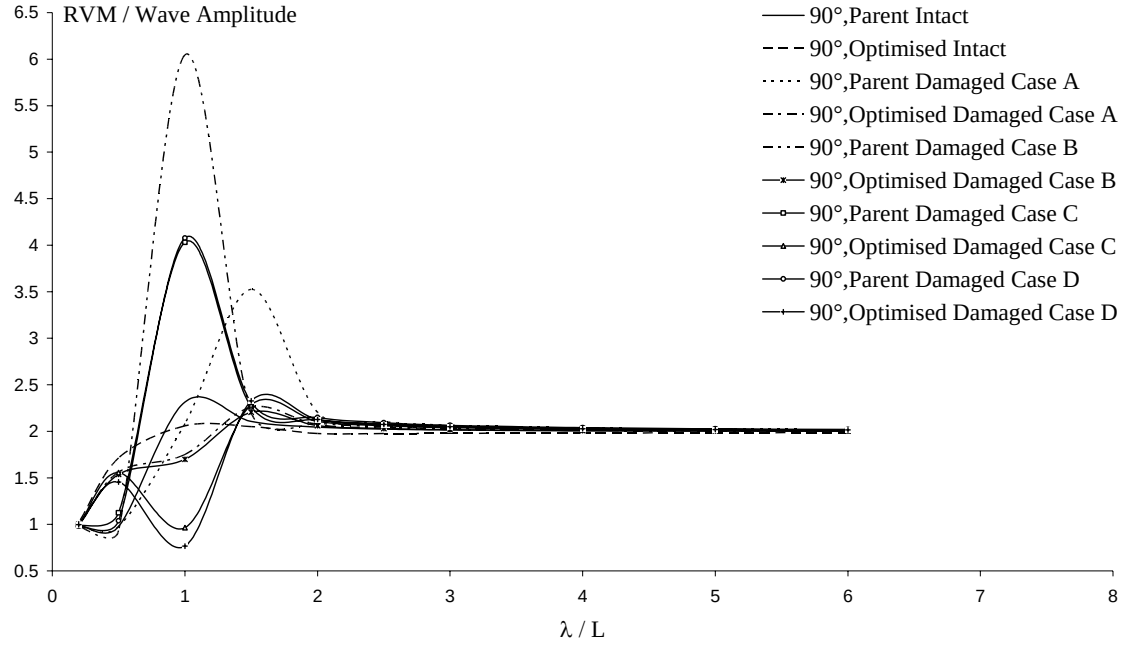

Figure J.63: Relative vertical motion responses for the intact and damaged hull forms for point G (in beam seas).

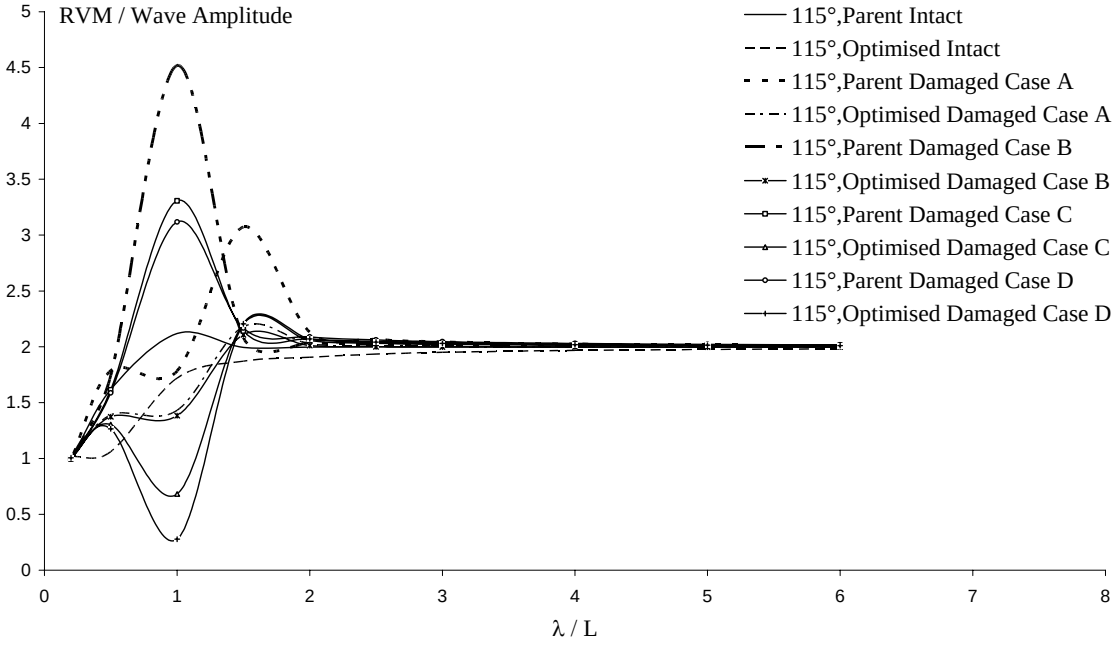

Figure J.64: Relative vertical motion responses for the intact and damaged hull forms for point G (in beam seas).

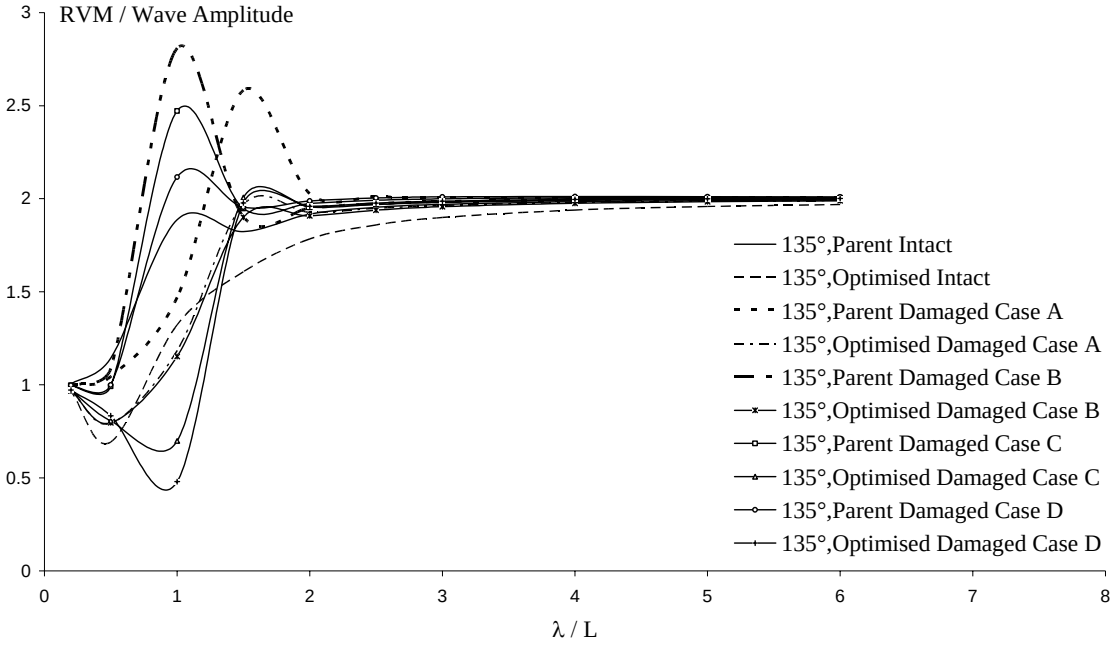

Figure J.65: Relative vertical motion responses for the intact and damaged hull forms for point G (in bow seas).

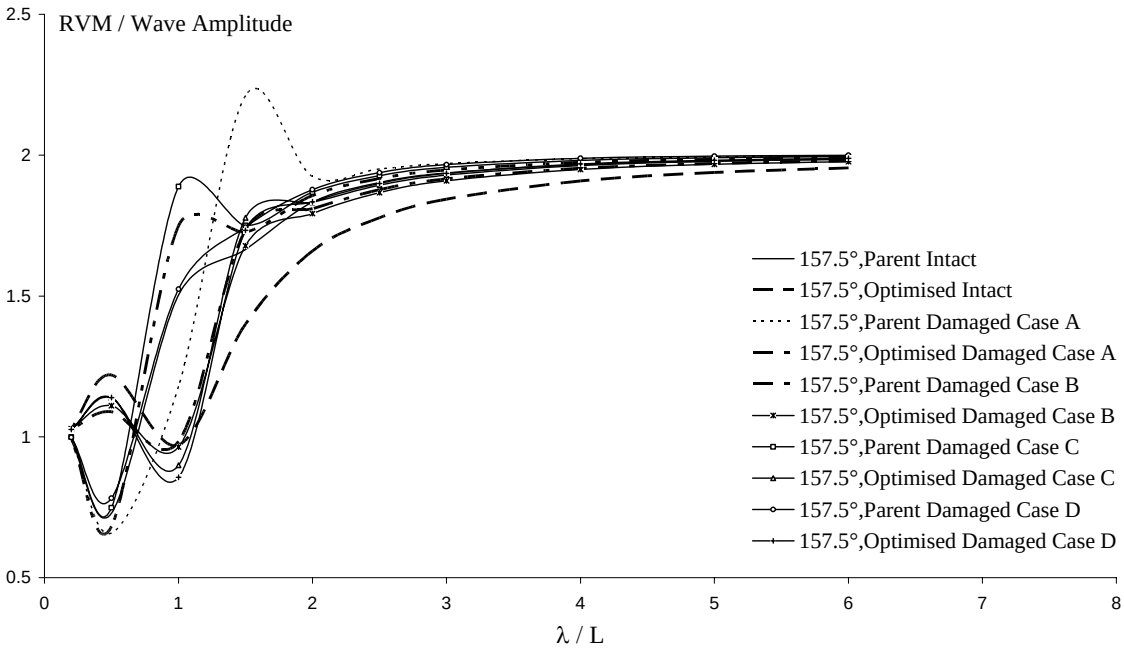

Figure J.66: Relative vertical motion responses for the intact and damaged hull forms for point G (in head seas).

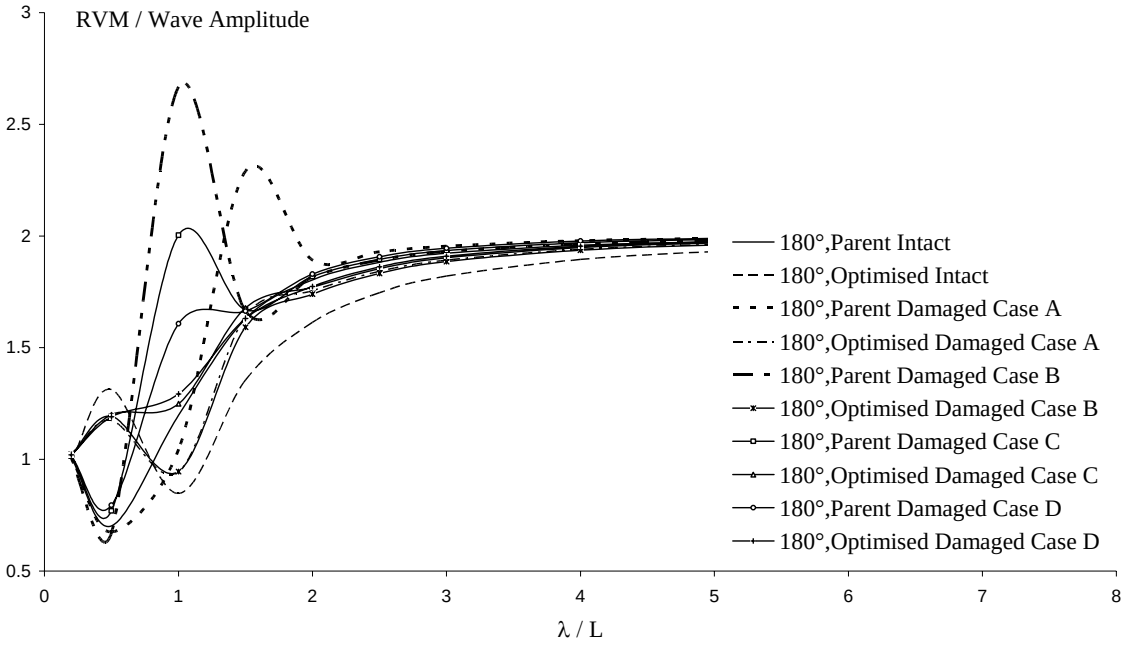

Figure J.67: Relative vertical motion responses for the intact and damaged hull forms for point G (in head seas).

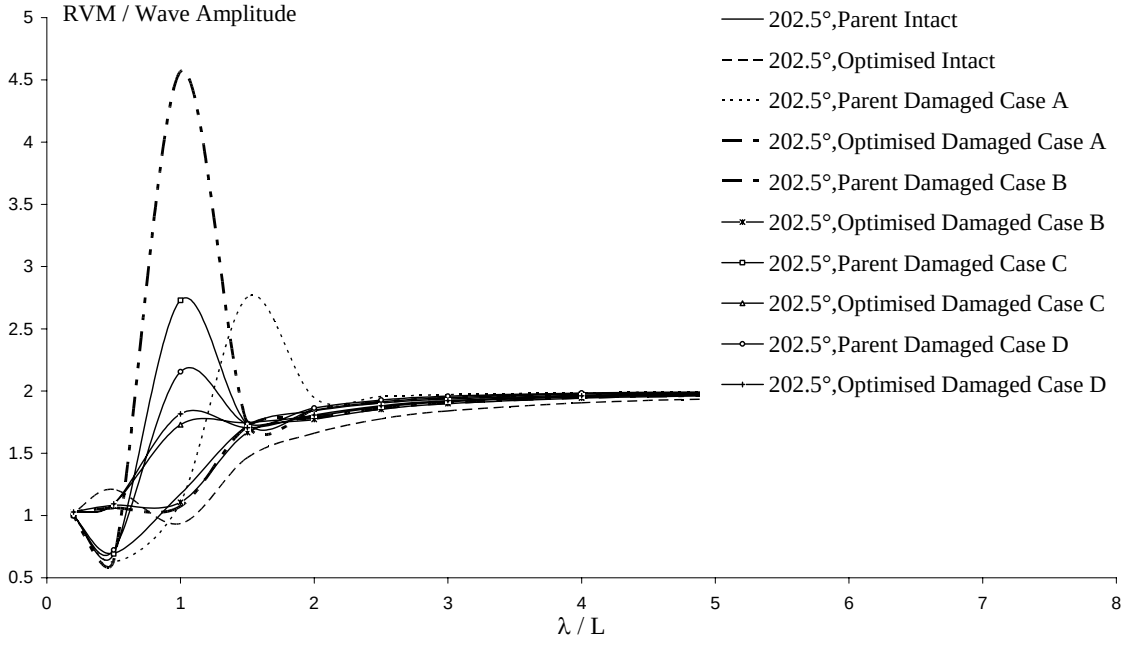

Figure J.68: Relative vertical motion responses for the intact and damaged hull forms for point G (in head seas).

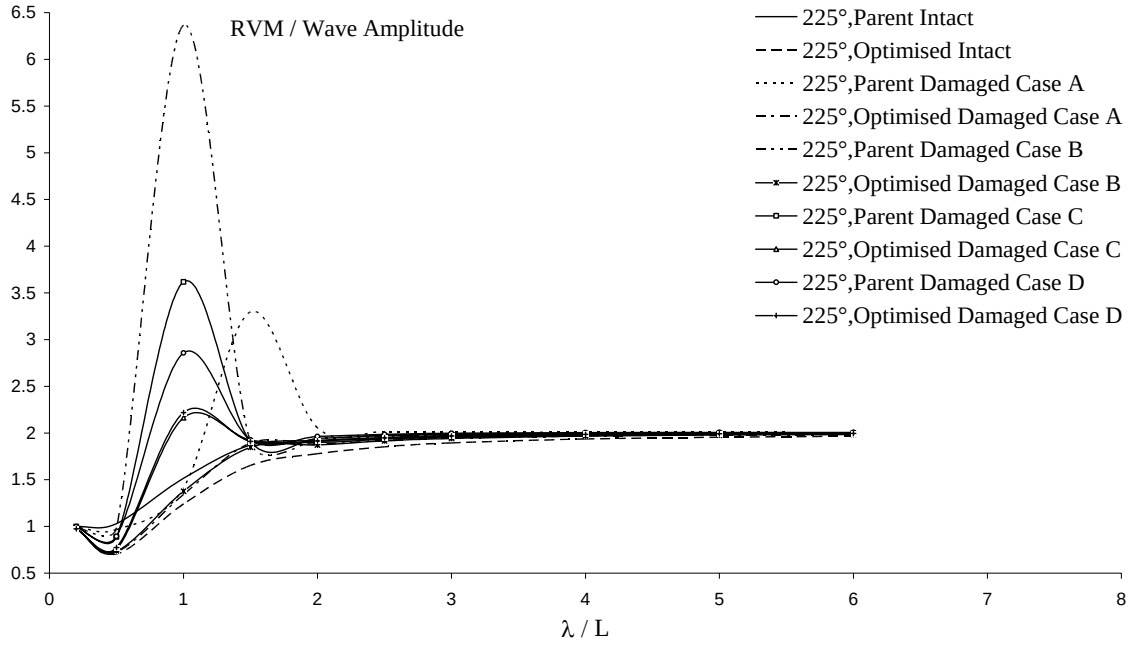

Figure J.69: Relative vertical motion responses for the intact and damaged hull forms for point G (in bow seas).

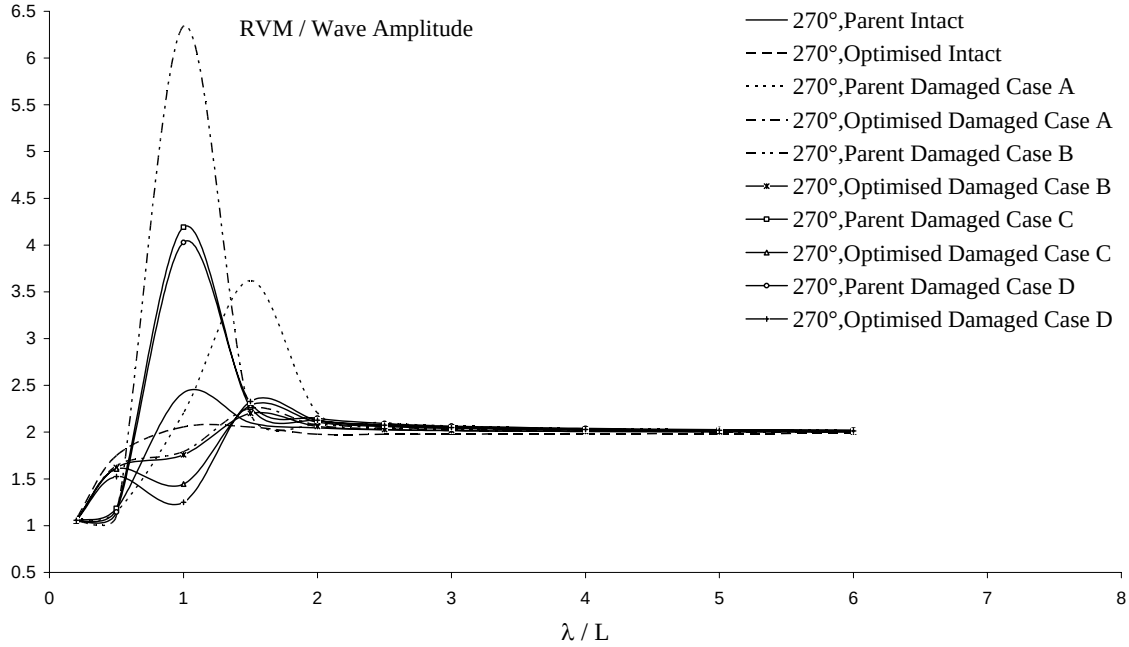

Figure J.70: Relative vertical motion responses for the intact and damaged hull forms for point G (in beam seas).

APPENDIX K – EXTENSION OF EQUATIONS OF MOTION FOR A SHIP TO INCLUDE INFLUENCES OF INGRESSED WATER WITHIN THE DAMAGED HOLD(S)

Within the dissertation the damaged ship has been modelled by considering the external fluid structure interaction. The ingressed water has influenced the motion dynamics through the hydrodynamics reactive and excitation loads reflecting the heeled-trimmed orientation of damaged ship and the mass-inertia matrix changes noting changes in equivalent point mass model and the inclusion of the products of inertia.

Another aspect of the ingressed water is that as the ship moves so will the internal free-surfaces within any damaged hull form. These free surfaces may be modelled as structural massless flat plates with heave, roll and pitch degrees of freedom. Here the hydrodynamic coupling of such a free surface and the ship are provided to indicate how the nine degrees of freedom system may be modelled. The extension to damage scenario C with two holds flooded is readily undertaken by extending the ideas encompassed in the following equations. The distinct hydrostatic restoration coefficients for the massless plate and the ship together with all the hydrodynamic reactive and active force and moments may be readily calculated using the Matthew Diffraction Suite.

Equations (K.1) to (K.6) provide the surge, sway, heave, roll, pitch and yaw equations of motion for the ship. Motion amplitude terms with the superscript ‘FS’ denote the motions (to be determined) of the internal free surface. On the hydrodynamic reactive coefficients superscripts of the form ‘/FS’ indicate that the loads included are the hydrodynamic loads experienced by the ship as a consequence of the motions of the free-surface. Equations (K.7) to (K.9) provide the heave, roll and pitch motion equations for the internal free surface. In this case the superscript ‘FS/’ indicates loads induced on the free-surface as a result of the motions of the ship. Because the free-surface is modelled as a massless plate there are no structural cross-coupling terms in the free-surface motion equations.

$$\left[-\omega^2\left(M+A_{11}\right)-i\omega B_{11}\right]\eta_1+\left[-\omega^2 A_{12}-i\omega B_{12}\right]\eta_2+\left[-\omega^2 A_{13}-i\omega B_{13}\right]\eta_3+\left[-\omega^2 A_{14}-i\omega B_{14}\right]\eta_4$$
$$+\left[-\omega^2 A_{15}-i\omega B_{15}+MY_G\omega^2\right]\eta_5+\left[-\omega^2 A_{16}-i\omega B_{16}-MX_G\omega^2\right]\eta_6+\left[-\omega^2 A_{13}^{/FS}-i\omega B_{13}^{/FS}\right]\eta_3^{FS}$$
$$+\left[-\omega^2 A_{14}^{/FS}-i\omega B_{14}^{/FS}\right]\eta_4^{FS}+\left[-\omega^2 A_{15}^{/FS}-i\omega B_{15}^{/FS}\right]\eta_5^{FS}=F_1$$

(K.1)

$$\left[-\omega^2 A_{21}-i\omega B_{21}\right]\eta_1+\left[-\omega^2\left(M+A_{22}\right)-i\omega B_{22}\right]\eta_2+\left[-\omega^2 A_{23}-i\omega B_{23}\right]\eta_3$$
$$+\left[-\omega^2 A_{24}-i\omega B_{24}-MY_G\omega^2\right]\eta_4+\left[-\omega^2 A_{25}-i\omega B_{25}\right]\eta_5+\left[-\omega^2 A_{26}-i\omega B_{26}+MZ_G\omega^2\right]\eta_6$$
$$+\left[-\omega^2 A_{23}^{/FS}-i\omega B_{23}^{/FS}\right]\eta_3^{FS}+\left[-\omega^2 A_{24}^{/FS}-i\omega B_{24}^{/FS}\right]\eta_4^{FS}+\left[-\omega^2 A_{25}^{/FS}-i\omega B_{25}^{/FS}\right]\eta_5^{FS}=F_2$$

(K.2)

$$\left[-\omega^2 A_{31}-i\omega B_{31}\right]\eta_1+\left[-\omega^2 A_{32}-i\omega B_{32}\right]\eta_2+\left[C_{33}-\omega^2\left(M+A_{33}\right)-i\omega B_{33}\right]\eta_3$$
$$+\left[C_{34}-\omega^2 A_{34}-i\omega B_{34}+MX_G\omega^2\right]\eta_4+\left[C_{35}-\omega^2 A_{35}-i\omega B_{35}-MZ_G\omega^2\right]\eta_5$$
$$+\left[-\omega^2 A_{36}-i\omega B_{36}\right]\eta_6+\left[-\omega^2 A_{33}^{/FS}-i\omega B_{33}^{/FS}\right]\eta_3^{FS}+\left[-\omega^2 A_{34}^{/FS}-i\omega B_{34}^{/FS}\right]\eta_4^{FS}$$
$$+\left[-\omega^2 A_{35}^{/FS}-i\omega B_{35}^{/FS}\right]\eta_5^{FS}=F_3$$

(K.3)

$$\left[-\omega^2 A_{41}-i\omega B_{41}\right]\eta_1+\left[-\omega^2 A_{42}-i\omega B_{42}-\omega^2 MY_G\right]\eta_2+\left[C_{43}-\omega^2 A_{43}-i\omega B_{43}+\omega^2 MX_G\right]\eta_3$$
$$+\left[C_{44}-\omega^2\left(I_{44}+A_{44}\right)-i\omega B_{44}\right]\eta_4+\left[C_{45}-\omega^2 A_{45}-i\omega B_{45}-\omega^2 I_{45}\right]\eta_5$$
$$+\left[-\omega^2 A_{46}-i\omega B_{46}-\omega^2 I_{46}\right]\eta_6+\left[-\omega^2 A_{43}^{/FS}-i\omega B_{43}^{/FS}\right]\eta_3^{FS}+\left[-\omega^2 A_{44}^{/FS}-i\omega B_{44}^{/FS}\right]\eta_4^{FS}$$
$$+\left[-\omega^2 A_{45}^{/FS}-i\omega B_{45}^{/FS}\right]\eta_5^{FS}=F_4$$

(K.4)

$$\left[-\omega^2 A_{51}-i\omega B_{51}+M\omega^2 Y_G\right]\eta_1+\left[-\omega^2 A_{52}-i\omega B_{52}\right]\eta_2+\left[C_{53}-\omega^2 A_{53}-i\omega B_{53}-\omega^2 MZ_G\right]\eta_3$$
$$+\left[C_{54}-\omega^2 A_{54}-i\omega B_{54}-\omega^2 I_{54}\right]\eta_4+\left[C_{55}-\omega^2\left(I_{55}+A_{55}\right)-i\omega B_{55}\right]\eta_5$$
$$+\left[-\omega^2 A_{56}-i\omega B_{56}-\omega^2 I_{56}\right]\eta_6+\left[-\omega^2 A_{53}^{/FS}-i\omega B_{53}^{/FS}\right]\eta_3^{FS}+\left[-\omega^2 A_{54}^{/FS}-i\omega B_{54}^{/FS}\right]\eta_4^{FS}$$
$$+\left[-\omega^2 A_{55}^{/FS}-i\omega B_{55}^{/FS}\right]\eta_5^{FS}=F_5$$

(K.5)

$$\left[-\omega^2 A_{61} - i\omega B_{61} - \omega^2 MX_G\right]\eta_1 + \left[-\omega^2 A_{62} - i\omega B_{62} + \omega^2 MZ_G\right]\eta_2 + \left[-\omega^2 A_{63} - i\omega B_{63}\right]\eta_3$$
$$+\left[-\omega^2 A_{64} - i\omega B_{64} - \omega^2 I_{64}\right]\eta_4 + \left[-\omega^2 A_{65} - i\omega B_{65} - \omega^2 I_{65}\right]\eta_5 + \left[-\omega^2\left(I_{66} + A_{66}\right) - i\omega B_{66}\right]\eta_6$$
$$+\left[-\omega^2 A_{63}^{/FS} - i\omega B_{63}^{/FS}\right]\eta_3^{FS} + \left[-\omega^2 A_{64}^{/FS} - i\omega B_{64}^{/FS}\right]\eta_4^{FS} + \left[-\omega^2 A_{65}^{/FS} - i\omega B_{65}^{/FS}\right]\eta_5^{FS} = F_6$$

(K.6)

$$\left[C_{33}^{FS} - \omega^2 A_{33}^{FS} - i\omega B_{33}^{FS}\right]\eta_3^{FS} + \left[C_{34}^{FS} - \omega^2 A_{34}^{FS} - i\omega B_{34}^{FS}\right]\eta_4^{FS} + \left[C_{35}^{FS} - \omega^2 A_{35}^{FS} - i\omega B_{35}^{FS}\right]\eta_5^{FS}$$
$$+\left[-\omega^2 A_{31}^{FS/} - i\omega B_{31}^{FS/}\right]\eta_1 + \left[-\omega^2 A_{32}^{FS/} - i\omega B_{32}^{FS/}\right]\eta_2 + \left[-\omega^2 A_{33}^{FS/} - i\omega B_{33}^{FS/}\right]\eta_3$$
$$+\left[-\omega^2 A_{34}^{FS/} - i\omega B_{34}^{FS/}\right]\eta_4 + \left[-\omega^2 A_{35}^{FS/} - i\omega B_{35}^{FS/}\right]\eta_5 + \left[-\omega^2 A_{36}^{FS/} - i\omega B_{36}^{FS/}\right]\eta_6 = F_3^{FS}$$

(K.7)

$$\left[C_{43}^{FS} - \omega^2 A_{43}^{FS} - i\omega B_{43}^{FS}\right]\eta_3^{FS} + \left[C_{44}^{FS} - \omega^2 A_{44}^{FS} - i\omega B_{44}^{FS}\right]\eta_4^{FS} + \left[C_{45}^{FS} - \omega^2 A_{45}^{FS} - i\omega B_{45}^{FS}\right]\eta_5^{FS}$$
$$+\left[-\omega^2 A_{41}^{FS/} - i\omega B_{41}^{FS/}\right]\eta_1 + \left[-\omega^2 A_{42}^{FS/} - i\omega B_{42}^{FS/}\right]\eta_2 + \left[-\omega^2 A_{43}^{FS/} - i\omega B_{43}^{FS/}\right]\eta_3$$
$$+\left[-\omega^2 A_{44}^{FS/} - i\omega B_{44}^{FS/}\right]\eta_4 + \left[-\omega^2 A_{45}^{FS/} - i\omega B_{45}^{FS/}\right]\eta_5 + \left[-\omega^2 A_{46}^{FS/} - i\omega B_{46}^{FS/}\right]\eta_6 = F_4^{FS}$$

(K.8)

$$\left[C_{53}^{FS} - \omega^2 A_{53}^{FS} - i\omega B_{53}^{FS}\right]\eta_3^{FS} + \left[C_{54}^{FS} - \omega^2 A_{54}^{FS} - i\omega B_{54}^{FS}\right]\eta_4^{FS} + \left[C_{55}^{FS} - \omega^2 A_{55}^{FS} - i\omega B_{55}^{FS}\right]\eta_5^{FS}$$
$$+\left[-\omega^2 A_{51}^{FS/} - i\omega B_{51}^{FS/}\right]\eta_1 + \left[-\omega^2 A_{52}^{FS/} - i\omega B_{52}^{FS/}\right]\eta_2 + \left[-\omega^2 A_{53}^{FS/} - i\omega B_{53}^{FS/}\right]\eta_3$$
$$+\left[-\omega^2 A_{54}^{FS/} - i\omega B_{54}^{FS/}\right]\eta_4 + \left[-\omega^2 A_{55}^{FS/} - i\omega B_{55}^{FS/}\right]\eta_5 + \left[-\omega^2 A_{56}^{FS/} - i\omega B_{56}^{FS/}\right]\eta_6 = F_5^{FS}$$

(K.9)